Topics:
Soils
Testing
Foundations
Transmission towers
Transmission lines
Design

EPRI EL-6800
Project 1493-6
Final Report
August 1990

Manual on Estimating Soil Properties for Foundation Design

Prepared by
Cornell University
Ithaca, New York

REPORT SUMMARY

SUBJECTS Overhead structures and foundations / Overhead transmission

TOPICS Soils, Testing, Foundations, Transmission towers, Transmission lines, Design

AUDIENCE Transmission managers and engineers

Manual on Estimating Soil Properties for Foundation Design

This manual provides foundation engineers with a comprehensive reference on estimating engineering soil parameters from field or laboratory test data. Empirical correlations are used extensively to evaluate soil parameters. The manual describes the most important of these correlations completely and systematically with an emphasis on the correlations of relatively common tests, including those that are seeing increased usage in practice.

BACKGROUND The analysis of all geotechnical problems, such as transmission structure foundation design, requires the adoption of a soil behavioral model that must include all relevant soil properties. These soil properties are not known in advance and require the design engineer to either measure or estimate properties using correlations. However, the source, extent, and limitations of correlations are most often obscured in the presentation of the relationships. When plotted, most correlations are presented as a simple line, but in reality they may be based on a veritable shotgun blast of data points.

OBJECTIVE To present a readily usable, comprehensive set of correlations for estimating soil properties with each correlation presented in the context of its historical evolution and statistical variability; to update existing correlations with new data when possible.

APPROACH The researchers established a context for basic soil characterization, including simple soil descriptions, classification, unit weight, relative density, and consistency. Next, they developed correlations for in situ state of stress, strength, elastic behavior, time-dependent deformability, and permeability—both for common tests and for newer tests coming into increasing use.

RESULTS This work is a collection of correlations that organize a huge body of dispersed knowledge into a coherent framework. Comprehensive correlations are given for basic soil characterizations, in situ stress state tests, strength tests, tests of elastic and time-dependent deformability, permeability tests, and liquefaction resistance tests. Each correlation is constructed from its beginnings in the literature. Some correlations are original amalgams of several different presentations, and several correlations are considerably enhanced by the addition of new data. Further, many new correlations were developed when sufficient data were available. All of the presentations give the foundation designer an immediate feel for the variability of each relationship.

EPRI PERSPECTIVE

This manual is intended to make the job of the transmission structure foundation designer easier. A second application is to aid in the development of local soil property correlations specific to particular utility service areas. This use of the soil properties manual will tie in directly with the use of the TLWorkstation™ foundation task modules, CUFAD and MFAD (EPRI report EL-6420, volumes 16 and 17), and the recently released CUFAD+ EPRIGEMS module (report EL-6583-CCML). Finally, the manual can serve to alert the design engineer, who previously had only standard penetration test data on which to base soil characterizations, that several other in situ tests are vastly superior predictors of soil properties. The engineer is thus presented with the data to make a cost-benefits analysis of the worth of better data on which to base design. For other EPRI work on soil properties and foundation design see EPRI reports EL-2870 and EL-6420, volume 2.

PROJECT

RP1493-6
EPRI Project Manager: Vito Longo
Electrical Systems Division
Contractor: Cornell University

Manual on Estimating Soil Properties for Foundation Design

EL-6800
Research Project 1493-6

Final Report, August 1990

Prepared by

CORNELL UNIVERSITY
Geotechnical Engineering Group
Hollister Hall
Ithaca, New York 14853-3501

Authors
F. H. Kulhawy
P. W. Mayne

Principal Investigator
F. H. Kulhawy

Prepared for

Electric Power Research Institute
3412 Hillview Avenue
Palo Alto, California 94304

EPRI Project Manager
V. J. Longo

Overhead Transmission Lines Program
Electrical Systems Division

ORDERING INFORMATION

Requests for copies of this report should be directed to Research Reports Center (RRC), Box 50490, Palo Alto, CA 94303, (415) 965-4081. There is no charge for reports requested by EPRI member utilities and affiliates, U.S. utility associations, U.S. government agencies (federal, state, and local), media, and foreign organizations with which EPRI has an information exchange agreement. On request, RRC will send a catalog of EPRI reports.

NOTICE

Prepared by
Cornell University
Ithaca, New York

ABSTRACT

This manual focuses on the needs of engineers involved in the geotechnical design of foundations for transmission line structures. It also will serve as a useful reference for other geotechnical problems. In all foundation design, it is necessary to know the pertinent parameters controlling the soil behavior. When it is not feasible to measure the necessary soil parameters directly, estimates will have to be made from other available data, such as the results of laboratory index tests and in-situ tests. Numerous correlations between these types of tests and the necessary soil parameters exist in the literature, but they have not been synthesized previously into readily usable form in a collective work. This manual summarizes the most pertinent of these available correlations for estimating soil parameters. In many cases, the existing correlations have been updated with new data, and new correlations have been developed where sufficient data have been available. For each soil parameter, representative correlations commonly are presented in chronological order to illustrate the evolutionary development of the particular correlation. The emphasis is on relatively common laboratory and in-situ tests and correlations, including those tests that are seeing increased use in practice.

ACKNOWLEDGMENTS

The authors appreciate the assistance of numerous people during the course of this study and want to acknowledge their contributions. C. H. Trautmann and H. E. Stewart of Cornell University provided many useful comments and suggestions as this report was compiled, and they provided detailed review comments on both the first and final drafts of this report. K. J. Stewart prepared the text, and A. Avcisoy drafted the figures.

Several colleagues graciously responded to a request for review and evaluation of the first draft of this report. These included: J. I. Adams, Consultant; R. G. Campanella, University of British Columbia; A. M. DiGioia, Jr. and L. F. Rojas-Gonzalez, GAI Consultants; M. D. Grigoriu and S. Vidić, Cornell University; E. B. Lawless, III, Potomac Electric Power Company; V. J. Longo, EPRI; J. K. Mitchell, University of California at Berkeley; H. S. Radhakrishna, Ontario Hydro; T. E. Rodgers, Jr., Virginia Power; J. W. Rustvold, Bonneville Power Administration; J. H. Schmertmann, Schmertmann and Crapps; J. J. Wolf, Western Area Power Administration; and C. P. Wroth, University of Oxford. The detailed reviewers' comments were very helpful in preparing the final text of this report.

CONTENTS

Section		Page

ILLUSTRATIONS

Figure		Page

Figure		Page
4-57	s_u as a Function of K_D from the DMT	4-60
5-1	Modulus Definitions	5-2
5-2	Drained Poisson's Ratio Parameters for Granular Soils	5-5
5-3	Drained Poisson's Ratio versus PI for Several LOC Soils	5-5
5-4	Drained Poisson's Ratio versus OCR and Stress Level for Sydney Kaolin	5-5
5-5	Normalized Undrained Modulus versus Stress Level and OCR	5-8
5-6	Generalized Undrained Modulus Ratio versus OCR and PI	5-8
5-7	Cam Clay Prediction of Undrained Initial Tangent Modulus Ratio	5-9
5-8	PMT Modulus of Clay versus N Value	5-10
5-9	Undrained Modulus for Deep Foundations in Compression	5-11
5-10	Undrained Modulus for (a) Drilled Shafts in Compression and Uplift and (b) Spread Foundations in Uplift	5-11
5-11	Shear Modulus versus Shear Strain for Sands	5-13
5-12	Dynamic Shear Modulus versus N for Cohesive Soils	5-14
5-13	Comparative Plot of Drained Modulus Correlations for Sand	5-17
5-14	PMT Modulus of Sand versus N Value	5-18
5-15	Trend Between Dilatometer Modulus and N in Piedmont Sandy Silts	5-19
5-16	Variation of α with D_r for Sands in Calibration Chambers	5-21
5-17	CPT α Correlation for Ticino Sand	5-22
5-18	Normalized Drained Modulus for (a) Drilled Shafts in Uplift and (b) Spread Foundations in Uplift	5-22
5-19	Variation of Shear Modulus of Dry Sands with Void Ratio and Confining Stress	5-23
6-1	Consolidation Behavior	6-2
6-2	Time-Settlement Behavior	6-3
6-3	Representative C_c Relationships for Cohesive Soils	6-4
6-4	Compression and Unload-Reload Indices versus PI	6-5
6-5	Sensitivity-Compression Index Relationships	6-6
6-6	Compression Ratio versus Water Content	6-6

TABLES

SYMBOLS

ENGLISH LETTERS - UPPER CASE

A - dilatometer test reading

$\bar{A}_f$ - pore water stress parameter at failure

A_s - surface area of cone sleeve

A_{s1} - cone area over which u_{bt} acts

A_{s2} - cone area over which u_s acts

ASTM - American Society for Testing and Materials

B - foundation diameter or width; cone diameter; dilatometer test reading

B_c - calibration chamber diameter

B_q - piezocone parameter

C - experimental constant in modified Cam clay model

C_A - N correction for aging

C_B - N correction for borehole diameter

C_{ER} - N correction for energy ratio

C_N - N correction for overburden stress

C_{OCR} - N correction for overconsolidation

C_P - N correction for particle size

C_R - N correction for rod length

C_S - N correction for sampling method

C_c - compression index

C_q - q_c correction for overburden stress

C_s - swelling index

C_u - uniformity coefficient = D_{60}/D_{10}

C_{ur} - unload-reload index

C_α - coefficient of secondary compression

$C_{\alpha e}$ - C_α in terms of void ratio

$C_{\alpha \epsilon}$ - C_α in terms of vertical strain

CAUC - consolidated anisotropic undrained triaxial compression

CF - clay fraction

CI - consistency index

CIDC - consolidated isotropic drained triaxial compression

CIUC - consolidated isotropic undrained triaxial compression

CIUE - consolidated isotropic undrained triaxial extension

CK_oUC - K_o consolidated undrained triaxial compression

CK_oUE - K_o consolidated undrained triaxial extension

COV - coefficient of variation (standard deviation/mean)

CPT - cone penetration test

CPTU - piezocone test

CR - compression ratio = $C_c/(1 + e_o)$

CSL - critical state line

CSSM - critical state soil mechanics

D - depth; vane diameter; cone diameter

D_5 - particle size at 5 percent finer

D_{10} - particle size at 10 percent finer

D_{50} - particle size at 50 percent finer

D_{60} - particle size at 60 percent finer

D_{max} - maximum particle size

D_{min} - minimum particle size

D_r - relative density = $(e_{max} - e)/(e_{max} - e_{min})$

DMT - dilatometer test

DS - direct shear

DSS - direct simple shear

E - Young's modulus

E_D - dilatometer modulus

E_{PMT} - pressuremeter modulus

E_d - drained modulus

E_{ds} - drained secant modulus

E_f - Young's modulus of foundation

E_i - initial tangent modulus

E_s - secant modulus

E_t - tangent modulus

E_u - undrained modulus

E_{ui} - undrained initial tangent modulus

E_{us} - undrained secant modulus

E_{ut} - undrained tangent modulus

ECPT - electric CPT

ER - energy ratio

F - percent passing No. 200 sieve

F_ν - Poisson's ratio parameter

FR - cone friction ratio = f_s/q_c (alternate for R_f)

G - shear modulus = $E/2(1 + \nu)$

G_i - initial tangent G

G_{max} - dynamic shear modulus

G_{ru} - reload-unload G

G_s - specific gravity of solids; secant G

G_{ur} - unload-reload G

G_ν - Poisson's ratio parameter

H - vane height; height of drainage path

HOC - heavily overconsolidated

I_D - density index; DMT material index

I_{RD} - relative dilatancy index

I_f - moment of inertia of foundation

I_r - rigidity index

I_{rr} - reduced rigidity index

K - coefficient of horizontal soil stress = $\bar{\sigma}_h/\bar{\sigma}_v$; vane constant

K_A - coefficient of minimum active soil stress

K_D - DMT horizontal stress index

K_P - coefficient of maximum passive soil stress

K_o - in-situ or at-rest K = $\bar{\sigma}_{ho}/\bar{\sigma}_{vo}$

K_{onc} - normally consolidated K_o

K_{ou} - K_o during primary unloading

K_q - calibration chamber correction factor

K_s - subgrade reaction modulus; ratio of s_u in extension to compression

LI - liquidity index = $(w_n - w_P)/(w_L - w_P)$

LOC - lightly overconsolidated

M - critical state failure parameter; constrained modulus; earthquake magnitude; exponent in G_{max} relationship

M_d - drained constrained modulus

M_{ds} - drained secant constrained modulus

M_{dt} - drained tangent constrained modulus

MCPT - mechanical CPT

N - standard penetration test value

N_{60} - corrected N for field procedures

N_k - cone bearing factor

N_p - PMT bearing factor

$(N_1)_{60}$ - N_{60} corrected to reference stress of one atmosphere

$N_{\Delta u}$ - piezocone factor

NC - normally consolidated

OC - overconsolidated

OCR - overconsolidation ratio = $\bar{\sigma}_p/\bar{\sigma}_{vo}$

OCR_i - isotropic OCR = $\bar{p}_{max}/\bar{p}_o$

OCR_{limit} - limiting OCR at which passive failure occurs

OCR_{max} - maximum OCR

PI - plasticity index = $w_L - w_P$

PMT - pressuremeter test

PSC - plane strain compression

PSE - plane strain extension

Q - soil mineralogy and compressibility coefficient for strength dilatancy

Q_C - soil mineralogy and compressibility coefficient for cone

Q_{CD} - dimensionless cone tip resistance = $(q_c/p_a)/(\bar{\sigma}_{vo}/p_a)^{0.5}$

Q_{OCR} - q_c correction for overconsolidation (equal to C_{OCR})

R - particle roundness; fitting coefficient; radius

R_e - equivalent radius

R_f - failure ratio; cone friction ratio = f_s/q_c

S - dynamic stiffness coefficient; particle sphericity

S_t - sensitivity

SBPMT - self-boring pressuremeter test

S.D. - standard deviation

SL - stress level (fraction of strength mobilized)

SPT - standard penetration test

T - time factor; torque

TC - triaxial compression

TE - triaxial extension

U - unconfined compression test

UU - unconsolidated-undrained triaxial compression test

V - volume

VST - vane shear test

ENGLISH LETTERS - LOWER CASE

a - cone area ratio; modified Cam clay parameter for anisotropic compression

a_{OCR} - s_u correction for overconsolidation

a_{RATE} - s_u correction for strain rate

a_{TEST} - s_u correction for test mode

a_{max} - maximum horizontal acceleration at ground surface

b - intermediate effective principal stress factor

c - cohesion intercept

$\bar{c}$ - effective stress cohesion intercept

c_u - alternative form of s_u

c_v - coefficient of consolidation

c_{vh} - horizontal c_v

d - internal cone diameter; modified Cam clay parameter for plane strain compression

e - void ratio (usually in-situ)

e_{max} - maximum void ratio

e_{min} - minimum void ratio

e_o - initial void ratio

f - unit side resistance; SPT modulus coefficient

f_s - cone side resistance

f_{sn} - normalized cone side resistance

f_t - corrected cone side resistance

g - gravitational acceleration

k - coefficient of permeability

k_h - horizontal k; alternative form for k_s

k_s - subgrade reaction modulus

k_v - vertical k

m - modulus number; OCR exponent

m_r - reload coefficient

m_v - coefficient of volumetric compressibility

n - hyperbolic modulus exponent; cone exponent; porosity = e/(1 + e); number of measurements or data points

n_h - coefficient of subgrade reaction

p - alternative form of $\bar{\sigma}_{vo}$; applied stress

$\bar{p}$ - effective mean normal stress = $(\bar{\sigma}_1 + \bar{\sigma}_2 + \bar{\sigma}_3)/3$; applied stress

p_1 - DMT expansion stress

p_2 - dilatometer C reading at a particular time

p_L - PMT limit stress

p_a - atmospheric pressure or stress (See Appendix I for numerical values.)

$\bar{p}_c$ - alternative form of $\bar{\sigma}_p$

p_e - PMT expansion stress

p_f - PMT yield stress

$\bar{p}_f$ - $\bar{p}$ at failure

$\bar{p}_{max}$ - maximum $\bar{p}$

p_o - DMT contact stress; PMT total horizontal stress

$\bar{p}_o$ - initial effective $\bar{p}$

q - shear stress

q_D - DMT tip resistance

q_T - corrected q_c

q_c - cone tip resistance

q_n - q_c standardized to reference stress of one atmosphere

q_u - unconfined compression strength = 2 s_u

r - critical state spacing ratio; sample correlation coefficient

r^2 - coefficient of determination

s - slope of PMT plot of p_e vs. ϵ_c

s_u - undrained shear strength

s_{ur} - remolded s_u

$s_{u(VST)}$ - s_u from VST

t - time

u_{bt} - pore water stress behind cone tip

u_m - measured pore water stress during cone penetration

u_o - hydrostatic stress

u_s - pore water stress behind cone sleeve

u_t - pore water stress on cone tip/face

w_n - in-situ, natural water content

w_L - liquid limit

w_P - plastic limit

z - depth

z_m - DMT gage pressure deviation

GREEK LETTERS - UPPER CASE

ΔV - volume change

Δu - excess pore water stress

Δu_{bt} - excess pore water stress measured behind the cone tip

Δu_o - Δu at time zero

Δu_t - excess pore water stress measured on the cone tip or face

$\Delta \sigma_{1,3}$ - major, minor principal stress increment

$\Delta \phi_{1-5}$ - corrections to $\bar{\phi}_{cv}$

$\Delta \bar{\phi}_r$ - change in residual friction angle

Λ - critical state parameter

GREEK LETTERS - LOWER CASE

α - CPT parameter relating modulus to q_c; K_o unload coefficient

α_{VST} - empirical vane factor

β_k - DMT K_o coefficient

β_o - DMT OCR coefficient

γ - unit weight; shear strain

$\bar{\gamma}$ - effective unit weight

γ_d - dry γ

γ_{sat} - saturated γ

γ_{total} - total γ

γ_w - γ of water

δ - stress rotation angle; displacement

ϵ - strain

$\dot{\epsilon}$ - strain rate

ϵ_a - axial strain

ϵ_c - cavity strain

ϵ_r - radial strain

ϵ_v - vertical or volumetric strain

κ - modulus number; critical state parameter for isotropic swelling index

λ - critical state parameter for isotropic compression index

μ - micron (10^{-6} meters); VST correction factor

ν - Poisson's ratio

ν_d - drained ν

ν_{di} - initial tangent drained ν

ν_u - undrained $\nu = 0.5$

ρ - density

ρ_d - in-situ dry density

ρ_{dmax} - maximum ρ_d

ρ_{dmin} - minimum ρ_d

σ - total normal stress

$\bar{\sigma}$ - effective normal stress

$\sigma_{1,2,3}$ - major, intermediate, minor principal σ

$\bar{\sigma}_{1,2,3}$ - major, intermediate, minor principal $\bar{\sigma}$

$\sigma_{a,b,c}$ - confining stress a, b, and c

$\bar{\sigma}_{3c}$ - minor principal effective confining stress

σ_{ho} - initial horizontal σ

$\bar{\sigma}_{ho}$ - initial horizontal $\bar{\sigma}$

$\bar{\sigma}_i$ - isotropic overburden $\bar{\sigma}$

$\bar{\sigma}_o$ - current vertical $\bar{\sigma}$; mean principal $\bar{\sigma}$

$\bar{\sigma}_p$ - maximum vertical $\bar{\sigma}$; preconsolidation stress

σ_v - vertical σ

$\bar{\sigma}_v$ - vertical $\bar{\sigma}$

σ_{vm} - mean σ_v

$\bar{\sigma}_{vm}$ - mean $\bar{\sigma}_v$

$\bar{\sigma}_{vmax}$ - alternative form of $\bar{\sigma}_p$

σ_{vo} - vertical (or overburden) σ

$\bar{\sigma}_{vo}$ - vertical (or overburden) $\bar{\sigma}$

τ - shear strength; shear stress

τ_{av} - average cyclic stress

τ_h - shear stress in DSS

ϕ - friction angle

$\bar{\phi}$ - effective stress friction angle

$\bar{\phi}_{cv}$ - fully softened, constant volume, or critical state $\bar{\phi}$

$\bar{\phi}_{ds}$ - direct shear $\bar{\phi}$

$\bar{\phi}_p$ - peak $\bar{\phi}$

$\bar{\phi}_{psc}$ - plane strain compression $\bar{\phi}$

$\bar{\phi}_r$ - residual $\bar{\phi}$

ϕ_{rel} - relative friction angle = $(\bar{\phi}_{tc} - 25°)/(45° - 25°)$

$\bar{\phi}_{secant}$ - secant $\bar{\phi}$

$\bar{\phi}_{tc}$ - triaxial compression $\bar{\phi}$

$\bar{\phi}_{te}$ - triaxial extension $\bar{\phi}$

ψ - dilation angle

Section 1

INTRODUCTION AND BACKGROUND

This manual has been prepared to assist foundation engineers in the selection of soil parameters, primarily for the geotechnical foundation design of transmission line structures. It also will serve as a useful reference for other geotechnical problems. Soil is a complex engineering material, and its properties are not unique or constant. Instead, they vary with many environmental factors (e.g., time, stress history, water table fluctuation, etc.), as discussed in most geotechnical reference books.

Because of the complexity of soil behavior, empirical correlations are used extensively in evaluating soil parameters. In this manual, an attempt has been made to summarize the most pertinent of these empirical laboratory and in-situ test correlations in an organized manner. The emphasis is on relatively common tests and several newer tests that are seeing increased use in practice.

Within this section, the necessary background is presented to understand and appreciate the nature of soil correlations and modeling, and the scope of this manual is outlined.

SOIL CORRELATIONS

The analysis of all geotechnical problems requires the adoption of a soil behavioral model, complete with all relevant soil properties. These soil properties are not known beforehand, and therefore the design engineer must either measure the properties under controlled conditions in the laboratory or field or estimate the properties from other test data. These estimates are made most often from laboratory index tests and in-situ test results, which are correlated to the soil properties either by calibration studies or by back-calculation from full-scale load test data obtained in the field.

Comprehensive characterization of the soil at a particular site would require an elaborate and costly testing program, well beyond the scope of most project budgets. Instead, the design engineer must rely upon more limited soil information, and that is when correlations become most useful. However, caution must always be exercised when using broad, generalized correlations of index parameters or in-situ test results with soil properties. The source, extent, and limitations of each correlation should be examined carefully before use to ensure that extrapolation is not being done beyond the original boundary conditions. "Local" calibrations, where available, are to be preferred over the broad, generalized correlations.

In addition, many of the common correlations in the literature have been developed from test data on relatively insensitive clays of low to moderate plasticity and on unaged quartz sands reconstituted in the laboratory. Extrapolation of these correlations to "special" soils, such as very soft clays, organic clays, sensitive clays, fissured clays, cemented soils, calcareous sands, micaceous sands, collapsible soils, and frozen soils, should be done with particular care because the correlations do not apply strictly to these soil deposits. Careful examination of the soil samples and reference to available geologic and soil survey maps should be made to detect the possible presence of these soils. The same special care should be exercised in remote areas and where no prior experience has been gained. If any "special" soils are present, or if no experience has been documented in a given area, a qualified geotechnical expert should be consulted for guidance.

SOIL AND TEST VARIABILITY

Soil is a complex engineering material which has been formed by a combination of various geologic, environmental, and chemical processes. Many of these processes are continuing and may be modifying the soil in-situ. Because of these natural processes, all soil properties in-situ will vary vertically and horizontally. Even under the most controlled laboratory test conditions, soil properties will exhibit variability. This variability becomes more pronounced in the field where the natural geologic environment is introduced. When empirical correlations are used, additional uncertainty is introduced. These levels of uncertainty must be considered when assessing the reliability of a particular foundation design.

Variability also may be introduced by the type of laboratory or in-situ test used. Each available test will provide a different test result because of differing boundary conditions and loading mechanisms. Figure 1-1 illustrates these variables for some of the common laboratory strength tests and field tests. For the laboratory strength tests, corrections are necessary to interrelate the particular test results because of the different boundary conditions. For the field tests, different in-situ responses are being measured in the different tests, as described in Appendices A through E. Each test has its own variability, and the relative merits

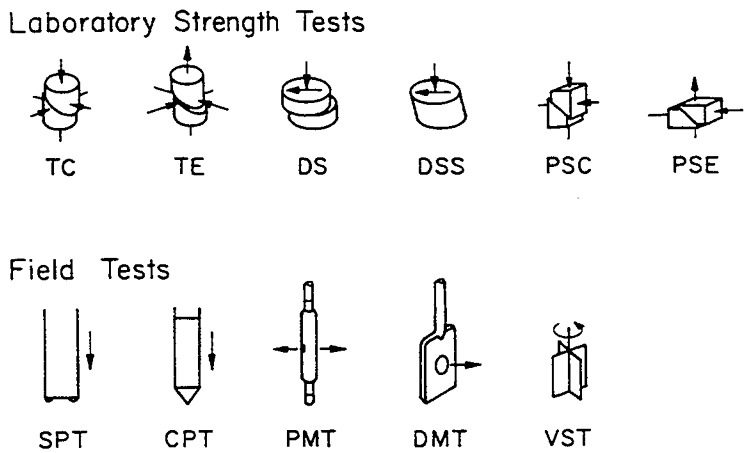

SYMBOLS:

TC - triaxial compression
TE - triaxial extension
DS - direct shear
DSS - direct simple shear
PSC - plane strain compression
PSE - plane strain extension

SPT - standard penetration test
CPT - cone penetration test
PMT - pressuremeter test
DMT - dilatometer test
VST - vane shear test

Figure 1-1. Common Laboratory Strength Tests and Field Tests

of each test should be considered within the overall project context. Appendix F provides a general comparison of these field test methods.

SOIL MODELING

Wroth and Houlsby (1) have stated succinctly that correlations ideally should be (a) based on a physical appreciation of why the properties can be expected to be related, (b) set against a background of theory, and (c) expressed in terms of dimensionless variables to allow scaling. These thoughts should always be kept in mind when using any type of correlation.

It also must be remembered how complex soil behavior really is. Ladd, et al. (2) described this complexity as follows.

> "A generalized model of the stress-strain behavior of soils should ideally account for nonlinearity, yielding, variable dilatancy (volume changes caused by shear stress), and anisotropy (both inherent and stress system induced), plus the behavioral dependence on stress path, stress system (orientation of σ_1 and relative magnitude of σ_2), and stress history (both initial and changes due to consolidation)".

Table 1-1 summarizes the major categories of analytical models that currently are available for representing the behavior of soils. These models range from rather complex (I) to advanced (II) to simple (III) descriptions of soil. Constitutive models for soil behavior require input in the form of soil properties and in-situ parameters. In most cases for transmission line structure foundations, Category III models may be most appropriate at the present time.

Jamiolkowski, et al. (3) also discuss the available laboratory and field tests in use for characterizing soil. Their discussion focuses on a wide range of soil behavior issues and might suggest that soil modeling is a most difficult task. However, new efforts in research and development have resulted in considerable progress in understanding soil behavior. The calibration and modification of soil models have been made possible by the back-analysis of performance data from full-scale field structures, such as deep foundations, embankments, tunnels, offshore platforms, and high-rise buildings. As additional field performance data become available, newer and more reliable correlations undoubtedly will be developed. This progress in research ideally will allow foundation design to evolve from Category III in Table 1-1 to Categories II and then I, at which time all of the necessary soil behavior issues will be addressed.

Table 1-1

CATEGORIES OF ANALYTICAL METHODS FOR SOIL MODELING

Category	Main Features of Models	Determination of Soil Parameters
I	Very advanced models using nonlinear elastic-plastic time-dependent laws which possibly incorporate anisotropic behavior	Only from sophisticated laboratory tests, with the exception of variables which must be obtained from in-situ tests
II	Advanced models using constitutive incremental elastic-plastic laws and nonlinear elastic relationships	Laboratory tests which are only a little more sophisticated than conventional tests; in-situ tests also appropriate
III	Simple continuum, such as isotropic elastic continuum, including layering and empirical models	Conventional laboratory and in-situ tests

Source: Adapted from Jamiolkowski, et al. (3), p. 58.

At the present time, there is one modeling concept of soil behavior which is of some practical use for estimating soil properties. This concept is known as Critical State Soil Mechanics (CSSM) and is described in Appendix G. With this concept, a general predictor for soil behavior has emerged. Strictly speaking, CSSM is applicable only to remolded, insensitive soils without aging, cementing, and other environmental influences. However, the resulting model predicts well the behavior of normally consolidated, insensitive soils, also without aging, cementing, and other environmental influences. In other soils, the model effectively provides a lower bound on the predicted property, such as the undrained shear strength. For these reasons, property prediction by CSSM has been included in this manual as a valuable reference on probable lower bound behavior of natural soils.

SCOPE OF MANUAL

In the following sections, commonly used correlations have been compiled that are helpful for estimating soil properties. Within a particular topic, these correlations are selected and presented in an approximate evolutionary order to represent the development of the relationship as newer research findings became available. In certain instances, it was necessary to develop new correlations to supplement existing ones. Where new correlations have been developed, the complete data set and regression analysis results are presented to provide a measure of the validity of the relationship. The regression equation is presented first, normally using an assumed intercept of zero for simplicity. The number of data points in the correlation is denoted by n, and the standard deviation (S.D.) is given to allow assessment of the dispersion around the regression line. Also given is the coefficient of determination, r^2, which is the ratio of the explained variation to the total variation. For $r^2 = 1$, a perfect correlation exists; for $r^2 = 0$, no correlation exists; and for $r^2 = 0.75$, 75 percent of the observed variation in y may be attributed to x. In almost all cases presented, the value of r^2 for a zero intercept was only 1 or 2 percent less than the r^2 for a regression line with an intercept. The sample correlation coefficient, r, is the statistic for testing the significance of a simple two-variable linear relationship (i.e., how well the data fit a linear relationship). For $r = 0$, no linearity exists while, for $r = \pm 1$, direct linearity exists.

By presenting the complete data set, the regression equation, and some pertinent statistics (n, S.D., r^2), the user will be able to assess the quality of the relationship and use the results accordingly. This format also will allow direct incorporation of the results into evolving reliability-based design procedures. Moroney (4) states rather directly in Figure 1-2 the importance of presenting the

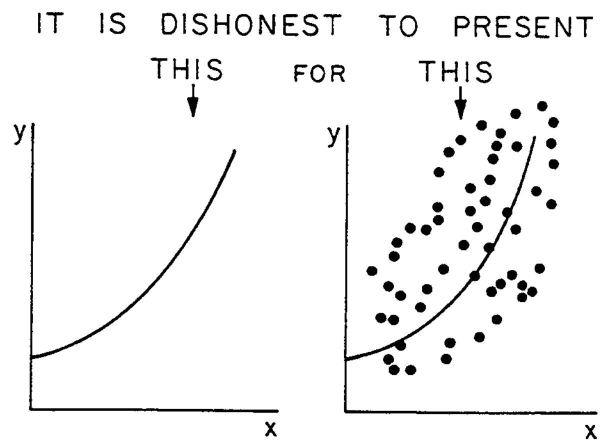

Figure 1-2. Importance of Proper Data Presentation

Source: Moroney (4), p. 29.

data properly.

Since this manual is directed toward the practicing engineer, its focus has been limited to the more common tests available on a commercial basis and to those tests that are seeing increased use in practice. Included are the common laboratory index and performance tests and the field standard penetration test (SPT), cone penetration test (CPT), pressuremeter test (PMT), and vane shear test (VST). The newer tests included are the dilatometer test (DMT), piezocone or cone penetration test with pore water stress measurement (CPTU), and the self-boring pressuremeter test (SBPMT). Intentionally not included are the wide variety of simple hand devices which are intended primarily for field inspection purposes, such as the pocket penetrometer, torvane, geostick, dynamic cone, etc. These are not design or performance devices and should not be used as such. Also not included are scaled tests such as the plate load test or centrifuge test, which may be used to model full-scale foundation performance on a smaller scale.

Section 2 addresses basic soil characterization to define the soil material, while Section 3 focuses on evaluating the in-situ soil stresses. The evaluation of soil strength is covered in Section 4, while Sections 5 and 6 address elastic and time-dependent soil deformability, respectively. Section 7 covers soil permeability, while Section 8 briefly addresses the special topic of liquefaction resistance.

Appendices A through F provide information on the various in-situ tests used in the correlations, primarily for those readers who are not familiar with the tests.

This information was extracted largely from EPRI Reports EL-2870 (5) and EL-5507, Vol. 2 (6). These reports should be consulted for further details on the tests. Appendix G gives a brief summary of the Critical State Soil Mechanics concept, and Appendix H summarizes available CPT calibration chamber data used to develop a number of correlations in this manual.

Within this manual, an effort has been made to present the relationships in dimensionless form for ease in scaling to whatever units are desired by the user. Therefore, stresses have been made dimensionless by the atmospheric pressure or stress, p_a, which is equal to 1.058 tsf, 14.7 psi, 101.3 kN/m^2, etc. A simple, approximate conversion for preliminary work is that 1 atm $\approx$ 1 tsf $\approx$ 1 kg/cm^2 $\approx$ 100 kN/m^2. These approximate conversions have been used liberally with previously published work where the 1 or 2 percent variation would not be significant. All unit weights have been made dimensionless by the unit weight of fresh water, γ_w, which is equal to 62.4 pcf or 9.80 kN/m^3. Where lengths are included, dual units are given. A detailed unit conversions guide is given as Appendix I.

Lastly, Appendix J presents summary tables to assist the user in locating specific recommended correlations in this manual. These tables are not intended to be a substitute for the text, which puts the correlations in proper perspective. Instead, they are intended to be a quick reference guide for the experienced user.

REFERENCES

1. Wroth, C. P. and Houlsby, G. T., "Soil Mechanics - Property Characterization and Analysis Procedures", Proceedings, 11th International Conference on Soil Mechanics and Foundation Engineering, Vol. 1, San Francisco, 1985, pp. 1-55.

2. Ladd, C. C., Foott, R., Ishihara, K., Schlosser, F., and Poulos, H. G., "Stress-Deformation and Strength Characteristics", Proceedings, 9th International Conference on Soil Mechanics and Foundation Engineering, Vol. 2, Tokyo, 1977, pp. 421-494.

3. Jamiolkowski, M., Ladd, C. C., Germaine, J. T., and Lancellotta, R., "New Developments in Field and Laboratory Testing of Soils", Proceedings, 11th International Conference on Soil Mechanics and Foundation Engineering, Vol. 1, San Francisco, 1985, pp. 57-154.

4. Moroney, M. J., Facts From Figures, 3rd Ed., Penguin Books, Baltimore, 1956, 472 p.

5. Kulhawy, F. H., Trautmann, C. H., Beech, J. F., O'Rourke, T. D., McGuire, W., Wood, W. A., and Capano, C., "Transmission Line Structure Foundations for Uplift-Compression Loading", Report El-2870, Electric Power Research Institute, Palo Alto, 1983, 412 p.

6. Orchant, C. J., Kulhawy, F. H., and Trautmann, C. H., "Reliability-Based Foundation Design for Transmission Line Structures: Critical Evaluation of In-Situ Test Methods", Report EL-5507, Vol. 2, Electric Power Research Institute, Palo Alto, 1988, 214 p.

Section 2

BASIC SOIL CHARACTERIZATION

One of the first steps in any geotechnical design problem is to develop an understanding and knowledge of the soil materials at the site. Soil is a complex engineering material, and therefore it is important to know its basic characteristics as thoroughly as possible before attempting to define its engineering design properties. In this section, procedures are presented to describe and classify soil, to estimate its unit weight, and to estimate its physical characteristics. General descriptions, simple index tests, and correlations with in-situ test results are used where available.

SIMPLE DESCRIPTIONS

Simple descriptions for soil are useful because they help to establish the nature and/or physical characteristics of the soil material in the laboratory or in-situ. In terms of basic behavior, soils often are described simply as either cohesionless or cohesive. Cohesionless soils include coarser-grained granular materials, such as sands, gravels, and non-plastic silts. Cohesive soils include finer-grained plastic materials, such as clays and plastic silts.

Particle Size and Distribution

The particle size and distribution are necessary to describe the basic nature of soil. For coarse-grained soils, the size and distribution are determined using nested sieves, as described in ASTM D422 (1) and D2217 (2). Identification by particle size is given in Table 2-1. For fine-grained soils, the size and distribution are determined by a hydrometer test (1). Clay-size particles generally are defined as those being less than 2 microns (0.002 mm).

From the particle size analyses, several parameters are defined which are of use in later sections of this manual. These parameters are: D_{60} = particle size at which 60 percent of the sample is finer (by weight), D_{50} = mean grain size = particle size at which 50 percent of the sample is finer, D_{10} = effective grain size = particle size at which 10 percent of the sample is finer, and $C_u = D_{60}/D_{10}$ = uniformity coefficient. Soils with a high value of C_u are well-graded and contain a wide

Table 2-1

SOIL PARTICLE SIZE IDENTIFICATION

Broad Group	Name	Size Limits: ASTM Sieve Number	Size Limits: mm
Coarse-Grained	Boulder	> 12 in	> 305
	Cobble	12 in to 3 in	305 to 76
	Coarse gravel	3 in to 3/4 in	76 to 19
	Fine gravel	3/4 in to No. 4 sieve	19 to 4.75
	Coarse sand	No. 4 to No. 10 sieve	4.75 to 2.0
	Medium sand	No. 10 to No. 40 sieve	2.0 to 0.42
	Fine sand	No. 40 to No. 200 sieve	0.42 to 0.075
Fine-Grained	Silt and/or clay	< No. 200 sieve	< 0.075

Note: Particles finer than fine sand can not be discerned with the naked eye at a distance of 8 in. (203 mm).

range of particle sizes, while soils with a low value of C_u are uniformly graded and contain particles of similar sizes.

Index Parameters for Cohesive Soils

The relative consistency of cohesive soils is described by several useful index parameters which are expressed as water contents at particular soil states. These consistency states are known as Atterberg limits, determined by ASTM D4318 (3). The most common index parameters are: w_n = in-situ natural water content, w_L = liquid limit, w_P = plastic limit, PI = $w_L - w_P$ = plasticity index, and LI = $(w_n - w_P)/(w_L - w_P)$ = liquidity index. Soils with a liquid limit (w_L) greater than 50 percent are termed "highly plastic". A plasticity index (PI) greater than 25 to 30 may mean troublesome soils with low strength, high compressibility, high shrink-swell potential, etc. The liquidity index (LI) is an excellent indicator of geologic history and relative soil properties, as shown schematically in Figure 2-1.

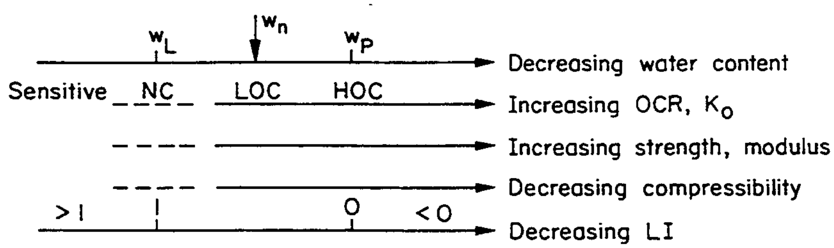

NC = normally consolidated

LOC = lightly overconsolidated

HOC = heavily overconsolidated

OCR = overconsolidation ratio = $\bar{\sigma}_p/\bar{\sigma}_{vo}$

$\bar{\sigma}_p$ = maximum vertical effective stress in soil during its geologic history

$\bar{\sigma}_{vo}$ = vertical effective stress in-situ

$\bar{\sigma}_{ho}$ = horizontal effective stress in-situ

K_o = in-situ coefficient of horizontal soil stress = $\bar{\sigma}_{ho}/\bar{\sigma}_{vo}$

Figure 2-1. Liquidity Index Variations

Index Parameters for Cohesionless Soils

Cohesionless soils also can be represented by simple index parameters, generally expressed in terms of either "unit weight" or "density". Unit weight (γ) is defined as the soil weight per unit volume and is given by the units kN/m^3 or $lb\text{-}force/ft^3$. Density (ρ) is defined as the soil mass per unit volume, with units of kg/m^3 or $lb\text{-}mass/ft^3$. Although density actually is the preferred term in modern SI usage, conventional engineering practice has favored unit weight, which will be used in this manual. The ratio (γ/ρ) is the gravitational acceleration (g), which is equal to 9.807 m/sec^2 or 32.17 ft/sec^2.

For cohesionless soils, the relative density (D_r) expresses the degree of compactness with respect to both the loosest and densest states achieved by standard laboratory procedures [ASTM D4253 (4) and D4254 (5)]. Most commonly, the relative density is expressed in terms of void ratio:

$$D_r = \frac{e_{max} - e}{e_{max} - e_{min}} \tag{2-1}$$

in which e = in-situ void ratio, e_{max} = maximum void ratio (loosest), and e_{min} = minimum void ratio (densest). Alternatively, D_r can be expressed as:

$$D_r = \frac{\rho_{dmax}(\rho_d - \rho_{dmin})}{\rho_d(\rho_{dmax} - \rho_{dmin})} \quad (2\text{-}2)$$

in which ρ_d = in-situ dry density, ρ_{dmax} = maximum dry density, and ρ_{dmin} = minimum dry density. In this equation, unit weight can be used alternatively in place of density. In some instances, the degree of relative compactness is described in terms of the density index (I_D):

$$I_D = \frac{\rho_d - \rho_{dmin}}{\rho_{dmax} - \rho_{dmin}} \quad (2\text{-}3)$$

Relative density is a useful parameter for describing the relative behavior of cohesionless soils. Standard terminology is given in Table 2-2. Column (a) tends to be used more commonly in the U.S. Increasing D_r generally means increasing strength and decreasing compressibility. If D_r is negative, a collapsible soil structure may be present, such as can occur with honeycombed soils and very loose cemented or calcareous sands with $e > e_{max}$. The applicability of D_r is limited to cohesionless soils having less than 15 percent fines. In practice, it has been misapplied occasionally to soils having greater than 15 percent fines, with questionable results. Since it is very difficult to obtain truly undisturbed samples of clean sands, the direct measurement of D_r also is difficult. In addition, the

Table 2-2

RELATIVE DENSITY OF COHESIONLESS SOILS

Relative Density	D_r (%)	
	(a)	(b)
Very loose	0 to 15	0 to 20
Loose	15 to 35	20 to 40
Medium	35 to 65	40 to 60
Dense	65 to 85	60 to 80
Very dense	85 to 100	80 to 100

a - Source: Lambe and Whitman (6), p. 31.
b - Source: Meyerhof (7), p. 17.

in-situ void ratio (e) is compared to e_{max} and e_{min}, both of which are subject to considerable error in their determination in the laboratory. For these reasons, D_r should be considered only as an index parameter.

For a variety of natural and artificially-prepared mixtures of sands, e_{max} and e_{min} depend primarily on the particle roundness (R) and the uniformity coefficient (C_u). The roundness is defined as the ratio of the minimum radius of the particle edges to the inscribed radius of the entire particle. Although R is difficult to measure, it can be estimated from the apparent angularity of the grains, as shown in Figure 2-2. Combined with a particle size analysis, the e_{max} and e_{min} values can be estimated from Figure 2-3. This figure is valid for clean sands with normal to moderately-skewed particle size distributions.

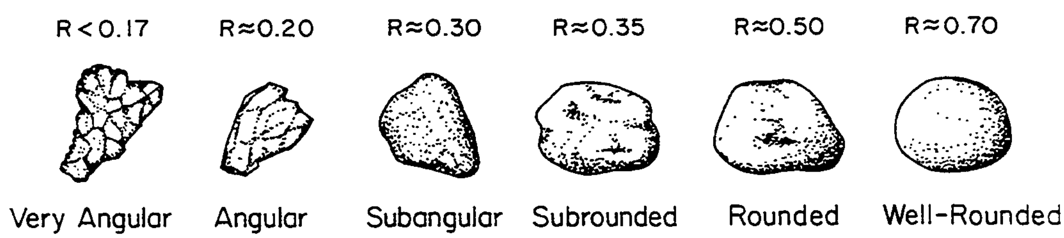

Figure 2-2. Particle Roundness Definitions

Source: Adapted from Youd (8).

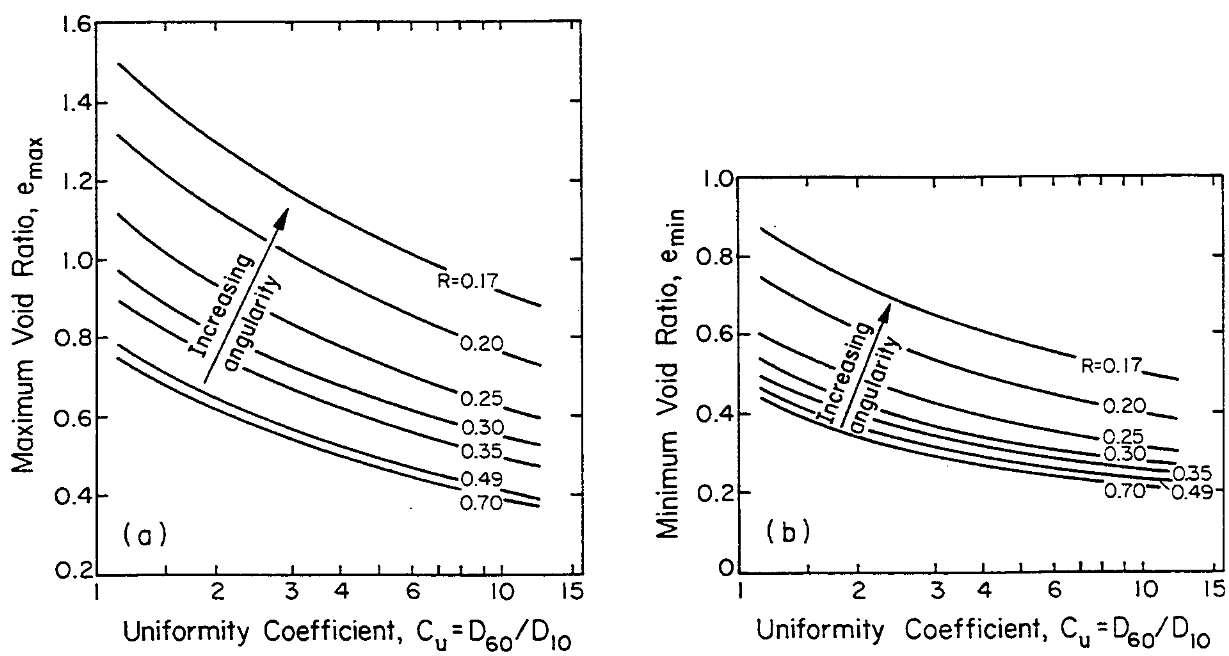

Figure 2-3. Generalized Curves for Estimating e_{max} and e_{min}

Source: Youd (8), p. 108.

Characterization by Simple Field Tests

For preliminary reconnaissance studies and quality control during construction, simple manual field tests are useful in describing the characteristics of in-place soils. For cohesive soils, Table 2-3 provides guidelines for approximate plasticity characteristics. Similarly, manual tests can provide a crude index of the unconfined compressive strength (q_u) or undrained shear strength (s_u) of cohesive soils, as indicated in Table 2-4. A pocket penetrometer (for q_u) or torvane (for s_u) also can be used to provide these approximate values, even though these measurements are crude.

Simple field tests similarly are available for evaluating the characteristics of cohesionless soils. Table 2-5 provides rough guidelines for this purpose by use of a reinforcing bar.

Color and Odor

Color also may be a useful indicator of some soil characteristics. For example, yellow and red hues often represent iron oxides in deeply weathered soil profiles. Dark greens and browns often indicate organic soils, particularly when coupled with the distinctive odor of decaying organic matter. Odor sometimes is an indicator of contaminants as well. Color also can assist in differentiating topsoil and the depth and extent of weathering. For these reasons, color and odor (if any) should always be considered an integral part of any soil description.

Table 2-3

APPROXIMATE PLASTICITY AND DRY STRENGTH OF SOIL BY SIMPLE TESTS

Plasticity	PI (%)	Dry Strength	Field Test on Air-Dried Sample
Nonplastic	0 to 3	Very low	Falls apart easily
Slightly plastic	3 to 15	Slight	Easily crushed with fingers
Medium plastic	15 to 30	Medium	Difficult to crush
Highly plastic	> 30	High	Impossible to crush with fingers

Source: Sowers (9), p. 83.

Table 2-4

APPROXIMATE COHESIVE SOIL STRENGTH BY SIMPLE TESTS

Strength	q_u (ksf)	q_u (kN/m^2)	Field Test
Very soft	0 to 1/2	0 to 25	Squeezes between fingers when fist is closed
Soft	1/2 to 1	25 to 50	Easily molded by fingers
Firm	1 to 2	50 to 100	Molded by strong pressure of fingers
Stiff	2 to 3	100 to 150	Dented by strong pressure of fingers
Very stiff	3 to 4	150 to 200	Dented only slightly by finger pressure
Hard	> 4	> 200	Dented only slightly by pencil point

Note: q_u = unconfined compressive strength = 2 s_u
s_u = undrained shear strength

Source: Sowers (9), p. 80.

Table 2-5

APPROXIMATE COHESIONLESS SOIL RELATIVE DENSITY BY SIMPLE TESTS

Density	D_r (%)	Field Test
Loose	0 to 50	Easily penetrated with 0.5 in. (12 mm) reinforcing rod pushed by hand
Firm	50 to 70	Easily penetrated with 0.5 in. (12 mm) reinforcing rod driven with 5 lb (2.3 kg) hammer
Dense	70 to 90	Penetrated a foot with 0.5 in. (12 mm) reinforcing rod driven with 5 lb (2.3 kg) hammer
Very dense	90 to 100	Penetrated only a few inches with 0.5 in. (12 mm) reinforcing rod driven with 5 lb (2.3 kg) hammer

Note: generally refers to shallow depths in uncemented quartz and feldspar sands

Source: Sowers (9), p. 81.

CLASSIFICATION

General Classification and Identification Systems

Classification systems are useful for grouping together soils of similar particle size and plasticity characteristics. By this grouping into pre-established categories, consistent terminology can be employed to represent a soil fitting within the bounds of a particular category. The most widely used of these systems is the Unified Soil Classification System [ASTM D2487 (10) and D2488 (11)], given in Table 2-6. To use this system properly, both particle size and Atterberg limits data are needed. With the particle size and Atterberg limits data, the soil is classified using the pre-established group symbols in Table 2-6. Plastic soils utilize the plasticity chart shown as well. Note that if any soils plot above the "U" line in the plasticity chart, the data should be questioned and verified. Further details are given in the ASTM Standards.

Other well-known special purpose classification systems have been developed by the U. S. Department of Agriculture (USDA) for agricultural purposes, the Federal Aviation Administration (FAA) for airport pavements, and the American Association of State Highway and Transportation Officials (AASHTO) for highway pavements. These systems normally are not used in foundation engineering.

As an alternative, Burmister (12, 13) developed a soil identification system for both field and laboratory use. As compared with the classification systems which use pre-established soil group categories, Burmister's approach uses rapid and simple visual-manual procedures to approximate the particle size and gradation and overall plasticity index. Essential features of the resulting soil identification are given in Table 2-7. With this system, approximate percentages of the principal and minor components are estimated using the notation in Table 2-7a. Particle size and gradation terms are defined in Tables 2-7b and c. For the fines (percent < No. 200 sieve), the overall plasticity is estimated and then described using the notation in Table 2-7d. Example identifications also are given with this table. Once the straightforward visual-manual procedures are mastered, some 15 to 30 samples per hour can be identified in terms of their approximate particle size distribution and plasticity index.

Cone Penetration Test (CPT) Classifications

The CPT has been used widely for many years as a site investigation device. Although no soil sample is recovered, the cone tip resistance (q_c), cone side resistance (f_s), and friction ratio ($R_f = FR = f_s/q_c$) have been employed to

Table 2-6

UNIFIED SOIL CLASSIFICATION SYSTEM

Criteria for Assigning Group Symbols and Group Names Using Laboratory Tests[A]				Soil Classification: Group Symbol	Soil Classification: Group Name[B]
Coarse-Grained Soils More than 50 % retained on No. 200 sieve	Gravels More than 50 % of coarse fraction retained on No. 4 sieve	Clean Gravels Less than 5 % fines[C]	$Cu \geq 4$ and $1 \leq Cc \leq 3$[E]	GW	Well-graded gravel[F]
			$Cu < 4$ and/or $1 > Cc > 3$[E]	GP	Poorly graded gravel[F]
		Gravels with Fines More than 12 % fines[C]	Fines classify as ML or MH	GM	Silty gravel[F,G,H]
			Fines classify as CL or CH	GC	Clayey gravel[F,G,H]
	Sands 50 % or more of coarse fraction passes No. 4 sieve	Clean Sands Less than 5 % fines[D]	$Cu \geq 6$ and $1 \leq Cc \leq 3$[E]	SW	Well-graded sand
			$Cu < 6$ and/or $1 > Cc > 3$[E]	SP	Poorly graded sand[I]
		Sands with Fines More than 12 % fines[D]	Fines classify as ML or MH	SM	Silty sand[G,H,I]
			Fines classify as CL or CH	SC	Clayey sand[G,H,I]
Fine-Grained Soils 50 % or more passes the No. 200 sieve	Silts and Clays Liquid limit less than 50	inorganic	PI > 7 and plots on or above "A" line[J]	CL	Lean clay[K,L,M]
			PI < 4 or plots below "A" line[J]	ML	Silt[K,L,M]
		organic	$\frac{\text{Liquid limit – oven dried}}{\text{Liquid limit – not dried}} < 0.75$	OL	Organic clay[K,L,M,N] / Organic silt[K,L,M,O]
	Silts and Clays Liquid limit 50 or more	inorganic	PI plots on or above "A" line	CH	Fat clay[K,L,M]
			PI plots below "A" line	MH	Elastic silt[K,L,M]
		organic	$\frac{\text{Liquid limit – oven dried}}{\text{Liquid limit – not dried}} < 0.75$	OH	Organic clay[K,L,M,P] / Organic silt[K,L,M,Q]
Highly organic soils	Primarily organic matter, dark in color, and organic odor			PT	Peat

[A] Based on the material passing the 3-in. (75-mm) sieve.

[B] If field sample contained cobbles or boulders, or both, add "with cobbles or boulders, or both" to group name.

[C] Gravels with 5 to 12 % fines require dual symbols:
GW-GM well-graded gravel with silt
GW-GC well-graded gravel with clay
GP-GM poorly graded gravel with silt
GP-GC poorly graded gravel with clay

[D] Sands with 5 to 12 % fines require dual symbols:
SW-SM well-graded sand with silt
SW-SC well-graded sand with clay
SP-SM poorly graded sand with silt
SP-SC poorly graded sand with clay

[E] $Cu = D_{60}/D_{10}$ $\quad Cc = \frac{(D_{30})^2}{D_{10} \times D_{60}}$

[F] If soil contains ≥ 15 % sand, add "with sand" to group name.

[G] If fines classify as CL-ML, use dual symbol GC-GM, or SC-SM.

[H] If fines are organic, add "with organic fines" to group name.

[I] If soil contains ≥ 15 % gravel, add "with gravel" to group name.

[J] If Atterberg limits plot in hatched area, soil is a CL-ML, silty clay.

[K] If soil contains 15 to 29 % plus No. 200, add "with sand" or "with gravel," whichever is predominant.

[L] If soil contains ≥ 30 % plus No. 200, predominantly sand, add "sandy" to group name.

[M] If soil contains ≥ 30 % plus No. 200, predominantly gravel, add "gravelly" to group name.

[N] PI ≥ 4 and plots on or above "A" line.

[O] PI < 4 or plots below "A" line.

[P] PI plots on or above "A" line.

[Q] PI plots below "A" line.

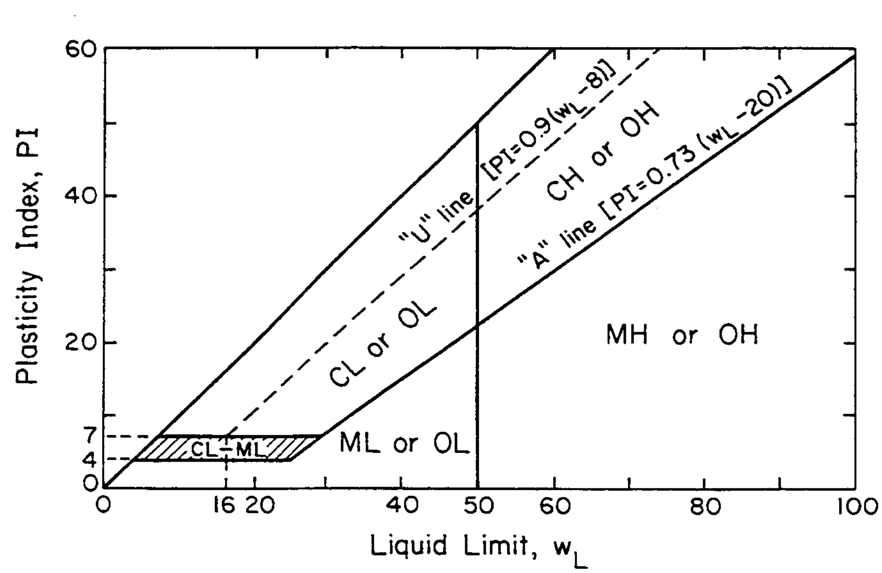

Source: American Society for Testing and Materials (10), pp. 289, 292.

Table 2-7

BURMISTER SOIL IDENTIFICATION SYSTEM

(a) Terms Describing Composition of Cohesionless Soils

Component	Identification		Proportion		
	Written	Symbol	Written	Symbol	% by Weight
Principal	GRAVEL	G	-	-	≥ 50
	SAND	S	-	-	≥ 50
	SILT	$	-	-	≥ 50
Minor	Gravel	G	and	a	35 to 50
	Sand	S	some	s	20 to 35
	Silt	$	little	l	10 to 20
			trace	t	1 to 10

(b) Terms Describing Gradation of Cohesionless Soils

Designation		
Written	Symbol	Defining Proportions
coarse medium to fine	cmf	all fractions > 10%
coarse to medium	cm	< 10% fine
medium to fine	mf	< 10% coarse
coarse	c	< 10% medium and fine
medium	m	< 10% coarse and fine
fine	f	< 10% coarse and medium

NOTE: For proportions in (a) and (b), use + for upper limit and - for lower limit.

Table 2-7 (cont'd)

BURMISTER SOIL IDENTIFICATION SYSTEM

(c) Particle Size Definitions

Soil	Fraction	Sieve Number and Size	
Gravel	coarse	3 in to 1 in	(76 mm to 25 mm)
	medium	1 in to 3/8 in	(25 mm to 9.5 mm)
	fine	3/8 in to No. 10	(9.5 mm to 2.0 mm)
Sand	coarse	No. 10 to No. 30	(2.0 mm to 0.6 mm)
	medium	No. 30 to No. 60	(0.6 mm to 0.25 mm)
	fine	No. 60 to No. 200	(0.25 mm to 0.075 mm)
Silt	-	< No. 200	(< 0.075 mm)

(d) Terms Describing Cohesive Soils Based on Overall Plasticity

Overall Plasticity			Principal Component		Minor Component	
Written	Symbol	Plasticity Index	Written	Symbol	Written	Symbol
Non-plastic	-	0	SILT	S̸	Silt	S̸
Slight	Sl	1 to 5	Clayey SILT	CyS̸	Clayey Silt	CyS̸
Low	L	5 to 10	SILT & CLAY	S̸ & C	Silt & Clay	S̸ & C
Medium	M	10 to 20	CLAY & SILT	C & S̸	Clay & Silt	C & S̸
High	H	20 to 40	Silty CLAY	S̸yC	Silty Clay	S̸yC
Very High	VH	> 40	CLAY	C	Clay	C

EXAMPLES:

Full - coarse^{+} medium to fine^{-} SAND, some^{-} medium fine Gravel, trace^{+} Silt

Abbreviated - c^{+}mf^{-} SAND, s^{-}·mf Gravel, t^{+}·Silt

Shorthand - c^{+}mf^{-} S, s^{-}·mfG, t^{+}·S̸

Full - CLAY & SILT, little^{+} coarse^{-} medium to fine^{+} Sand, Medium Plasticity

Abbreviated - CLAY & SILT, l^{+}·c^{-}mf^{+} S, M·Pl

Shorthand - C & S̸, l^{+}·c^{-}mf^{+}S, M·Pl

NOTE: Principal component (> 50%) always listed first. If no principal component, list sand first.

Source: Burmister (12, 13).

classify the soil in-situ. Since soil classification by the CPT is an empirical approach, it has been an evolutionary process which has required periodic updates as new and larger data bases have been collected and evaluated. Two representative examples of the earlier interpretations of CPT data are shown in Figure 2-4. Further research led to empirical classification charts for the mechanical Begemann friction-cone, as shown in Figure 2-5. Similar developments led to classification charts for electric friction cones, as shown in Figure 2-6 in original form and in Figure 2-7 in simplified form.

Recently, it has been realized that the correlations should be made dimensionless by appropriate scaling factors (Wroth, 18). Numerous field studies have shown that the cone side resistance increases proportionally with confining stress. For the tip resistance, the proportionality varies with soil type (e.g., Jamiolkowski, et al., 19). Therefore, at the present time, the most rational approach to soil classification by the CPT is by using dimensionless parameters, as given in Figure 2-8.

Soil classification using Figure 2-8 requires an iterative approach, since q_c is divided by a power function of the vertical effective stress, $(\bar{\sigma}_{vo})^n$, and the exponent (n) depends upon the soil type. This exponent (n) increases from about 0.5 for sands to approximately 1 for clays. An initial estimate of soil type may be obtained from Figure 2-7. A first estimate of n for the iterative solution then

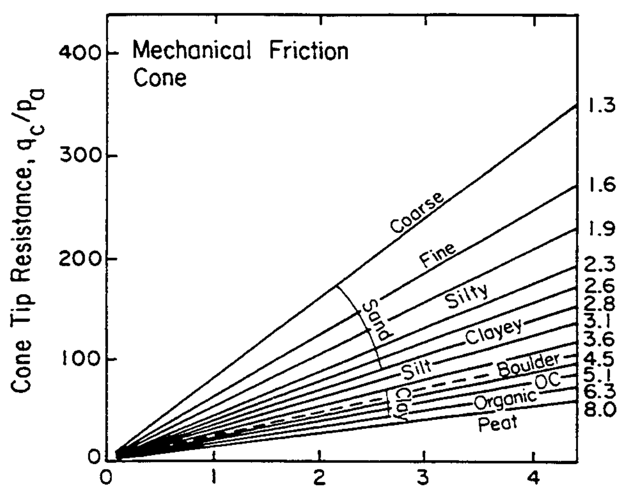

a. Mechanical Friction Cone

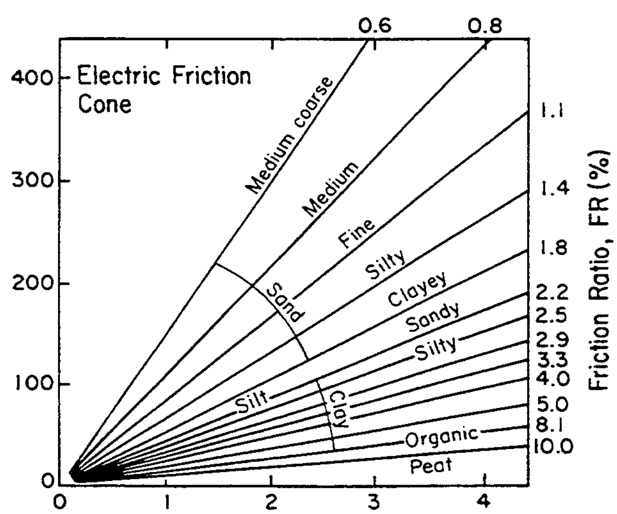

b. Electric Friction Cone

Figure 2-4. Early Soil Classification by CPT

Source: Laboratorium voor Grondmechanica (14), p. 29.

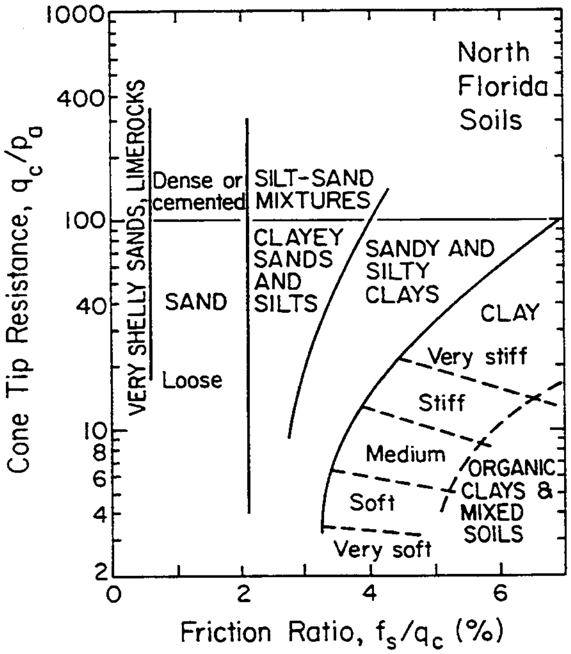

Figure 2-5. Soil Classification by Mechanical Friction CPT

Source: Schmertmann (<u>15</u>), p. 7.

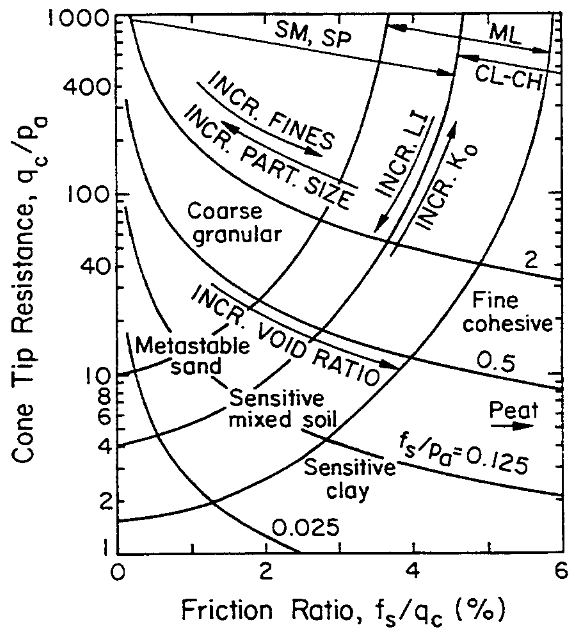

Figure 2-6. Soil Classification by Fugro Electric Friction CPT

Source: Douglas and Olsen (<u>16</u>), p. 222.

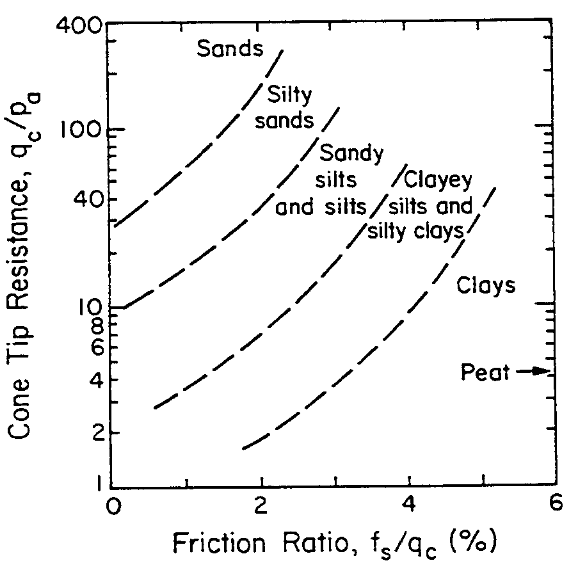

Figure 2-7. Simplified Soil Classification by Fugro Electric Friction CPT

Source: Robertson and Campanella (<u>17</u>), p. 721.

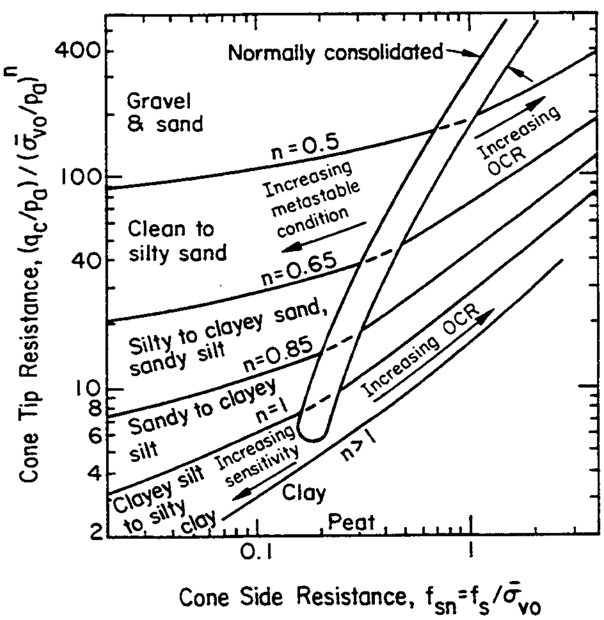

Figure 2-8. Most Recent Soil Classification by Fugro Electric Friction CPT

Source: Olsen and Farr (<u>20</u>), p. 858.

can be made from Figure 2-8.

As described in Appendix B, different results commonly are obtained using different cones. Therefore, adjustments to the following figures may be warranted as a function of cone type and shape, as given in Appendix B.

Piezocone Penetration Test (CPTU) Classifications

With the recent development of the piezocone, which measures the total penetration pore water stress (u_m) in addition to q_c and f_s, the ability of the cone penetrometer to delineate soil stratigraphy and provide an accurate classification of soil type is enhanced greatly. In loose, contractive sands, the value of u_m closely follows the hydrostatic stress (u_o). In dense, dilatant sands, u_m may be less than u_o. In clays, cone penetration generates excess pore water stresses which are recorded by the pore water transducer. Two of the recent soil classification systems based on CPTU measurements are given in Figures 2-9 and 2-10. Other classification charts are given by Robertson, et al. (23). In the first of these figures, the parameter B_q is used, which is defined as:

$$B_q = \frac{u_m - u_o}{q_T - \sigma_{vo}} \qquad (2\text{-}4)$$

in which u_m = measured total pore water stress (usually behind the tip), u_o = hydrostatic pore water stress, q_T = corrected cone tip resistance, and σ_{vo} = total overburden stress.

One important finding which has evolved from the development of piezocones is that the cone tip and side resistances must be corrected for pore water stress effects acting on unequal areas of the cone geometry. The corrected tip resistance is given by:

$$q_T = q_c + (1 - a)u_{bt} \qquad (2\text{-}5)$$

in which q_c = measured cone tip resistance, a = net area ratio for the particular cone (See Figure 2-11.), and u_{bt} = pore water stress behind the tip. Similarly, the correction for cone side resistance is given by:

$$f_t = f_s + (u_s A_{s2} - u_{bt} A_{s1})/A_s \qquad (2\text{-}6)$$

in which u_s = pore water stress behind the sleeve, A_s = surface area of the sleeve,

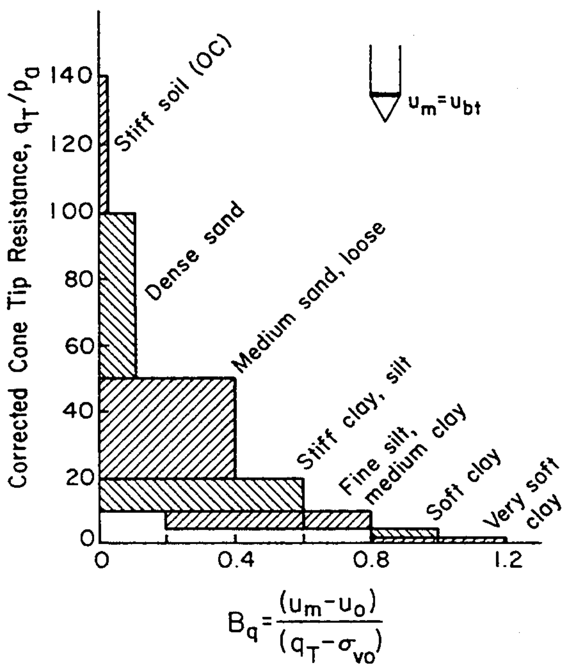

Figure 2-9. Soil Classification Based on q_T and B_q

Source: Senneset and Janbu (21), p. 48.

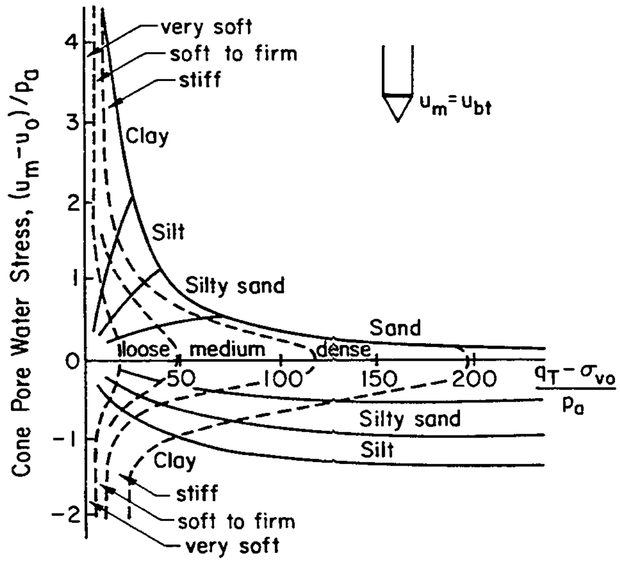

Figure 2-10. Soil Classification Based on CPTU Data

Source: Jones and Rust (22), p. 612.

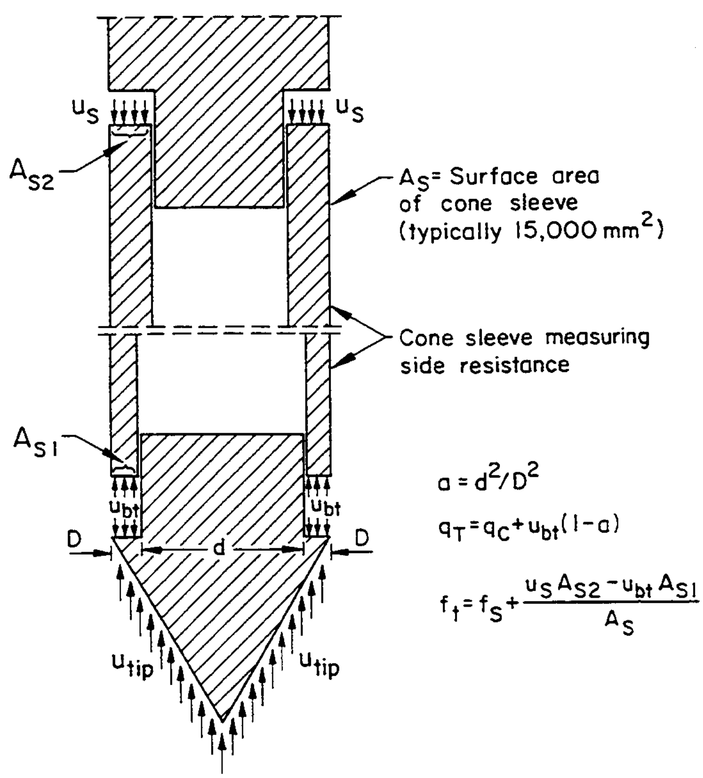

Figure 2-11. Unequal End Areas of Electric Friction Cone

f_s = measured cone side resistance, and A_{s1} and A_{s2} are the net internal areas of the sleeve, as given in Figure 2-11.

Dilatometer Test (DMT) Classifications

The flat dilatometer test (DMT) also is capable of providing an estimate of the soil type and consistency. The original development of the DMT (Marchetti, 24) included a classification based on the material index, I_D, defined as:

$$I_D = \frac{p_1 - p_o}{p_o - u_o} \qquad (2\text{-}7)$$

in which p_o = contact stress, p_1 = stress to expand membrane 1 mm into soil, and u_o = ambient equilibrium pore water stress (often assumed to be hydrostatic, although not necessarily so). A more recent interpretation is shown in Figure 2-12, which is based on I_D and the dilatometer modulus, E_D, defined as:

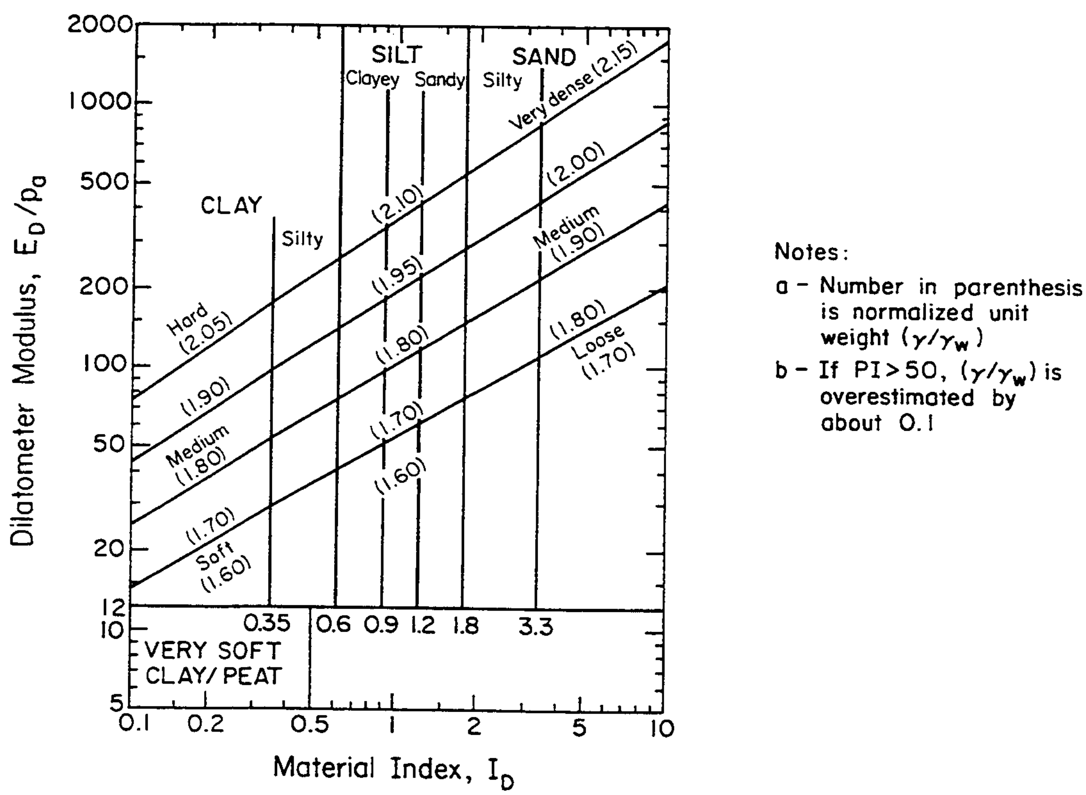

Figure 2-12. Determination of Soil Description and Unit Weight by DMT

Source: Schmertmann (25), p. 98.

$$E_D = 34.7(p_1 - p_o) \qquad (2\text{-}8)$$

This correlation also provides an estimate of the soil unit weight.

UNIT WEIGHT

As previously defined, the soil unit weight (γ) is determined as the weight of soil per unit volume. The relationship between dry (γ_d) and total (γ_{total}) unit weight is:

$$\gamma_{total} = (1 + w_n)\gamma_d \qquad (2\text{-}9)$$

in which w_n = natural water content (as a decimal). Table 2-8 presents typical soil unit weights.

RELATIVE DENSITY OF COHESIONLESS SOILS FROM IN-SITU TEST CORRELATIONS

The standard penetration test (SPT) N value and the CPT cone tip resistance (q_c) have been used extensively to estimate the relative density of cohesionless soils in-situ. Although they are used commonly in practice, different approaches have been adopted by different authors. Some of these differences in methodology result from improvements in the understanding of penetration tests and the relevant factors affecting the test values. Also, the estimation of the relative density using the SPT and CPT results is an evolutionary process during which newer and larger data bases are compiled to allow for more statistically significant trends to be established. Furthermore, some earlier studies were based on penetration tests conducted in one type of soil. Testing of more soils of differing geologic origins, stress histories, and mineralogies allows for refinements and adjustments to existing correlations.

Standard Penetration Test (SPT) Correlations

Early work on this subject simply correlated the SPT N value directly with relative density, as shown in Table 2-9. Later laboratory research demonstrated that the SPT N value also was influenced significantly by the overburden stress. Figure 2-13 shows these results, which were based on calibration chamber tests. For practical use in estimating D_r from N and $\bar{\sigma}_{vo}$, these results were presented in alternative forms such as that shown in Figure 2-14.

Additional research showed that these relationships are even more complex and dependent upon other factors, including vertical stress, stress history, and sand

Table 2-8

TYPICAL SOIL UNIT WEIGHTS

Soil Type	Approximate Particle Size (mm)			Uniformity Coefficient	Void Ratio		Normalized Unit Weight			
							Dry, γ_{dry}/γ_w		Saturated, γ_{sat}/γ_w	
	D_{max}	D_{min}	D_{10}	D_{60}/D_{10}	e_{max}	e_{min}	Min.	Max.	Min.	Max.
Uniform granular soil										
Equal spheres (theoretical)	-	-	-	1.0	0.92	0.35	-	-	-	-
Standard Ottawa sand	0.84	0.59	0.67	1.1	0.80	0.50	1.47	1.76	1.49	2.10
Clean, uniform sand	-	-	-	1.2 to 2.0	1.00	0.40	1.33	1.89	1.35	2.18
Uniform, inorganic silt	0.05	0.005	0.012	1.2 to 2.0	1.10	0.40	1.28	1.89	1.30	2.18
Well-graded granular soil										
Silty sand	2.0	0.005	0.02	5 to 10	0.90	0.30	1.39	2.04	1.41	2.28
Clean, fine to coarse sand	2.0	0.05	0.09	4 to 6	0.95	0.20	1.36	2.21	1.38	2.37
Micaceous sand	-	-	-	-	1.20	0.40	1.22	1.92	1.23	2.21
Silty sand and gravel	100	0.005	0.02	15 to 300	0.85	0.14	1.43	2.34	1.44	2.48
Silty or sandy clay	2.0	0.001	0.003	10 to 30	1.80	0.25	0.96	2.16	1.60	2.36
Gap-graded silty clay w. gravel or larger	250	0.001	-	-	1.00	0.20	1.35	2.24	1.84	2.42
Well-graded gravel, sand, silt, and clay	250	0.001	0.002	25 to 1000	0.70	0.13	1.60	2.37	2.00	2.50
Clay (30 to 50% < 2μ size)	0.05	0.5μ	0.001	-	2.40	0.50	0.80	1.79	1.51	2.13
Colloidal clay (over 50% < 2μ size)	0.01	10Å	-	-	12.00	0.60	0.21	1.70	1.14	2.05
Organic silt	-	-	-	-	3.00	0.55	0.64	1.76	1.39	2.10
Organic clay (30 to 50% < 2μ size)	-	-	-	-	4.40	0.70	0.48	1.60	1.30	2.00

Note: γ_w = 62.4 lb/ft^3 = 1 gm/cm^3 = 0.983 t/m^3 = 9.80 kN/m^3 (at STP conditions).

Source: Hough (26), pp. 34, 35.

Table 2-9

RELATIVE DENSITY OF SAND VERSUS N

N Value (blows/ft or 305 mm)	Relative Density	D_r (%)
0 to 4	very loose	0 to 15
4 to 10	loose	15 to 35
10 to 30	medium	35 to 65
30 to 50	dense	65 to 85
> 50	very dense	85 to 100

Source: Terzaghi and Peck (27), p. 341 and Lambe and Whitman (6), p. 31.

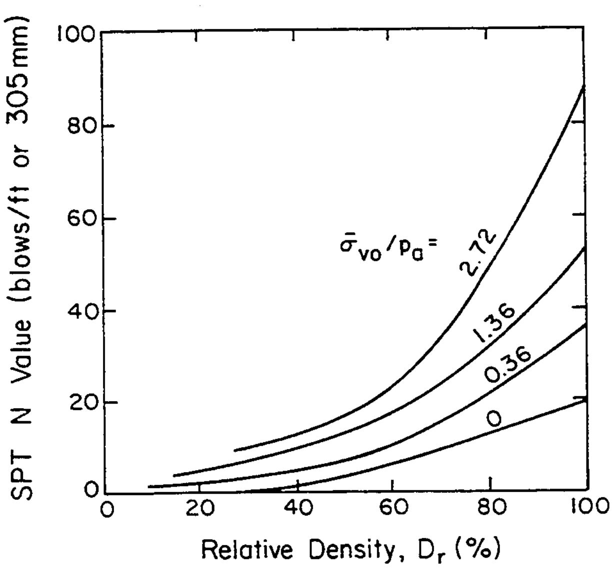

Figure 2-13. Effect of Overburden Stress and D_r on SPT N Value

Source: Gibbs and Holtz (28), p. 37.

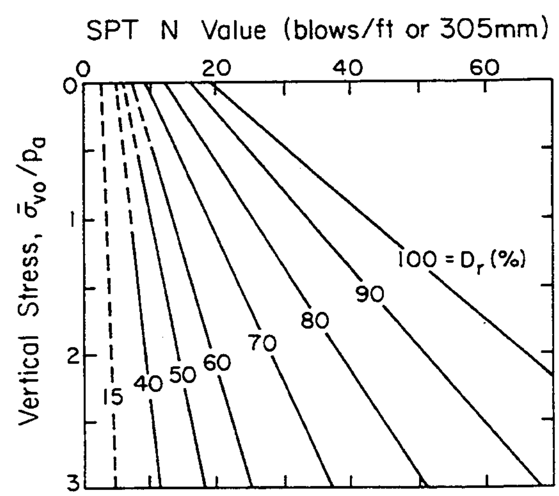

Figure 2-14. Relative Density-N-Stress Relationship

Source: Holtz and Gibbs (29), p. 441.

type (primarily compressibility influences), as a minimum. Figure 2-15 illustrates some of these complexities. The studies presented in Figure 2-15 led to a correlation for estimating D_r from SPT N values that includes the effect of overburden

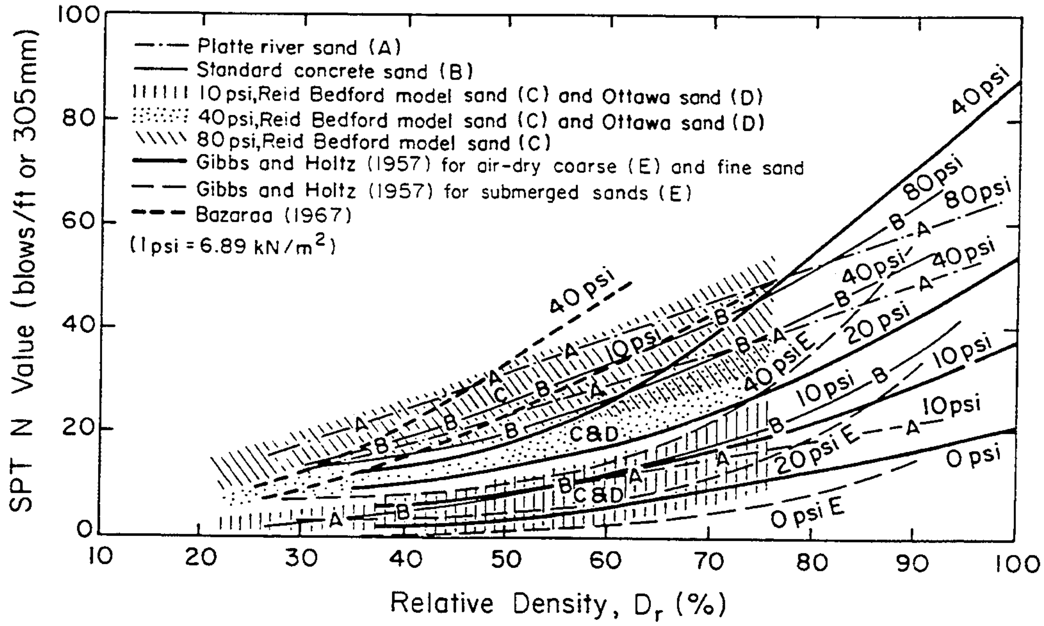

Figure 2-15. Relative Density-N-Stress Relationships for Several Sands

Source: Marcuson and Bieganousky (30), p. 1301.

stress ($\bar{\sigma}_{vo}$), particle size distribution (C_u), and stress history ($OCR = \bar{\sigma}_p/\bar{\sigma}_{vo}$), as given below:

$$D_r(\%) = 12.2 + 0.75[222N + 2311 - 711\ OCR - 779(\bar{\sigma}_{vo}/p_a) - 50\ C_u^2]^{0.5} \quad (2\text{-}10)$$

Regression analyses of the data gave $r^2 = 0.77$. The data all were unaged with OCR equal to 1 or 3.

An important factor affecting the SPT N value is the energy efficiency of the drop hammer onto the drill rods. The theoretical free-fall energy for the SPT is 140 lb (0.623 kN) times 30 in (0.76 m) or 4200 in-lb (0.475 kN-m). Typically, the average energy ratio (ER) is about 55 to 60 percent in the U.S.A., although this value can vary from 30 to 90 percent for particular drillers and SPT equipment in practice.

Skempton (31) reviewed SPT calibration data from Japan, China, the U.K., and the U.S.A. and suggested correction factors based on standard practice in these countries. Some of the variables affecting the energy efficiency include the type of hammer, age of the rope, borehole size, and use of liners in the split spoon sampler. For example, the donut hammer is less efficient than the safety hammer, as shown by the energy ratio examples in Figure 2-16. Correcting the hammers to a

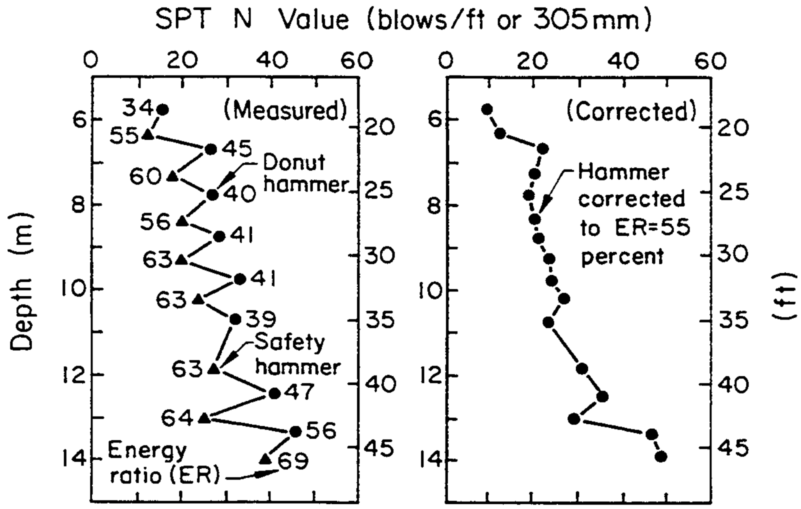

Figure 2-16. Donut and Safety Hammer Comparisons

Source: Robertson, et al. (32), p. 1454.

constant energy ratio eliminates the differences. The energy efficiency also depends upon the size of cathead and number of turns of the rope, as indicated in Figure 2-17. Standard U.S. practice is two turns of rope on a large cathead.

The SPT N value, corrected for field procedures, is given below:

$$N_{60} = C_{ER}\ C_B\ C_S\ C_R\ N \qquad (2\text{-}11)$$

in which N_{60} = N value corrected for field procedures to an average energy ratio of 60 percent, N = measured SPT N value, and C_{ER}, C_B, C_S, and C_R are correction factors for energy ratio, borehole diameter, sampling method, and rod length, respectively, as given in Table 2-10.

Since the SPT N value also varies with stress level, overburden stress correction factors are used to provide a consistent point of reference. This correction takes the form:

$$(N_1)_{60} = C_N\ N_{60} \qquad (2\text{-}12)$$

in which $(N_1)_{60}$ = N_{60} value corrected to a reference stress of one atmosphere and C_N = correction factor for overburden stress.

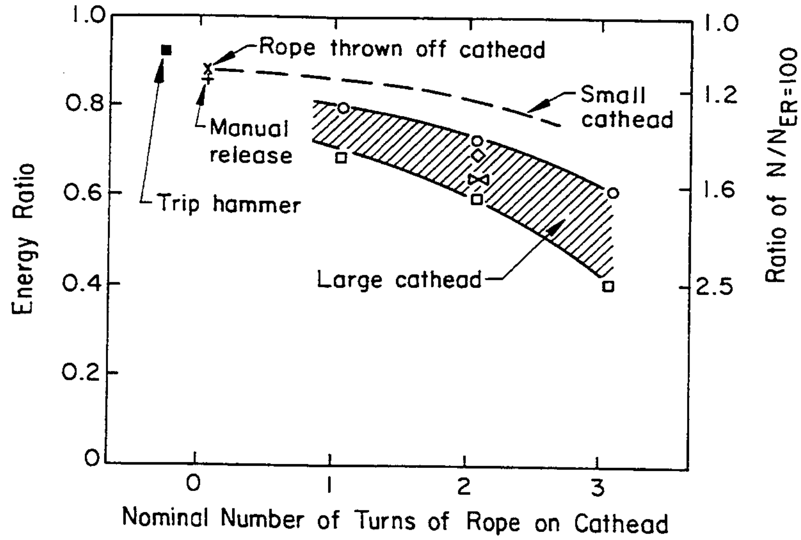

Figure 2-17. Energy Ratio Variations

Source: Modified after Skempton (31), p. 427.

Table 2-10

SPT CORRECTION FACTORS FOR FIELD PROCEDURES

Factor	Equipment Variables	Correction Term	Correction Value
Energy ratio	Safety hammer	C_{ER}	0.9
	Donut hammer		0.75
Borehole diameter	65 to 115 mm (2.5 to 4.5 in)	C_B	1.0
	150 mm (6 in)		1.05
	200 mm (8 in)		1.15
Sampling method	Standard sampler	C_S	1.0
	Sampler without liner		1.2
Rod length	> 10 m (> 30 ft)	C_R	1.0
	6 to 10 m (20 to 30 ft)		0.95
	4 to 6 m (13 to 20 ft)		0.85
	3 to 4 m (10 to 13 ft)		0.75

Source: Based on Skempton (31).

Perhaps the simplest expression for C_N is given below (Liao and Whitman, 33):

$$C_N = (p_a/\bar{\sigma}_{vo})^{0.5} \qquad (2\text{-}13)$$

A comparison of different C_N recommendations is given in Figure 2-18. Basically, all methods give similar corrections for $\bar{\sigma}_{vo} > 0.5\ p_a$ within the range of expected accuracy for the SPT. The correction factors proposed by Skempton are based largely on laboratory test data, while the others have been derived from field data.

Although Equation 2-13 is simple, high values of C_N develop at very low values of $\bar{\sigma}_{vo}$. Alternatively, Skempton (31) suggested the following for fine sands:

$$C_N = 2/(1 + \bar{\sigma}_{vo}/p_a) \qquad (2\text{-}14)$$

This equation gives a maximum C_N of 2 at the ground surface. Figure 2-19 shows that both equations are adequate for $\bar{\sigma}_{vo} > 0.5\ p_a$ and also appear applicable for use in overconsolidated sands.

Once the SPT N value has been corrected for field procedures and overburden effects to give $(N_1)_{60}$, it can be used to evaluate the relative density as a function of the soil characteristics. Figure 2-20 shows $(N_1)_{60}/D_r^2$ as a function of the soil particle size (D_{50}). The laboratory data in this figure were obtained from studies

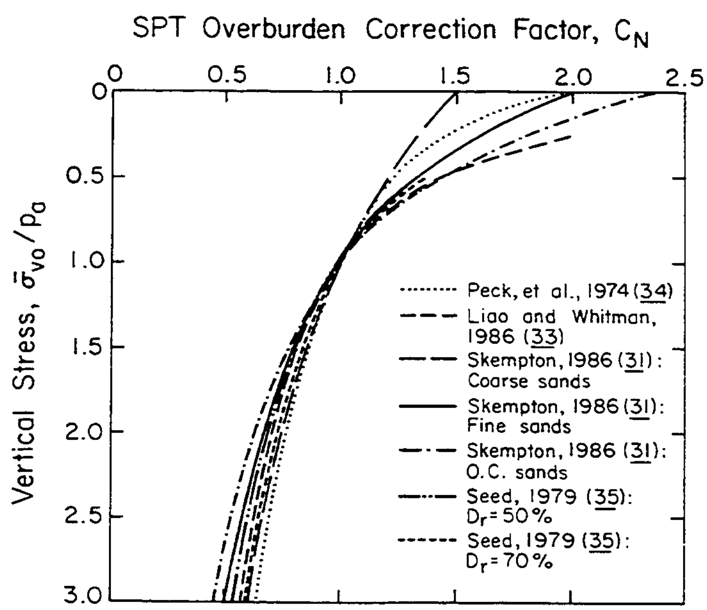

Figure 2-18. Comparison of SPT Overburden Corrections

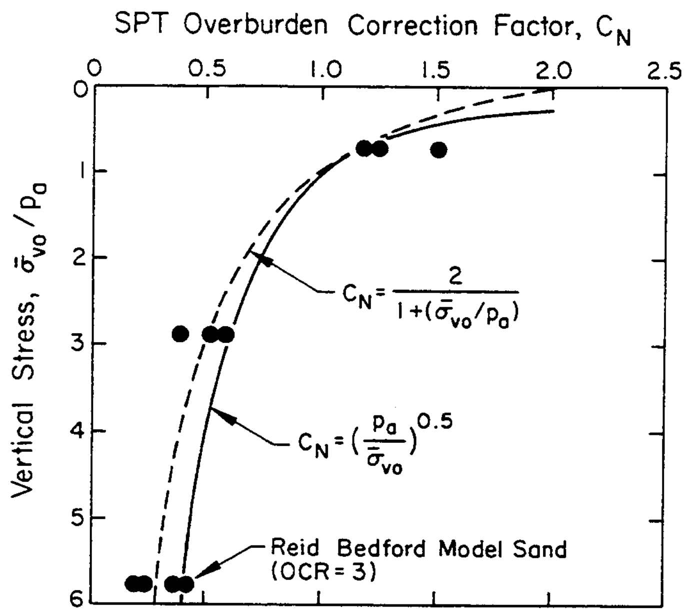

Figure 2-19. Comparison of Recommended C_N Factors and Available Data from OC Sands

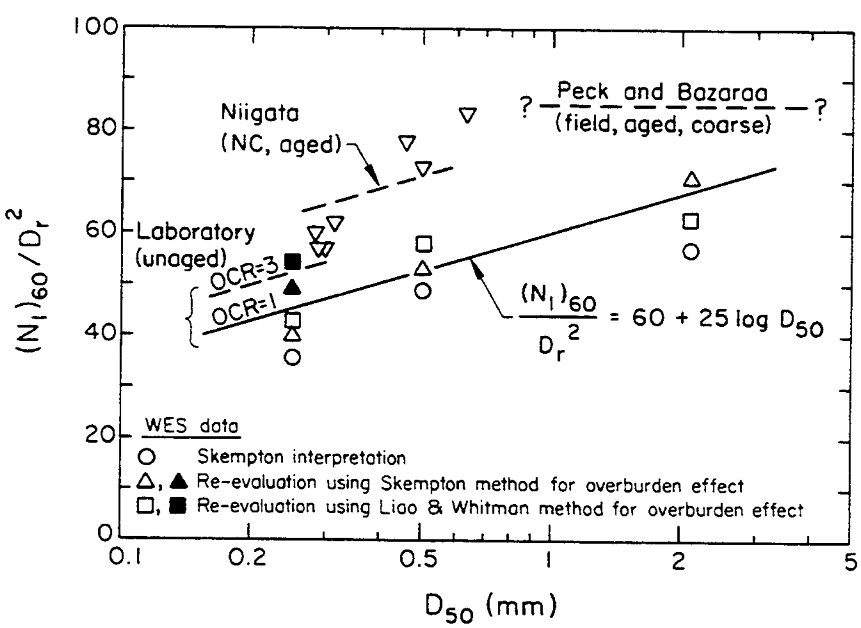

Figure 2-20. Particle Size Effect on Blow Count for Sands

at the Waterways Experiment Station (WES) on three sands (30, 36, 37). Most of the data were for unaged, normally consolidated (NC) sands (OCR = 1), although a small series of tests was conducted on overconsolidated sands with OCR = 3. Skempton's interpretation (31) of these data is shown, but it is believed that the averaged curves and smoothed data he used led to an underestimation of $(N_1)_{60}/D_r^2$. Re-evaluation of the original data (36, 37) leads to the higher values shown, using either Skempton's linearized overburden effect (31) or Liao and Whitman's (33) nonlinear overburden effect. These results can be approximated as follows:

$$(N_1)_{60}/D_r^2 = 60 + 25 \log D_{50} \tag{2-15}$$

which is applicable for NC, unaged sands. The OC data give higher values than Equation 2-15, and aged sands also give higher values. The data from Niigata, Japan were tabulated by Skempton (31), but they were re-evaluated individually. The Peck and Bazaraa (38) curve represents coarse sands (no exact particle size given) from field test evaluations. These data represent aged sands that likely were overconsolidated.

Figure 2-21 illustrates the data as a function of age of the deposits. The WES laboratory data are plotted at an age of several days. The Niigata, Ogishima, and Kawagishi data summarized by Skempton (31) represent NC recent fills that were assigned approximate ages of 30 to 40 years. The time is not known for the OC, aged, Peck and Bazaraa data, so it is estimated at 100 to 10,000 years. The other four sites (A, B, C, D) are given by Barton, et al. (39). They represent OC, aged, fine and fine to medium sands of four geologic periods, as noted.

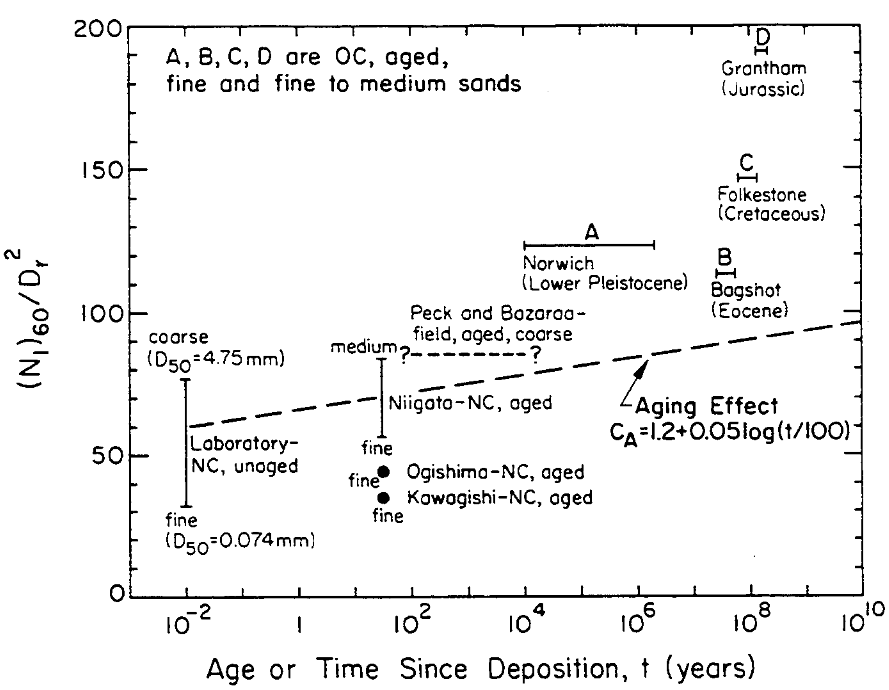

Figure 2-21. Aging Effect on Blow Count for Sands

Based on Figures 2-20 and 2-21, it is clear that particle size, aging, and overconsolidation significantly influence the $(N_1)_{60}/D_r^2$ ratio. These effects can be quantified as follows:

$$D_r^2 = \frac{(N_1)_{60}}{C_P\ C_A\ C_{OCR}} \qquad (2\text{-}16)$$

in which C_P, C_A, and C_{OCR} are the correction factors given in Table 2-11. C_P is based on Figure 2-20. C_A is based on a conservative interpretation of the imprecise data in Figure 2-21. C_{OCR} is based on direct evaluation of the WES data and interpretation of the Niigata data. It also is consistent with the studies presented by Tokimatsu (40).

Finally, the complete expression for relative density (D_r) in terms of SPT N value, including all corrections and modifying terms, is:

$$D_r^2 = \frac{C_{ER}\ C_B\ C_S\ C_R\ C_N\ N}{C_P\ C_A\ C_{OCR}} \qquad \text{(with } D_r \text{ in decimal form)} \qquad (2\text{-}17)$$

in which N = measured N value and the corrections are as follows: energy ratio (C_{ER}), borehole diameter (C_B), sampling method (C_S), rod length (C_R), overburden stress (C_N), particle size (C_P), aging (C_A), and overconsolidation (C_{OCR}).

Cone Penetration Test (CPT) Correlations

Early work on this subject was similar to the SPT, and therefore the CPT q_c value

Table 2-11

SPT CORRECTION FACTORS FOR SAND VARIABLES

Effect	Parameter	Correction Term	Correction Value
Particle size	D_{50} of sand	C_P	$60 + 25 \log D_{50}$ (D_{50} in mm)
Aging	Time (t)	C_A	$1.2 + 0.05 \log (t/100)$
Overconsolidation	$OCR = \bar{\sigma}_p/\bar{\sigma}_{vo}$	C_{OCR}	$OCR^{0.18}$

simply was correlated directly to relative density, as shown in Table 2-12. As with the N values, recent research has shown that the relationships are more complex. Figure 2-22 shows the generalized relationship for Ticino sand, which is of medium compressibility. The vertical effective stress can be used with this figure if the sand is unaged and normally consolidated. The horizontal effective stress should be used if the sand is aged or overconsolidated.

Figure 2-23 illustrates that the generalized CPT correlations vary for soils of different compressibilities. Curve 3 corresponds to data on Monterey sand, which is of low compressibility. Monterey sand is characterized by subrounded to subangular grains, which are composed mainly of quartz and some feldspar, with zero percent fines. Curve 2 is for Ticino sand, a granular soil of moderate compressibility with subangular grains composed of quartz and 5 percent mica, with less than 1 percent fines. Curve 3 is for the high compressibility Hilton Mines sand, consisting of angular iron mine tailings of quartz, feldspar, and mica composition, with 3 percent fines.

To compare cone tip resistances obtained at different depths, it is necessary to reference the values to a standardized reference stress level, usually taken as $\bar{\sigma}_{vo}/p_a$ = 1 atmosphere. The standardized cone tip resistance (q_n) then becomes:

$$q_n = C_q \, q_c \tag{2-18}$$

Table 2-12

RELATIVE DENSITY OF SAND VERSUS q_c

Cone Tip Resistance, q_c/p_a	Relative Density	D_r (%)
< 20	Very loose	< 20
20 to 40	Loose	20 to 40
40 to 120	Medium	40 to 60
120 to 200	Dense	60 to 80
> 200	Very dense	> 80

Source: Meyerhof (7), p. 17.

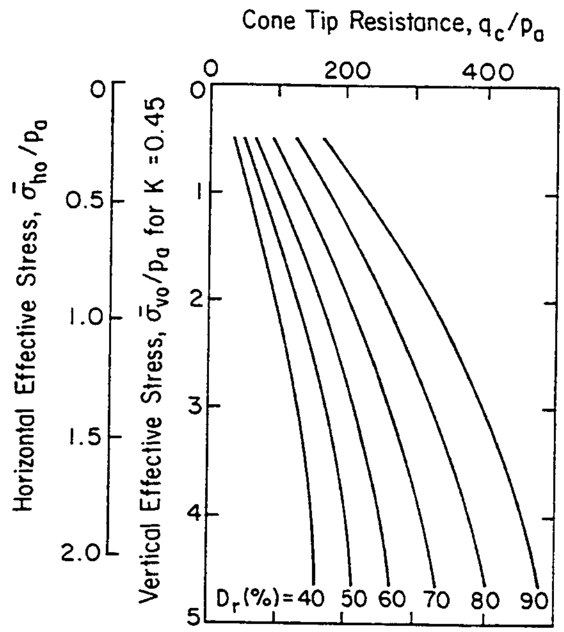

Figure 2-22. Relative Density from CPT for Uncemented and Unaged Quartz Sands

Source: Robertson and Campanella (17), p. 723.

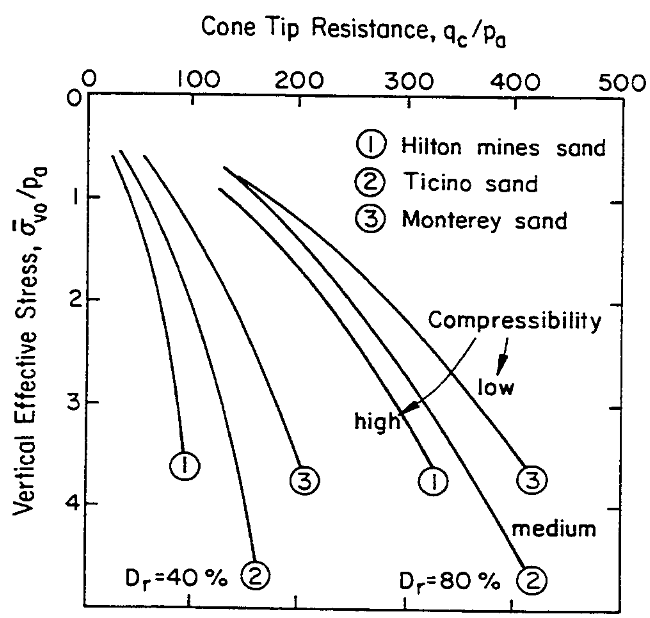

Figure 2-23. Relative Density from CPT, Including Soil Compressibility

Source: Robertson and Campanella (17), p. 722.

in which q_c = measured cone tip resistance, and C_q = overburden stress correction factor. For all practical purposes, C_q is nearly identical to C_N, proposed for the SPT and given as:

$$C_q \approx C_N = (p_a/\bar{\sigma}_{vo})^{0.5} \quad (2\text{-}19)$$

Much research on the CPT has been conducted in calibration chambers, which are described briefly in Appendix H. These studies allow the use of controlled sand properties and in-situ stresses, which is not possible in the field. One summary of D_r data from calibration chamber tests on five different normally consolidated sands is shown in Figure 2-24. This figure illustrates the range in actual data taken under controlled laboratory conditions after uniform soil placement. The generalized figures shown earlier in this section do not show the data range and perhaps suggest a high confidence level. Figure 2-24 shows what the actual ranges are for only five sands under controlled laboratory conditions; field cases are likely to exhibit more variability.

Calibration chamber data are useful, but the tests are performed with flexible walls of limited dimensions. Therefore, the boundary effects result in lower q_c values than obtained for "field conditions", corresponding to an infinite half-space. To correlate the field and chamber q_c values, Jamiolkowski, et al. (19) recommended dividing the field value of q_c by K_q, as given below:

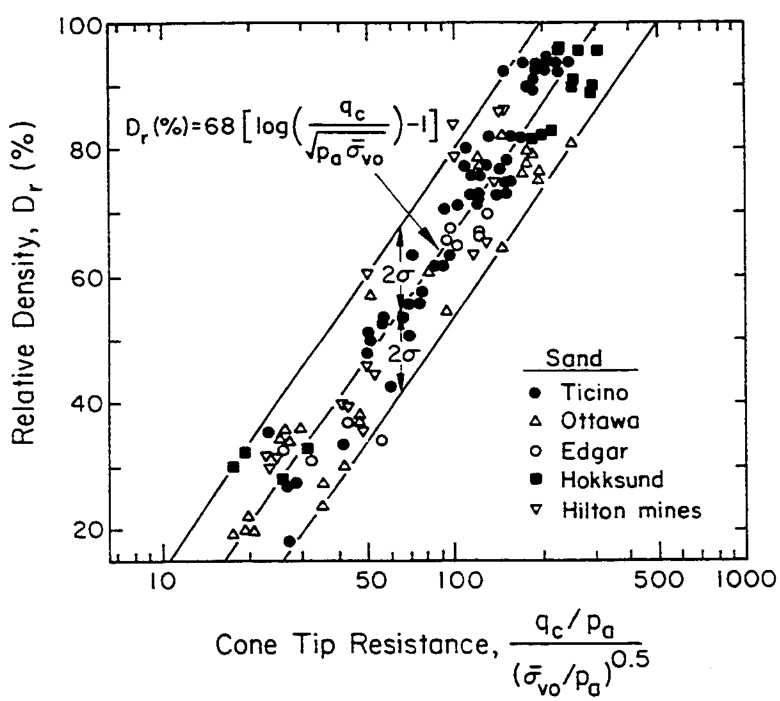

Figure 2-24. Correlation Between D_r and Dimensionless q_c (Uncorrected for Boundary Effects)

Source: Jamiolkowski, et al. (19), p. 120.

$$K_q = 1 + (D_r - 30)/300 \quad (2\text{-}20)$$

before entering Figure 2-24. The equivalent chamber values then can be used to evaluate D_r. This process requires iteration, because the value of D_r is not known.

As an alternative approach, the results of 24 sets of calibration chamber tests on sands were compiled, in which the values of q_c were corrected for the effects of boundary conditions. These sands were predominantly fine and medium sands. A summary of this compilation is given in Appendix H. For the majority of chambers with flexible walls, the boundary correction required an increase in q_c to reflect "field" values.

The results of this study are given in Figures 2-25 and 2-26 for unaged, uncemented sands. In all cases, a linear relationship was obtained for the square of the relative density (D_r^2) versus the dimensionless cone tip resistance, given as shown by Q_{CD}. Figure 2-25 shows the normally consolidated sands, separated into low, medium, and high compressibility. Low compressibility (Figure 2-25a) generally corresponds to quartz sands with little, if any, fines. Medium compressibility (Figure 2-25b) suggests quartz with some feldspar, with perhaps several percent fines. High compressibility (Figure 2-25c) indicates more fines, mica, and other compressible minerals. Most natural sands likely will be more toward the medium to high range of compressibility. As shown in these figures, the correlation is good below the limit of possible particle crushing. This limit was established by statistical analysis of the data, optimizing the r^2 value as a function of different limiting Q_{CD} values from 250 up to the entire data set. The limiting Q_{CD} values shown provide the maximum r^2 for the data and define the boundary of possible particle crushing. Data points beyond the limiting Q_{CD} values are not included in the statistics.

Figure 2-26 shows comparable calibration chamber data on overconsolidated sands, separated into low (< 3), medium (3 to 8), and high (8 to 15) OCR ranges. These data also were optimized using r^2 for different Q_{CD} limiting values, resulting in the regression lines and possible particle crushing limits shown.

A summary of these relationships is given in Figure 2-27 for all of the corrected calibration chamber data. This figure clearly shows the influence of compressibility and OCR on the relationship between D_r^2 and the dimensionless cone tip resistance. These relationships can be quantified approximately as follows:

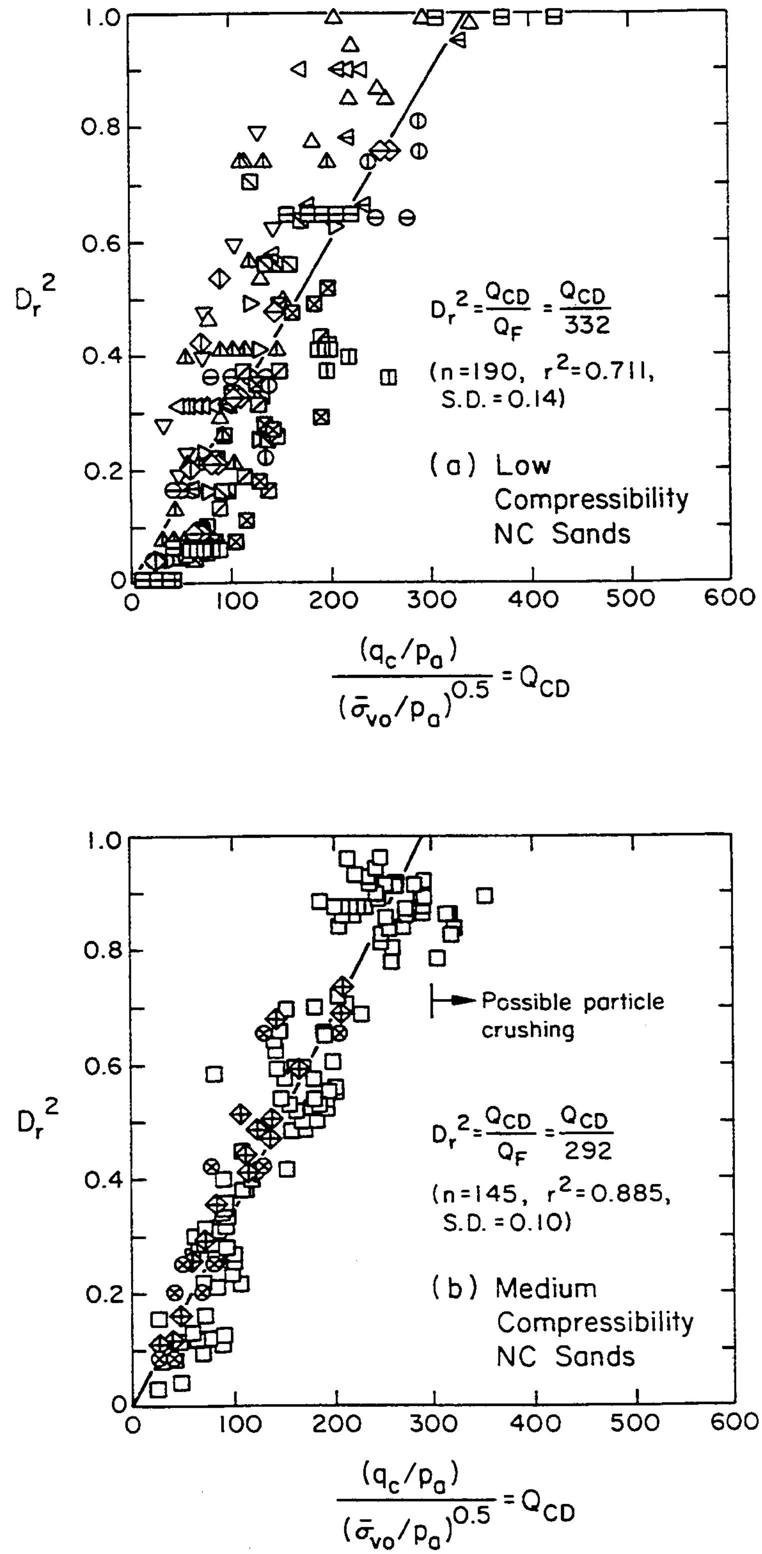

Figure 2-25. Calibration Chamber Data on NC Sands

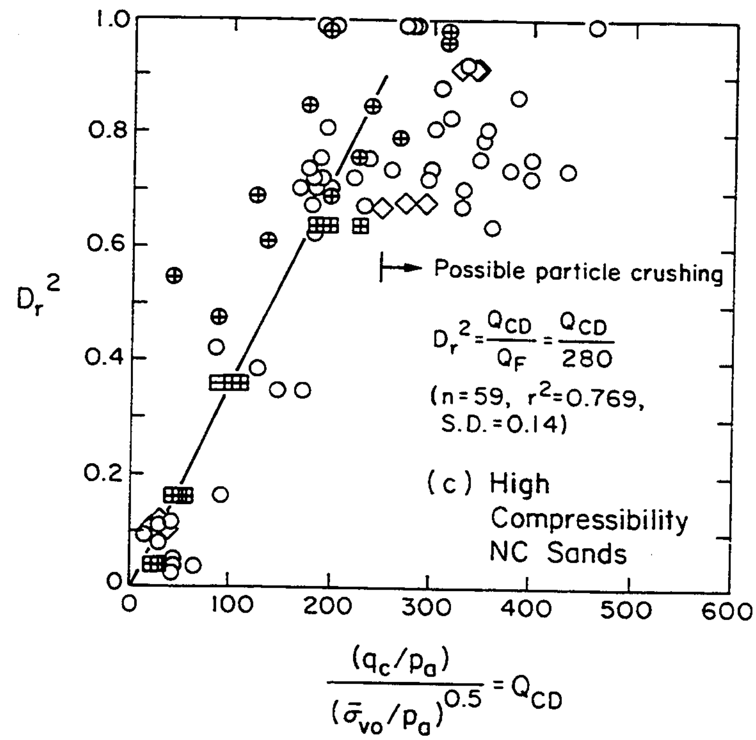

Figure 2-25. Calibration Chamber Data on NC Sands (continued)

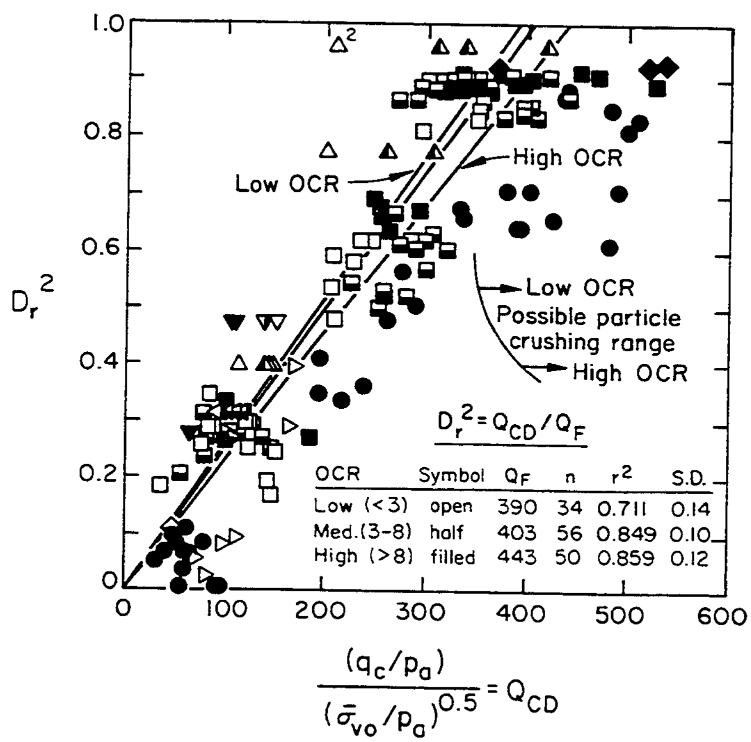

Figure 2-26. Calibration Chamber Data on OC Sands

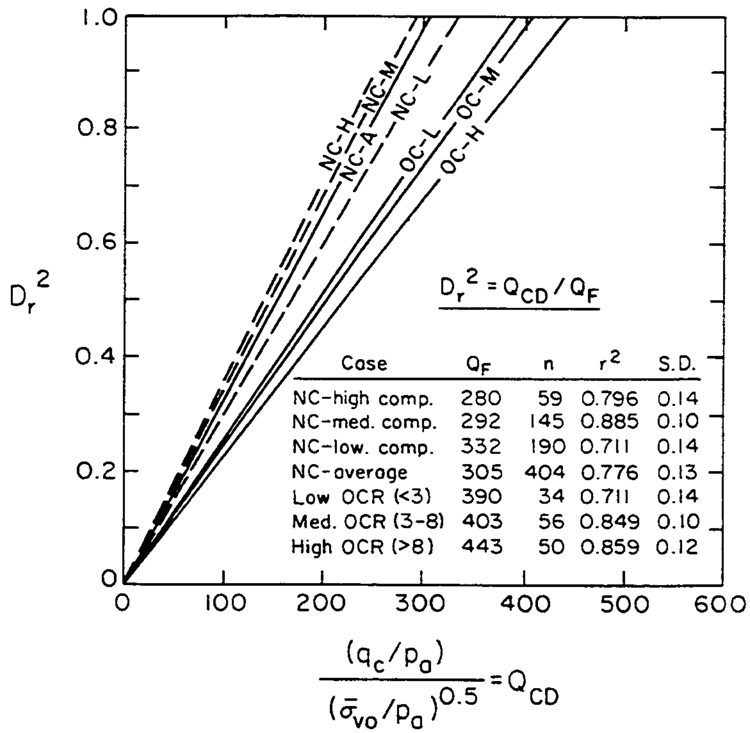

Figure 2-27. Summary of Calibration Chamber Studies

$$D_r^2 = \frac{Q_{CD}}{305\ Q_C\ Q_{OCR}} \tag{2-21a}$$

$$D_r^2 = \frac{C_q(q_c/p_a)}{305\ Q_C\ Q_{OCR}} \tag{2-21b}$$

$$D_r^2 = \frac{1}{305\ Q_C\ OCR^{0.18}} \frac{(q_c/p_a)}{(\bar{\sigma}_{vo}/p_a)^{0.5}} \tag{2-21c}$$

in which Q_C = compressibility factor (0.91 for high, 1.0 for medium, and 1.09 for low) and Q_{OCR} = overconsolidation factor (= $OCR^{0.18}$), comparable to C_{OCR} for the standard penetration test. The Q_{OCR} factor was evaluated using the mean OCR values for the low, medium, and high OCR data equal to 2.3, 5.1, and 10.1, respectively. The majority of natural sands are likely to be of medium to high compressibility and low to medium OCR.

It should be noted that Equation 2-17 for the SPT is similar in form to Equation 2-21 for the CPT, although some differences are evident. Perhaps the most important difference is that the SPT relationship includes aging, while the CPT relationship is only for unaged sands. If the same functional relationship for aging holds for both the SPT and CPT, then C_A (as given in Table 2-11) would be introduced into the denominator of Equation 2-21. This addition is speculation at this time. However, the C_A changes qualitatively explain the effects of aging in a reasonable manner.

Dilatometer Test (DMT) Correlations

The DMT is a relatively new test for which broad correlations have not yet been developed for relative density (D_r). However, it has been used to estimate D_r in normally consolidated, uncemented sands. This correlation is shown in Figure 2-28 for D_r as a function of the DMT horizontal stress index (K_D), described in Appendix D and defined as:

$$K_D = (p_o - u_o)/\bar{\sigma}_{vo} \qquad (2\text{-}22)$$

in which p_o = initial contact stress, u_o = hydrostatic stress, and $\bar{\sigma}_{vo}$ = effective vertical stress. This correlation is based on few data and should be considered preliminary at this time.

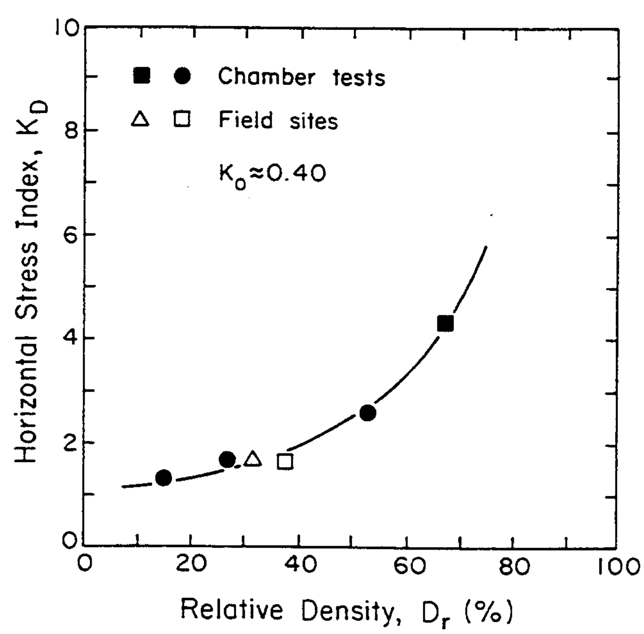

Figure 2-28. Correlation Between DMT Horizontal Stress Index and Relative Density for Normally Consolidated, Uncemented Sand

Source: Robertson and Campanella (41), p. 39.

CONSISTENCY OF COHESIVE SOILS FROM IN-SITU TEST CORRELATIONS

The standard penetration test (SPT) N value and the cone penetration test (CPT) q_c value also have been used to estimate the consistency of cohesive soils in-situ. However, little published work has been presented on these correlations, and therefore all should be considered approximate at best.

Standard Penetration Test (SPT) Correlations

The consistency of cohesive soils has been correlated with the N value, as shown in Table 2-13. In general, these values are to be considered only approximate guidelines, since clay sensitivity can greatly affect the N value (Schmertmann, 42).

Although the correlations with N value in clay commonly are considered to be less reliable than those in sand, increasing N values do, in general, reflect increasing stiffness and therefore decreasing liquidity index. To express this general correlation, the consistency index (CI) has been defined as follows:

$$CI = \frac{w_L - w_n}{w_L - w_P} = 1 - LI \qquad (2\text{-}23)$$

which effectively is a mirror image of the liquidity index. Table 2-14 is

Table 2-13

CONSISTENCY OF CLAY VERSUS N

N Value (blows/ft or 305 mm)	Consistency
0 to 2	Very soft
2 to 4	Soft
4 to 8	Medium
8 to 15	Stiff
15 to 30	Very stiff
> 30	Hard

Source: Terzaghi and Peck (27), p. 347.

Table 2-14

CONSISTENCY INDEX OF CLAY VERSUS N and q_c

N Value (blows/ft or 305 mm)	Cone Tip Resistance, q_c/p_a	Consistency	Consistency Index
< 2	< 5	Very soft	< 0.5
2 to 8	5 to 15	Soft to medium	0.5 to 0.75
8 to 15	15 to 30	Stiff	0.75 to 1.0
15 to 30	30 to 60	Very stiff	1.0 to 1.5
> 30	> 60	Hard	> 1.5

Source: Szechy and Varga (43), p. 105.

representative of the CI correlations.

Cone Penetration Test (CPT) Correlations

The consistency of cohesive soils also has been related to the cone tip resistance. Again, as with the N values, the correlations in clay are less reliable. A typical correlation is given also in Table 2-14.

RELATIONSHIP BETWEEN SPT N AND CPT q_c VALUES

Because of the numerous relationships developed for either SPT or CPT data, it is advantageous to have a procedure to interrelate N and q_c. Both are penetration resistances (although the SPT is dynamic and the CPT is quasi-static), and they are the most common forms of in-situ testing used worldwide today.

A number of investigators have proposed single numerical values of q_c/N. However, recent studies have shown that q_c/N generally correlates with grain size, as shown in Figure 2-29. Unfortunately, most of these data do not include N or q_c value corrections as noted previously.

Newer data (44 - 50) have been combined with the previous results in Figure 2-29 to result in Figure 2-30. This new relationship confirms the general trend of the data, and it extends the relationship to mean grain sizes up to 10 mm. The new

REFERENCES

1. American Society for Testing and Materials, "Standard Method for Particle-Size Analysis of Soils [D422-63(1972)]", Annual Book of Standards, Vol. 4.08, ASTM, Philadelphia, 1989, pp. 86-92.

2. American Society for Testing and Materials, "Standard Practice for Wet Preparation of Soil Samples for Particle-Size Analysis and Determination of Soil Constants (D2217-85)", Annual Book of Standards, Vol. 4.08, ASTM, Philadelphia, 1989, pp. 270-272.

3. American Society for Testing and Materials, "Standard Test Method for Liquid Limit, Plastic Limit, and Plasticity Index of Soils (D4318-84)", Annual Book of Standards, Vol. 4.08, ASTM, Philadelphia, 1989, pp. 579-589.

4. American Society for Testing and Materials, "Standard Test Methods for Maximum Index Density of Soils Using a Vibratory Table (D4253-83)", Annual Book of Standards, Vol. 4.08, ASTM, Philadelphia, 1989, pp. 560-571.

5. American Society for Testing and Materials, "Standard Test Methods for Minimum Index Density of Soils and Calculation of Relative Density (D4254-83)", Annual Book of Standards, Vol. 4.08, ASTM, Philadelphia, 1989, pp. 572-578.

6. Lambe, T. W. and Whitman, R. V., Soil Mechanics, John Wiley and Sons, New York, 1969, 553 p.

7. Meyerhof, G. G., "Penetration Tests and Bearing Capacity of Cohesionless Soils", Journal of the Soil Mechanics and Foundations Division, ASCE, Vol. 82, No. SM1, Jan. 1956, pp. 1-19.

8. Youd, T. L., "Factors Controlling Maximum and Minimum Densities of Sands", Evaluation of Relative Density and Its Role in Geotechnical Projects Involving Cohesionless Soils (STP 523), ASTM, Philadelphia, 1973, pp. 98-122.

9. Sowers, G. F., Introductory Soil Mechanics and Foundations: Geotechnical Engineering, 4th Ed., Macmillan Publishing Co., New York, 1979, 621 p.

10. American Society for Testing and Materials, "Standard Test Method for Classification of Soils for Engineering Purposes (D2487-85)", Annual Book of Standards, Vol. 4.08, ASTM, Philadelphia, 1989, pp. 288-297.

11. American Society for Testing and Materials, "Standard Practice for Description and Identification of Soils (Visual-Manual Procedure) (D2488-84)", Annual Book of Standards, Vol. 4.08, ASTM, Philadelphia, 1989, pp. 298-307.

12. Burmister, D. M., "Physical, Stress-Strain, and Strength Responses of Granular Soils", Symposium on Field Testing of Soils (STP 322), ASTM, Philadelphia, 1962, pp. 67-97.

13. Burmister, D. M., "Suggested Methods of Test for Identification of Soils", Special Procedures for Testing Soil and Rock for Engineering Purposes (STP 479), ASTM, Philadelphia, 1970, pp. 311-332.

14. Laboratorium voor Grondmechanica, "Cone Penetration Testing", Civiele and Bouwkundige Techniek, No. 3, May 1982, pp. 16-36.

15. Schmertmann, J. H., "Guidelines for Cone Penetration Test Performance and Design", Report FHWA-TS-78-209, U.S. Department of Transportation, Washington, 1978, 145 p.

16. Douglas, B. J. and Olsen, R. S., "Soil Classification Using Electric Cone Penetrometer", Cone Penetration Testing and Experience, Eds. G. M. Norris and R. D. Holtz, ASCE, New York, 1981, pp. 209-227.

17. Robertson, P. K. and Campanella, R. G., "Interpretation of Cone Penetration Tests. Part I: Sand", Canadian Geotechnical Journal, Vol. 20, No. 4, Nov. 1983, pp. 718-733.

18. Wroth, C. P., "Penetration Testing - A More Rigorous Approach to Interpretation", Proceedings, 1st International Symposium on Penetration Testing (ISOPT-1), Vol. 1, Orlando, 1988, pp. 303-311.

19. Jamiolkowski, M., Ladd, C. C., Germaine, J. T., and Lancellotta, R., "New Developments in Field and Laboratory Testing of Soils", Proceedings, 11th International Conference on Soil Mechanics and Foundation Engineering, Vol. 1, San Francisco, 1985, pp. 57-153.

20. Olsen, R. S. and Farr, J. V., "Site Characterization Using the Cone Penetrometer Test", Use of In-Situ Tests in Geotechnical Engineering (GSP No. 6), Ed. S. P. Clemence, ASCE, New York, 1986, pp. 854-868.

21. Senneset, K. and Janbu, N., "Shear Strength Parameters Obtained from Static CPT", Strength Testing of Marine Sediments (STP 883), Eds. R. C. Chaney and K. R. Demars, ASTM, Philadelphia, 1985, pp. 41-54.

22. Jones, G. and Rust, E., "Piezometer Penetration Testing", Proceedings, 2nd European Symposium on Penetration Testing, Vol. 2, Amsterdam, 1982, pp. 607-613.

23. Robertson, P. K., Campanella, R. G., Gillespie, D., and Grieg, J., "Use of Piezometer Cone Data", Use of In-Situ Tests in Geotechnical Engineering (GSP No. 6, Ed. S. P. Clemence, ASCE, New York, 1986, pp. 1263-1280.

24. Marchetti, S., "In-Situ Tests by Flat Dilatometer", Journal of the Geotechnical Engineering Division, ASCE, Vol. 106, No. GT3, Mar. 1980, pp. 299-321.

25. Schmertmann, J., "Suggested Method for Performing the Flat Dilatometer Test", Geotechnical Testing Journal, ASTM, Vol. 9, No. 2, June 1986, pp. 93-101.

26. Hough, B. K., Basic Soils Engineering, 2nd Ed., Ronald Press, New York, 1969, 634 p.

27. Terzaghi, K. and Peck, R. B., Soil Mechanics in Engineering Practice, 2nd Ed., John Wiley and Sons, New York, 1967, 729 p.

28. Gibbs, H. J. and Holtz, W. G., "Research on Determining the Density of Sands by Spoon Penetration Testing", Proceedings, 4th International Conference on Soil Mechanics and Foundation Engineering, Vol. 1, London, 1957, pp. 35-39.

29. Holtz, W. G. and Gibbs, H. J., Discussion of "SPT and Relative Density in Coarse Sand", Journal of the Geotechnical Engineering Division, ASCE, Vol. 105, No. GT3, Mar. 1979, pp. 439-441.

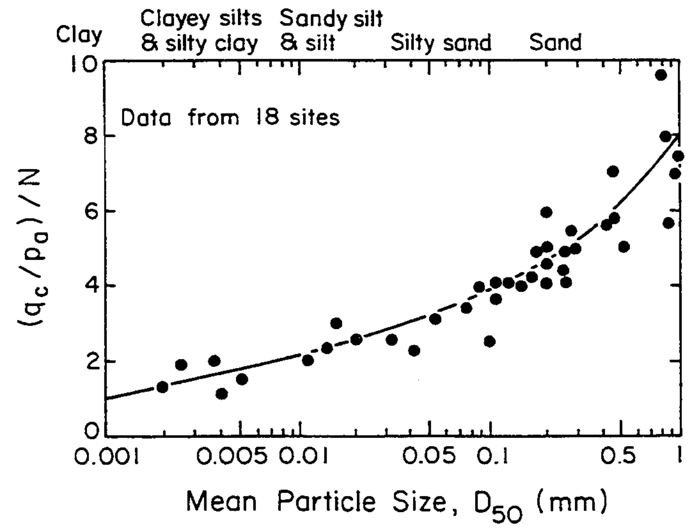

Figure 2-29. Variation of q_c/N with Grain Size for Electric and Mechanical Friction Cones

Source: Robertson and Campanella (17), p. 730.

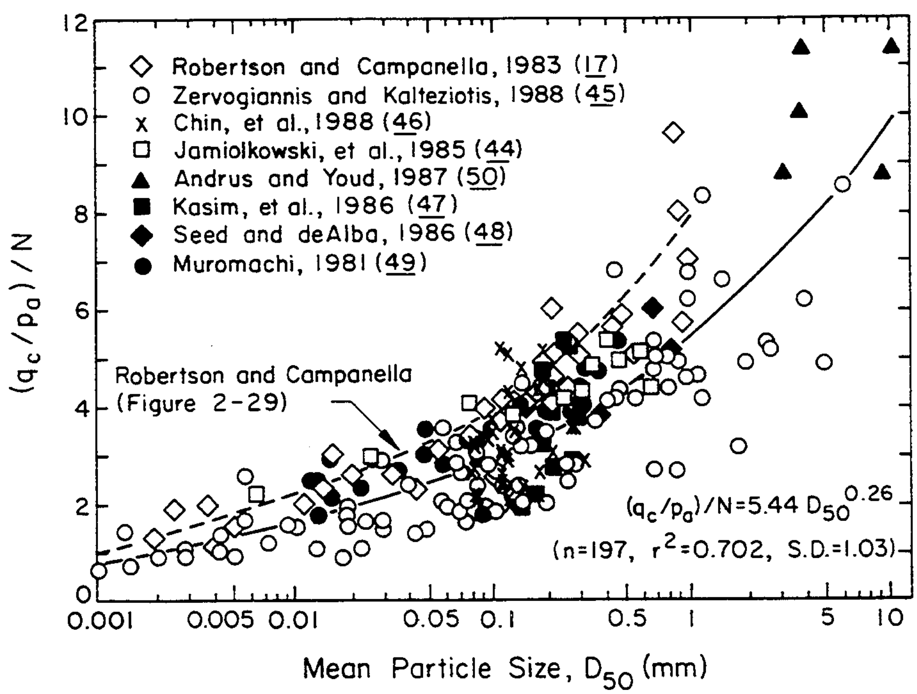

Figure 2-30. Recommended Variation of q_c/N with Grain Size for Fugro Electric Friction Cones

recommended relationship is given by the solid line and regression equation on the figure.

In other studies, the ratio of q_c/N has been correlated to the percentage of fines (clay and silt sizes). For example, Jamiolkowski, et al. (44) indicate the trend presented in Figure 2-31 for Italian soils. In addition to these data, other available data were summarized (46, 47, 49) to substantiate a general trend between the q_c/N ratio and fines content, as shown in Figure 2-32. Use of Figures 2-30 and 2-32 will provide the best estimate relationship between q_c and N, with the ratio decreasing with increasing fines content.

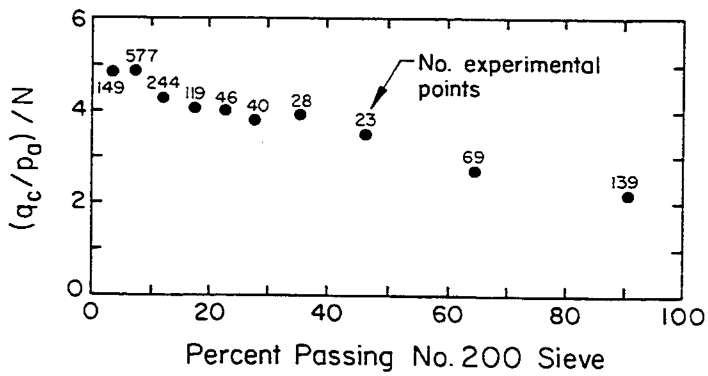

Figure 2-31. Variation of q_c/N with Fines Content

Source: Jamiolkowski, et al. (44), p. 1895.

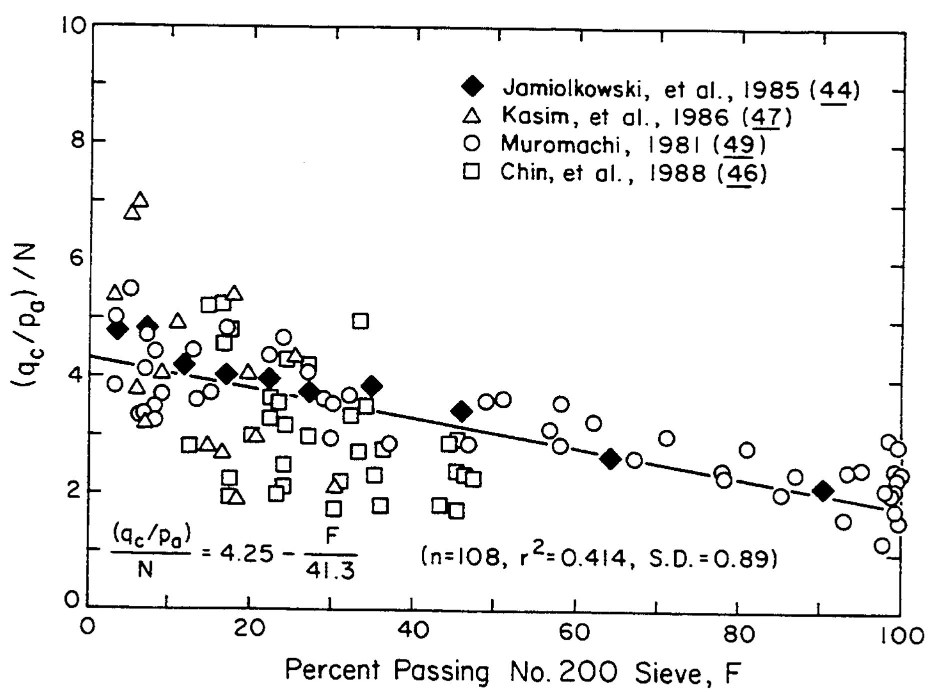

Figure 2-32. Recommended Variation of q_c/N with Fines Content

30. Marcuson, W. F., III and Bieganousky, W. A., "SPT and Relative Density in Coarse Sands", Journal of the Geotechnical Engineering Division, ASCE, Vol. 103, No. GT11, Nov. 1977, pp. 1295-1309.

31. Skempton, A. W., "Standard Penetration Test Procedures and the Effects in Sands of Overburden Pressure, Relative Density, Particle Size, Aging, and Overconsolidation", Geotechnique, Vol. 36, No. 3, Sept. 1986, pp. 425-447.

32. Robertson, P. K., Campanella, R. G., and Wightman, A., "SPT-CPT Correlations", Journal of the Geotechnical Engineering Division, ASCE, Vol. 109, No. 11, Nov. 1983, pp. 1449-1459.

33. Liao, S. S. and Whitman, R. V., "Overburden Correction Factors for SPT in Sand", Journal of Geotechnical Engineering, ASCE, Vol. 112, No. 3, Mar. 1986, pp. 373-377.

34. Peck, R. B., Hansen, W. E., and Thornburn, T. H., Foundation Engineering, 2nd Ed., John Wiley and Sons, New York, 1974, 514 p.

35. Seed, H. B., "Soil Liquefaction and Cyclic Mobility Evaluation for Level Ground During Earthquakes", Journal of the Geotechnical Engineering Division, ASCE, Vol. 105, No. 2, Feb. 1979, pp. 201-255.

36. Bieganousky, W. A. and Marcuson, W. F., III, "Liquefaction Potential of Dams and Foundations: Laboratory Standard Penetration Tests on Reid Bedford Model and Ottawa Sands", Research Report S-76-2 (Report 1), U.S. Army Engineer Waterways Experiment Station, Vicksburg, 1976, 156 p.

37. Bieganousky, W. A. and Marcuson, W. F., III, "Liquefaction Potential of Dams and Foundations: Laboratory Standard Penetration Tests on Platte River Sand and Standard Concrete Sand", Research Report S-76-2 (Report 2), U.S. Army Engineer Waterways Experiment Station, Vicksburg, 1977, 87 p.

38. Peck, R. B. and Bazaraa, A. R. S., Discussion of "Settlement of Spread Footings on Sand", Journal of the Soil Mechanics and Foundations Division, ASCE, Vol. 95, No. SM3, May 1969, pp. 905-909.

39. Barton, M. E., Cooper, M. R., and Palmer, S. N., "Diagenetic Alteration and Micro-Structural Characteristics of Sands", Penetration Testing in the U.K., Thomas Telford, London, 1988, pp. 57-60.

40. Tokimatsu, K., "Penetration Tests for Dynamic Problems", Proceedings, 1st International Symposium on Penetration Testing (ISOPT-1), Vol. 1, Orlando, 1988, pp. 117-136.

41. Robertson, P. K. and Campanella, R. G., "Estimating Liquefaction Potential of Sands Using the Flat Plate Dilatometer", Geotechnical Testing Journal, ASTM, Vol. 9, No. 1, Mar. 1986, pp. 38-40.

42. Schmertmann, J. H., "Measurement of In-Situ Shear Strength", Proceedings, ASCE Conference on In-Situ Measurement of Soil Properties, Vol. 2, Raleigh, 1975, pp. 57-138. (closure: pp. 175-179).

43. Szechy, K. and Varga, L., Foundation Engineering - Soil Exploration and Spread Foundations, Akademiai Kiado, Budapest, 1978, 508 p.

44. Jamiolkowski, M., Baldi, G., Bellotti, R., Ghionna, V., and Pasqualini, E., "Penetration Resistance and Liquefaction of Sands", Proceedings, 11th International Conference on Soil Mechanics and Foundation Engineering, Vol. 4, San Francisco, 1985, pp. 1891-1896.

45. Zervogiannis, C. S. and Kalteziotis, N. A., "Experiences and Relationships from Penetration Testing in Greece", Proceedings, 1st International Symposium on Penetration Testing (ISOPT-1), Vol. 2, Orlando, 1988, pp. 1063-1071.

46. Chin, C. T., Duann, S. W., and Kao, T. C., "SPT-CPT Correlations for Granular Soils", Proceedings, 1st International Symposium on Penetration Testing (ISOPT-1), Vol. 1, Orlando, 1988, pp. 335-339.

47. Kasim, A. G., Chu, M. Y., and Jensen, C. N., "Field Correlation of Cone and Standard Penetration Tests", Journal of Geotechnical Engineering, ASCE, Vol. 112, No. 3, Mar. 1986, pp. 368-372.

48. Seed, H. B. and de Alba, P., "Use of SPT and CPT Tests for Evaluating the Liquefaction Resistance of Sands", Use of In-Situ Tests in Geotechnical Engineering (GSP 6), Ed. S. P. Clemence, ASCE, New York, 1986, pp. 281-302.

49. Muromachi, T., "Cone Penetration Testing in Japan", Cone Penetration Testing and Experience, Eds. G. M. Norris and R. D. Holtz, ASCE, New York, 1981, pp. 49-75.

50. Andrus, R. D. and Youd, T. L., "Subsurface Investigation of a Liquefaction-Induced Lateral Spread, Thousand Springs Valley, Idaho", Miscellaneous Paper GL-87-8, U.S. Army Engineer Waterways Experiment Station, Vicksburg, 1987, 131 p.

Section 3

IN-SITU STRESS STATE

In most geotechnical engineering problems, a knowledge of the in-situ state of stress is necessary for two reasons. First, these stresses represent the original conditions onto which any engineered construction imposes stress increments. These initial through final stress conditions are used to evaluate the overall engineering performance of the constructed facility. Second, nearly all engineering properties of soil are a function of the soil stresses, either directly or indirectly. Therefore, the stresses are needed to evaluate the soil properties.

In this section, procedures are presented to evaluate the in-situ stresses in both cohesive and cohesionless soils. Vertical stresses are covered first, followed by horizontal stresses. In each case, correlations are presented with soil index parameters and in-situ test results, where available.

BASIC DEFINITIONS

The in-situ state of stress in soil is defined in terms of the current values of effective vertical stress ($\bar{\sigma}_{vo}$) and effective horizontal stress ($\bar{\sigma}_{ho}$). For horizontal, level ground, the in-situ stress state is shown in Figure 3-1.

The current vertical stress is determined in a straightforward manner, being equal to the effective overburden stress in which $\bar{\sigma}_{vo} = \bar{\gamma}z$. However, the horizontal stress is more difficult to evaluate. The stress ratio is K_o, the at-rest coefficient of horizontal soil stress, which is defined as $\bar{\sigma}_{ho}/\bar{\sigma}_{vo}$. As a lower bound, K_o could equal K_A, the coefficient of minimum active soil stress. The upper bound for K_o is K_P, the coefficient of maximum passive soil stress. For horizontal, level

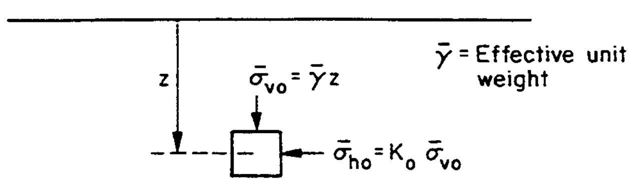

Figure 3-1. Stresses in Soil

ground and an effective stress cohesion ($\bar{c}$) = 0, these limit states are given by Rankine theory as below:

$$K_P = \frac{1}{K_A} = \frac{1 + \sin \bar{\phi}_{psc}}{1 - \sin \bar{\phi}_{psc}} \tag{3-1}$$

in which $\bar{\phi}_{psc}$ = effective stress friction angle for plane strain compression conditions. Using these limits for a cohesionless soil with $\bar{\phi}_{psc} = 40°$, for example, K_o could range from 0.2 to 4.6.

Many factors affect the in-situ state of stress in soil, including overconsolidation, aging, chemical bonding, etc. Overconsolidation is probably most influential for the majority of soils, because it is caused by glaciation, erosion, desiccation, excavation, ground water fluctuations, and possibly other factors. In this regard, the effective vertical preconsolidation stress (denoted $\bar{\sigma}_p$, $\bar{\sigma}_{vmax}$, or $\bar{p}_c$) is an important measure of the soil stress history. This maximum past stress affects the compressibility, strength, consistency, and overall state of stress. It is often convenient to represent the stress history in terms of a dimensionless parameter defined as the overconsolidation ratio (OCR):

$$OCR = \bar{\sigma}_p/\bar{\sigma}_{vo} \tag{3-2}$$

The magnitude of $\bar{\sigma}_p$ and OCR can be evaluated directly from the results of one-dimensional consolidation tests conducted on undisturbed cohesive soil samples. Correlations with other tests and soil types are presented in this section.

The magnitude of K_o may be measured directly either in the laboratory using special testing equipment, or in the field using devices such as the pressuremeter or total stress cells. However, these direct methods may be subject to unavoidable disturbance effects during sampling and in-situ testing. Alternatively, several empirical approaches can be used to evaluate the in-situ value of K_o, including: (1) reconstruction of stress history, (2) correlations with soil index parameters, and (3) correlations with in-situ test results. All three approaches are described in this section.

RECONSTRUCTION OF STRESS HISTORY

Reconstruction of the soil stress history involves tracing the stress paths of the soil as in Figure 3-2, from virgin loading, to primary unloading, to primary

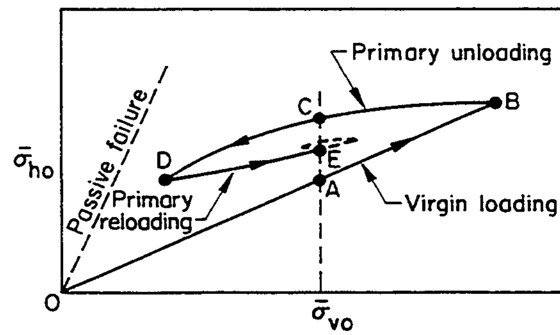

Figure 3-2. Stress Paths for Simple Stress Histories

reloading, and then cyclical load-unload looping from water table fluctuations, etc. (above point E in figure). Virgin loading represents normally consolidated (NC) soils with OCR = 1. All other stress paths represent overconsolidated (OC) soils with OCR > 1.

Based on a study of 171 different laboratory-tested soils, Mayne and Kulhawy (1) showed that a general equation can be used to model stress paths OB-BD-DE, as given below:

$$K_o = K_{onc} \left[\frac{OCR}{OCR_{max}^{1-\alpha}} + m_r \left(1 - \frac{OCR}{OCR_{max}}\right) \right] \tag{3-3}$$

in which K_{onc} = K_o during virgin (normally consolidated) loading, α = at-rest unload coefficient, m_r = reload coefficient, OCR = current overconsolidation ratio, and OCR_{max} = maximum past OCR (e.g., point D for a soil currently at point E).

For virgin loading, the simplified Jáky equation (2) provides reasonable estimates for K_{onc}, as given below:

$$K_{onc} = 1 - \sin \bar{\phi}_{tc} \tag{3-4}$$

in which $\bar{\phi}_{tc}$ = effective stress friction angle for triaxial compression. Figure 3-3 shows this equation to be a reasonable estimate for a wide range of soils. In this figure, K_{onc} was determined from oedometer or triaxial tests.

During rebound or unloading, the general relationship for K_o is often expressed as:

$$K_o = K_{onc}\ OCR^{\alpha} \tag{3-5}$$

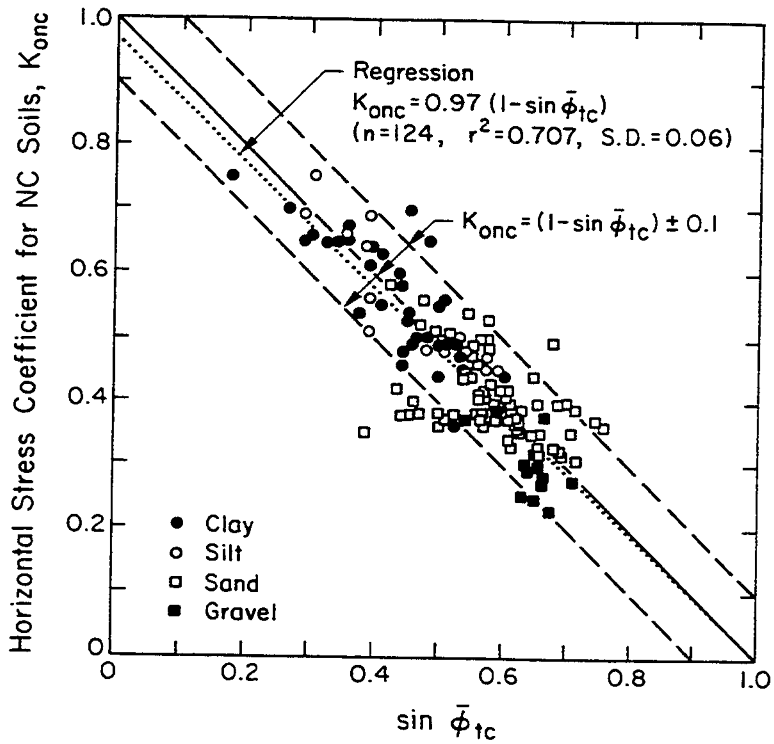

Figure 3-3. Horizontal Stress Coefficient for NC Soils from Laboratory Tests

Source: Mayne and Kulhawy (1), p. 862.

As suggested by Schmidt (3), the exponent α may be expressed as a function of $\bar{\phi}_{tc}$:

$$\alpha = \sin \bar{\phi}_{tc} \qquad (3\text{-}6)$$

Alternatively, the exponent may be expressed as:

$$\alpha = 1 - K_{onc} \qquad (3\text{-}7)$$

which also appears reasonable, as shown in Figure 3-4. For reloading, the stress path from D to E in Figure 3-2 may be approximated as a straight line with slope $m_r = \partial\bar{\sigma}_{ho}/\partial\bar{\sigma}_{vo}$. Review of laboratory data from 35 soils (Figure 3-5) indicates that the reload coefficient can be estimated adequately from:

$$m_r = 0.75(1 - \sin \bar{\phi}_{tc}) \qquad (3\text{-}8)$$

Linear regressions on these data for m_r give 0.76 K_{onc} (r^2 = 0.583 and S.D. = 0.06) and 0.77(1 - sin $\bar{\phi}_{tc}$) with r^2 = 0.534 and S.D. = 0.06.

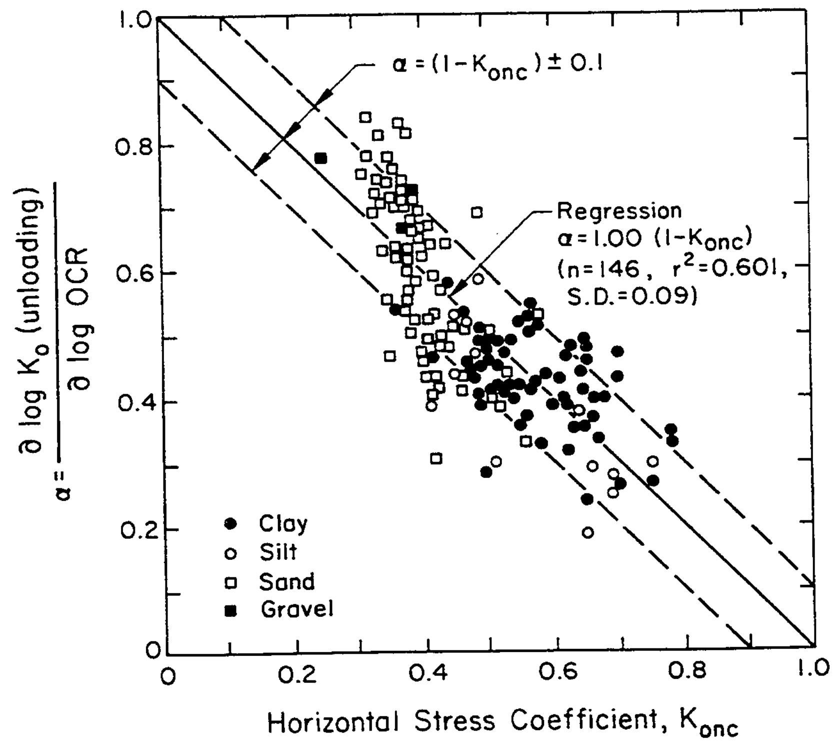

Figure 3-4. Unload Coefficient for OC Soils

Source: Mayne and Kulhawy (1), p. 864.

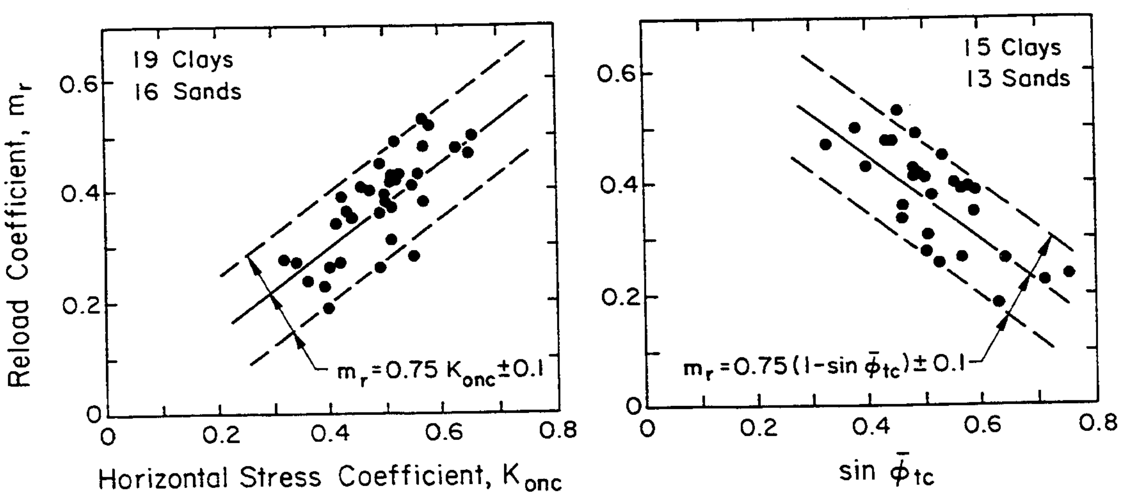

Figure 3-5. Reload Coefficient for OC Soils

Source: Mayne (4), p. 269.

Combining the above relationships gives:

$$K_o = (1 - \sin \bar{\phi}_{tc}) \left[\frac{OCR}{OCR_{max}^{(1 - \sin \bar{\phi}_{tc})}} + \frac{3}{4} \left(1 - \frac{OCR}{OCR_{max}}\right)\right] \quad (3\text{-}9)$$

in which OCR_{max} is the OCR at point D in Figure 3-2. For primary unloading, OCR = OCR_{max} and therefore:

$$K_o = (1 - \sin \bar{\phi}_{tc}) \; OCR^{\sin \bar{\phi}_{tc}} = K_{ou} \quad (3\text{-}10)$$

For virgin loading, OCR = 1 and therefore:

$$K_o = 1 - \sin \bar{\phi}_{tc} = K_{onc} \quad (3\text{-}11)$$

Most natural soils have undergone a stress history of loading-unloading-reloading, and therefore K_o is likely to be within points C and E in Figure 3-2. Therefore, K_o at point E is an appropriate lower bound for the in-situ K_o. All that is needed is $\bar{\phi}_{tc}$, OCR, and OCR_{max}, which can be evaluated by direct laboratory measurements, geologic generalization of the soil stress history, or experimental test programs in-situ to establish the values. It should be noted that, if an NC assumption is made (Equation 3-11), it will underestimate K_o in the majority of soil deposits.

One last point to mention regarding Figure 3-2 is that the soil can reach passive failure during primary unloading if the vertical effective stress is reduced sufficiently. This limit state can be developed from Equations 3-1 and 3-10 and is given by:

$$OCR_{limit} = [(1 + \sin \bar{\phi}_{psc})/(1 - \sin \bar{\phi}_{psc})(1 - \sin \bar{\phi}_{tc})]^{(1/\sin \bar{\phi}_{tc})} \quad (3\text{-}12)$$

As shown in Section 4, $\bar{\phi}_{psc} = 1.1 \; \bar{\phi}_{tc}$. If this limit state is reached, soil failure occurs, and the stresses change. It is uncertain what this stress state may be, although K_o might approach 1.

EFFECTIVE PRECONSOLIDATION STRESS IN COHESIVE SOILS

Cohesive soils consolidate and stiffen during overconsolidation and effectively retain a "memory" of the largest preconsolidation stress ($\bar{\sigma}_p$) to which they have been subjected (e.g., point B in Figure 3-2). This process was illustrated qualitatively in Figure 2-1 as a function of the water content and Atterberg limits. Therefore, these index parameters represent a starting point for estimating $\bar{\sigma}_p$. Correlations with in-situ test results follow the index parameter correlations.

Details on the in-situ test strength parameters are given in Section 4.

Correlations with Index Parameters

The effective preconsolidation stress ($\bar{\sigma}_p$) has been correlated with the liquidity index by several authors. A recent analysis of laboratory consolidation test data by Stas and Kulhawy (5) suggested the following:

$$\bar{\sigma}_p/p_a = 10^{(1.11 - 1.62\ LI)} \qquad (3\text{-}13)$$

in which p_a = atmospheric stress in the desired stress units and LI = liquidity index. This equation is based on 150 data points for clays with a sensitivity between 1 and 10. This relationship has a standard deviation of 0.33 and r^2 equal to 0.740.

Other generalized relationships are shown in Figure 3-6, which gives the preconsolidation stress as a function of liquidity index (LI) and sensitivity (S_t).

For comparison purposes to evaluate the soil stress history, the effective vertical stress ($\bar{\sigma}_{vo}$) is needed. This stress can be evaluated directly as in Figure 3-1, or it can be estimated from the liquidity index. Based on the modified Cam clay model and empirical observations, Wood (7) developed the following approximation for $\bar{\sigma}_{vo}$:

$$\bar{\sigma}_{vo}/p_a \approx 0.063 \cdot 10^{2(1-LI)} \qquad (3\text{-}14)$$

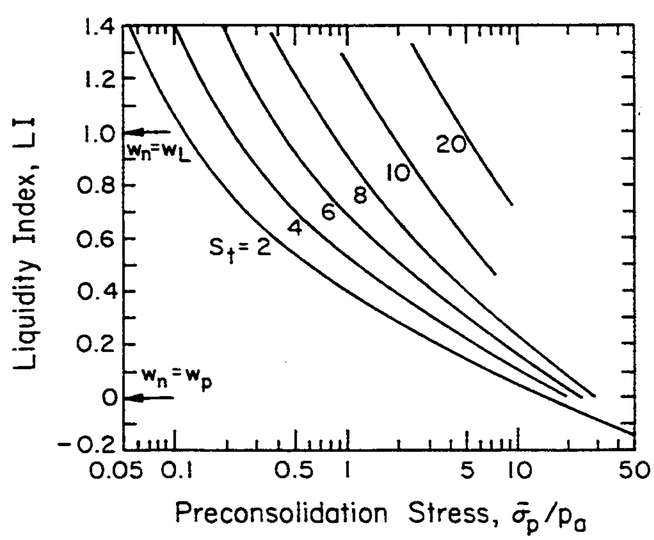

Figure 3-6. Generalized $\bar{\sigma}_p$ - Liquidity Index - Sensitivity Relationships

Source: NAVFAC (6), p. 7.1-142.

Although this equation strictly applies only to insensitive soils at the critical state, it is a useful approximation for uncemented, low sensitivity soils.

Comments on Field Test Correlations

It should be noted that the following figures correlating $\bar{\sigma}_p$ with field test measurements are presented all in similar form, on log-log plots because of the range in the parameters involved. These figures were developed from the sources noted, and the symbols used correspond to the clay types referenced in the source papers. For each figure, the number of intact and fissured clays is noted, the fissured clays are located separately because their behavior is different, and a linear regression equation is presented for the intact clays only. The regression was done assuming a linear, arithmetic relationship through the origin. The statistics given with each regression include the number of data points (n), coefficient of determination (r^2), and the standard deviation of $\bar{\sigma}_p$ (S.D.) for a given field test measurement. The given relationships should be used only as predictors for $\bar{\sigma}_p$.

Correlations with VST Strength

The field vane shear test (VST) has been used for many years as an estimator of $\bar{\sigma}_p$. In 1957, Hansbo (8) developed the following equation for Swedish clays:

$$\bar{\sigma}_p = \alpha_{VST}\ s_u(VST) \tag{3-15}$$

in which α_{VST} is an empirical factor approximately equal to $222/w_L$, with w_L = liquid limit (in percent).

A more recent compilation of worldwide clays, shown in Figure 3-7, indicated the general nature of Equation 3-15. This study further showed that α_{VST} could be correlated weakly with the plasticity index (PI), as shown in Figure 3-8.

Correlations with SPT N Value

The standard penetration test (SPT) N value may be used to provide a first-order estimate of $\bar{\sigma}_p$ for cohesive soils. Figure 3-9 shows the available data for 51 clays. The regression shows a fair correlation with a relatively large standard deviation.

It should be noted that the reported N values have not been corrected for the factors which significantly affect the SPT N value. Until the N values are corrected to a consistent standard, the SPT is likely to be of limited use in evaluating $\bar{\sigma}_p$.

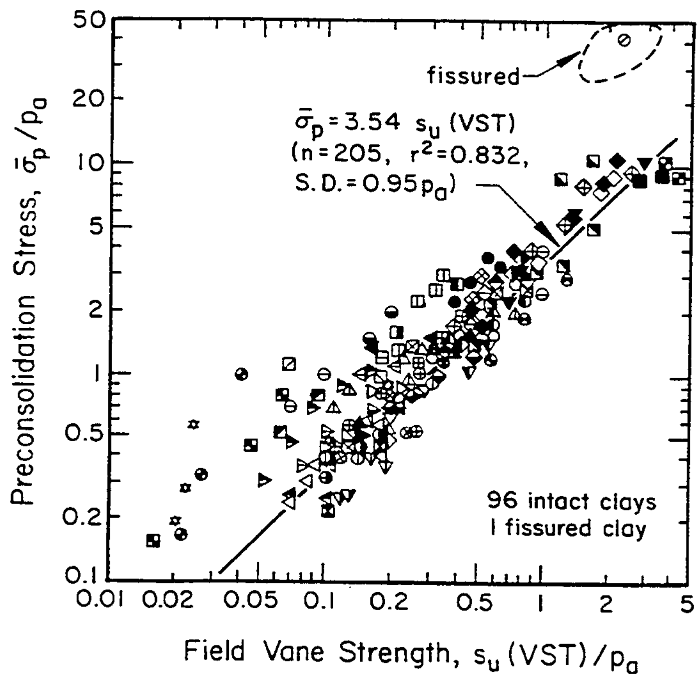

Figure 3-7. $\bar{\sigma}_p$ Correlated with VST s_u

Source: Based on Mayne and Mitchell (9), p. 154, and others (10).

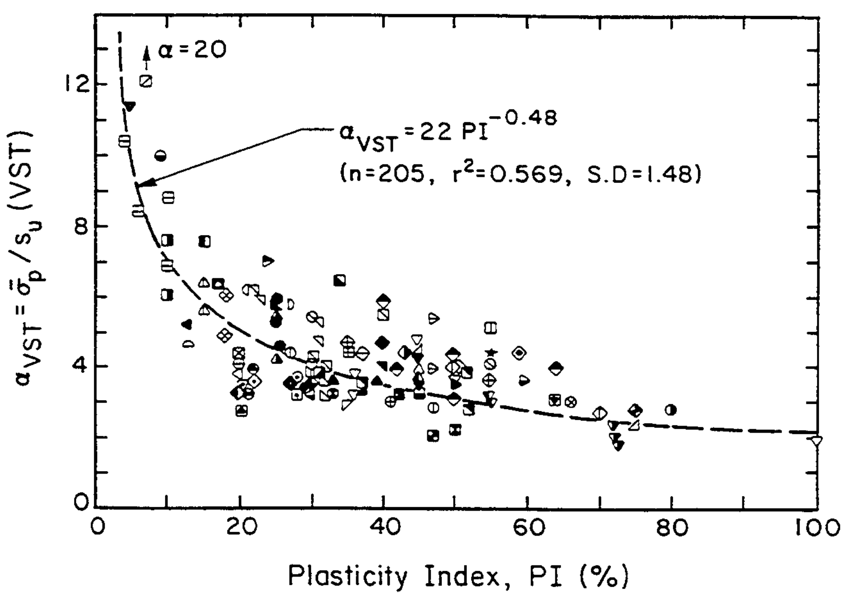

Figure 3-8. Field Vane Coefficient versus PI

Source: Mayne and Mitchell (9), p. 154.

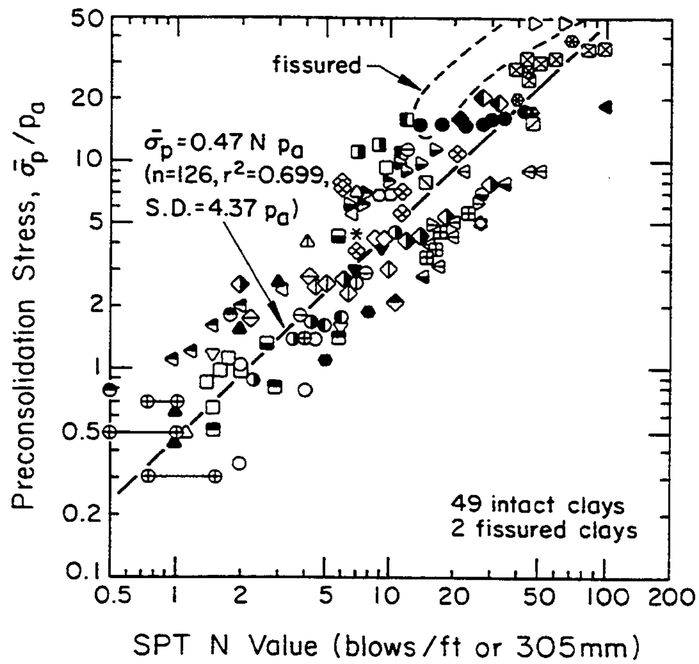

Figure 3-9. $\bar{\sigma}_p$ Correlated with SPT N

Source: Based on Mayne and Kemper (11), p. 144, and others (12).

Correlations with CPT q_c Value

The cone penetration test (CPT) tip resistance, q_c, has been used effectively to profile the preconsolidation stress in clays. Figure 3-10 presents the available data from 49 clays. This correlation is somewhat better than with the N value, and the standard deviation is smaller. This correlation also shows more clearly that the fissured clays behave differently from the intact clays. However, it is important to note that the data in Figure 3-10 are not corrected for pore water stress effects.

Correlations with CPTU Results

The piezocone (CPTU) provides additional data during penetration and generally is considered to be a more sensitive type of cone penetration test. Tavenas and Leroueil (20) demonstrated that the preconsolidation stress ($\bar{\sigma}_p$) was well-correlated with the net corrected cone tip resistance (q_T - σ_{vo}) for eleven Canadian clays. A larger sample of piezocone data is shown in Figure 3-11. The regression in this case gave an even higher r^2 with lower standard deviation.

In addition to measurements of cone tip resistance, piezocones provide the

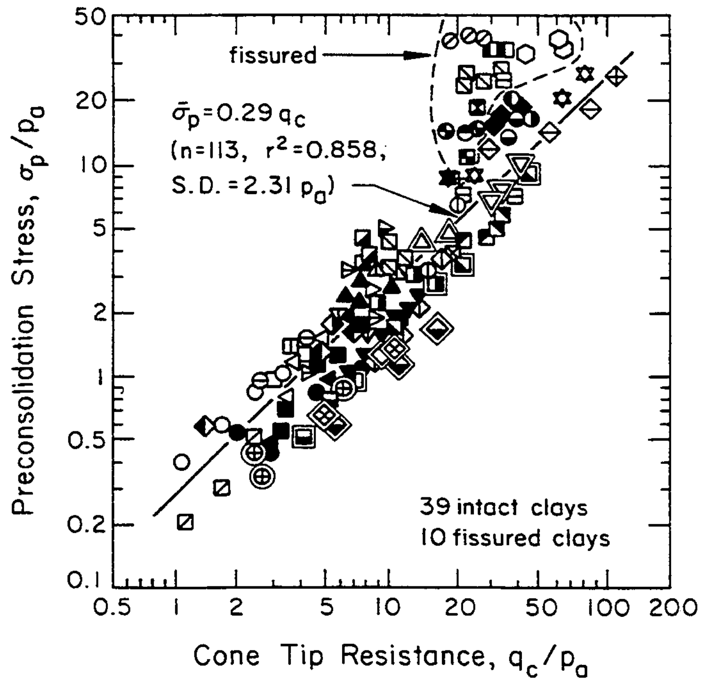

Figure 3-10. $\bar{\sigma}_p$ Correlated with CPT q_c

Source: Based on Mayne (13), p. 786, and others (14 - 19).

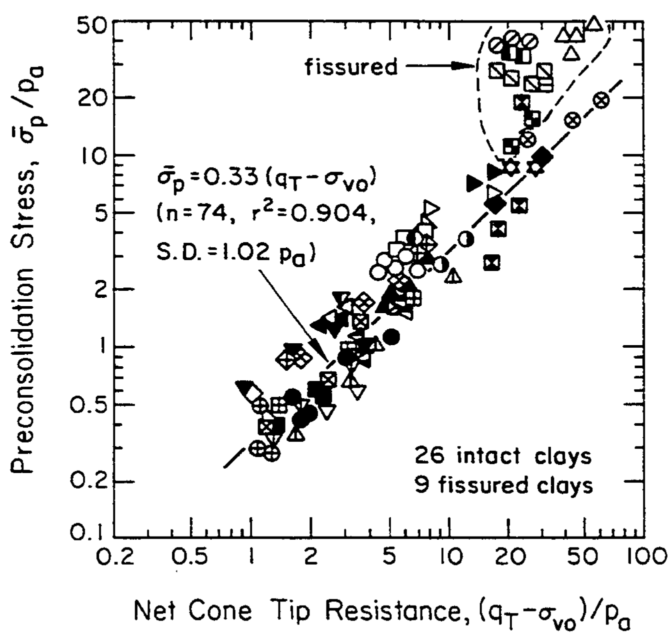

Figure 3-11. $\bar{\sigma}_p$ Correlated with CPTU q_T

Source: Based on Mayne and Holtz (21), p. 25, and others (14, 15, 17 - 19).

magnitude of pore water stress (Δu) caused by penetration. A relationship between $\bar{\sigma}_p$ and Δu_t from CPTU tests with tip or face pore water stress measurements is shown in Figure 3-12. For pore water stress measurements behind the tip, the relationship is given in Figure 3-13. The results are similar for the intact clays. However, for piezocones in heavily overconsolidated fissured clays, pore water stresses measured behind the tip are near zero and sometimes are even negative. On the cone tip, positive pore water stresses are observed for all clays at all OCR values, regardless of whether fissuring is present.

From cavity expansion theory, the general relationship between $\bar{\sigma}_p$ and the excess pore water stress measured at the tip during piezocone penetration can be given by the following (23):

$$\bar{\sigma}_p/\Delta u = 3/(M \ln I_r) \tag{3-16}$$

in which M = critical state parameter (Appendix G) and I_r = rigidity index (G/s_u). For measurements behind the tip, the coefficient 3 becomes equal to 4. This equation gives values consistent with those in Figures 3-12 and 3-13 for the intact

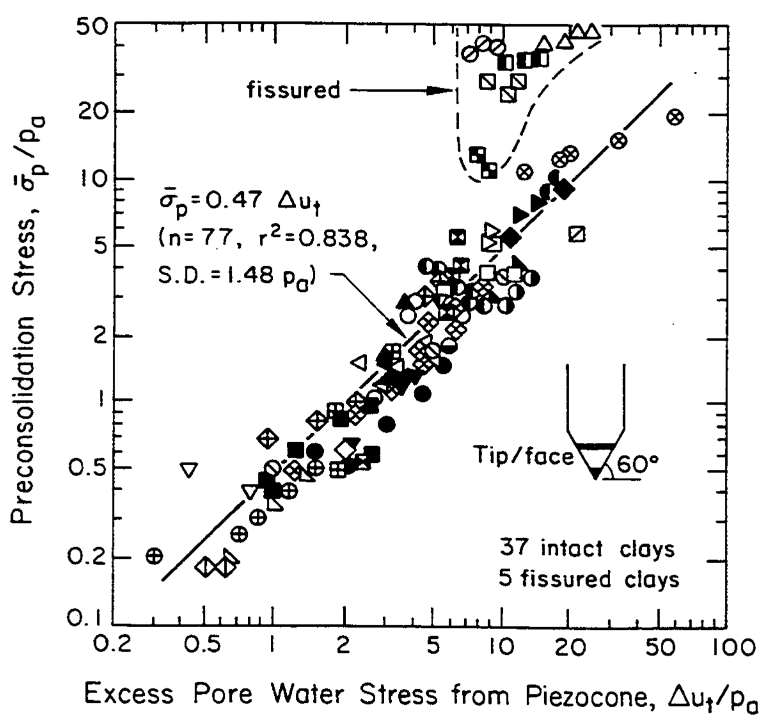

Figure 3-12. $\bar{\sigma}_p$ Correlated with CPTU Δu_t

Source: Based on Mayne and Holtz (21), p. 23, and others (14, 18, 22).

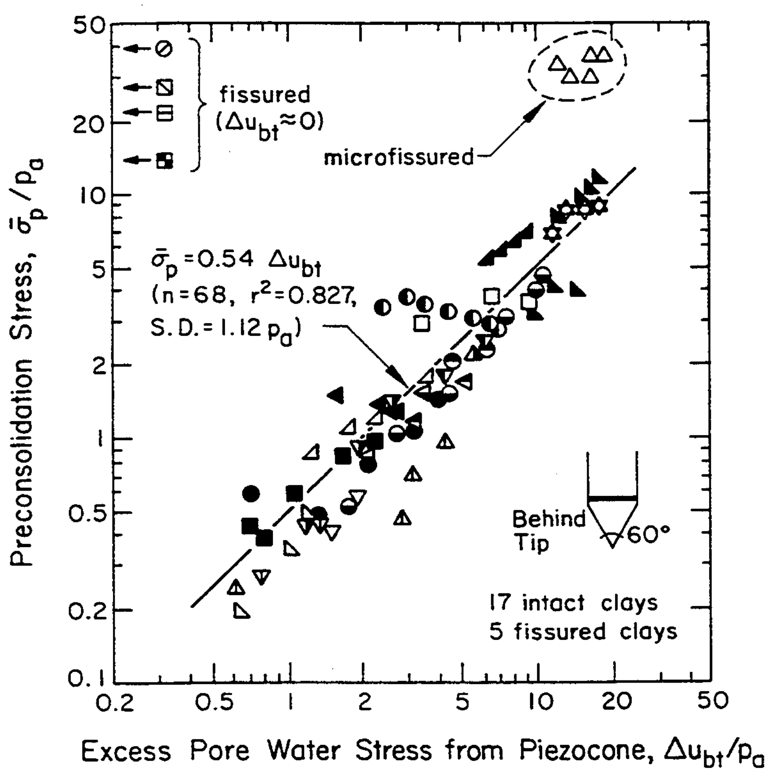

Figure 3-13. $\bar{\sigma}_p$ Correlated with CPTU Δu_{bt}

Source: Based on Mayne and Holtz (21), p. 24, and others (14, 15, 17, 19, 22).

clays.

Correlations with PMT Results

Several correlations have been attempted with the pressuremeter test (PMT) to estimate the value of $\bar{\sigma}_p$. Early work with the Menard pressuremeter indicated that the PMT creep pressure was approximately equal to $\bar{\sigma}_p$ for Chicago area lake clays (24). Later work showed that the limit stress from the self-boring pressuremeter test (SBPMT) could be correlated with $\bar{\sigma}_p$, as shown in Figure 3-14. Other studies have shown the correlations given in Figure 3-15, including the undrained shear strength (s_u) and the rigidity index (I_r).

Correlations with DMT Results

The initial contact stress (p_o) from the dilatometer test (DMT) is a measure of the induced total pore water stress caused by insertion of the DMT blade. Analogous to the previous relationship between $\bar{\sigma}_p$ and Δu for piezocone tests, a similar relationship applies for the DMT between $\bar{\sigma}_p$ and (p_o - u_o), as shown in Figure 3-16.

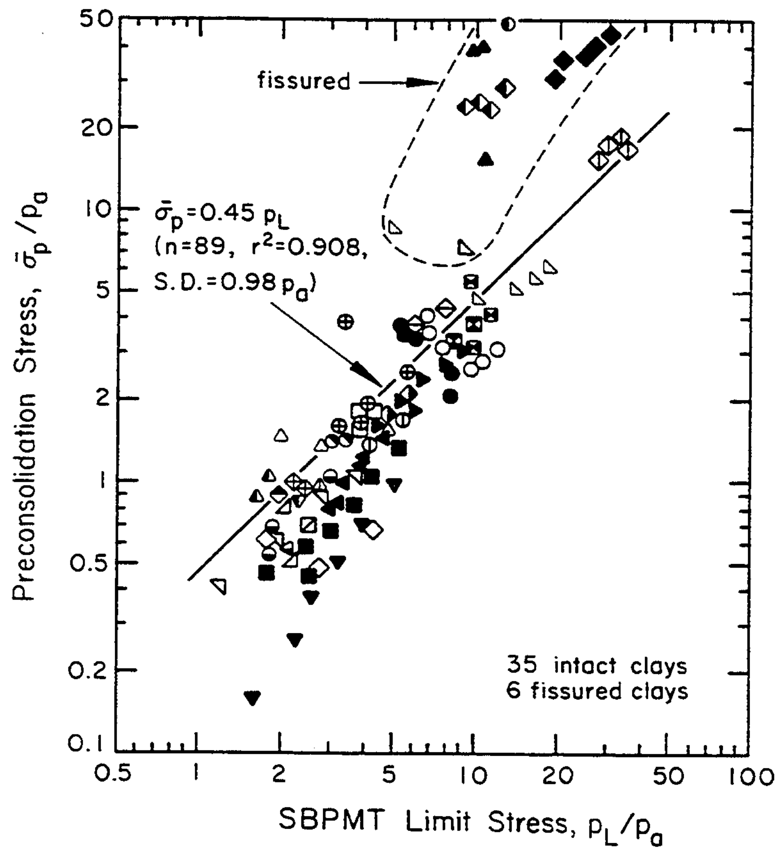

Figure 3-14. $\bar{\sigma}_p$ Correlated with SBPMT p_L

Source: Data from Mayne and Kulhawy (25), and others (12, 16, 19, 26).

EFFECTIVE PRECONSOLIDATION STRESS IN COHESIONLESS SOILS

Cohesionless soils also consolidate and stiffen during overconsolidation and retain a "memory" of the preconsolidation stress. However, cohesionless soils are difficult to sample and test in the laboratory in the undisturbed state, and therefore little correlation information is available to estimate the preconsolidation stress in these soils. More work has focused on evaluating OCR and K_o directly, as described later.

OVERCONSOLIDATION RATIO FOR COHESIVE SOILS

In lieu of describing soil stress history by the preconsolidation stress ($\bar{\sigma}_p$), the in-situ overconsolidation ratio (OCR) may be estimated directly using normalized parameters developed from laboratory or field test measurements. These correlations strictly apply only to insensitive clays. Furthermore, the same comments made previously on field test correlations with respect to $\bar{\sigma}_p$ also apply to the OCR

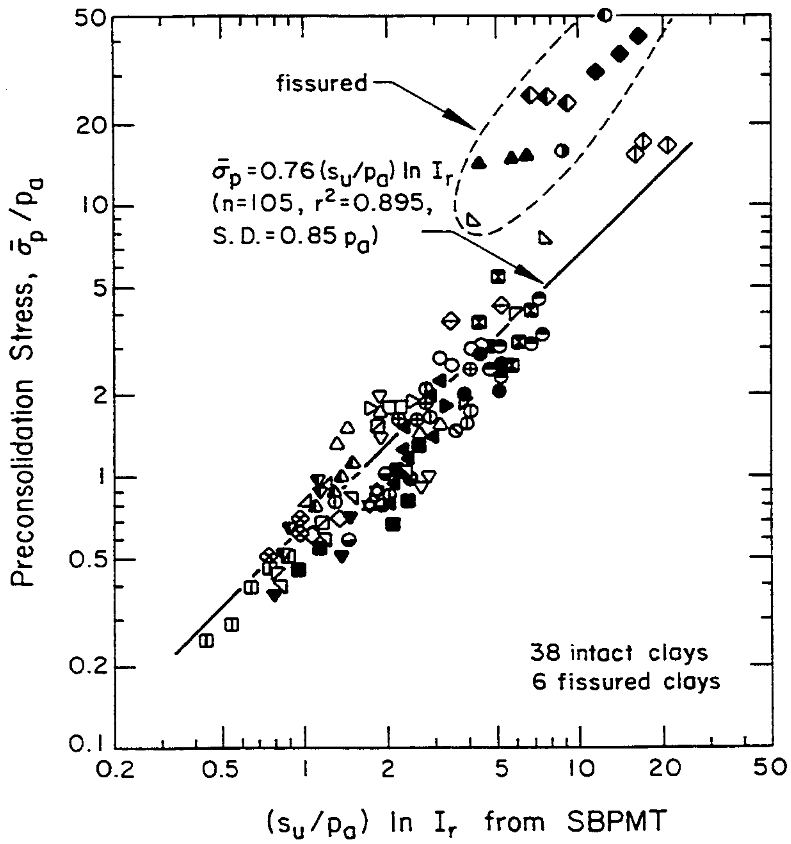

Figure 3-15. $\bar{\sigma}_p$ Correlated with SBPMT s_u and I_r

Source: Based on Mayne and Bachus (23), p. 293, and others (12, 16, 19, 26).

correlations.

Correlations with Index Parameters

Equation 3-13 can be re-cast in terms of OCR as follows:

$$OCR = (p_a/\bar{\sigma}_{vo})\ 10^{(1.11 - 1.62\ LI)} \qquad (3\text{-}17)$$

As noted previously, this relationship is based on statistical analysis of laboratory consolidation test data on clays with sensitivity from 1 to 10.

Based on the modified Cam clay model and empirical observations, Wood (7) developed Equation 3-14 to correlate $\bar{\sigma}_{vo}$ with LI. He also developed the following:

$$\log OCR \approx [2 - 2\ LI - \log (15.87\ \bar{\sigma}_{vo}/p_a)]/\Lambda \qquad (3\text{-}18)$$

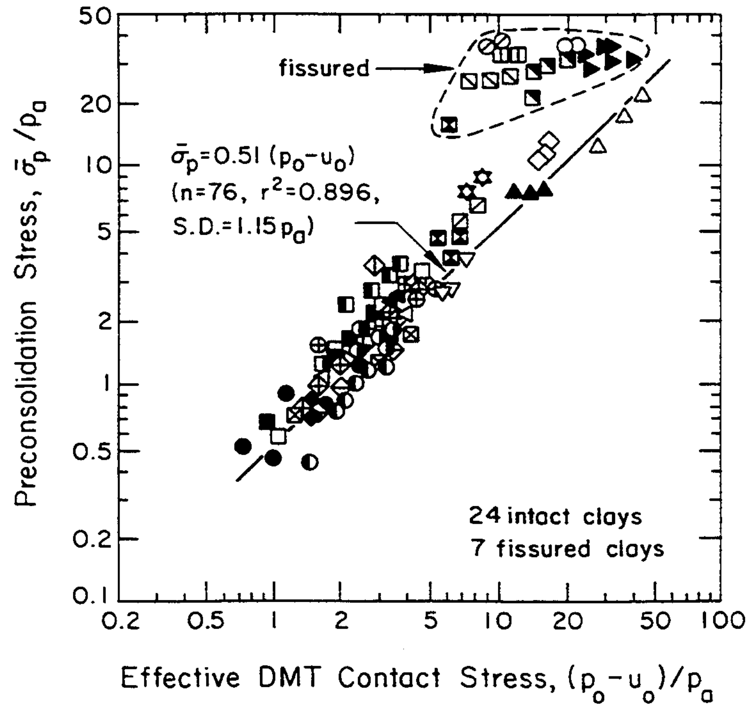

Figure 3-16. $\bar{\sigma}_p$ Correlated with DMT p_o

Source: Based on Mayne (27), p. 148, and others (26).

in which Λ = critical state parameter (Appendix G). Using a typical value of Λ = 0.8, and combining Equations 3-14 and 3-18, results in the following:

$$OCR = 10^{[1 - 2.5\ LI - 1.25 \log (\bar{\sigma}_{vo}/p_a)]} \tag{3-19}$$

Although this equation strictly applies only to insensitive soils at the critical state, it is a useful approximation for uncemented, low sensitivity soils, as noted previously.

Correlations with Laboratory Strength

Laboratory undrained shear strength (s_u) data may be used to estimate the in-situ OCR of clays. Using empirical observations from isotropically and anisotropically consolidated triaxial compression tests, Mayne (28) observed the following for OCR:

$$OCR_{CIUC} = [(s_u/\bar{\sigma}_{vo})/0.75 \sin \bar{\phi}_{tc}]^{1.43} \tag{3-20}$$

$$OCR_{CAUC} = [(s_u/\bar{\sigma}_{vo})/0.67 \sin \bar{\phi}_{tc}]^{1.28} \tag{3-21}$$

These results are consistent with the modified Cam clay model, which would predict the following:

$$OCR = 2[(s_u/\bar{\sigma}_{vo})/0.5\ M]^{-1/\Lambda} \qquad (3\text{-}22)$$

Correlations with VST Strength

The undrained strength from the field vane shear test (VST) may be related to the in-situ OCR according to:

$$OCR = \alpha_{VST}\ (s_u/\bar{\sigma}_{vo})_{VST} \qquad (3\text{-}23)$$

in which α_{VST} has been shown in Figure 3-8 to be related weakly to plasticity index (PI). Figure 3-17 shows a direct relationship between OCR and $s_u/\bar{\sigma}_{vo}$ for 96 clays.

Correlations with SPT N Value

Attempts have been made to correlate the SPT N value with OCR. Figure 3-18 is typical of these correlations, using uncorrected N values. This relationship is only a first-order estimator.

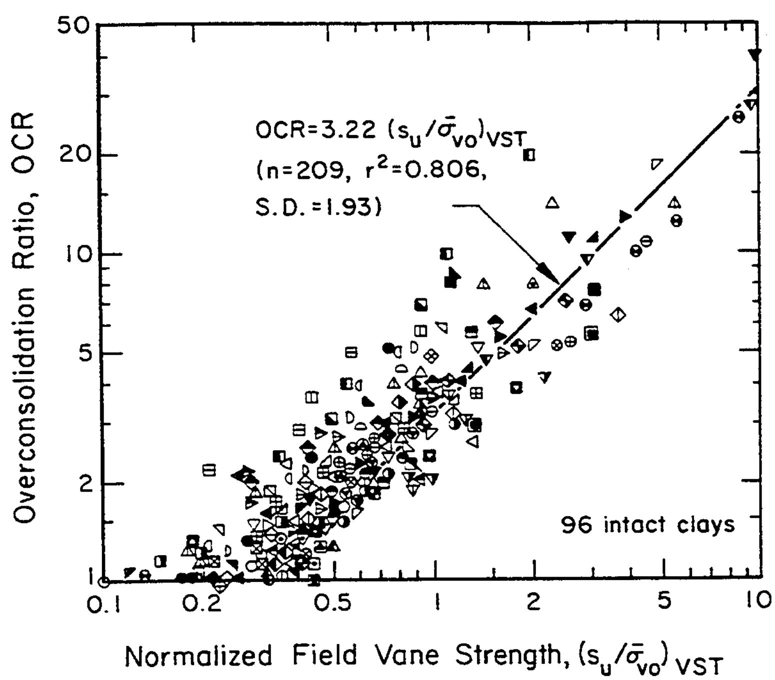

Figure 3-17. OCR Correlated with VST s_u

Source: Based on Mayne and Mitchell (9), p. 152.

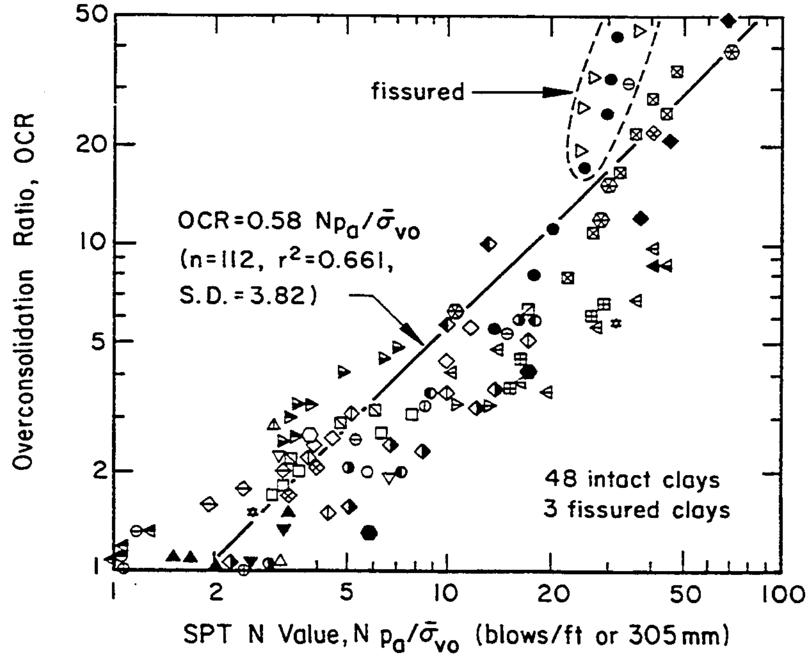

Figure 3-18. OCR Correlated with SPT N

Source: Based on Mayne and Kemper (11), p. 143, and others (12).

Correlations with CPT and CPTU Results

A number of authors (e.g., 13, 29) have demonstrated that OCR correlates with the CPT q_c value through the normalized cone tip resistance, $(q_c - \sigma_{vo})/\bar{\sigma}_{vo}$. However, q_c also should be corrected for pore water stresses acting on unequal areas of the cone. Figure 3-19 shows the variation of OCR with the corrected cone tip resistance, q_T, as obtained from piezocones.

Other piezocone studies (31) suggested a general trend with B_q (Equation 2-4) and OCR that was strongly dependent on the rigidity index. However, B_q is so site-dependent that the relationship was of little predictive use. More recent work (32) considered a combined critical state/cavity expansion model to correlate OCR with piezocone results. However, at the present time, the relationship given in Figure 3-19 probably is most appropriate to use.

Correlations with DMT Results

In the initial introduction of the dilatometer test, Marchetti (33) proposed the correlation in Figure 3-20 between OCR and the DMT parameter K_D, given by:

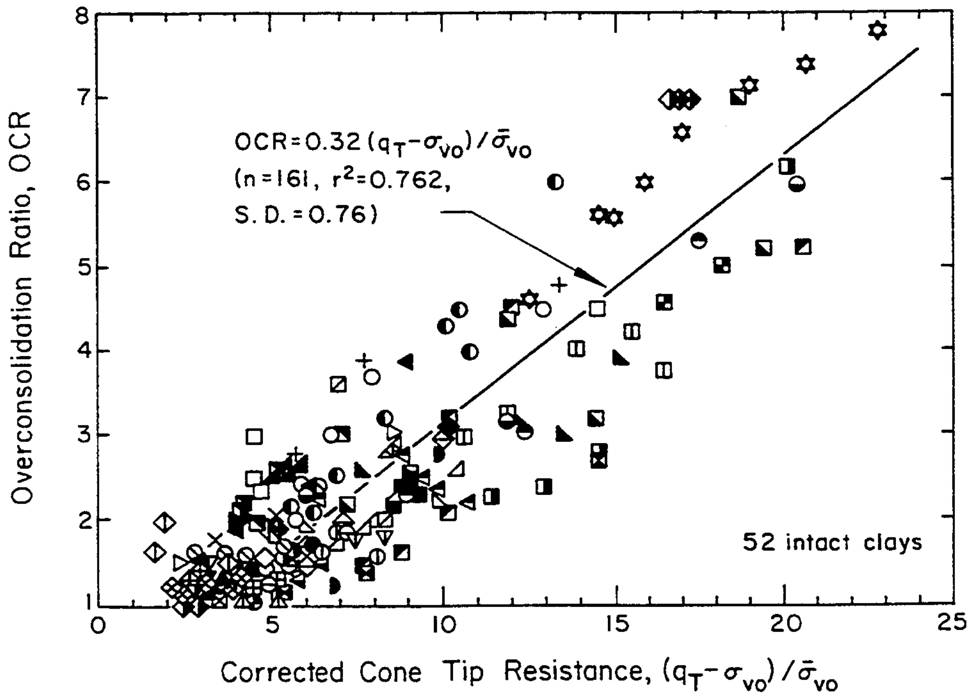

Figure 3-19. OCR Correlated with CPTU q_T

Source: Data from Mayne (30), and others (18, 19, 22).

$$OCR = (0.5\ K_D)^{1.56} \qquad (3\text{-}24)$$

in which K_D = horizontal stress index = $(p_o - u_o)/\bar{\sigma}_{vo}$, p_o = initial contact stress, u_o = hydrostatic pore water stress, and $\bar{\sigma}_{vo}$ = effective vertical stress. Subsequent research with the DMT in other countries suggests a more general expression:

$$OCR = (\beta_o\ K_D)^{1.56} \qquad (3\text{-}25)$$

in which the parameter β_o depends upon the degree of fissuring, sensitivity, and geologic origin, as shown in Figure 3-21.

OVERCONSOLIDATION RATIO IN COHESIONLESS SOILS

It is difficult to estimate the in-situ OCR of natural sand deposits. The best approach is through a detailed geologic study to evaluate the stress history of the formation. Indirectly, oedometer tests on interbedded clay strata or seams may give clues to the in-situ OCR of the surrounding sands. With the DMT, a value of OCR in sands can be back-calculated from the estimated K_o as (Bullock, 36):

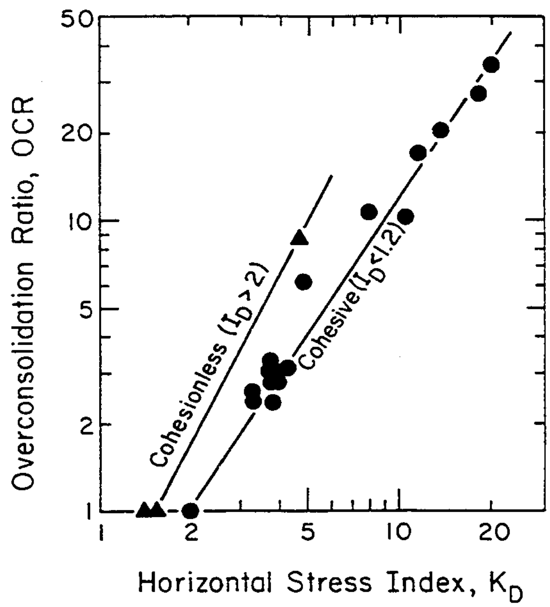

Figure 3-20. OCR Correlated with DMT K_D

Source: Marchetti (33), p. 315.

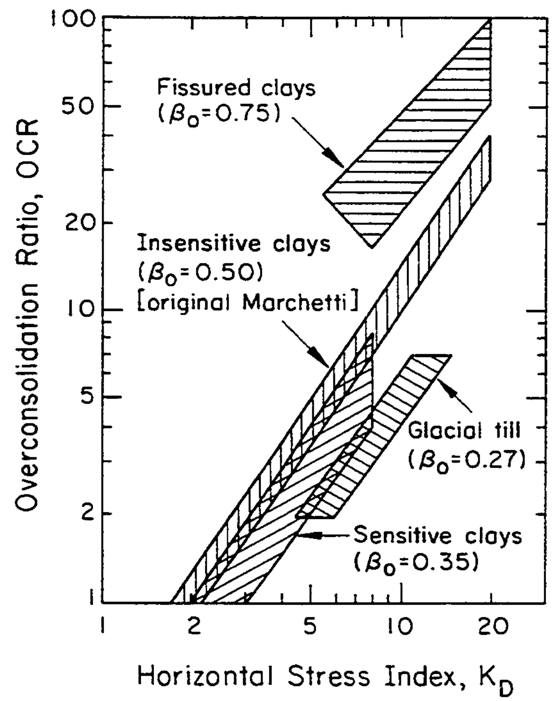

Figure 3-21. OCR - K_D Relationships for Clays of Varied Geologic Origin

Source: Based on Marchetti (33), Powell and Uglow (34), and Lacasse and Lunne (35).

$$OCR = [K_o/(1 - \sin \bar{\phi}_{tc})]^{(1.25/\sin \bar{\phi}_{tc})} \quad (3\text{-}26)$$

which is a form of Equation 3-10 that has been rearranged and modified to fit the results of laboratory calibration chamber tests on sands.

EFFECTIVE HORIZONTAL STRESS IN COHESIVE SOILS

As noted previously, soils retain a "memory" of preconsolidation. With vertical stresses, this memory is reflected by the preconsolidation stress ($\bar{\sigma}_p$) which, in OC soils, is greater than the effective overburden stress ($\bar{\sigma}_{vo}$). In the horizontal direction, the process is somewhat different, because the soil can not unload as freely as it can in the vertical direction. The result is that the retained memory of the maximum horizontal effective stress is less clear. If the soil is young and has experienced only a relatively simple stress history, then the procedures described earlier under "Reconstruction of Stress History" can be used to evaluate the horizontal effective stress in terms of K_o, defined as $\bar{\sigma}_{ho}/\bar{\sigma}_{vo}$. For older soils or soils with more complex stress history, the reconstruction process can be more difficult. By default in these cases, it may be necessary to assume only primary unloading, as shown in Figure 3-2. This assumption will result in an upper bound on K_o, which must be used with some considered engineering judgment, taking into account the loading level and differences between the virgin loading and primary unloading values of K_o.

Alternatively, K_o may be estimated from index parameters or correlations with in-situ measurements. Ideally, these approaches reflect the soil in-situ and therefore should be good indicators of the current K_o. However, all correlations contain uncertainties and must be considered within the context of the stress history of the soil. The predicted K_o should be consistent with this information.

Correlations with Index Parameters

A number of studies have attempted to correlate K_o with the Atterberg limits. Figure 3-22 shows one of these relationships for NC clay. As shown, organic clays should be excluded from the general trend. For OC soils, an early study demonstrated the behavior shown in Figure 3-23, with the overconsolidation ratio (OCR) dominating the resulting K_o value. These two figures suggest a high degree of correlation with the Atterberg limits. However, more comprehensive data compilations show the lack of correlation given in Figure 3-24, which has an r^2 equal to 0.147.

One simple alternative estimator is to assume overconsolidation by simple unloading, which was described previously as:

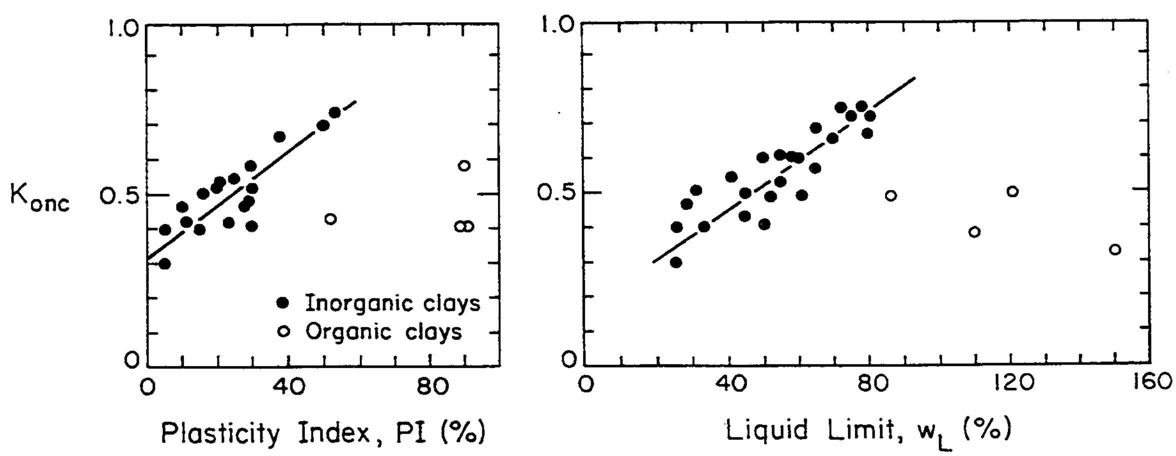

Figure 3-22. K_{onc} Correlated with Atterberg Limits

Source: Larsson (37), p. 21.

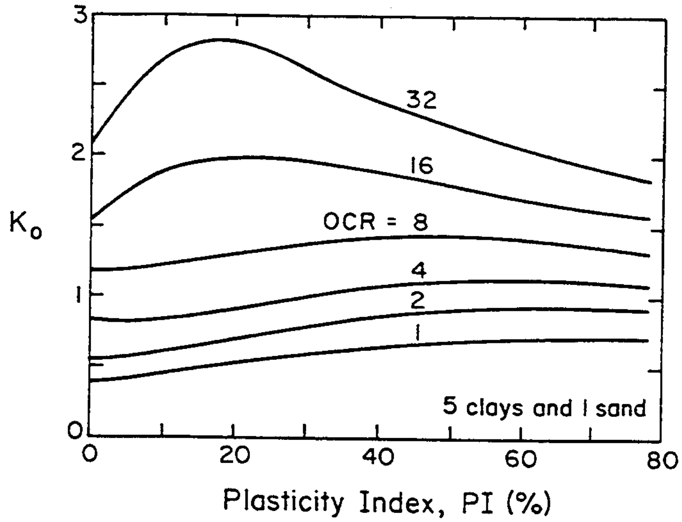

Figure 3-23. K_o Correlated with PI and OCR

Source: Brooker and Ireland (38), p. 14.

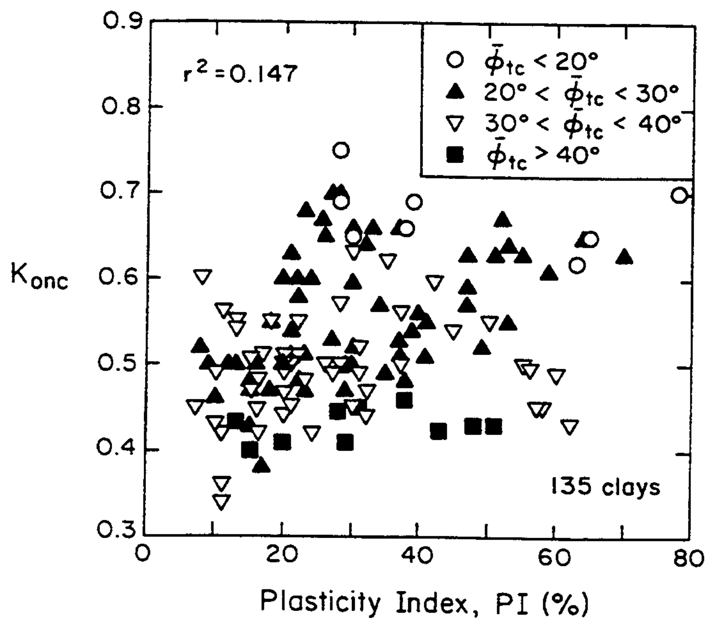

Figure 3-24. Apparent Lack of Trend Between K_{onc} and PI for 135 Clay Soils

$$K_o = (1 - \sin \bar{\phi}_{tc})\ OCR^{\sin \bar{\phi}_{tc}} \tag{3-10}$$

Figure 3-25 illustrates this approach for 48 clay soils. Also, the following approximation was given earlier:

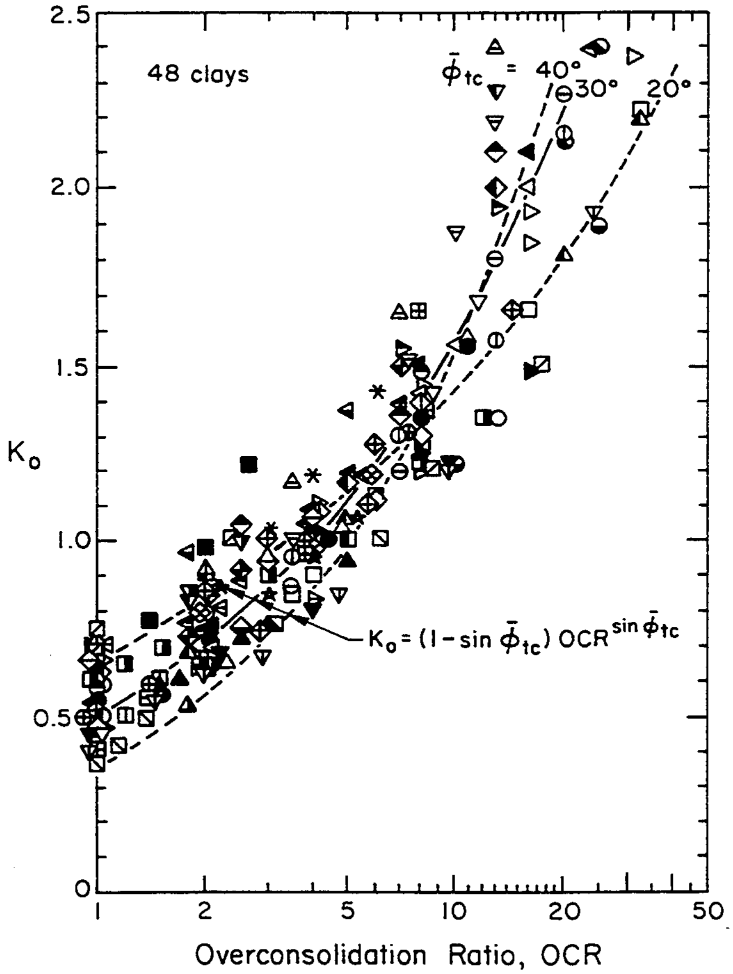

Figure 3-25. K_o Correlated with OCR

Source: Data from Mayne and Kulhawy (1).

$$OCR = (p_a/\bar{\sigma}_{vo})\ 10^{(1.11\ -\ 1.62\ LI)} \qquad (3\text{-}17)$$

By combining these two equations, K_o can be estimated simply from a knowledge of $\bar{\phi}_{tc}$, $\bar{\sigma}_{vo}$, and LI.

One further simplification is to note that $\bar{\phi}_{tc}$ = 30° is a reasonable fit of the data in Figure 3-25. Using this value, Equation 3-10 reduces to:

$$K_o \approx 0.5\ OCR^{0.5} \qquad (3\text{-}27)$$

Then, combining this result with Equation 3-17 yields:

$$K_o \approx 0.5[(p_a/\bar{\sigma}_{vo})^{0.5}\ 10^{(0.56\ -\ 0.81\ LI)}] \tag{3-28}$$

which is a simple, first-order estimator requiring only $\bar{\sigma}_{vo}$ and LI.

If information is available for the undrained shear strength (s_u), then the correlation shown in Figure 3-26 can provide an estimate for K_o.

Direct Correlations with SBPMT and DMT Results

The self-boring pressuremeter test (SBPMT) has shown promise as one of the few devices capable of providing a direct measurement of the in-situ horizontal stress. There is no need for correlations because the stress is measured directly, taking into account equipment calibrations. Figure 3-27 shows results summarized for 56 clays in the literature, in which both K_o and OCR values were given. As can be seen, the trends are consistent with those shown previously (Figure 3-25) for laboratory data. It should be noted that the fissured and intact clays behave similarly when tested with the SBPMT because this test involves an expanding device which compresses the soil and fissures to mimic an intact soil.

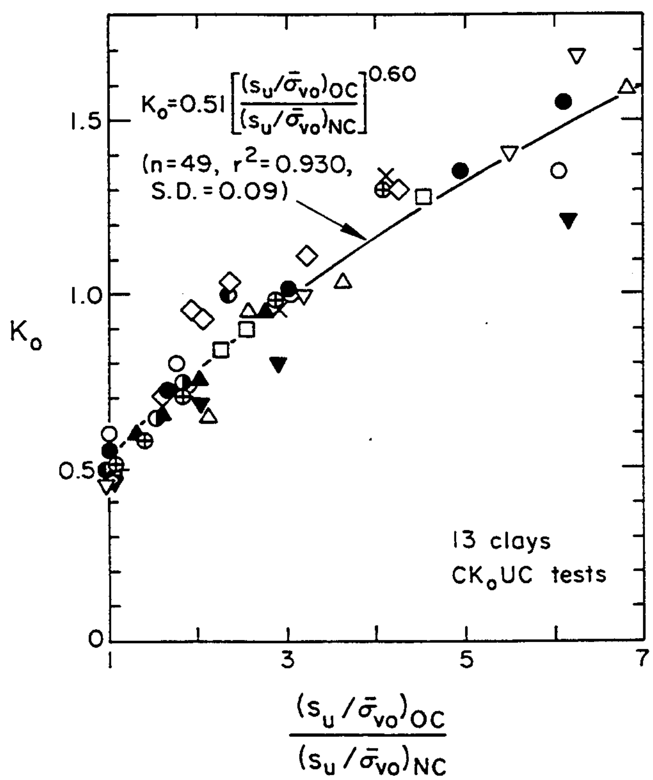

Figure 3-26. K_o Correlated with Undrained Strength Ratio

Source: Modified after Mayne (39).

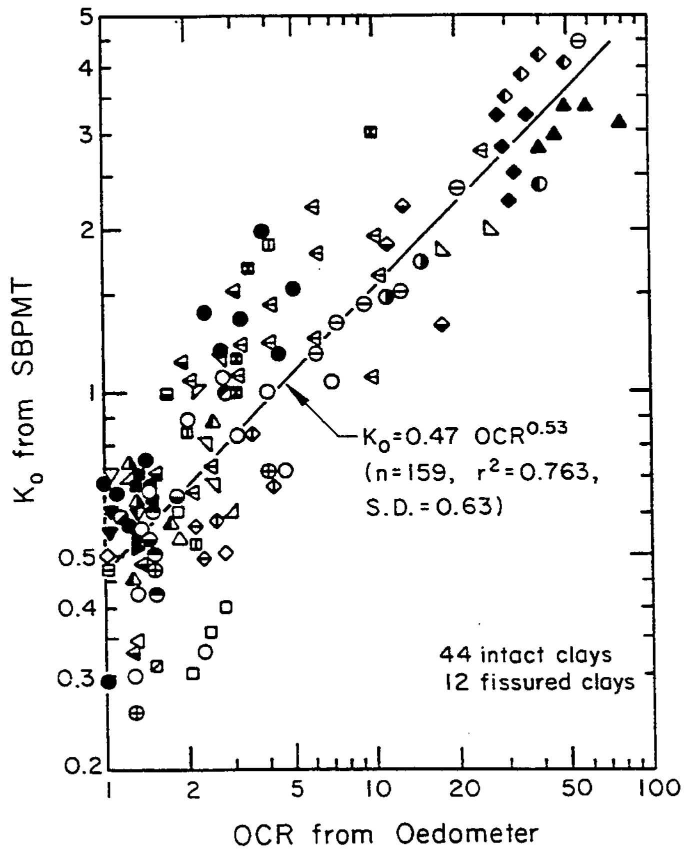

Figure 3-27. K_o from SBPMT Correlated with OCR

Source: Based on Mayne and Kulhawy (25 and 40).

The original intent of the dilatometer test (DMT) was to model the soil modulus for the laterally loaded pile problem, which requires an assessment of the horizontal stress. However, all in-situ testing devices cause some disturbance upon insertion into the ground. Therefore, Marchetti (33) found it necessary to develop a correlation between a best estimate K_o and the DMT horizontal stress index (K_D), as shown in Figure 3-28. The original Marchetti equation was based primarily upon data from insensitive Italian clays and uncemented normally consolidated sands and was given as:

$$K_o = (K_D/1.5)^{0.47} - 0.6 \qquad (3\text{-}29)$$

Powell and Uglow (34) tested heavily overconsolidated and fissured clays from the United Kingdom with the DMT and found that, although the in-situ K_o trended with K_D, the relationship was offset from the original one established for Italian clays. Similarly, Lacasse and Lunne (35) used the DMT at several Norwegian sites

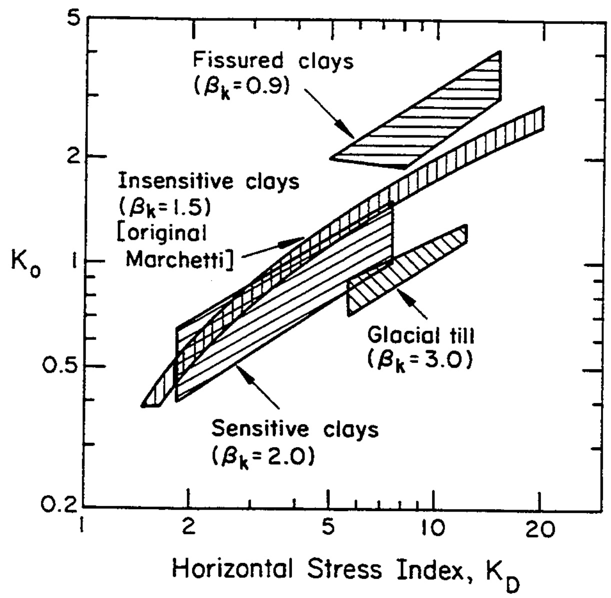

Figure 3-28. K_o Correlated with K_D

Source: Based on Marchetti (33), Powell and Uglow (34), and Lacasse and Lunne (35).

and suggested further modifications to the original Marchetti correlation. Both data sets also are shown in Figure 3-28. Considering these other data, a general equation for K_o is:

$$K_o = (K_D/\beta_k)^{0.47} - 0.6 \qquad (3\text{-}30)$$

in which β_k depends upon soil type and geologic origin.

Where possible, local calibration of the DMT should be made relative to K_o measurements obtained with SBPMT or push-in spade cells. For preliminary estimating purposes, the values of β_k in Figure 3-28 may be used.

Figure 3-29 shows a direct comparison of K_o from the SBPMT with K_D from the DMT. As can be seen, the SBPMT K_o for stiffer clays is higher than the original K_o prediction by Marchetti (33).

Indirect Correlations with SPT, CPT, CPTU, and DMT Results

The standard penetration test (SPT), cone penetration test (CPT), and piezocone test (CPTU) all are measurements of vertical penetration, and therefore they do not address K_o directly. However, vertical penetration is coupled with the horizontal

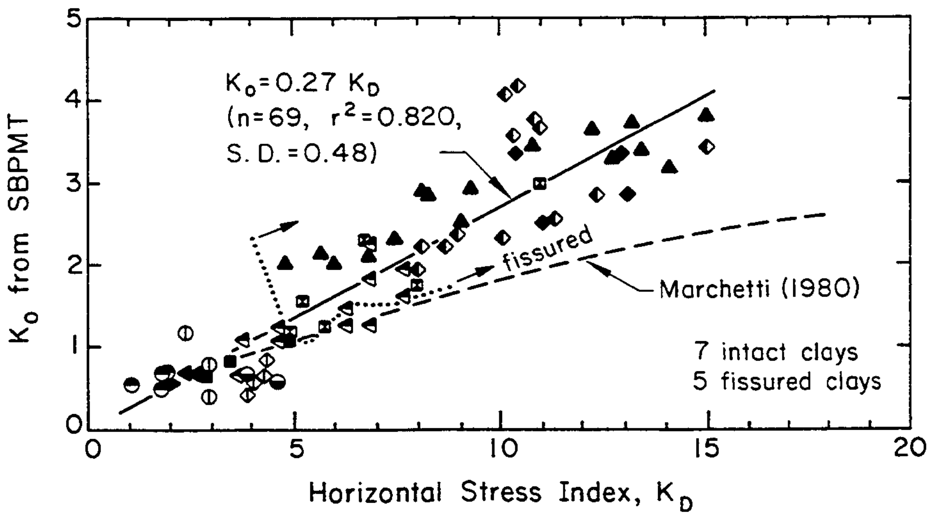

Figure 3-29. K_o from SBPMT Correlated with K_D

Source: Data from Mayne and Kulhawy (25 and 40).

stresses because they control the vertical "stiffness" of the soil and the shearing resistance of the advancing in-situ device. Alternatively, the DMT provides measurements of horizontal total stress. These measurements are taken immediately after penetration of the blade into the clay and, as such, reflect large increases in total horizontal and pore water stresses over the geostatic state of stress. Consequently, the SPT, CPT, CPTU, and DMT provide indirect measurements of K_o.

Figure 3-30 shows the trend of K_o obtained from laboratory tests and DMT, PMT, and SBPMT measurements with the normalized SPT N value. From regression analyses of these data, K_o can be given by the following:

$$K_o = 0.073 \; Np_a/\bar{\sigma}_{vo} \tag{3-31}$$

Figure 3-31 shows the trend of K_o from SBPMT measurements with the normalized cone tip resistance. From these data, K_o can be given by the following:

$$K_o = 0.10(q_T - \sigma_{vo})/\bar{\sigma}_{vo} \tag{3-32}$$

K_o also can be estimated from the piezocone pore water stress, as shown in Figure 3-32. These data show that K_o can be given by:

$$K_o = 0.24 \; \Delta u_t/\bar{\sigma}_{vo} \tag{3-33}$$

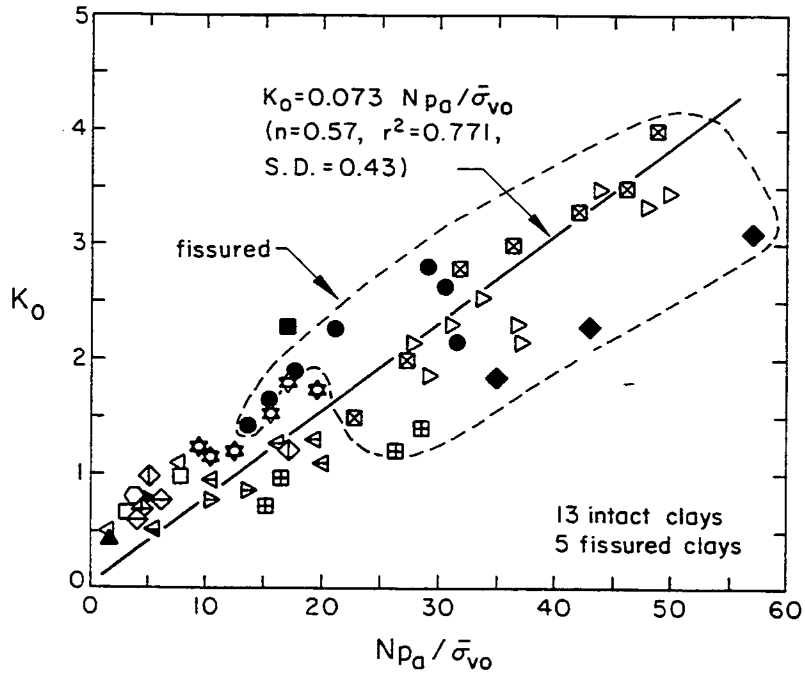

Figure 3-30. K_o Correlated with SPT N

Source: Kulhawy, et al. (41), p. 129.

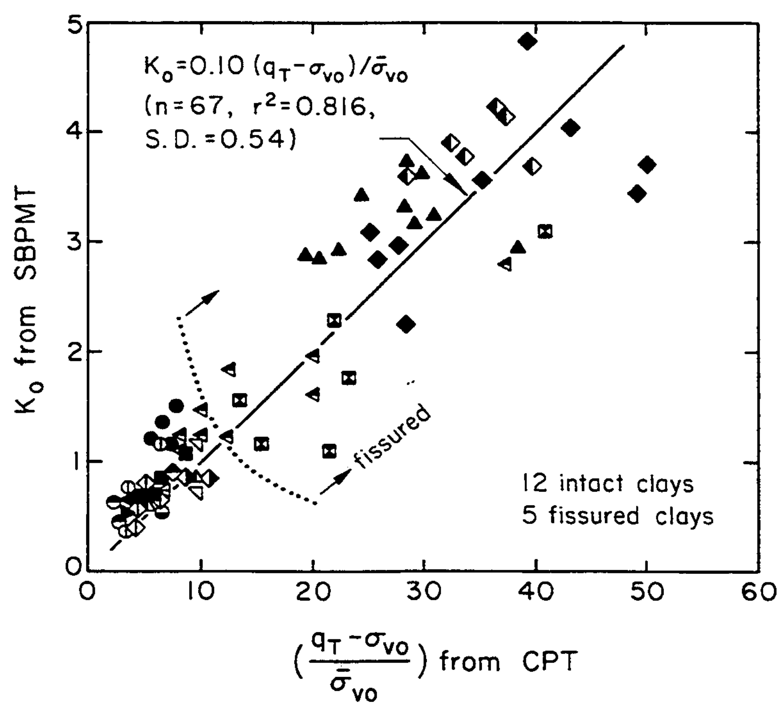

Figure 3-31. K_o Correlated with CPTU q_T

Source: Kulhawy, et al. (41), p. 128, and others (40).

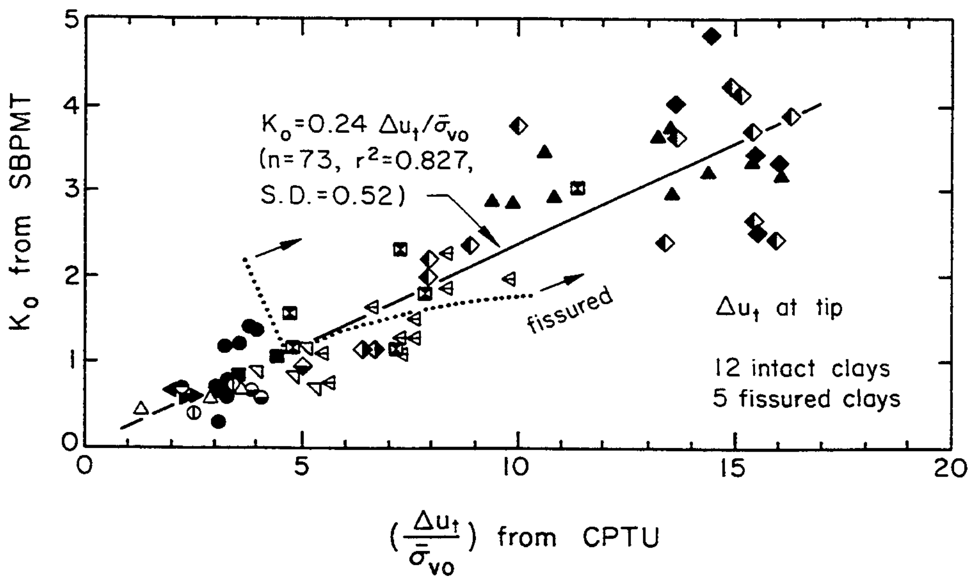

Figure 3-32. K_o Correlated with CPTU Δu

Source: Data from Mayne and Kulhawy (15 and 40).

An example of K_o profiling by several in-situ tests in London clay is presented in Figure 3-33. Measured values from the SBPMT and estimated values using the original Marchetti (33) DMT correlation are given, along with correlations developed from the SPT, CPT, and the liquidity index. Although there is obvious scatter, all of the results are consistent with each other.

EFFECTIVE HORIZONTAL STRESS IN COHESIONLESS SOILS

Cohesionless soils also retain a "memory" of preconsolidation. However, as noted previously, the stress history in cohesionless soils is more difficult to determine because of sampling problems. Therefore, the focus has been almost exclusively on in-situ tests.

Direct Correlations with SBPMT and DMT Results

The self-boring pressuremeter test (SBPMT) has shown promise as one of the few devices capable of providing a direct measurement of the in-situ horizontal stress. As such, there is no need for correlations because the stress ideally is measured directly. However, the SBPMT has not been used widely in cohesionless soils because of the relatively high cost, low productivity, and difficulties in advancing the device in the field.

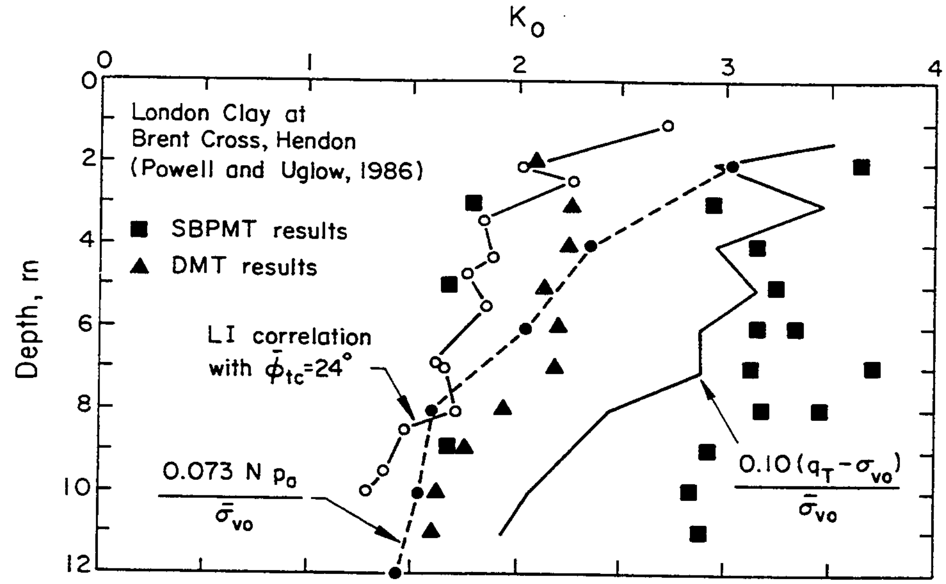

Figure 3-33. Comparison of K_o Values for London Clay at Brent Cross

Source: Kulhawy, et al. (41), p. 129.

One intent of the dilatometer test (DMT) was to provide a measurement of the horizontal soil stress, as noted previously. Unfortunately, all in-situ testing devices cause some disturbance upon insertion into the ground. Therefore, Marchetti (33) found it necessary to develop a correlation between a best estimate K_o and the DMT horizontal stress index (K_D), as shown in Figures 3-28 and 3-29. However, Schmertmann (42) showed by calibration chamber tests that the original relationship should also be dependent upon the effective stress friction angle ($\bar{\phi}_{tc}$), as given in Figure 3-34. Other correlations with CPT results are given below.

Indirect Correlations with SPT and CPT Results

No correlations have been developed to date between K_o and the standard penetration test (SPT) N value. However, it was shown in Section 2 that the N value could be correlated with the cone penetration test (CPT) q_c value. Therefore, the q_c correlations below could be used approximately with N values converted to "equivalent" q_c values.

For the CPT q_c value, Durgunoglu and Mitchell (44) developed a theory to relate the cone factor, K_o, $\bar{\phi}_{tc}$, and depth (D) to diameter (B) ratio. This theory has been used to develop Figure 3-35, from which an estimate of K_o can be made. This figure must be used cautiously because small changes in the cone factor or $\bar{\phi}_{tc}$ can result

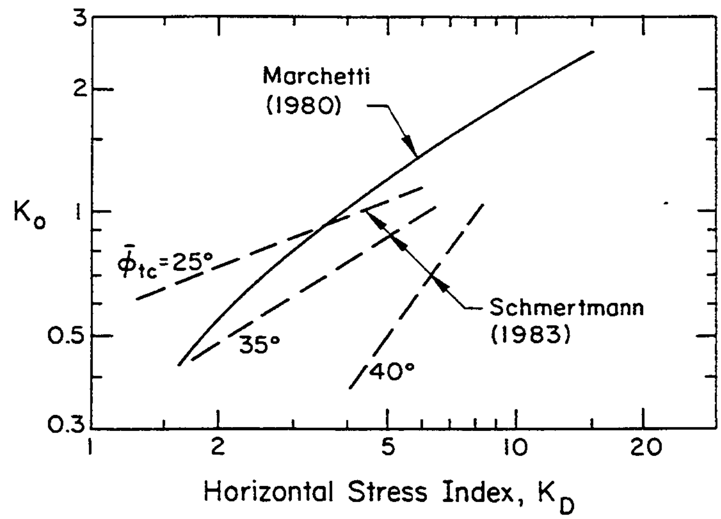

Figure 3-34. K_o Correlated with K_D in Sands

Source: Marchetti (43), p. 2668.

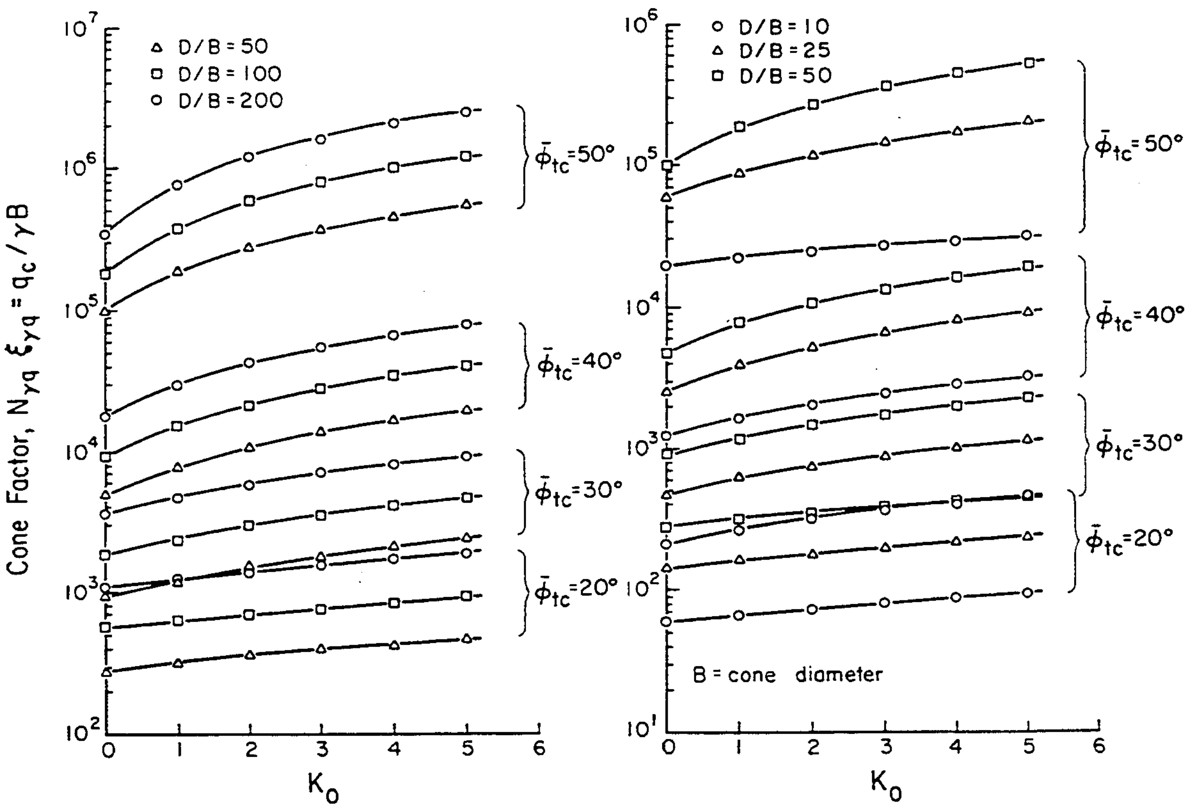

Figure 3-35. Cone Factor versus K_o as a Function of $\bar{\phi}_{tc}$ and D/B

in large K_o changes. However, careful use of this figure with a good knowledge of the soil stress history can result in reasonable K_o predictions. An example using this approach is given in Figure 3-36.

Marchetti (43) also used this theory and developed a more simplified relationship, as shown in Figure 3-37. In this figure, B = 35.7 mm for a standard cone was introduced. Note that these curves also are quite flat, and that small changes in the input parameters can give large K_o changes.

Combined DMT/CPT Approach for K_o of Sands

In a novel approach, the combined results of DMT and CPT calibration chamber tests on laboratory-prepared sand (Figure 3-38) indicated a best fit expression for K_o in terms of both the horizontal stress index (K_D) and normalized cone tip resistance ($q_c/\bar{\sigma}_{vo}$), as given below:

$$K_o = 0.359 + 0.071\ K_D - 0.00093\ (q_c/\bar{\sigma}_{vo}) \qquad (3\text{-}34)$$

This equation was modified to account for field CPT and DMT measurements obtained in a natural sand deposit. The differences between the laboratory and field relationships may be a result of aging effects. This phenomenon of aging is quite important, but it is not very well understood at present, as noted in Section 2.

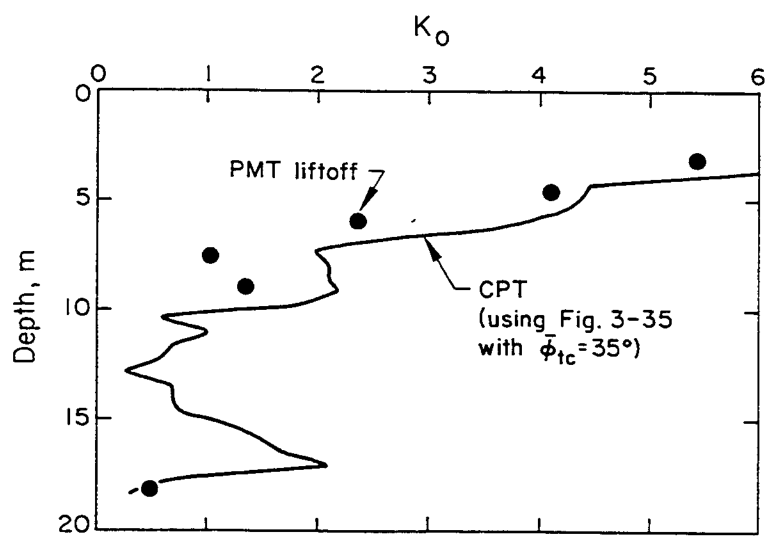

Figure 3-36. Estimation of K_o in Coastal Plain Sand from CPT

Source: Kulhawy, et al. (41), p. 130.

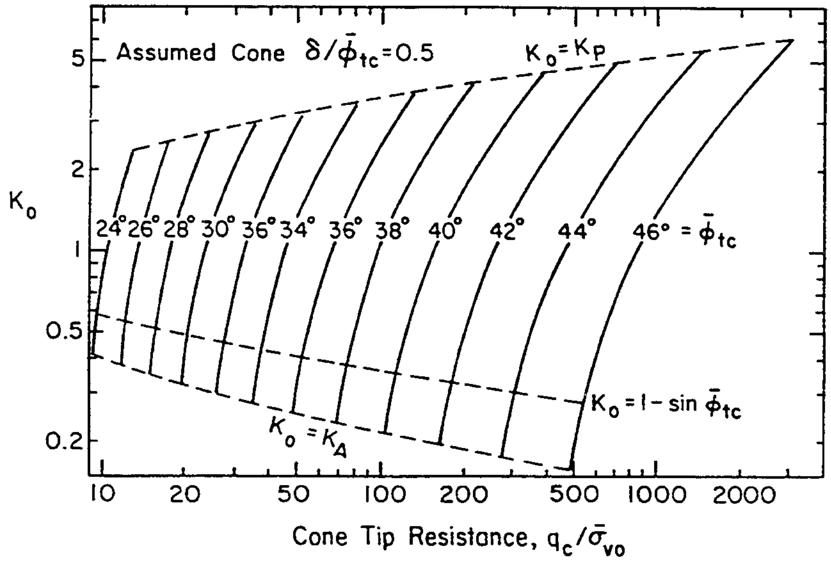

Figure 3-37. Simplified q_c - K_o - $\bar{\phi}_{tc}$ Relationships

Source: Marchetti (43), p. 2668.

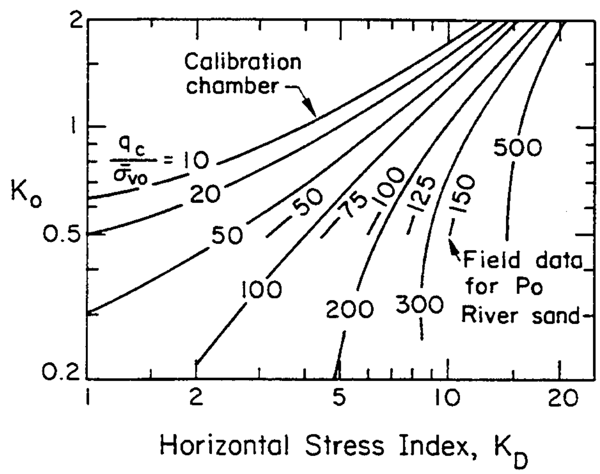

Figure 3-38. K_o Correlated with q_c and K_D

Source: Marchetti (43), p. 2672.

Empirical Approach

Data from CPT studies using electric cones in calibration chamber tests (e.g., Appendix H) indicate that the initial effective horizontal stress ($\bar{\sigma}_{ho}$) is more influential on the magnitude of q_c than the vertical stress. Furthermore, the relationship between $\bar{\sigma}_{ho}$ and q_c appears to be independent of OCR. The advantages of using laboratory chamber tests include known stress state, stress history, and in-place density prior to penetration.

A tentative evaluation of the calibration chamber data is shown in Figure 3-39, indicating a general trend between $\bar{\sigma}_{ho}$, q_c, and D_r. The value of $\bar{\sigma}_{ho}$ is the imposed effective horizontal stress prior to cone penetration. With this figure, measured values of q_c and D_r are used to obtain $\bar{\sigma}_{ho}$, as given below:

$$\frac{\bar{\sigma}_{ho}}{p_a} = \frac{(q_c/p_a)^{1.25}}{35 \exp(D_r/20)} \qquad (3\text{-}35)$$

Once $\bar{\sigma}_{ho}$ is known, K_o can be computed from $\bar{\sigma}_{ho}/\bar{\sigma}_{vo}$.

Application of this empirical approach for estimating in-situ K_o from CPT data in an overconsolidated sand near Stockholm is shown in Figure 3-40. The stress history of this sand has been documented well in the literature, and Equation 3-34 was

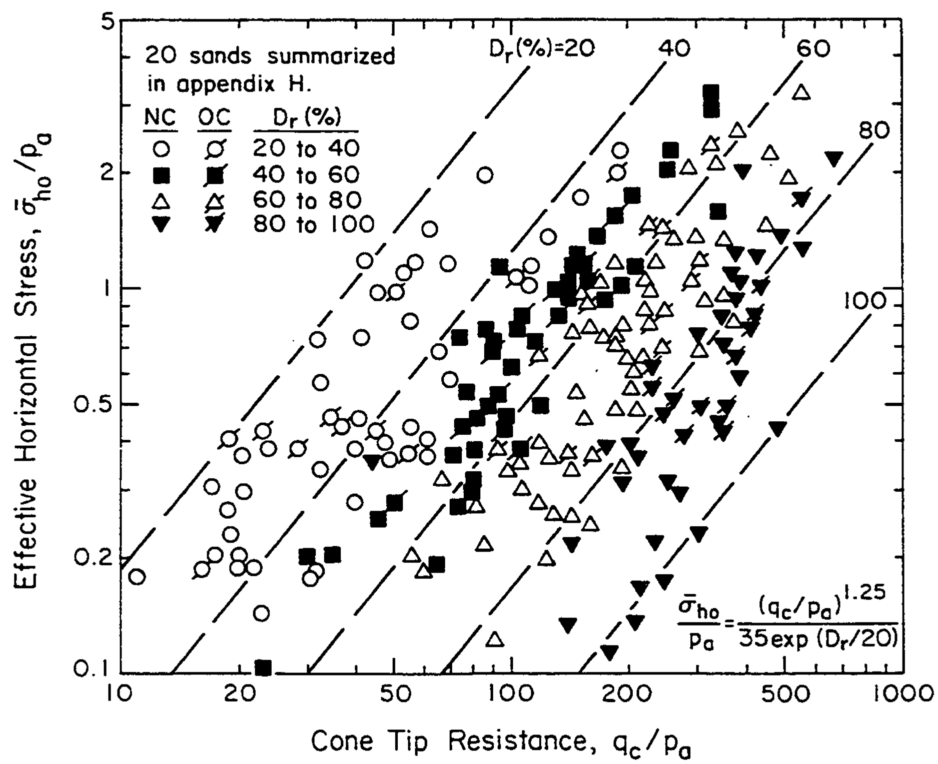

Figure 3-39. Tentative Correlation Between $\bar{\sigma}_{ho}$, q_c, and D_r for NC and OC Sands Tested in Calibration Chambers

Source: Kulhawy, et al. (41), p. 132.

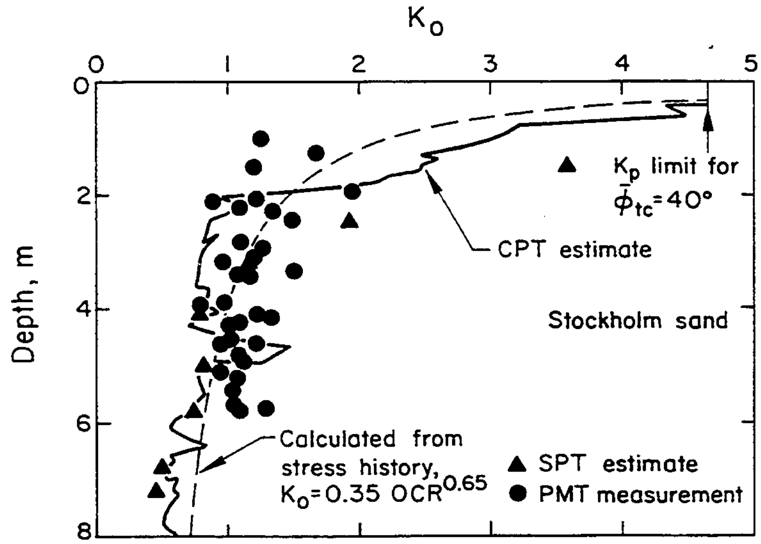

Figure 3-40. Comparison of K_o Values at Stockholm Site

Source: Kulhawy, et al. (41), p. 132.

used to evaluate the in-situ K_o. As can be seen, the agreements are quite good.

The CPT approach may be extended to SPT results through an approximate correlation between the cone tip resistance and N value. The ratio of q_c to N has been correlated to mean particle size (expressed as D_{50}), as shown in Figure 2-30. For the Stockholm site, the value of D_{50} averages about 0.9 $\pm$ 0.1 mm, suggesting a q_c/N ratio of about 6.5. This conversion has been used to estimate a profile of K_o from SPT data using the CPT empirical procedure. Figure 3-40 shows reasonable agreement between the profiles of K_o estimated from CPT and SPT resistances and values determined from the known stress history and PMT data.

REFERENCES

1. Mayne, P. W. and Kulhawy, F. H., "K_o - OCR Relationships in Soil", Journal of the Geotechnical Engineering Division, ASCE, Vol. 108, No. GT6, June 1982, pp. 851-872.

2. Jáky, J., "The Coefficient of Earth Pressure at Rest", Journal of the Society of Hungarian Architects and Engineers, Budapest, Oct. 1944, pp. 355-358.

3. Schmidt, B., Discussion of "Earth Pressures at Rest Related to Stress History", Canadian Geotechnical Journal, Vol. 3, No. 4, Nov. 1966, pp. 239-242.

4. Mayne, P. W., Discussion of "C_α/C_c Concept and K_o During Secondary Compression", Journal of Geotechnical Engineering, ASCE, Vol. 115, No. 2, Feb. 1988, pp. 267-270.

5. Stas, C. V. and Kulhawy, F. H., "Critical Evaluation of Design Methods for Foundations Under Axial Uplift and Compression Loading", Report EL-3771, Electric Power Research Institute, Palo Alto, Nov. 1984, 198 p.

6. NAVFAC, Soil Mechanics (DM 7.1), Naval Facilities Engineering Command, Alexandria, 1982, 355 p.

7. Wood, D. M., "Index Properties and Critical State Soil Mechanics", Proceedings, Symposium on Recent Developments in Laboratory and Field Tests and Analysis of Geotechnical Problems, Bangkok, Dec. 1983, pp. 301-309.

8. Hansbo, S., "A New Approach to the Determination of Shear Strength of Clay by the Fall Cone Test", Report 14, Swedish Geotechnical Institute, Stockholm, 1957.

9. Mayne, P. W. and Mitchell, J. K., "Profiling of Overconsolidation Ratio in Clays by Field Vane", Canadian Geotechnical Journal, Vol. 25, No. 1, Feb. 1988, pp. 150-157.

10. Marsland, A., "Design Parameters for Stiff Clays", Proceedings, European Conference on Soil Mechanics and Foundation Engineering, Vol. 5, Brighton, 1979, pp. 159-162.

11. Mayne, P. W. and Kemper, J. B., "Profiling OCR in Stiff Clays by CPT and SPT", Geotechnical Testing Journal, ASTM, Vol. 11, No. 2, June 1988, pp. 139-147.

12. Garrett, C. and Barnes, S. J., "The Design and Performance of the Dunton Green Retaining Wall", Geotechnique, Vol. 34, No. 4, Dec. 1984, pp. 533-548.

13. Mayne, P. W., "CPT Indexing of In-Situ OCR in Clays", Use of In-Situ Tests in Geotechnical Engineering (GSP 6), Ed. S. P. Clemence, ASCE, New York, 1986, pp. 780-789.

14. Campanella, R. G. and Robertson, P. K., "Current Status of the Piezocone Test", Proceedings, 1st International Symposium on Penetration Testing (ISOPT-1), Vol. 1, Orlando, 1988, pp. 93-116.

15. Lunne, T., Eidsmoen, T., Powell, J., and Quarterman, R., "Piezocone Testing in Overconsolidated Clays", Proceedings, 39th Canadian Geotechnical Conference, Ottawa, 1986, pp. 209-218.

16. Mahar, L. and O'Neill, M. W., "Geotechnical Characteristics of Desiccated Clay", Journal of Geotechnical Engineering, ASCE, Vol. 109, No. 1, Jan. 1983, pp. 56-71.

17. Mayne, P. W. and Frost, D. D., "Geotechnical Report, White House Communications Agency, Anacostia, Washington, D.C.", Report W6-5523, Law Engineering, McLean, 1986, 95 p.

18. Powell, J. J. M., Quarterman, R., and Lunne, T., "Interpretation and Use of the Piezocone Test in U.K. Clays", Penetration Testing in the U.K., Thomas Telford, London, 1988, pp. 47-52.

19. Rad, N. S. and Lunne, T., "Direct Correlation Between Piezocone Test Results and Undrained Shear Strength of Clay", Proceedings, 1st International Symposium on Penetration Testing (ISOPT-1), Vol. 2, Orlando, 1988, pp. 911-917.

20. Tavenas, F. and Leroueil, S., "State-of-the-Art on Laboratory and In-Situ Stress-Strain-Time Behavior of Soft Clays", Proceedings, International Symposium on Geotechnical Engineering of Soft Soils, Mexico City, 1987, pp. 1-46.

21. Mayne, P. W. and Holtz, R. D., "Profiling Stress History from Piezocone Soundings", Soils and Foundations, Vol. 28, No. 1, Mar. 1988, pp. 16-28.

22. LaRochelle, P., Zebdi, M., Leroueil, S., Tavenas, F., and Virely, D., "Piezocone Tests in Sensitive Clays of Eastern Canada", Proceedings, 1st International Symposium on Penetration Testing (ISOPT-1), Vol. 2, Orlando, 1988, pp. 831-841.

23. Mayne, P. W. and Bachus, R. C., "Penetration Pore Pressures in Clay from CPTU, DMT, and SBP", Proceedings, 12th International Conference on Soil Mechanics and Foundation Engineering, Vol. 1, Rio de Janeiro, 1989, pp. 291-294.

24. Lukas, R. G. and de Bussy, B., "Pressuremeter and Laboratory Test Correlations for Clays", Journal of the Geotechnical Engineering Division, ASCE, Vol. 102, No. GT9, Sept. 1976, pp. 945-962.

25. Mayne, P. W. and Kulhawy, F. H., Discussion of "Independence of Geostatic Stress from Overconsolidation in Some Beaufort Sea Clays", Canadian Geotechnical Journal, Vol. 25, No. 3, Aug. 1988, pp. 617-621.

26. Powell, J. J. M. and Uglow, I. M., "Marchetti Dilatometer Testing in U.K. Soils", Proceedings, 1st International Symposium on Penetration Testing (ISOPT-1), Vol. 1, Orlando, 1988, pp. 555-562.

27. Mayne, P. W., "Determining Preconsolidation Stress and Penetration Pore Pressures from DMT Contact Pressures", Geotechnical Testing Journal, ASTM, Vol. 10, No. 3, Sept. 1987, pp. 146-150.

28. Mayne, P. W., "Determining OCR in Clays from Laboratory Strength", Journal of Geotechnical Engineering, ASCE, Vol. 114, No. 1, Jan. 1988, pp. 76-92.

29. Wroth, C. P., "Penetration Testing - A Rigorous Approach to Interpretation", Proceedings, 1st International Symposium on Penetration Testing (ISOPT-1), Vol. 1, Orlando, 1988, pp. 303-311.

30. Mayne, P. W., "Cavity Expansion/Critical-State Theory for Piezocone Penetration in Clays", submitted for review in 1990.

31. Robertson, P. K., Campanella, R. G., Gillespie, D., and Greigs, J., "Use of Piezometer Cone Data", Use of In-Situ Tests in Geotechnical Engineering (GSP 6), Ed. S. P. Clemence, ASCE, New York, 1986, pp. 1263-1280.

32. Mayne, P. W. and Bachus, R. C., "Profiling OCR in Clays by Piezocone Soundings", Proceedings, 1st International Symposium on Penetration Testing (ISOPT-1), Vol. 2, Orlando, 1988, pp. 857-864.

33. Marchetti, S., "In-Situ Tests by Flat Dilatometer", Journal of the Geotechnical Engineering Division, ASCE, Vol. 106, No. GT3, Mar. 1980, pp. 299-321.

34. Powell, J. J. M. and Uglow, I. M., "Dilatometer Testing in Stiff Overconsolidated Clays", Proceedings, 39th Canadian Geotechnical Conference, Ottawa, 1986, pp. 317-326.

35. Lacasse, S. and Lunne, T., "Calibration of Dilatometer Correlations", Proceedings, 1st International Symposium on Penetration Testing (ISOPT-1), Vol. 1, Orlando, 1988, pp. 539-548.

36. Bullock, P., "The Dilatometer: Current Test Procedures and Data Interpretation", Civil Engineering Report, University of Florida, Gainesville, 1983, 308 p.

37. Larsson, R., "Basic Behavior of Scandinavian Soft Clays", Report 4, Swedish Geotechnical Institute, Linkoping, 1977, 125 p.

38. Brooker, E. W. and Ireland, H. O., "Earth Pressures at Rest Related to Stress History", Canadian Geotechnical Journal, Vol. 2, No. 1, Feb. 1965, pp. 1-15.

39. Mayne, P. W., "K_o-$c_u/\bar{\sigma}_{vo}$ Trends for Overconsolidated Clays", Journal of Geotechnical Engineering, ASCE, Vol. 110, No. 10, Oct. 1984, pp. 1511-1516.

40. Mayne, P. W. and Kulhawy, F. H., "Direct and Indirect Determinations of In-Situ K_o in Clays", Research Record xxxx, Transportation Research Board, Washington, 1990, in press.

41. Kulhawy, F. H., Jackson, C. S., and Mayne, P. W., "First-Order Estimation of K_o in Sands and Clays", Foundation Engineering: Current Principles and Practices, Ed. F. H. Kulhawy, ASCE, New York, 1989, pp. 121-134.

42. Schmertmann, J. H., DMT Digest No. 1, GPE Inc., Gainesville, 1983, 3 p.

43. Marchetti, S., "On the Field Determination of K_o in Sand", Proceedings, 11th International Conference on Soil Mechanics and Foundation Engineering, Vol. 5, San Francisco, 1985, pp. 2667-2672.

44. Durgunoglu, H. T. and Mitchell, J. K., "Static Penetration Resistance of Soils", Proceedings, ASCE Specialty Conference on In-Situ Measurement of Soil Properties, Vol. 1, Raleigh, 1975, pp. 151-189.

Section 4

STRENGTH

A knowledge of the strength of soils is necessary for most geotechnical analyses. From a foundation engineering standpoint, the strength is necessary primarily to evaluate the capacity. However, soil strength varies with many parameters, and therefore it is not uniquely defined. In this section, basic definitions are presented first to establish the general background, notation, and relevance of the strength tests to field conditions. Then methods for estimating the effective stress friction angle are presented, first for cohesionless soils and second for cohesive soils. For each soil type, typical values, influencing factors, and in-situ test correlations are presented. Finally, methods for estimating the undrained shear strength are presented, including typical values, influencing factors, and in-situ test correlations.

BASIC DEFINITIONS

The strength of soils commonly is expressed by the Coulomb-Mohr failure criterion, as illustrated in Figure 4-1. For this criterion, failure is given by:

$$\tau = c + \sigma \tan \phi \qquad (4\text{-}1)$$

in which τ = shear stress at failure (i.e., shear strength), c = cohesion intercept, σ = normal stress, and ϕ = friction angle.

Effective Stress Analysis

Although Equation 4-1 is the general form of the criterion, it is rarely appropriate to use the complete equation. Instead, the criterion is used in two alternative forms. First, when effective stress analyses of cohesionless or cohesive soils are conducted, Equation 4-1 is expressed as:

$$\tau = \bar{\sigma} \tan \bar{\phi} \qquad (4\text{-}2)$$

in which $\bar{\sigma}$ = effective normal stress and $\bar{\phi}$ = effective stress friction angle, as shown in Figure 4-2.

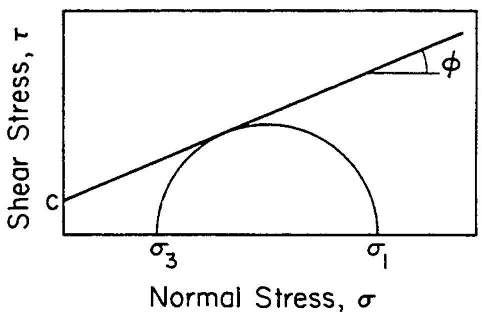

Figure 4-1. General Coulomb-Mohr Failure

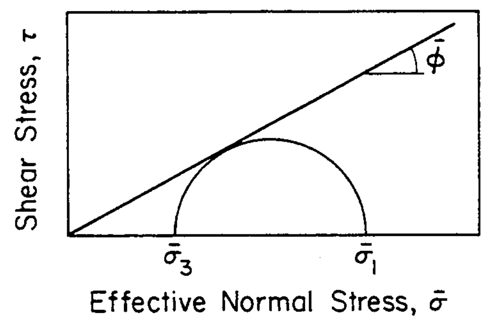

Figure 4-2. Effective Stress Coulomb-Mohr Failure

No effective stress cohesion intercept ($\bar{c}$) is shown because it occurs only in special cases, such as with truly cemented soils, partially saturated soils, and heavily overconsolidated clays, in which $\bar{c}$ is interpreted as gradually decaying with time on an engineering time-scale. For these special cases, $\bar{c}$ could be included in Equation 4-2. However, it is prudent to seek expert geotechnical advice before considering use of $\bar{c}$ for design.

Many times, effective stress laboratory test data are interpreted incorrectly to show a moderately high $\bar{c}$ and an unrealistically low $\bar{\phi}$ because the true failure envelope curvature is not being addressed. Figure 4-3 shows actual curved failure envelopes, with $\bar{c} = 0$, for a wide range of soils from clay to rockfill. Linear interpretation of any of these data over a limited stress range would suggest a $\bar{c}$ and $\bar{\phi}$, but these values would not be the true soil strength parameters.

The friction angle of soils also varies with many other factors, as will be described throughout this section. For a given soil at a constant normal effective stress ($\bar{\sigma}$), the friction angle varies with density state and strain, as shown in Figure 4-4. Expressing $\bar{\phi}$ in terms of the effective major and minor principal stresses ($\bar{\sigma}_1$ and $\bar{\sigma}_3$, respectively) gives:

$$\sin \bar{\phi} = \frac{(\bar{\sigma}_1/\bar{\sigma}_3)_f - 1}{(\bar{\sigma}_1/\bar{\sigma}_3)_f + 1} = \frac{(\bar{\sigma}_1 - \bar{\sigma}_3)_f}{(\bar{\sigma}_1 + \bar{\sigma}_3)_f} \qquad (4\text{-}3)$$

in which the subscript f represents failure conditions.

Different peak friction angles ($\bar{\phi}_p$) develop as a function of soil density state. At one limit is the very dense cohesionless soil or the heavily overconsolidated

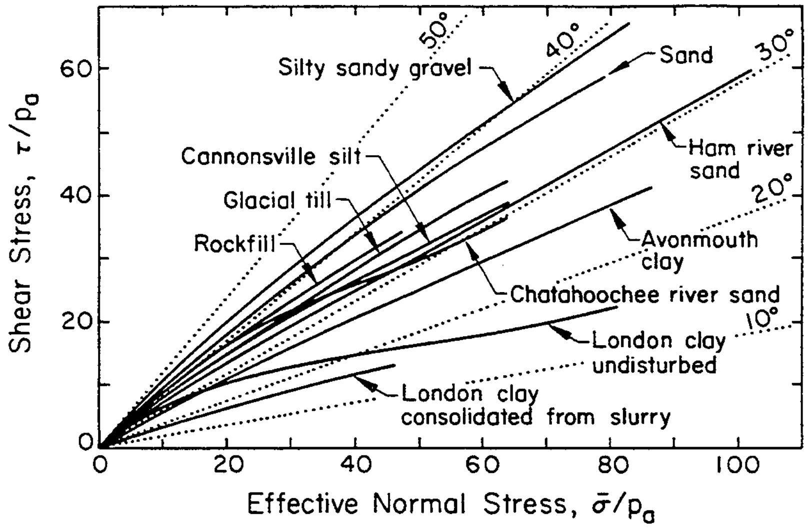

Figure 4-3. Strength Envelopes for a Range of Soil Types

Source: Bishop (1), p. 104.

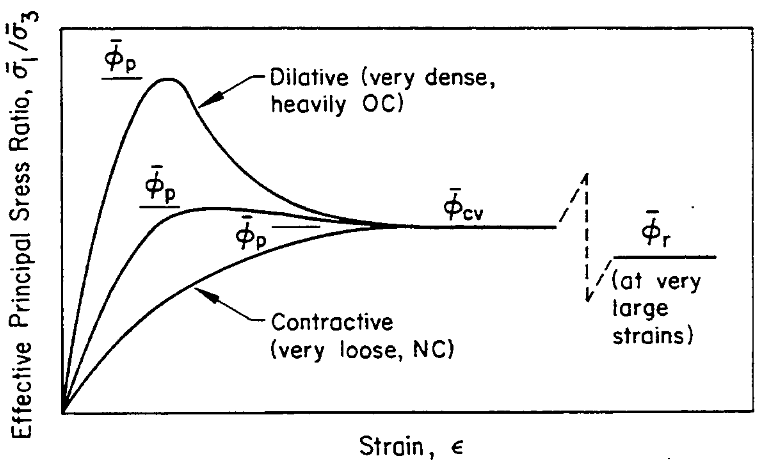

Figure 4-4. Friction Angle Definitions

cohesive soil which exhibits strongly dilative behavior during shear. For these soils, the peak friction angle is high, and it develops at very small strains, typically on the order of a few percent. At the other limit is the very loose cohesionless soil or the normally consolidated, insensitive, uncemented, cohesive soil, which exhibits contractive behavior during shear. For these soils, the peak friction angle is lower, and it develops at larger strains, typically upwards of 10 to 20 percent. The difference between these limits occurs because of the volume change behavior during shear (dilative to contractive). Different behavior is noted for sensitive, cemented, and other structured cohesive soils, which normally peak at small strains, much like the intermediate curve in Figure 4-4.

As a dilative soil is strained past its peak, it strain-softens to a limiting state known as the fully-softened or critical void ratio state ($\bar{\phi}_{cv}$). The contractive soil strain-hardens to reach the critical void ratio state, which also corresponds to its peak friction angle. The critical state ($\bar{\phi}_{cv}$) typically occurs at strains upwards of 10 to 20 percent. Therefore, regardless of the initial density state, $\bar{\phi}_{cv}$ is unique for a given soil at a constant normal effective stress.

With subsequent large straining in cohesive soils, typically in excess of 100 percent, $\bar{\phi}_{cv}$ is gradually reduced to an ultimate limit known as the residual state ($\bar{\phi}_r$). The resulting $\bar{\phi}_r$ is commonly several degrees lower than $\bar{\phi}_{cv}$. For cohesionless soils, $\bar{\phi}_r$ is essentially equal to $\bar{\phi}_{cv}$. The residual state would be considered in foundation engineering only for very large strain problems, such as siting in soils containing pre-existing shear failures. Common examples would be landslide debris or slopes in stiff-fissured clays.

Total Stress Analysis

The second use of Equation 4-1 is defined as the total stress (or $\phi = 0$) analysis of cohesive soils, given by:

$$\tau = c = c_u = s_u \tag{4-4}$$

in which all four terms can be used interchangeably to represent the undrained shear strength of the soil. This relationship is shown in Figure 4-5. Also in this figure, q_u is defined as the unconfined compressive strength = 2 s_u.

In many older references, the term "cohesion" was used to designate s_u. In recent

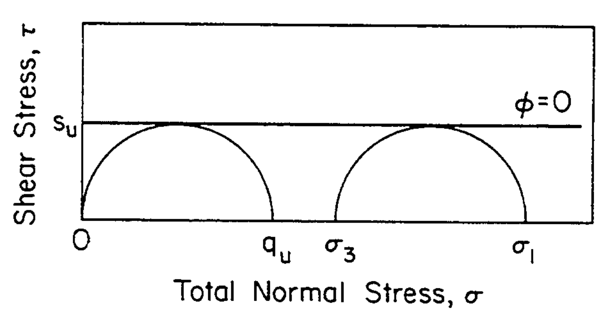

Figure 4-5. Total Stress Coulomb-Mohr Failure

references, s_u is referred to as the undrained shear strength or undrained shearing resistance. The older definition has led to much confusion and misinterpretation with the effective stress cohesion intercept ($\bar{c}$).

Total stress analysis normally is adopted for simplicity. In reality, the failure of all soils (sands, silts, and clays) occurs on the effective stress envelope shown in Figure 4-2. In low permeability soils such as clays, loading generates changes in pore water stresses (Δu). These pore water stresses change the effective stresses, which in turn influence the state of stress relative to the effective stress envelope. Since the total stress loading path and the magnitude of the changes in pore water stresses may not be known with confidence, a total stress analysis provides a simple analysis alternative. However, it must be remembered that s_u includes $\bar{\phi}$ and Δu, and it varies with stress level in-situ. Therefore, s_u must be determined carefully to represent the in-situ conditions at a particular depth, as described in detail later in this section.

Relevance of Laboratory Strength Tests to Field Conditions

The strength of soils can be measured by a number of different laboratory strength tests, as noted previously in Figure 1-1. Each of these tests will give different results because each subjects the soil to different boundary conditions and loading stress paths.

In the field, different elements of soil also will be subjected to different boundary conditions and loading stress paths. Figure 4-6 shows a number of common field loading cases and the test types pertinent for each case. For an embankment loading, the bearing capacity is represented most correctly by a combination of compression (PSC or TC), direct simple shear (DSS), and extension (PSE or TE) tests along the potential shear surface noted. For ease in computation, an average of these three test types normally is used. With a loaded wall, the direct simple shear and extension test types are averaged. With a vertical cut, the compression test is most relevant.

When addressing foundations, different strengths are appropriate for different field loading and behavior modes. These modes are described in detail by Kulhawy, et al. (2). For a drilled shaft in compression, the tip resistance can be evaluated from an average of the triaxial compression, direct simple shear, and triaxial extension tests. The side resistance is modeled by the direct simple shear test up to first yield or slippage along the interface, after which direct shear is more appropriate. The results of these two tests are similar, so they commonly are used

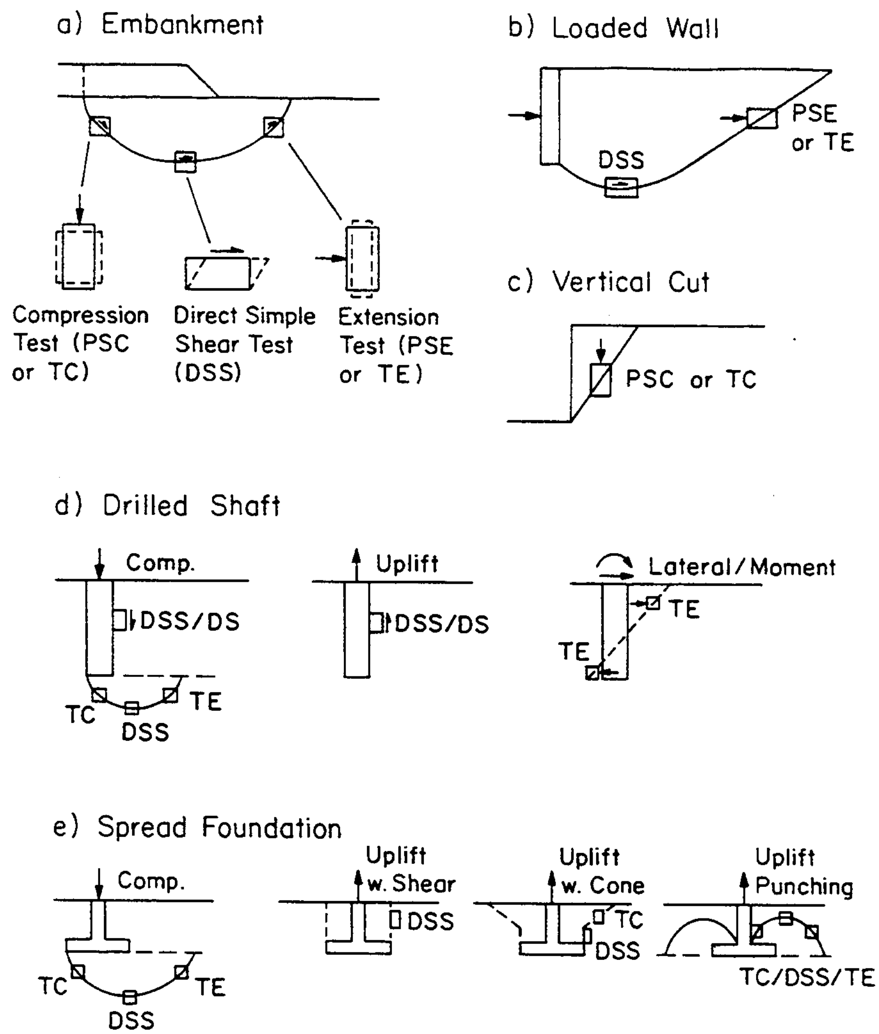

Note: Plane strain tests (PSC/PSE) used for long features
Triaxial tests (TC/TE) used for near symmetrical features
Direct shear (DS) normally substituted for DDS to evaluate $\bar{\phi}$

Figure 4-6. Relevance of Laboratory Strength Tests to Field Conditions

where they are best-suited, the DS being used for sands with the DSS being used for clays. For a shaft in uplift, the side resistance is the same as in compression. For lateral or moment loading, triaxial extension is more appropriate.

For spread foundations in compression, the same bearing capacity approach is used. In uplift, the behavior can range from the normal situation of a vertical shear surface to a vertical shear with cone breakout to a punching limit controlled by bearing capacity. As noted in the figure, the shear case is given by the DSS. The cone case is an average of TC and DSS. The punching is evaluated using an average of TC, DSS, and TE.

The various tests pertinent for a particular field condition are likely to be an excessive requirement for common and routine design cases. Therefore, it is more convenient to establish a standard "test of reference" which would be appropriate for many design cases, and which would be simple and expedient from a commercial testing standpoint. The recommended test (e.g., Wroth, 3) is the isotropically consolidated, triaxial compression test for undrained loading (CIUC) and for drained loading (CIDC). Using the results of this test as a standard reference, the results of all other tests can be compared simply and conveniently.

It should be noted that most soils in-situ actually will be consolidated anisotropically. This difference in consolidation stresses has no appreciable influence on the soil friction angle ($\bar{\phi}$). However, it does influence the evaluation of the undrained shear strength, as will be shown later.

EFFECTIVE STRESS FRICTION ANGLE OF COHESIONLESS SOILS - GENERAL EVALUATION BASIS

Correlations for estimating the effective stress friction angle for cohesionless soils have been presented by numerous authors. Representative relationships are given below.

Typical Values

Early work on this topic suggested simplified tabulated values for the effective stress friction angle, such as those given in Table 4-1. Although never stated explicitly, it is probable that these values refer to peak values measured in triaxial compression tests ($\bar{\phi}_{tc}$). Tabulated values such as these only establish the general order of magnitude for $\bar{\phi}_{tc}$. They should not be used for design.

Correlations with Index Parameters

Subsequent approaches have correlated the value of $\bar{\phi}_{tc}$ with one or more soil index parameters, such as soil type, relative density, and unit weight or void ratio. Figures 4-7 and 4-8 show two common relationships for estimating $\bar{\phi}_{tc}$ from soil index parameters. Figure 4-7 refers specifically to $\bar{\phi}_{tc}$ from triaxial compression tests on soils composed of hard minerals, at stress levels typical of those used in footing design. Figure 4-8 is a more general relationship based on the groups in the Unified Soil Classification System and presumably also refers to $\bar{\phi}_{tc}$. Although these figures address more of the variables, they still are simplifications of actual behavior and tend to be somewhat conservative.

Table 4-1

REPRESENTATIVE VALUES OF $\bar{\phi}_{tc}$

Soil Material	$\bar{\phi}_{tc}$ (degrees) Loose	Dense
Sand, round grains, uniform	27.5	34
Sand, angular grains, well-graded	33	45
Sandy gravels	35	50
Silty sand	27 to 33	30 to 34
Inorganic silt	27 to 30	30 to 35

Source: Terzaghi and Peck (4), p. 107.

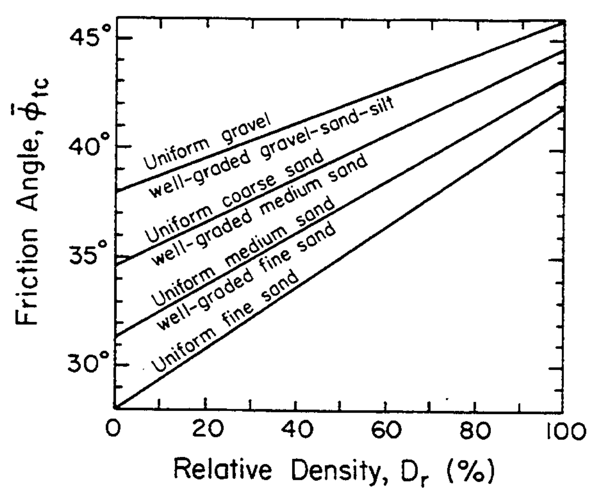

Figure 4-7. $\bar{\phi}_{tc}$ versus Relative Density

Source: Schmertmann (5), p. 41.

Influence of Strength Envelope Curvature

Table 4-1 and Figures 4-7 and 4-8 imply that the soil failure envelope is linear, although data such as that in Figure 4-3 show that the failure envelopes normally are nonlinear. This nonlinearity is well-established in the literature (e.g., 1, 7, 8) and is attributed to soil dilatancy. This dilatancy increases with increasing relative density and decreases with increasing stress level.

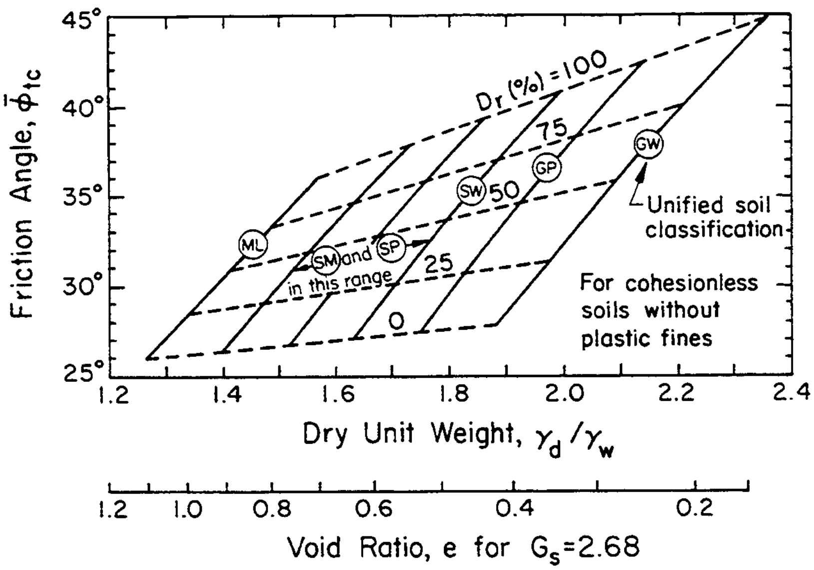

Figure 4-8. $\bar{\phi}_{tc}$ versus Relative Density and Unit Weight

Source: NAVFAC (6), p. 7.1-149.

The most convenient way to include the strength envelope curvature is to use secant peak friction angles which vary with stress level, as illustrated in Figure 4-9. By taking successive secants through the origin at varying normal stresses, the values of $\bar{\phi}_{secant}$ with normal stress can be obtained. Loose soils approximate $\bar{\phi}_{cv}$ and exhibit an essentially linear envelope.

It should be noted at this point that the soil behavior illustrated in Figures 4-3, 4-4, and 4-9 is general and that the same patterns will develop regardless of the laboratory test type. From this point forward, it will be presumed that the friction angle given represents a peak value obtained as a secant to the failure

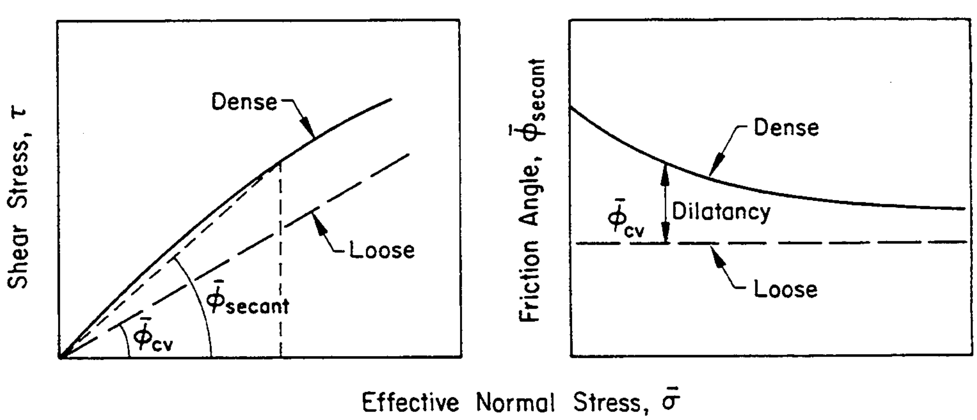

Figure 4-9. Nonlinear Failure Envelope Representation

envelope. For clarity, the subscripts to be used will refer only to the test type, such as $\bar{\phi}_{tc}$ for peak secant friction angle in triaxial compression. No test designation is needed for the critical void ratio friction angle ($\bar{\phi}_{cv}$) because this value is unique and independent of test type (e.g., 8, 9). The same is true for the residual friction angle ($\bar{\phi}_r$).

Recent work by Bolton (6) has unified much prior research in a convenient way, utilizing critical state concepts and a data base primarily of clean sands. This work demonstrated that the dilatancy component of the friction angle can be estimated as follows:

$$(\bar{\phi}_{psc} - \bar{\phi}_{cv}) = 5\ I_{RD} \text{ for plane strain compression} \qquad (4\text{-}5)$$

$$(\bar{\phi}_{tc} - \bar{\phi}_{cv}) = 3\ I_{RD} \text{ for triaxial compression} \qquad (4\text{-}6)$$

in which I_{RD} is a relative dilatancy index, given by:

$$I_{RD} = D_r[Q - \ln(100\ \bar{p}_f/p_a)] - R \qquad (I_{RD} \geq 0) \qquad (4\text{-}7)$$

In this equation, D_r = relative density, Q = soil mineralogy and compressibility coefficient (10 for quartz and feldspar, 8 for limestone, 7 for anthracite, 5.5 for chalk), $\bar{p}_f$ = mean principal effective stress at failure $[(\bar{\sigma}_1 + \bar{\sigma}_2 + \bar{\sigma}_3)_f/3]$, p_a = atmospheric stress in the same units as $\bar{p}_f$, and R = fitting coefficient (equal to 1 for the evaluated test conditions and data). Figure 4-10 illustrates this relationship for eight different quartz and feldspar sands. The equation noted on the figure would be typical of triaxial compression tests on silica-type sands. The relative dilatancy index (I_{RD}) should be limited to 4 unless detailed laboratory test data indicate otherwise.

Equation 4-7 unfortunately relates to the mean principal effective stress at failure, a parameter which includes the initial stress state, stress path to failure, test conditions, and foundation type. For preliminary estimating purposes, $\bar{p}_f$ can be assumed to approximate two times $\bar{\sigma}_{vo}$, which should lead to a computed $(\bar{\phi} - \bar{\phi}_{cv})$ within 1 to 2 degrees of the actual value for most cases. For final design, the value of $\bar{p}_f$ corresponding to the specific foundation conditions should be used.

To estimate the value of $\bar{\phi}_{cv}$, Koerner's work (10) on single mineral soils can be considered, which led to the following:

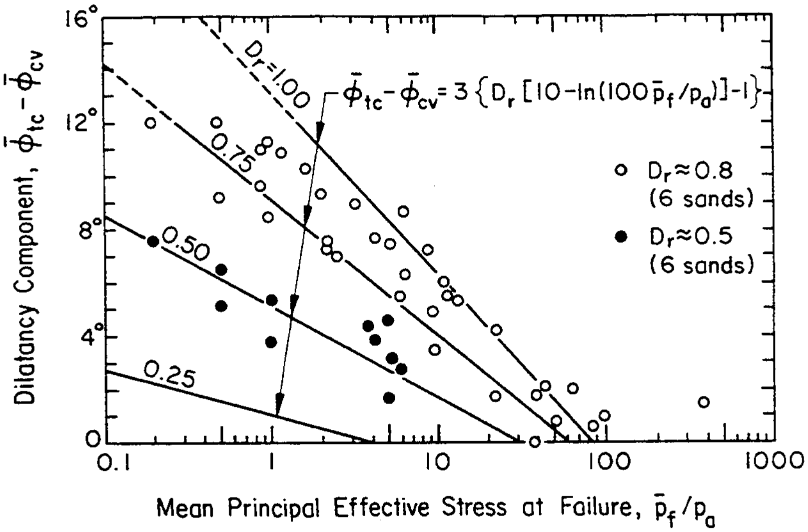

Figure 4-10. Dilatancy Angle Relationships

Source: Bolton (8), p. 73.

$$\bar{\phi}_{cv} = 36° + \Delta\phi_1 + \Delta\phi_2 + \Delta\phi_3 + \Delta\phi_4 + \Delta\phi_5 \quad (4\text{-}8)$$

in which: $\Delta\phi_1$ = correction for particle shape

- $\Delta\phi_1$ = -6° for high sphericity and subrounded shape
- $\Delta\phi_1$ = +2° for low sphericity and angular shape

$\Delta\phi_2$ = correction for particle size (effective size, d_{10})

- $\Delta\phi_2$ = -11° for d_{10} > 2.0 mm (gravel)
- $\Delta\phi_2$ = -9° for 2.0 > d_{10} > 0.6 (coarse sand)
- $\Delta\phi_2$ = -4° for 0.6 > d_{10} > 0.2 (medium sand)
- $\Delta\phi_2$ = 0 for 0.2 > d_{10} > 0.06 (fine sand)

$\Delta\phi_3$ = correction for gradation (uniformity coefficient, C_u)

- $\Delta\phi_3$ = -2° for C_u > 2.0 (well-graded)
- $\Delta\phi_3$ = -1° for C_u = 2.0 (medium graded)
- $\Delta\phi_3$ = 0 for C_u < 2.0 (poorly graded)

$\Delta\phi_4$ = correction for relative density (D_r)

- $\Delta\phi_4$ = -1° for 0 < D_r < 0.5 (loose)
- $\Delta\phi_4$ = 0 for 0.5 < D_r < 0.75 (intermediate)
- $\Delta\phi_4$ = +4° for 0.75 < D_r < 1.00 (dense)

$\Delta\phi_5$ = correction for type of mineral

- $\Delta\phi_5$ = 0 for quartz
- $\Delta\phi_5$ = +4° for feldspar, calcite, chlorite
- $\Delta\phi_5$ = +6° for muscovite mica

Current understanding (e.g., 8) is that $\bar{\phi}_{cv}$ is essentially independent of relative density, and therefore the relative density correction ($\Delta\phi_4$) should be set equal to zero. Relative density primarily influences the dilatancy component. Equation 4-8 also must be kept within the context of Bolton's work (8) on natural soils, which showed that $\bar{\phi}_{cv} \approx 33°$ for representative quartz sands and $\bar{\phi}_{cv} \approx 40°$ for representative feldspar sands. However, most natural deposits of sand include silt. Therefore, Bolton concluded that $\bar{\phi}_{cv}$ for most natural sand deposits rarely will be much above 30° to 33°, and may be as low as 27° when the silt content is high.

Influence of Test Boundary Conditions

For simplicity, most analyses assume that the peak, secant, effective stress friction angle is independent of direction of loading, and therefore the intermediate effective principal stress ($\bar{\sigma}_2$) is disregarded. However, this influence can be important in some loading cases. To evaluate this effect, the intermediate effective principal stress factor (b) can be defined as:

$$b = \frac{\bar{\sigma}_2 - \bar{\sigma}_3}{\bar{\sigma}_1 - \bar{\sigma}_3} \tag{4-9}$$

Normalized test data on five sands are shown in Figure 4-11 to illustrate the importance of b. The mean and range are shown for both the loose and dense sands. For plane strain compression (b = 0.3 to 0.4), the increase ranges from 7 to 18 percent with an average on the order of 12 percent. For triaxial extension (b = 1), the increase ranges from 0 to 23 percent, again with an average on the order of 12 percent. A similar increase should be expected when comparing plane strain extension to compression.

Other studies (e.g., 9) have shown that the plane strain compression (PSC) and direct shear (DS) tests can be interrelated as follows:

$$\tan \bar{\phi}_{ds} = \tan \bar{\phi}_{psc} \cos \bar{\phi}_{cv} \tag{4-10}$$

For typical ranges of $\bar{\phi}_{cv}$, the PSC values from this equation will be some 2 to 7 degrees higher than the direct shear values, corresponding to increases from 4 to 19 percent.

Comparison of the direct shear values from Equation 4-10 with the triaxial compression values from Equations 4-5 and 4-6 indicates that the triaxial compression values may be larger or smaller than the direct shear values, depending on the values

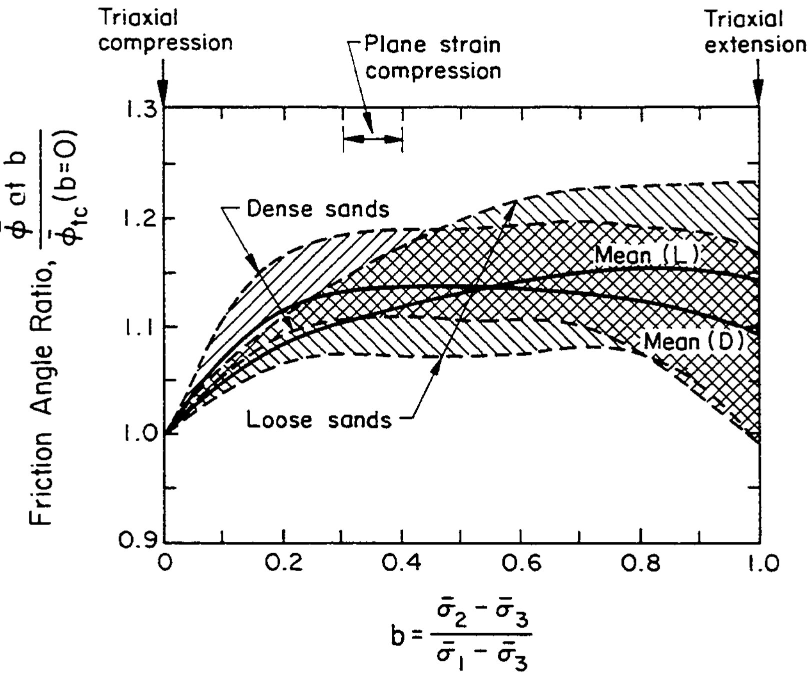

Figure 4-11. Influence of Intermediate Principal Stress on Friction Angle

Source: Data from Ladd, et al. (<u>11</u>), p. 431.

of $\bar{\phi}_{cv}$, relative density, and stress level.

Table 4-2 summarizes the relationships for friction angle as a function of test type. As can be seen from this table and Figure 4-6, use of the triaxial compression friction angle ($\bar{\phi}_{tc}$) alone will almost always be a conservative assumption.

EFFECTIVE STRESS FRICTION ANGLE OF COHESIONLESS SOILS CORRELATED WITH IN-SITU TESTS

At the present time, correlations of the effective stress friction angle have been made with the standard penetration test (SPT), cone penetration test (CPT), pressuremeter test (PMT), and dilatometer test (DMT). The CPT correlations are perhaps the best-developed, followed by the SPT. The PMT correlations are newer and less developed, while the DMT correlations are of limited use at this time. In all cases, it is presumed that the correlations use the triaxial compression friction angle ($\bar{\phi}_{tc}$) corresponding to the appropriate stress and/or relative density conditions.

<u>Correlations with SPT N Value</u>

Correlations of the effective stress friction angle with the SPT N value have been made for many years. Early work on this subject attempted to relate N to $\bar{\phi}_{tc}$

Table 4-2

RELATIVE VALUES OF EFFECTIVE STRESS FRICTION ANGLES FOR COHESIONLESS SOILS

Test Type	Friction Angle (degrees)
Triaxial compression (TC)	$1.0\ \bar{\phi}_{tc}$
Triaxial extension (TE)	$1.12\ \bar{\phi}_{tc}$
Plane strain compression (PSC)	$1.12\ \bar{\phi}_{tc}$
Plane strain extension (PSE)	1.12 (for PSC/TC) x 1.12 (for TE/TC) $= 1.25\ \bar{\phi}_{tc}$
Direct shear (DS)	$\tan^{-1}[\tan \bar{\phi}_{psc} \cos \bar{\phi}_{cv}]$ or $\tan^{-1}[\tan(1.12\ \bar{\phi}_{tc}) \cos \bar{\phi}_{cv}]$

directly, as shown in Table 4-3. The Peck, et al. (12) approach appears to be more common, perhaps because it is more conservative. These values also are shown in Figure 4-12.

As discussed in Section 2, the N value actually depends upon stress level. Figure 4-13 is representative of the correlations between N and $\bar{\phi}_{tc}$ as a function of stress level. This correlation can be approximated as follows:

$$\bar{\phi}_{tc} \approx \tan^{-1}[N/(12.2 + 20.3\ \bar{\sigma}_{vo}/p_a)]^{0.34} \qquad (4\text{-}11)$$

These results tend to be somewhat conservative and should not be used at very shallow depths, less than 1 to 2 m (3.3 to 6.6 ft). Improved correlations with the other variables described in Section 2 have not been developed to date.

Correlations with CPT q_c Value

Similarly, correlations of $\bar{\phi}_{tc}$ with cone tip resistance, q_c, have been developed. Early work attempted to correlate q_c to $\bar{\phi}_{tc}$ directly, as shown in Table 4-4.

As described in Section 2, q_c is affected by the vertical stress. Therefore, $\bar{\phi}_{tc}$ should be correlated to both q_c and $\bar{\sigma}_{vo}$, as shown in Figure 4-14. This correlation

Table 4-3

N VERSUS $\bar{\phi}_{tc}$ RELATIONSHIPS

N Value (blows/ft or 305 mm)	Relative Density	Approximate $\bar{\phi}_{tc}$ (degrees) (a)	(b)
0 to 4	very loose	< 28	< 30
4 to 10	loose	28 to 30	30 to 35
10 to 30	medium	30 to 36	35 to 40
30 to 50	dense	36 to 41	40 to 45
> 50	very dense	> 41	> 45

a - Source: Peck, Hanson, and Thornburn (12), p. 310.
b - Source: Meyerhof (13), p. 17.

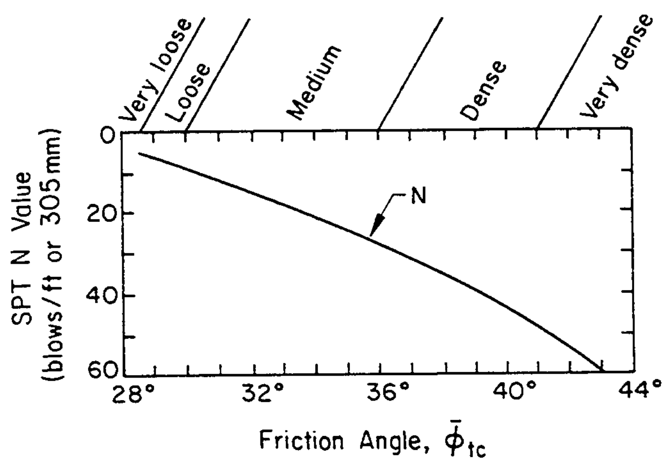

Figure 4-12. N versus $\bar{\phi}_{tc}$

Source: Peck, Hanson, and Thornburn (12), p. 310.

can be approximated as follows:

$$\bar{\phi}_{tc} \approx \tan^{-1} [0.1 + 0.38 \log (q_c/\bar{\sigma}_{vo})] \qquad (4\text{-}12)$$

Adjustments to this figure and equation for soils of different compressibility and stress history should be made as described in Section 2.

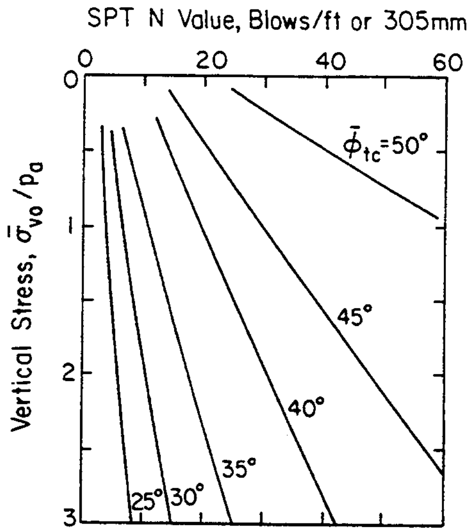

Figure 4-13. N versus $\bar{\phi}_{tc}$ and Overburden Stress

Source: Schmertmann (14), p. 63.

Table 4-4

q_c VERSUS $\bar{\phi}_{tc}$

Normalized Cone Tip Resistance, q_c/p_a	Relative Density	Approximate $\bar{\phi}_{tc}$ (degrees)
< 20	very loose	< 30
20 to 40	loose	30 to 35
40 to 120	medium	35 to 40
120 to 200	dense	40 to 45
> 200	very dense	> 45

Source: Meyerhof (13), p. 17.

Villet and Mitchell (16) presented a more general approach to evaluating $\bar{\phi}_{tc}$ from CPT data which includes q_c, stress level, shape effects, and soil stress history. Their results are shown in Figure 4-15 and are suitable for low compressibility sands.

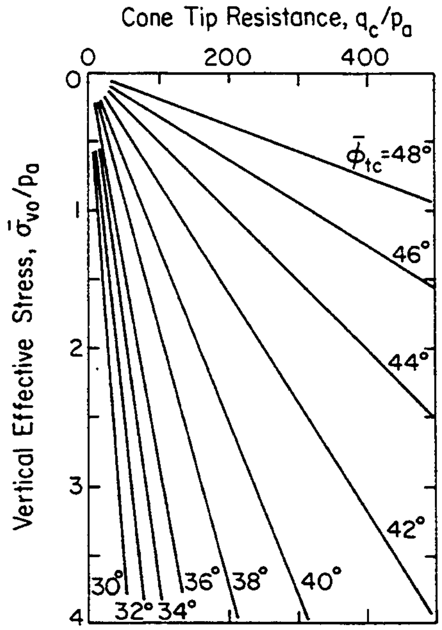

Figure 4-14. q_c versus $\bar{\phi}_{tc}$ and Vertical Stress for NC, Uncemented, Quartz Sands

Source: Robertson and Campanella (15), p. 726.

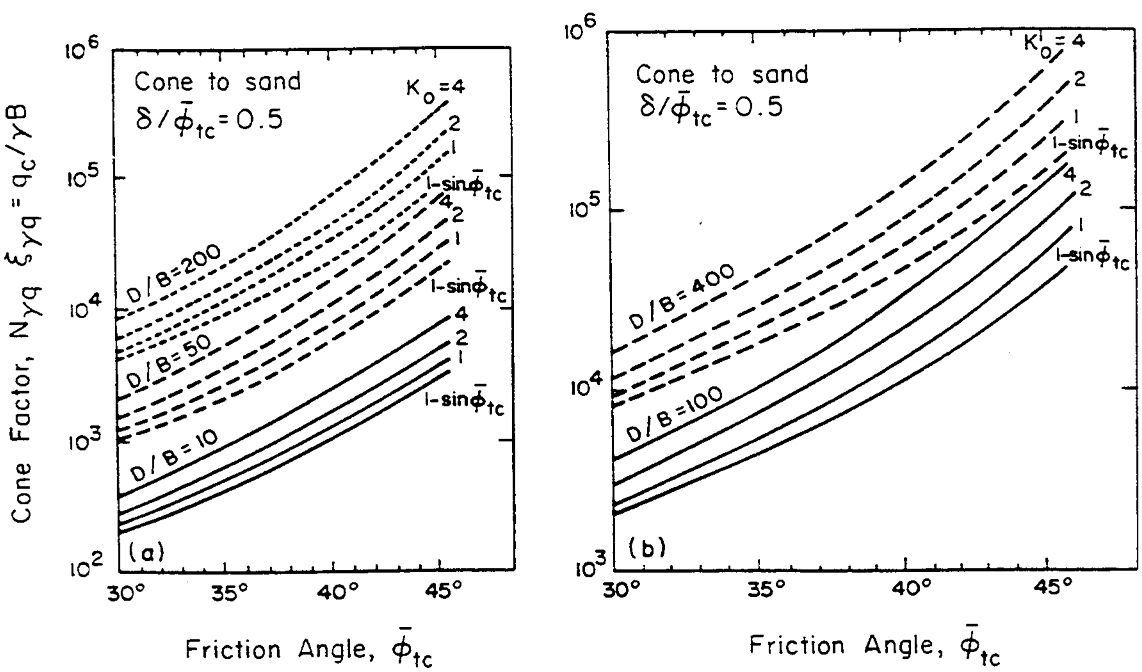

Figure 4-15. $\bar{\phi}_{tc}$ from CPT Data

Source: Villet and Mitchell (16), p. 193.

Using the standard cone diameter (B) of 35.7 mm, Marchetti (17) reworked the data in Figure 4-15 to result in the more simplified Figure 4-16. Consistent with the development in Section 2 which related relative density to the normalized cone tip resistance, a similar correlation has been developed from 20 data sets obtained in calibration chambers and is shown in Figure 4-17. Mineralogy, particle shape, compressibility, and percent fines largely account for the observed range of $\bar{\phi}_{tc}$ at any normalized q_c value.

Correlations with PMT Results

The results obtained from pressuremeter tests also can be correlated with the effective stress friction angle, using procedures developed by either Schmertmann (14) or Hughes, et al. (18). The Hughes, et al. approach is presented below.

In a pressuremeter test, the basic data obtained are the expansion stress (p_e) and the volume changes (ΔV) in the pressuremeter of known volume (V). The resulting data can be plotted as shown in Figure 4-18a, using the cavity strain (ϵ_c) which is defined as the change in membrane radius divided by the initial radius and is given by:

$$\epsilon_c = (1 - \epsilon_V)^{-0.5} - 1 \qquad (4\text{-}13)$$

in which $\epsilon_V = \Delta V/V$ = volumetric strain. These data then are re-plotted as in

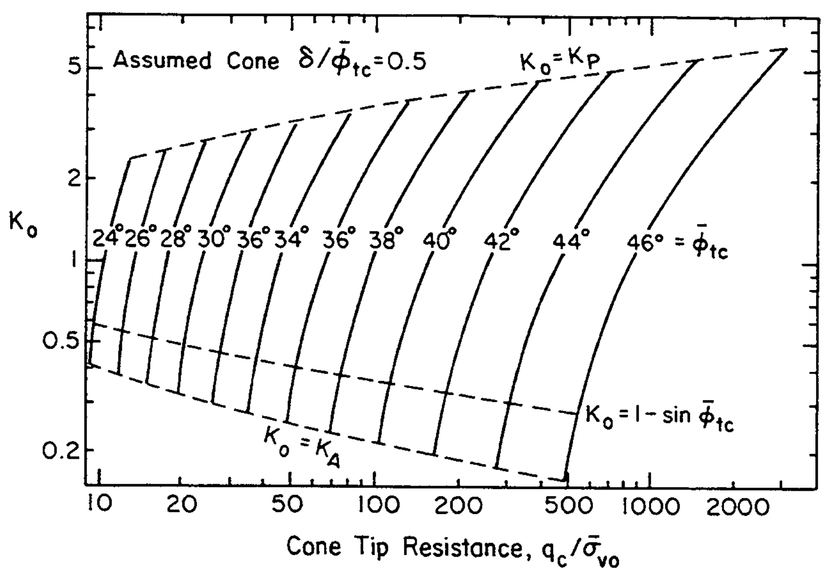

Figure 4-16. Simplified q_c - K_o - $\bar{\phi}_{tc}$ Relationships

Source: Marchetti (17), p. 2668.

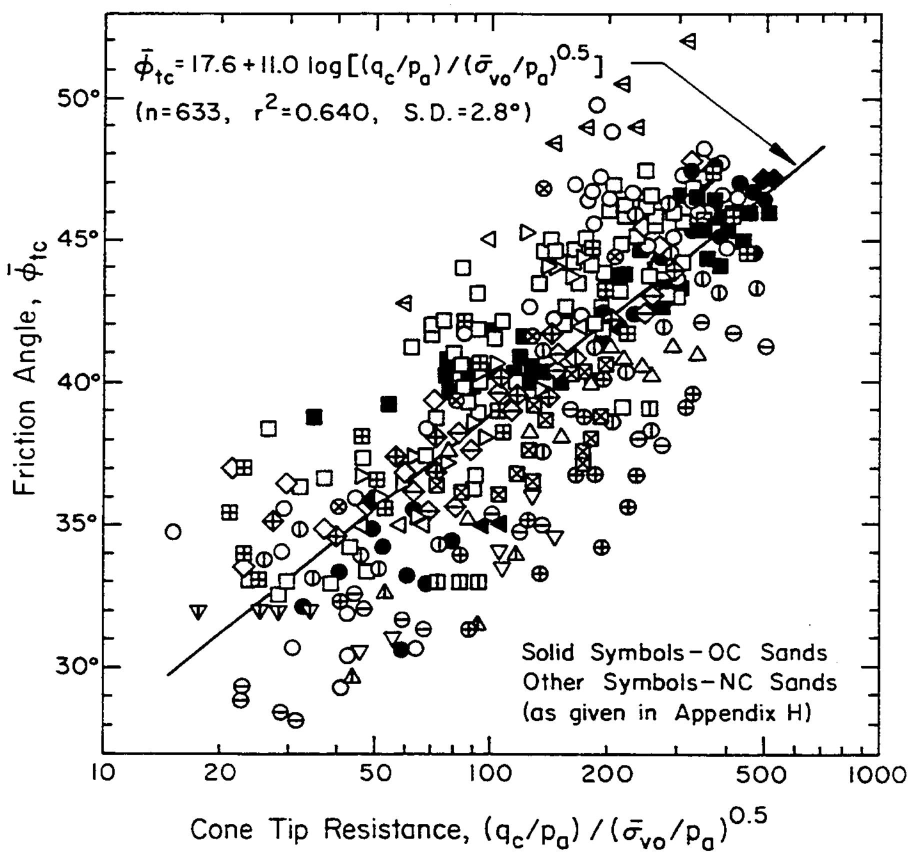

Figure 4-17. Trend of $\bar{\phi}_{tc}$ with Normalized q_c

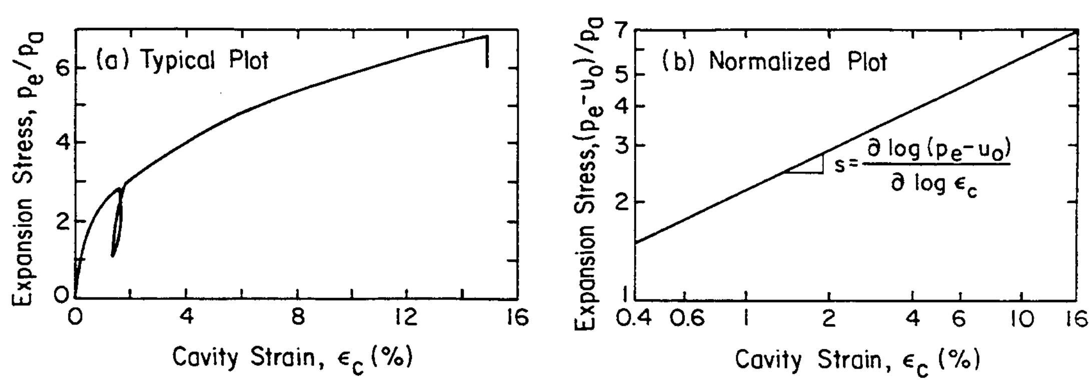

Figure 4-18. PMT Data Representations

Source: Mair and Wood (19), p. 76.

Figure 4-18b, subtracting the initial pore water stress at the pressuremeter level. The resulting log-log plot is essentially linear with a slope, s.

By considering cylindrical cavity expansion theory, s can be given by:

$$s = \sin \bar{\phi}_{cv} (1 + \sin \psi)/(1 + \sin \bar{\phi}_{cv}) \quad (4\text{-}14)$$

in which $\bar{\phi}_{cv}$ = critical void ratio friction angle and ψ = dilation angle ($\bar{\phi}_{tc}$ - $\bar{\phi}_{cv}$, as described previously). Equation 4-14 can be rearranged to give:

$$\sin \psi = s (1 + \sin \bar{\phi}_{cv})/\sin \bar{\phi}_{cv} \quad (4\text{-}15)$$

Therefore, by re-plotting the PMT data to give s and estimating $\bar{\phi}_{cv}$ as described previously, the friction angle ($\bar{\phi}_{tc}$) can be obtained. Figure 4-19 provides a graphical procedure to evaluate $\bar{\phi}_{tc}$, using Bolton's (8) approximation that:

$$\bar{\phi}_{tc} = \bar{\phi}_{cv} + 0.8 \psi \quad (4\text{-}16)$$

Correlations with DMT Results

Recently, a correlation also has been presented between the effective stress friction angle and the thrust pressure (tip resistance) on the dilatometer during penetration. Using the Durgunoglu and Mitchell (20) theory, Schmertmann (21) showed that the dilatometer tip resistance (q_D), obtained from thrust measurements during penetration of the blade, could be related to the cone tip resistance (q_c) and the effective stress friction angle ($\bar{\phi}_{psc}$) under plane strain compression. This

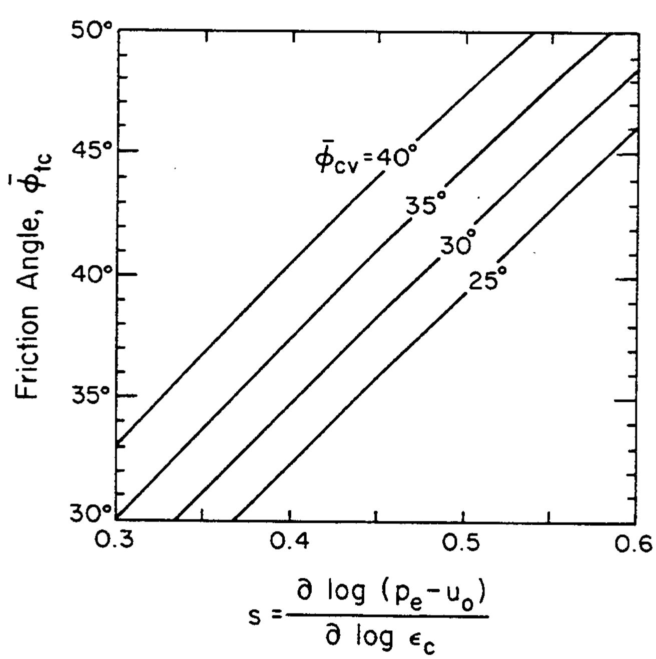

Figure 4-19. Friction Angle Evaluation from PMT Results

Source: Mair and Wood (19), p. 78.

relationship is given below:

$$\bar{\phi}_{psc} = 25(2.3 - q_D/q_c) \quad (4\text{-}17)$$

To evaluate $\bar{\phi}_{psc}$ from the DMT results, an iterative process is necessary. An initial estimate is made of $\bar{\phi}_{psc}$ for triaxial compression conditions, from which an equivalent q_c is determined from Figure 4-15 or 4-16. Using this q_c and the q_D measurement, $\bar{\phi}_{psc}$ is computed from Equation 4-17. This plane strain $\bar{\phi}_{psc}$ then is converted to an equivalent triaxial $\bar{\phi}_{tc}$ using the relationships shown in Figure 4-11 or Table 4-2. The final $\bar{\phi}_{tc}$ is compared with the initial assumption. If they agree, then $\bar{\phi}_{psc}$ is correct. Otherwise, iteration must be done until the initial estimate and final value converge. At the present time, the DMT versus $\bar{\phi}_{psc}$ correlation should be considered only as a first order approximation until sufficient field confirmations become available.

EFFECTIVE STRESS FRICTION ANGLE OF COHESIVE SOILS

Correlations for estimating the effective stress friction angle for cohesive soils have focused on only two areas: (1) the friction angle for normally consolidated (NC) and remolded clays, which will approximate $\bar{\phi}_{cv}$, and (2) the residual friction angle ($\bar{\phi}_r$). No generally accepted procedure has been presented for estimating the peak friction angle of overconsolidated (OC) clays as a function of overconsolidation ratio (OCR) and other controlling factors, although the behavior should be qualitatively similar to that for cohesionless soils. Similarly, no generally accepted correlations have been presented with in-situ test results.

Correlations with Critical Void Ratio Friction Angle

As described at the beginning of this section, the peak friction angle for insensitive, uncemented NC cohesive soils basically is equal to the critical void ratio friction angle ($\bar{\phi}_{cv}$). For sensitive, cemented, or other structured NC cohesive soils, $\bar{\phi}_{cv}$ will represent a lower bound for the peak friction angle. For OC soils, remolding will destroy the stress history and therefore result in "newly-created NC soil", with the friction angle being given by $\bar{\phi}_{cv}$. Other complex factors such as leaching, sensitivity, stress state, etc. influence this simple explanation to some degree. However, first-order correlations can be made using this simple approach.

Many authors have shown that $\bar{\phi}_{cv}$ can be correlated with simple index parameters such as the plasticity index. One such relationship is presented in Figure 4-20, which shows that $\bar{\phi}_{cv}$ decreases with increasing plasticity index and increasing clay

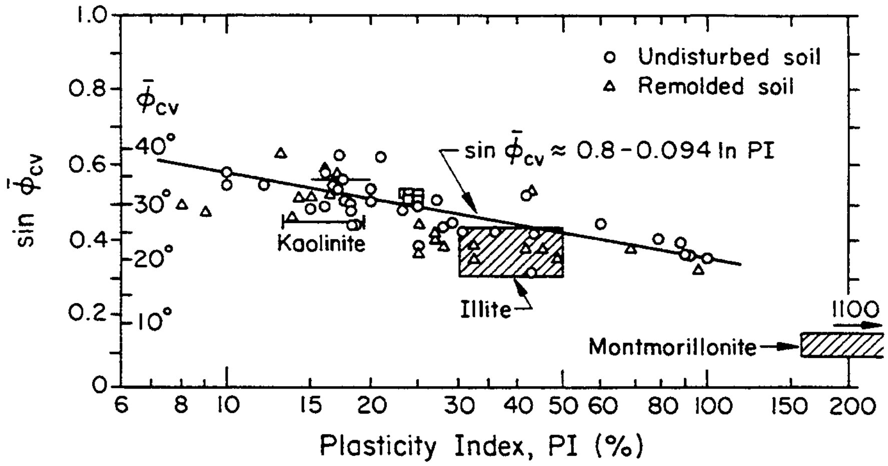

Figure 4-20. $\bar{\phi}_{cv}$ for NC Clays versus PI

Source: Mitchell (22), p. 284.

mineral activity (kaolinite → illite → montmorillonite). This general trend has been corroborated by others (e.g., 11, 23). However, it should be noted that the error band with this correlation is fairly large.

Influence of Test Boundary Conditions

Laboratory testing conditions can influence the friction angle of NC clays. The data in Figure 4-20 were obtained largely from isotropically consolidated, undrained triaxial compression (CIUC) tests with pore water stress measurements. In-situ, the initial stresses would correspond to anisotropic consolidation (CAUC), most commonly restricted to K_o consolidation (CK_oUC). Fortunately, comparative studies such as that shown in Figure 4-21 have demonstrated that $\bar{\phi}_{tc}$ essentially is the same, regardless of initial consolidation state. Although the regression shows a small variation from equality, this variation is small and can be ignored.

However, the same can not be said for other testing conditions. For plane strain compression, Wroth (3) suggested analytically that $\bar{\phi}_{psc}$ would be approximately 9/8 times $\bar{\phi}_{tc}$. Figure 4-22 illustrates that this relationship is satisfactory, although the regression gives a slightly lower value. This value is similar to that for sands. Figure 4-23 compares the friction angles for NC clays in extension and compression. As can be seen, $\bar{\phi}_{te}$ always is equal to or greater than $\bar{\phi}_{tc}$ and, on the average, $\bar{\phi}_{te}/\bar{\phi}_{tc}$ = 1.22. This average is the same for both anisotropic and isotropic test conditions, even though their statistics differ a small amount. Additional limited data (26) show that the pattern should be similar for plane strain conditions as well.

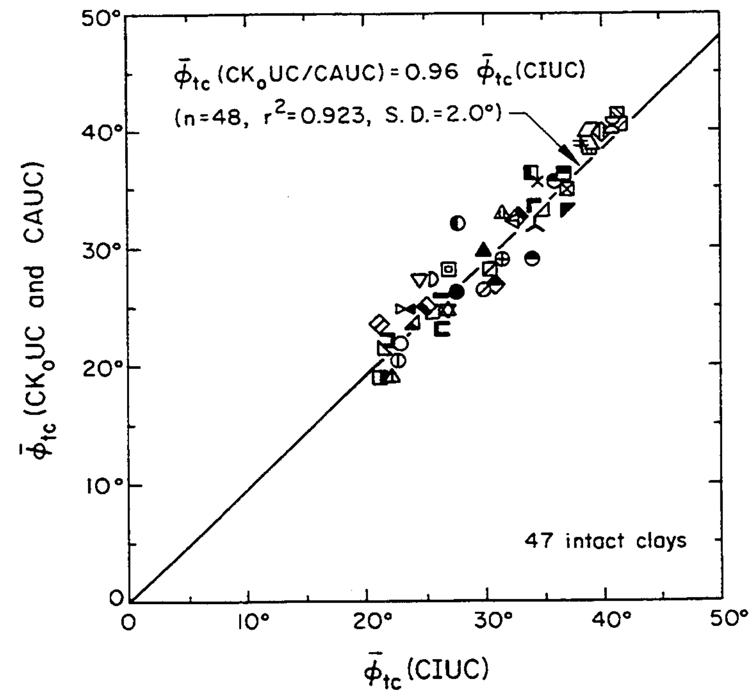

Figure 4-21. $\bar{\phi}_{tc}$ Variation as a Function of Consolidation Stress for NC Clays

Source: Data from Mayne (24) and Nakase and Kamei (25).

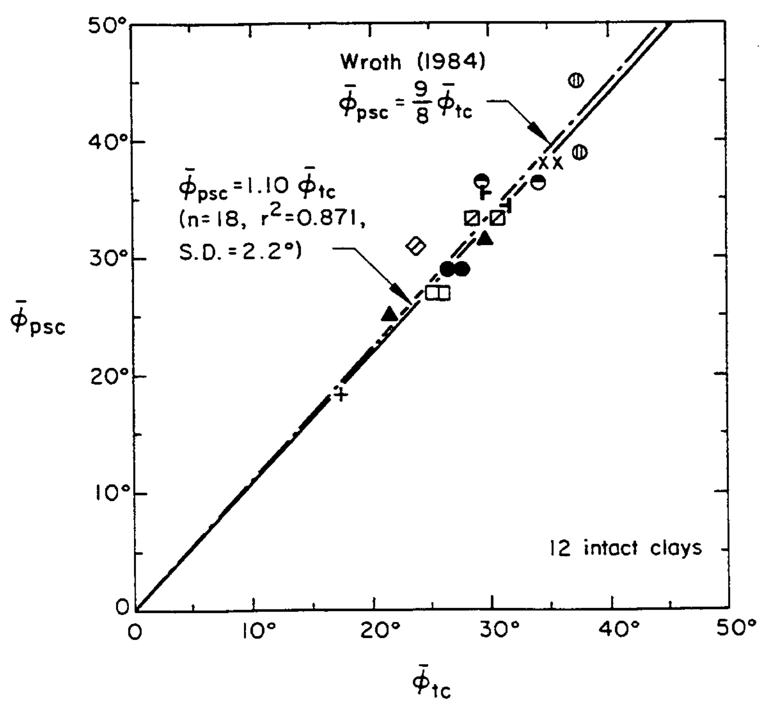

Figure 4-22. $\bar{\phi}_{psc}$ versus $\bar{\phi}_{tc}$ for NC Clays

Source: Data from Mayne and Holtz (26).

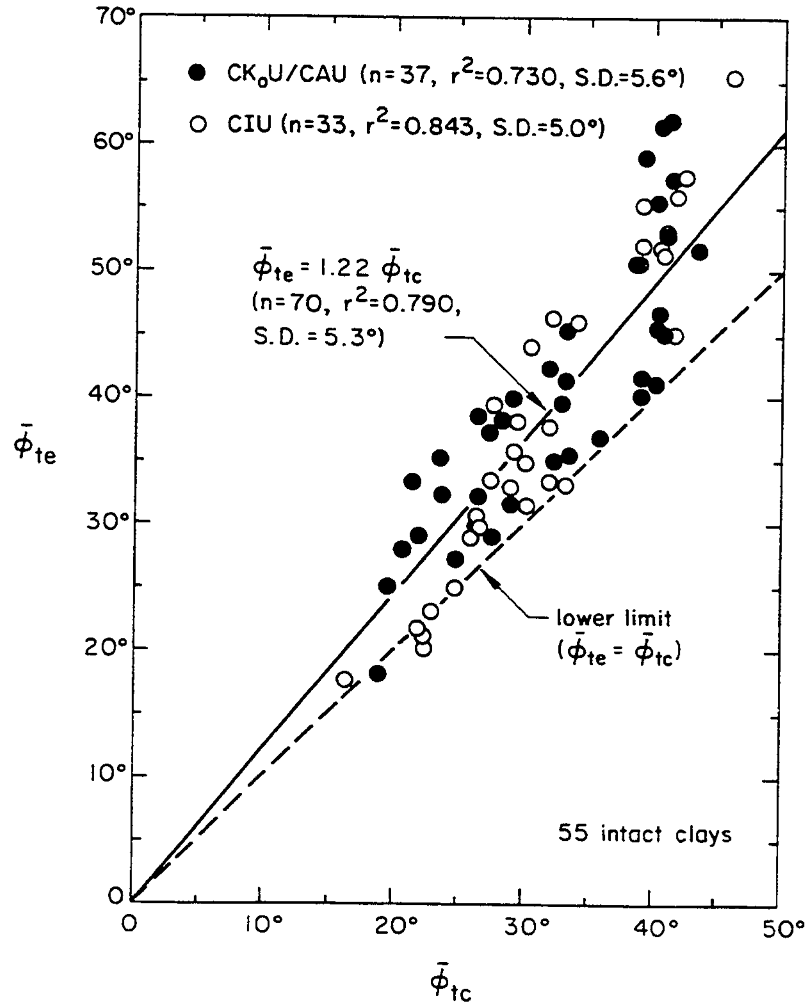

Figure 4-23. $\bar{\phi}_{te}$ versus $\bar{\phi}_{tc}$ for NC Clays

Source: Data from Mayne and Holtz (26) and Nakase and Kamei (25).

Table 4-5 summarizes the relative values of the friction angle for the different testing conditions. Although no detailed comparisons have been presented for the direct shear test, the results should exhibit patterns similar to those presented earlier for cohesionless soils. Therefore, the same relationship is proposed for cohesive soils. It should be noted that use of $\bar{\phi}_{tc}$ alone will almost always be a conservative assumption.

Correlations with Residual Friction Angle

As described earlier in this section, the residual friction angle ($\bar{\phi}_r$) develops when a cohesive soil undergoes very large strains, and the soil structure is totally remolded and re-oriented into a minimum strength orientation. Currently,

Table 4-5

RELATIVE VALUES OF EFFECTIVE STRESS FRICTION ANGLE FOR NORMALLY CONSOLIDATED COHESIVE SOILS

Test Type	Friction Angle (degrees)
Triaxial compression[1] (TC)	1.0 $\bar{\phi}_{tc}$
Triaxial extension (TE)	1.22 $\bar{\phi}_{tc}$
Plane strain compression (PSC)	1.10 $\bar{\phi}_{tc}$
Plane strain extension (PSE)	1.10 (for PSC/TC) x 1.22 (for TE/TC) = 1.34 $\bar{\phi}_{tc}$
Direct shear[2] (DS)	$\tan^{-1}$ [tan ϕ_{psc} cos $\bar{\phi}_{cv}$] or $\tan^{-1}$ [tan(1.10 $\bar{\phi}_{tc}$) cos $\bar{\phi}_{cv}$]

1 - CIUC, CK_oUC, or CAUC
2 - Speculative, based on results from sand

it is understood that the strains necessary to accomplish this remolding may exceed 100 percent. Earlier studies of this subject may not have subjected the soil to the necessary strains, and therefore residual angles quoted in earlier sources may be somewhat on the high side.

Extensive research (e.g., 27, 28) has shown that the clay fraction (percent finer than two microns) and mineralogy perhaps are most important in evaluating $\bar{\phi}_r$. If the soil clay fraction is less than about 15 percent, the soil behaves much like a cohesionless soil, with $\bar{\phi}_r$ typically greater than 25° and not much different from $\bar{\phi}_{cv}$. If the clay fraction is greater than 50 percent, $\bar{\phi}_r$ is appreciably lower than $\bar{\phi}_{cv}$ and is governed entirely by sliding of the clay minerals. For the most common clay minerals, $\bar{\phi}_r$ ranges approximately from 15° for kaolinite, to 10° for illite, and then to 5° for montmorillonite. Soils with clay fractions between 15 and 50 percent exhibit transitional behavior, as shown in Figure 4-24.

The value of $\bar{\phi}_r$ also is stress-dependent because of curvature of the failure envelope (22, 27, 29). Values given in Figure 4-24 are appropriate for an effective normal stress equal to about one atmosphere. Figure 4-25a illustrates the typical changes in $\bar{\phi}_r$ which occur with changes in effective normal stress and plasticity

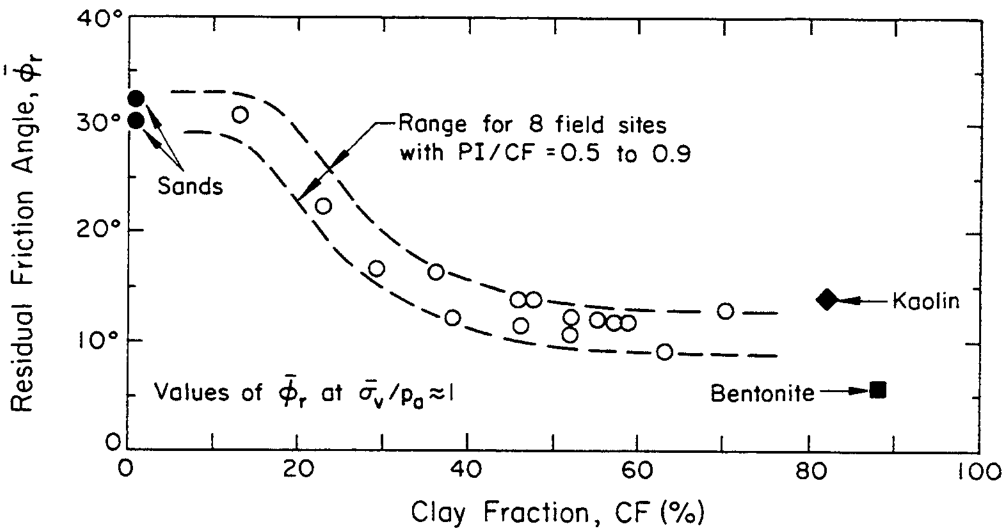

Figure 4-24. $\bar{\phi}_r$ from Ring Shear Tests and Field Studies

Source: Skempton (28), p. 14.

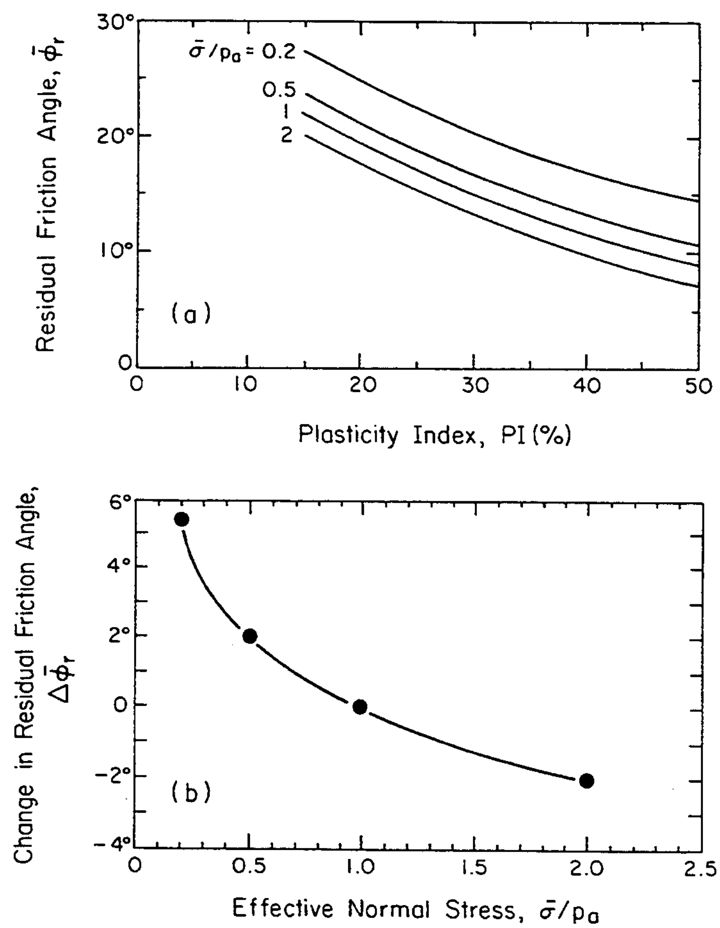

Figure 4-25. $\bar{\phi}_r$ for Amuay Soils

Source: Based on Lambe (29), p. 144.

index for the soils at the Amuay landslide sites. These curves essentially are parallel, indicating that the change in $\bar{\phi}_r$ as a function of stress change is independent of the plasticity index. Re-plotting these changes in friction angle ($\Delta\bar{\phi}_r$) results Figure 4-25b. Other data (e.g., 27) are consistent with these $\Delta\bar{\phi}_r$ values.

The final values of $\bar{\phi}_r$ therefore should be evaluated from Figure 4-24, modified for effective normal stress level as given in Figure 4-25b.

UNDRAINED SHEAR STRENGTH OF COHESIVE SOILS - GENERAL EVALUATION BASIS

The undrained shear strength (s_u) may very well be the most widely used parameter for describing the consistency of cohesive soils. However, s_u is not a fundamental material property. Instead, it is a measured response of soil during undrained loading which assumes zero volume change. As such, s_u is affected by the mode of testing, boundary conditions, rate of loading, confining stress level, initial stress state, and other variables. Consequently, although not fully appreciated by many users, s_u is and should be different for different test types (See Figure 1-1 for test types.).

As described earlier in this section, it is appropriate to use a standard "test of reference", which is the isotropically consolidated, triaxial compression test for undrained loading (CIUC). With the CIUC test as a standard reference, the results of all other tests can be compared simply and conveniently. It should be noted that simpler forms of triaxial test are available, such as the unconsolidated, undrained (UU) triaxial and unconfined (U) compression tests. With the UU test, a total confining stress is applied, but no soil consolidation is allowed under this confining stress. With the U test, the soil is unconfined with a zero confining stress.

Many detailed studies (e.g., 11, 23) have shown that the UU and U tests often are in gross error because of sampling disturbance effects and omission of a reconsolidation phase. Based on studies such as these, the CIUC test also is considered to be the minimum quality laboratory test for evaluating the undrained shear strength of cohesive soils. Other simple tests such as the torvane and pocket penetrometer have an error potential that is comparable to that of the UU and U tests. Therefore, these tests should only be considered general indicators of relative behavior. They should never be used directly for design.

Since s_u is stress-dependent, its value commonly is normalized by the vertical effective overburden stress ($\bar{\sigma}_{vo}$) at the depth where s_u is measured. This undrained strength ratio, $s_u/\bar{\sigma}_{vo}$, has been expressed in many alternate forms in the literature, including $s_u/\bar{\sigma}_o$, $c_u/\bar{\sigma}_o$, $c_u/\bar{\sigma}_v$, c/p, etc. All are equal to $s_u/\bar{\sigma}_{vo}$, which will be used in the remainder of this section.

Correlations with Index Parameters for Undisturbed Clays

Early work by Skempton (30) suggested the general correlation in Figure 4-26 for s_u determined from the field vane shear test (VST) as a function of the plasticity index. All of the data are for normally consolidated (NC) clays. A linear fit of these data results in:

$$s_u(VST)/\bar{\sigma}_{vo} = 0.11 + 0.0037\ PI \qquad (4\text{-}18)$$

In general, this relationship has been corroborated by others (e.g., 31), but there usually is more spread in the data than that shown in Figure 4-26. Recent work by Chandler (32) suggests that this approximation may also be valid for OC clays, using the modification below with the preconsolidation stress ($\bar{\sigma}_p$):

$$s_u(VST)/\bar{\sigma}_p \approx 0.11 + 0.0037\ PI \qquad (4\text{-}19)$$

He notes that the accuracy of this method will be on the order of ± 25 percent, but he cautions against its use in fissured, organic, sensitive, or other unusual clays.

However, in a surprisingly large number of case histories, direct use of s_u from the field VST in stability analyses of numerous embankments, excavations, and footings in clay has led to failures. Back-analysis of these failures has led to

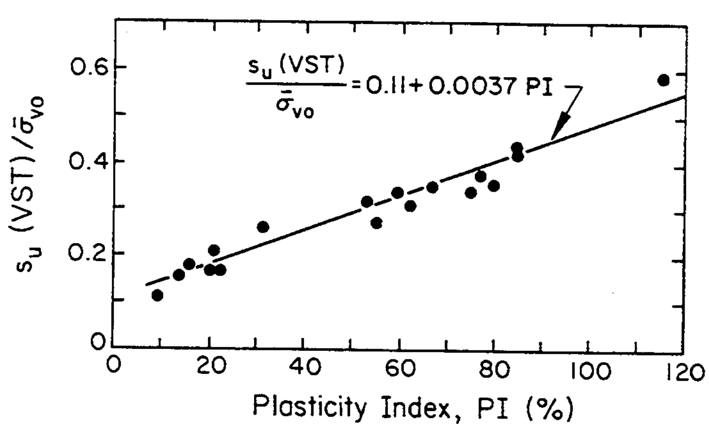

Figure 4-26. $s_u(VST)/\bar{\sigma}_{vo}$ versus PI for NC Clays

Source: Skempton (30), p. 306.

empirical correction factors for the field VST. These factors will be described later in the section on s_u correlations with the VST.

Subsequent studies (e.g., 33) showed that sensitive clays with high liquidity index did not fit the trend in Figure 4-26 very well. For these sensitive clays, the undrained strength ratio could be correlated better with the liquidity index, as shown in Figure 4-27. These data were obtained from triaxial compression tests on NC clays.

The undrained strength ratio for triaxial compression also can be determined from Critical State Soil Mechanics (CSSM) using the modified Cam clay model (e.g., 34). For NC clay, this relationship is given by:

$$s_u/\bar{\sigma}_i = 0.129 + 0.00435 \text{ PI} \quad (4\text{-}20)$$

in which $\bar{\sigma}_i$ = effective overburden stress after isotropic consolidation.

Other useful approximations include the following for low OCR clays with low to moderate PI (Jamiolkowski, et al., 35):

$$s_u/\bar{\sigma}_p = 0.23 \pm 0.04 \quad (4\text{-}21)$$

in which $\bar{\sigma}_p$ = preconsolidation stress. Alternatively, Mesri (36) suggested the following:

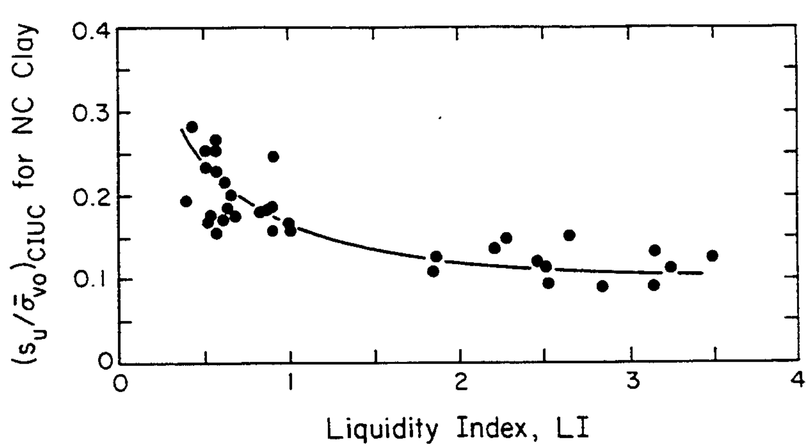

Figure 4-27. $s_u/\bar{\sigma}_{vo}$ for NC Clay versus Liquidity Index

Source: Bjerrum and Simons (33), p. 722.

$$s_u/\bar{\sigma}_p = 0.22 \tag{4-22}$$

In both cases, the s_u corresponds approximately to direct simple shear (DSS) conditions.

Correlations with Index Parameters for Remolded Clays

The sensitivity (S_t) is defined as s_u in the undisturbed state divided by s_u when remolded (both tested normally in unconfined compression at the same natural water content), and therefore it is a measure of strength loss upon disturbance. Table 4-6 gives the typical terminology used to describe sensitivity, while Figure 4-28 illustrates a generalized relationship for sensitivity as a function of liquidity index and effective stress. The undrained remolded strength represents the lower bound on s_u and, when S_t approaches one, $s_u \approx s_{ur}$.

Figure 4-29 indicates that s_{ur} correlates reasonably well with the liquidity index. Data on undisturbed natural clays of low sensitivity are presented in Figure 4-30 and indicate good agreement with Figure 4-29, suggesting that s_{ur} is a fair predictor of s_u for many clays of low sensitivity.

The undrained shear strength for triaxial compression also can be predicted from the modified Cam clay model as follows (Wroth and Wood, 38):

$$\ln S = (1 - LI) \ln R \tag{4-23}$$

Table 4-6

CLASSIFICATION OF SENSITIVITY

Clay Description	S_t	Clay Description	S_t
Insensitive	≈ 1	Slightly quick	8 to 16
Slightly sensitive	1 to 2	Medium quick	16 to 32
Medium sensitive	2 to 4	Very quick	32 to 64
Very sensitive	4 to 8	Extra quick	> 64

Source: Mitchell (22), p. 208.

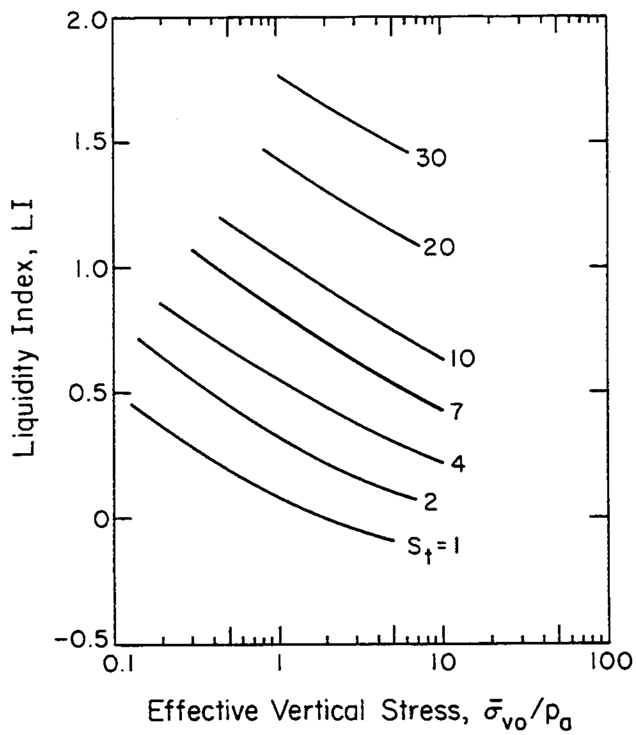

Figure 4-28. General Relationship Between Sensitivity, Liquidity Index, and Effective Stress

Source: Mitchell (22), p. 229.

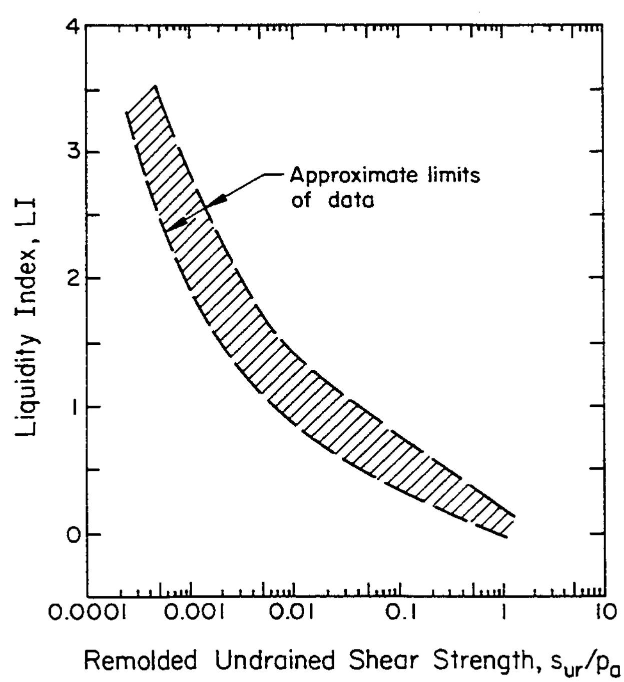

Figure 4-29. Remolded Undrained Shear Strength versus LI

Source: Mitchell (22), p. 228.

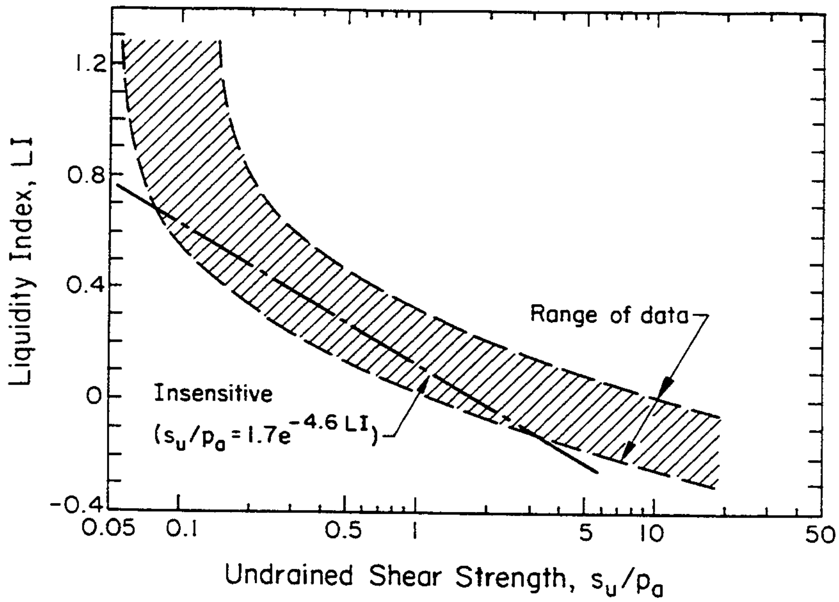

Figure 4-30. Undisturbed Undrained Shear Strength versus LI

Source: Wood (37), p. 7.

in which $S = s_u/(s_u \text{ at } w_L)$ and $R = (s_u \text{ at } w_p)/(s_u \text{ at } w_L)$. Typically, $R \approx 100$ and $(s_u \text{ at } w_L) \approx 0.017\ p_a$, yielding:

$$s_u/p_a = 1.7\ e^{-4.6\ LI} \tag{4-24}$$

This equation is plotted as the straight line in Figure 4-30 and shows good agreement with the data in the range $0.1 < s_u/p_a < 3$.

General Behavior Under Triaxial Compression Loading

The undrained strength ratio in triaxial compression can be expressed in terms of more fundamental soil parameters by analysis of the Coulomb-Mohr failure envelope geometry. For K_o consolidation, the undrained strength ratio is given as:

$$(s_u/\bar{\sigma}_{vo})_{CAUC} = \frac{[K_o + A_f(1 - K_o)]\ \sin \bar{\phi}_{tc}}{1 + (2A_f - 1)\ \sin \bar{\phi}_{tc}} \tag{4-25}$$

in which K_o = coefficient of horizontal soil stress and A_f = Skempton's pore water stress parameter, defined as:

$$A_f = \frac{\Delta u - \Delta\sigma_3}{\Delta\sigma_1 - \Delta\sigma_3} \tag{4-26}$$

for saturated soil with Δu = excess pore water stress developed during loading, $\Delta\sigma_1$ = major principal stress increment, and $\Delta\sigma_3$ = minor principal stress increment. Typical ranges in A_f are shown in Table 4-7. For isotropic consolidation (K_o = 1), Equation 4-25 reduces to:

$$(s_u/\bar{\sigma}_{vo})_{CIUC} = \frac{\sin \bar{\phi}_{tc}}{1 + (2A_f - 1) \sin \bar{\phi}_{tc}} \qquad (4\text{-}27)$$

In both cases, $\bar{\phi}_{tc}$ is used since it was shown earlier that the consolidation state does not influence the friction angle.

The undrained strength ratio in triaxial compression also can be predicted from the modified Cam clay model (e.g., 3). For isotropic consolidation, this ratio is:

$$(s_u/\bar{\sigma}_{vo})_{CIUC} = 0.5\ M\ (0.5)^{\Lambda} \qquad (4\text{-}28)$$

with M and Λ defined in Appendix G. For anisotropic consolidation, this ratio is:

$$(s_u/\bar{\sigma}_{vo})_{CAUC} = \frac{\sin \bar{\phi}_{tc}}{2a} \left(\frac{a^2 + 1}{2}\right)^{\Lambda} \qquad (4\text{-}29)$$

in which

Table 4-7

TYPICAL RANGES IN A_f FOR ISOTROPICALLY CONSOLIDATED CLAYS

Clay Type	A_f
High sensitivity	0.75 to 1.5
Normally consolidated (NC)	0.5 to 1.0
Lightly overconsolidated (LOC)	0 to 0.5
Heavily overconsolidated (HOC)	-0.5 to 0

Source: Skempton (39), p. 146.

$$a = \frac{3 - \sin \bar{\phi}_{tc}}{2(3 - 2 \sin \bar{\phi}_{tc})} \qquad (4\text{-}30)$$

For isotropic consolidation, this model also predicts A_f in NC clays, as follows:

$$A_f = [2^{\Lambda} + (M/3) - 1]/M \qquad (4\text{-}31)$$

Typical values of Λ range between 0.7 and 0.8, with 0.8 being used most often.

To examine the applicability of these relationships for predicting the undrained strength ratio of NC clays, a data base of 48 different clays (24, 25, 40) was used for comparison. Figure 4-31 shows the direct comparisons between the undrained strength ratios for isotropic consolidation and for K_o or anisotropic consolidation. It should be noted that the data base consisted of tests that were: (1) accurately consolidated using K_o testing procedures, (2) consolidated to estimated K_o stress values, or (3) consolidated to some general anisotropic stress which may or may not be equal to K_o. Linear regression of these data showed the following:

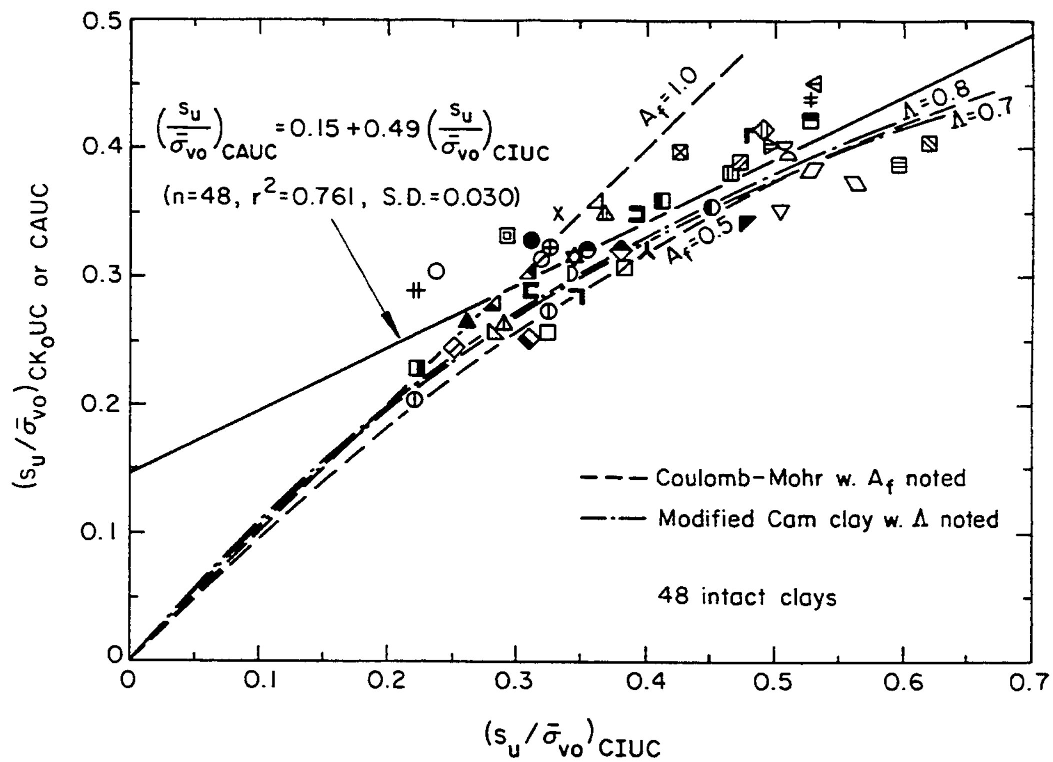

Figure 4-31. Comparison of Undrained Strength Ratio for NC Clays After Anisotropic and Isotropic Consolidation

Source: Data from Mayne (24) and others (25, 40).

$$(s_u/\bar{\sigma}_{vo})_{CAUC} = 0.15 + 0.49(s_u/\bar{\sigma}_{vo})_{CIUC} \tag{4-32}$$

with the statistics shown on the figure. A linear regression through the origin was inappropriate for these data. Also shown on this figure are the predictions from the Coulomb-Mohr failure envelope geometry (Equations 4-25 and 4-27), using typical limiting values for A_f and $K_o = (1 - \sin\bar{\phi}_{tc})$ from Section 3, and from the modified Cam clay model (Equations 4-28 and 4-29), using typical values for Λ. As can be seen, the Coulomb-Mohr predictions bound the data well and modified Cam clay provides an accurate prediction, although slightly conservative.

Figure 4-32 provides a more detailed comparison of these data, with each undrained strength ratio plotted versus $\bar{\phi}_{tc}$. For isotropic consolidation (Figure 4-32a), linear regression on these data gave the following:

$$(s_u/\bar{\sigma}_{vo})_{CIUC} = 0.0120\ \bar{\phi}_{tc} \tag{4-33}$$

with the statistics shown on the figure. The regression line and the modified Cam clay prediction agree well. The Coulomb-Mohr prediction bounds much of the data, but tends to be somewhat on the high side. It should be noted that the $\Lambda = 0.8$ line from the modified Cam clay model is identical to the Coulomb-Mohr model using A_f predicted by the modified Cam clay model (Equation 4-31). These data further show that the following provides a reasonable lower bound for the data:

$$(s_u/\bar{\sigma}_{vo})_{CIUC} = \bar{\phi}_{tc}/100 \qquad \text{for lower bound} \tag{4-34}$$

This observation is in general agreement with Wroth's suggestion (3) that:

$$(s_u/\bar{\sigma}_{vo})_{remolded} \approx \bar{\phi}_{cv}/100 \tag{4-35}$$

The remolded and critical void ratio values are consistent with lower bounds on natural soils.

For anisotropic consolidation (Figure 4-32b), linear regression on the data gave the following:

$$(s_u/\bar{\sigma}_{vo})_{CAUC} = 0.0117\ \bar{\phi}_{tc} \tag{4-36}$$

with the statistics shown on the figure. The Coulomb-Mohr predictions tend to be on the high side, while the modified Cam clay predictions tend to be on the low

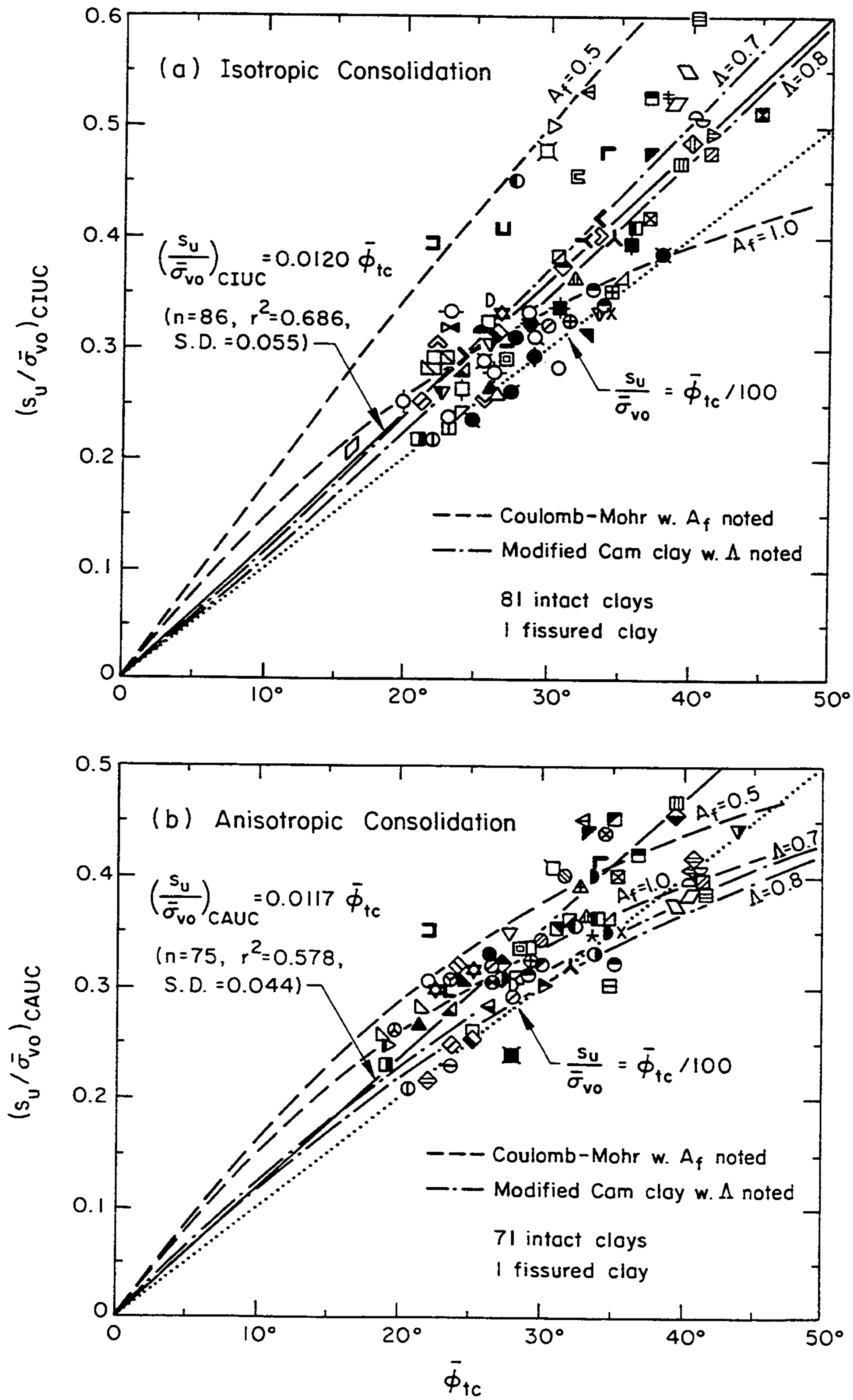

Figure 4-32. Undrained Strength Ratio versus $\bar{\phi}_{tc}$ for NC Clays

Source: Data from Mayne (41) and others (25, 26, 40).

side. The $\bar{\phi}_{tc}/100$ relationship still provides a lower bound estimate, although not as reliably as for isotropic consolidation.

Figures 4-32a and b suggest that the $s_u/\bar{\sigma}_{vo}$ ratios for isotropic and anisotropic consolidation are nearly the same, although it is clear from Figure 4-31 that the anisotropic value is less than the isotropic and the difference increases with increasing $s_u/\bar{\sigma}_{vo}$. Part of the reason for this apparent anomaly is that the data bases in these three figures are not the same. Also, it is clear that the data in Figure 4-32a exhibit a near-linear trend, while the data in Figure 4-32b exhibit a pronounced curved trend. For these reasons, it is believed that the regression lines given in Figures 4-31 and 4-32a should be more reliable and be used to interrelate $(s_u/\bar{\sigma}_{vo})_{CAUC}$, $(s_u/\bar{\sigma}_{vo})_{CIUC}$, and $\bar{\phi}_{tc}$ for $\bar{\phi}_{tc} > 20°$. As a preferred alternative, the modified Cam clay model (Equations 4-28 and 4-29) can be used directly. It agrees well with the regression line in Figure 4-32 for predicting $(s_u/\bar{\sigma}_{vo})_{CIUC}$, and it gives a slightly conservative value of $(s_u/\bar{\sigma}_{vo})_{CAUC}$, typically 0.01 to 0.02 less than the regression, and a better fit for low $s_u/\bar{\sigma}_{vo}$ values.

Influence of Overconsolidation

The undrained strength ratio increases with increasing overconsolidation, as measured by the overconsolidation ratio (OCR = $\bar{\sigma}_p/\bar{\sigma}_{vo}$). Figure 4-33 shows typical experimental data illustrating this OCR effect, as measured in direct simple shear (DSS) tests. The concept of SHANSEP (Stress History and Normalized Soil Engineering Parameters) addresses this phenomenon and uses this behavior to correct laboratory test results for sample disturbance effects (e.g., 11). For example, Figure 4-34 shows these same data in normalized form, indicating a rather narrow band. Based on data of this type, the following general equation was suggested (e.g., 11):

$$\frac{(s_u/\bar{\sigma}_{vo})_{OC}}{(s_u/\bar{\sigma}_{vo})_{NC}} = OCR^m \qquad (4\text{-}37)$$

with m = 0.8. However, a better fit occurs when m = 0.85 to 0.75 with increasing OCR. This experimental observation also is the basis for the approximation made by Jamiolkowski, et al. (35) for low to moderate PI soils, as given below:

$$s_u/\bar{\sigma}_{vo} = (0.23 \pm 0.04)\ OCR^{0.8} \qquad (4\text{-}38)$$

This equation basically is a revised form of Equation 4-21, corresponding approximately to DSS conditions.

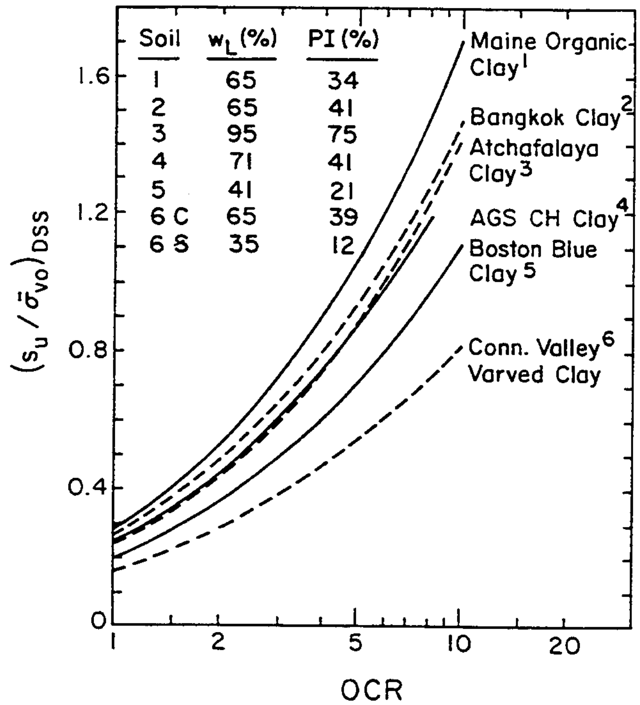

Figure 4-33. $s_u/\bar{\sigma}_{vo}$ versus OCR

Source: Ladd, et al. (11), p. 26.

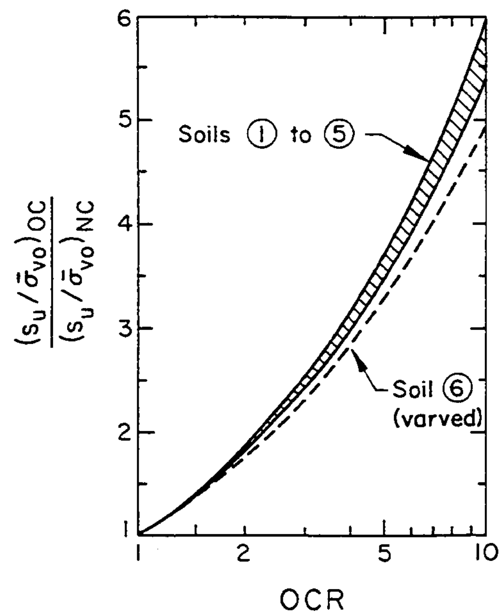

Figure 4-34. Normalized $s_u/\bar{\sigma}_{vo}$ versus OCR

Source: Ladd, et al. (11), p. 26.

It should be noted that the general form of Equation 4-37 will hold regardless of strength test type (e.g., 3, 35, 42). However, $(s_u/\bar{\sigma}_{vo})_{NC}$ will vary significantly with test type and m will vary to a limited degree, as described subsequently.

This general behavior also is predicted by the modified Cam clay model, as follows (e.g., 34):

$$\frac{(s_u/\bar{\sigma}_{vo})_{OC}}{(s_u/\bar{\sigma}_{vo})_{NC}} = OCR^{\Lambda} \qquad (4\text{-}39)$$

with Λ typically about 0.8. Fundamentally, this equation applies to CIUC test conditions (Equation 4-28).

The modified Cam clay model also can be used for predicting A_f, as follows:

$$A_f = [(2/OCR)^{\Lambda} + (M/3) - 1]/M \qquad (4\text{-}40)$$

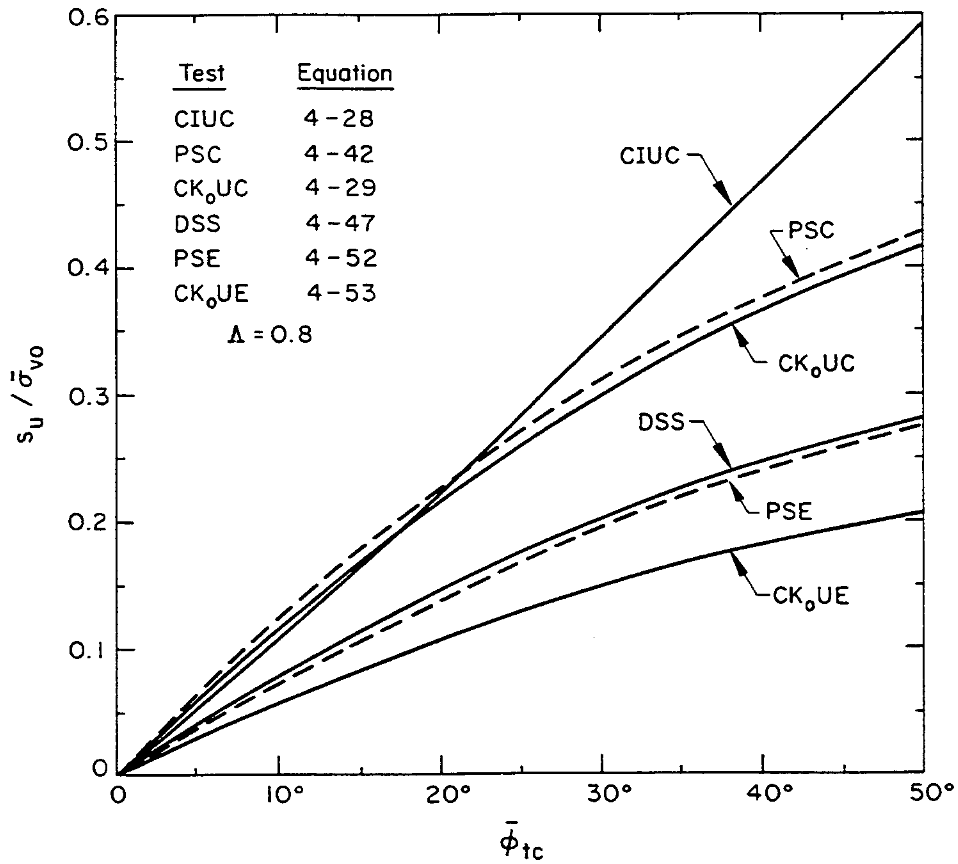

Figure 4-37. Undrained Strength Ratio as a Function of Test Type

and $\bar{\phi}_{psc} \approx 1.1\ \bar{\phi}_{tc}$, as shown previously. Figure 4-38 shows a comparison of these equations with the limited data available. The agreement is very good and slightly conservative. For comparison, Figure 4-39 shows the results for plane strain and triaxial extension tests. The plane strain extension results also are larger than the triaxial, and the differences in extension are larger than in compression. Equation 4-42 also is plotted on Figure 4-37 for reference with other test types.

The next important test boundary condition is the loading direction or stress rotation. For natural clays, strength anisotropy can develop from both stress anisotropy (K_o stresses) and structural anisotropy (layering, fabric, sensitivity, etc.). The complete range of loading angles and stress rotation effects can be investigated only in sophisticated, hollow cylinder tests. However, since these tests are rather expensive and difficult to perform, it is more common to use simpler tests with more limited loading directions (δ). Most commonly, triaxial compression (δ = 0°), direct simple shear ($\delta \approx$ 45°), and triaxial extension (δ = 90°) tests are used, as illustrated in Figure 4-40. This figure shows the general

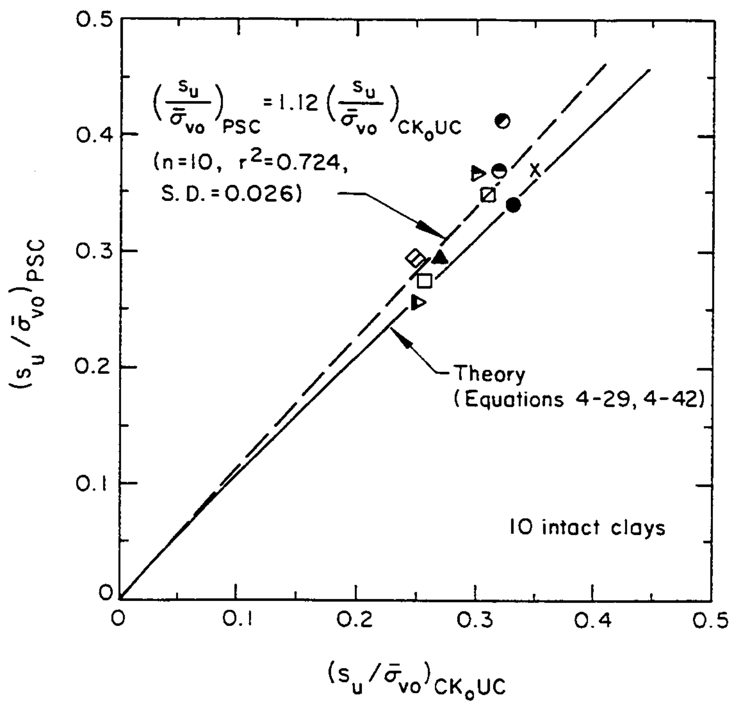

Figure 4-38. Comparison of Undrained Strength Ratios from PSC and CK_0UC Tests

Source: Data from Ladd, et al. (11) and Mayne and Holtz (26).

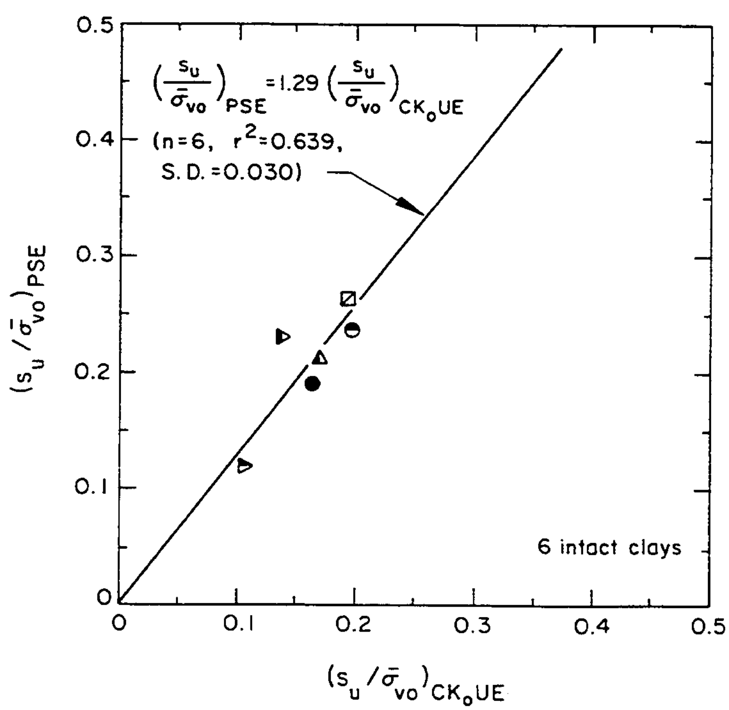

Figure 4-39. Comparison of Undrained Strength Ratios from PSE and CK_0UE Tests

Source: Data from Ladd, et al. (11) and Mayne and Holtz (26).

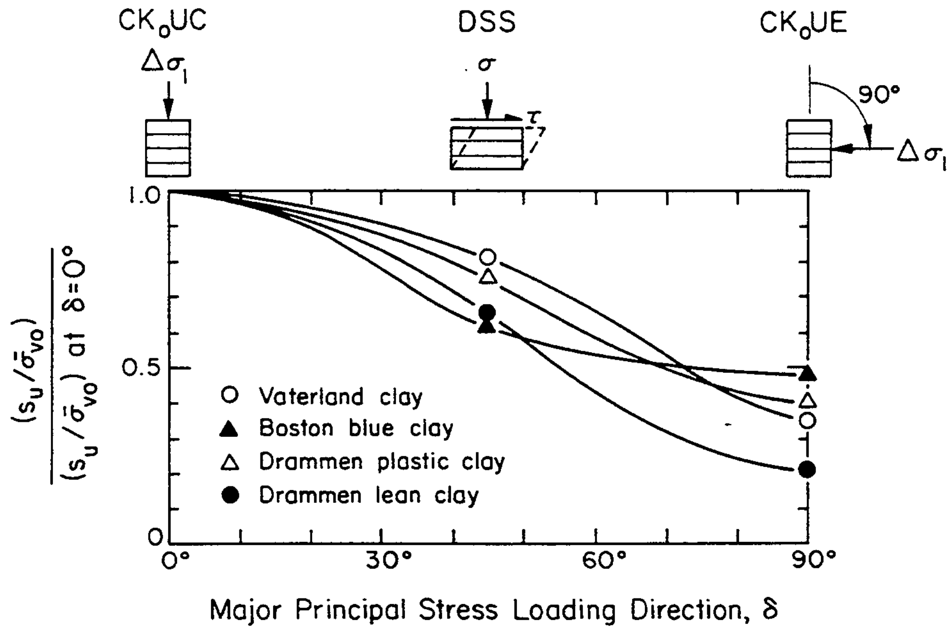

Figure 4-40. Effect of Loading Direction on s_u

Source: Hansen and Clough (43), p. 258.

observed pattern, with the DSS results intermediate between the triaxial compression and extension results.

At the present time, there is no general agreement on methods of interpreting the DSS test results in terms of effective stresses. Wroth (3) discusses many of the pertinent issues involved and presents three possible equations for interpretation, as given below:

$$(s_u/\bar{\sigma}_{vo})_{DSS\text{-}1} = 0.5 \sin \bar{\phi}_{tc} \tag{4-44}$$

$$(s_u/\bar{\sigma}_{vo})_{DSS\text{-}2} = \tan \bar{\phi}_{psc} \ (1 - \sin \bar{\phi}_{psc})/(1 + \sin \bar{\phi}_{psc}) \tag{4-45}$$

$$(s_u/\bar{\sigma}_{vo})_{DSS\text{-}3} = \sin \bar{\phi}_{psc}/(1 + \sin \bar{\phi}_{psc})^2 \tag{4-46}$$

with $\bar{\phi}_{psc} \approx 1.1 \ \bar{\phi}_{tc}$ as shown previously. Figure 4-41 compares these equations with available data on 41 clays. As can be seen, the DSS-1 interpretation typically is high, especially at high $\bar{\phi}_{tc}$ values. The DSS-2 interpretation is consistently very low, while the DSS-3 interpretation appears to be adequate.

Figure 4-42 shows the DSS data plotted against triaxial compression data, showing

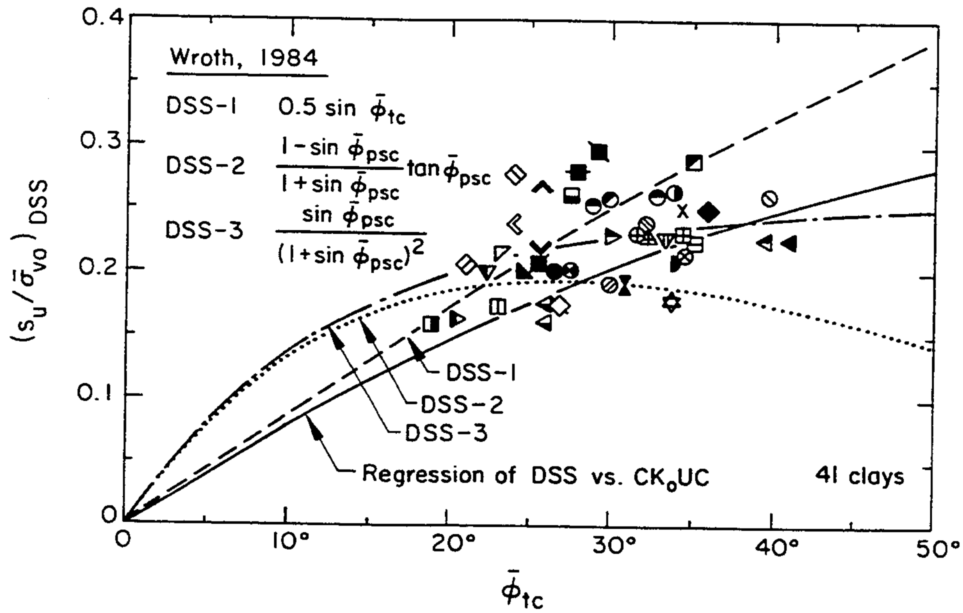

Figure 4-41. Undrained Strength Ratio from DSS versus $\bar{\phi}_{tc}$

Source: Data from Mayne (44) and others (26, 35, 41).

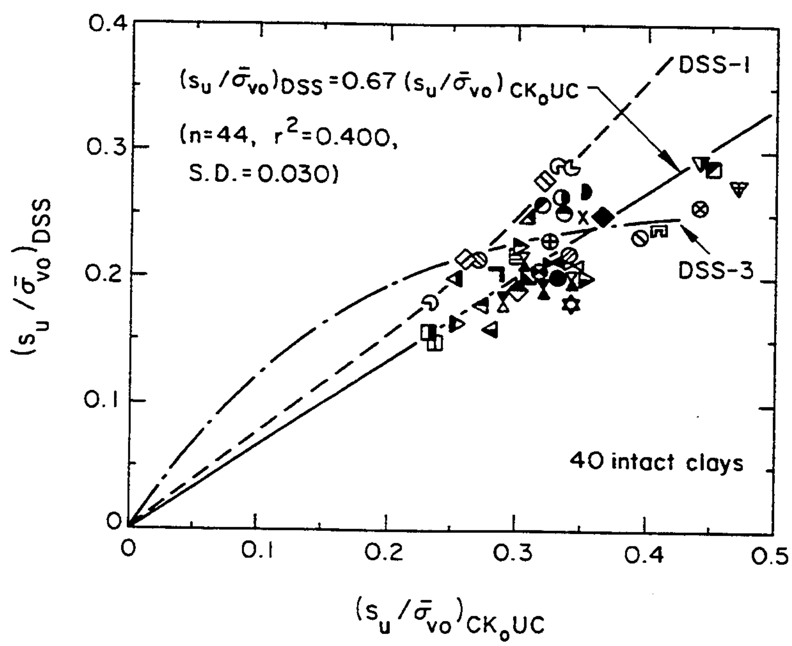

Figure 4-42. Comparison of Undrained Strength Ratios from DSS and CK_0UC Tests

Source: Data from Mayne (44) and others (26, 35, 41).

two of the DSS interpretation methods. The DSS-1 method is consistently high, while the DSS-3 method exhibits a high degree of curvature which is not evident in the data. Because of these problems with the theoretical models in describing the data, it is more prudent to rely on the regression line for the data, given by:

$$(s_u/\bar{\sigma}_{vo})_{DSS} = 0.67\ (s_u/\bar{\sigma}_{vo})_{CK_oUC} \qquad (4\text{-}47)$$

This regression line is plotted on Figure 4-41 and provides as good a predictor as the DSS-3 interpretation method. For these reasons, Equation 4-47 will be the recommended method for evaluating the DSS undrained strength ratio. This equation also is plotted in Figure 4-37 for comparison with the other test types.

Lastly, it is necessary to address the behavior in extension and compression. Prevost (45) developed simple relationships between the different tests, as given below:

$$(s_u/\bar{\sigma}_{vo})_{DSS} = 0.45\ [(s_u/\bar{\sigma}_{vo})_{PSC} + (s_u/\bar{\sigma}_{vo})_{PSE}] \qquad (4\text{-}48)$$

$$(s_u/\bar{\sigma}_{vo})_{DSS} = 0.52\ [(s_u/\bar{\sigma}_{vo})_{CK_oUC} + (s_u/\bar{\sigma}_{vo})_{CK_oUE}] \qquad (4\text{-}49)$$

These relationships generally are consistent with previous experimental observations (e.g., 46) that the DSS strength is roughly equal to the average of the triaxial compression and extension strengths. Available data for the DSS and triaxial tests are shown in Figure 4-43 and indicate general agreement. However, the regressions for both the triaxial and plane strain data are lower than Prevost's model (45). Therefore, to be consistent with the data, the relationships given by Equations 4-48 and 4-49 should be changed as follows:

$$(s_u/\bar{\sigma}_{vo})_{DSS} = 0.40\ [(s_u/\bar{\sigma}_{vo})_{PSC} + (s_u/\bar{\sigma}_{vo})_{PSE}] \qquad (4\text{-}50)$$

$$(s_u/\bar{\sigma}_{vo})_{DSS} = 0.45\ [(s_u/\bar{\sigma}_{vo})_{CK_oUC} + (s_u/\bar{\sigma}_{vo})_{CK_oUE}] \qquad (4\text{-}51)$$

Equations 4-50 and 4-51 then can be rearranged to yield the extension strengths directly, as below:

$$(s_u/\bar{\sigma}_{vo})_{PSE} = 2.50\ (s_u/\bar{\sigma}_{vo})_{DSS} - (s_u/\bar{\sigma}_{vo})_{PSC} \qquad (4\text{-}52)$$

$$(s_u/\bar{\sigma}_{vo})_{CK_oUE} = 2.22\ (s_u/\bar{\sigma}_{vo})_{DSS} - (s_u/\bar{\sigma}_{vo})_{CK_oUC} \qquad (4\text{-}53a)$$

$$\approx 0.487\ (s_u/\bar{\sigma}_{vo})_{CK_oUC} \quad \text{(using Equation 4-47]} \qquad (4\text{-}53b)$$

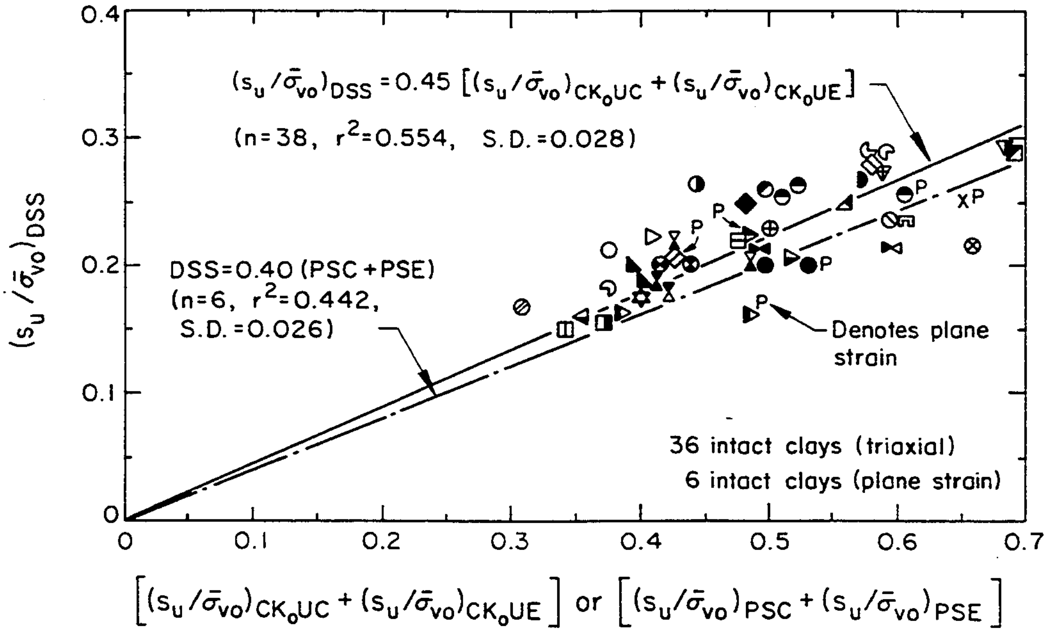

Figure 4-43. Comparison of Undrained Strength Ratios from DSS, CK_0UC and CK_0UE, and PSC and PSE Tests

Source: Data from Mayne (44) and others (26, 35).

These relationships then can be added to those on Figure 4-37 to provide a general comparison of the different test results. Available data comparing the CK_0UE and CIUC results with Equation 4-53 are shown in Figure 4-44. As can be seen, the theory underestimates the triaxial extension strength by a modest amount and therefore is somewhat conservative.

As an alternative approach for evaluating the extension strength, it has been suggested by Ladd, et al. (11) that the ratio of undrained strengths in extension to compression generally increases with increasing plasticity index, as shown in Figure 4-45. As can be seen, this is a fair alternative and could be used as a check on the analytical prediction from Equations 4-52 and 4-53.

The available data bases also provide an opportunity to evaluate the exponent Λ in the modified Cam clay model. Table 4-8 summarizes these data, showing that Λ ranges from 0.72 for compression tests, to 0.78 for shear tests, to 0.82 for extension tests. Overall, Λ is given by 0.75 with a coefficient of variation of 13 percent. This value is close to the common assumption that $\Lambda \approx 0.8$.

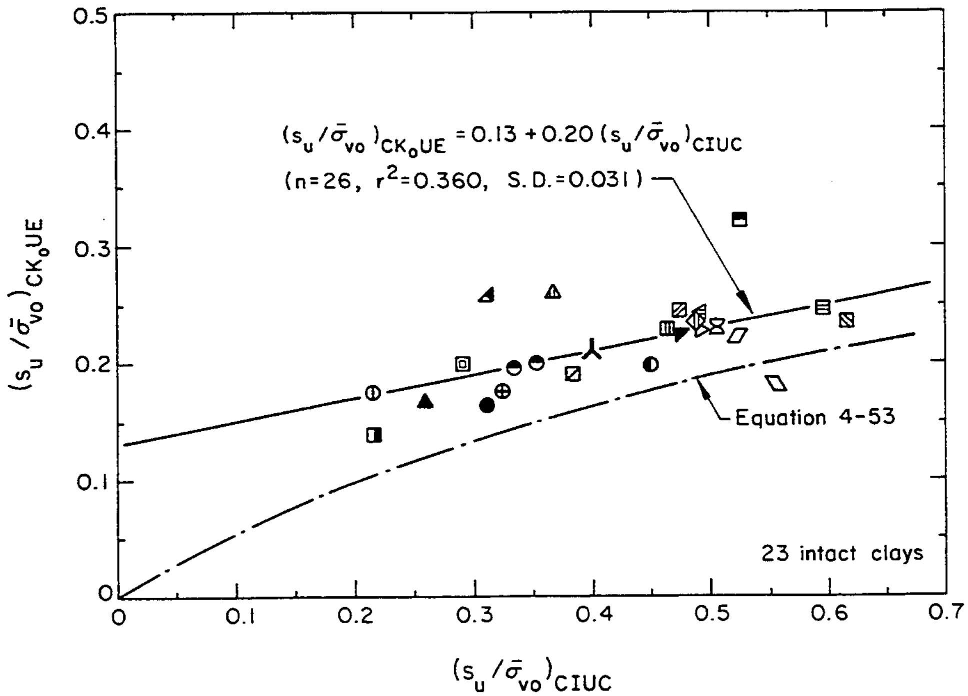

Figure 4-44. Comparison of Undrained Strength Ratios from CK_oUE and CIUC Tests

Source: Data from Mayne and others (26, 41).

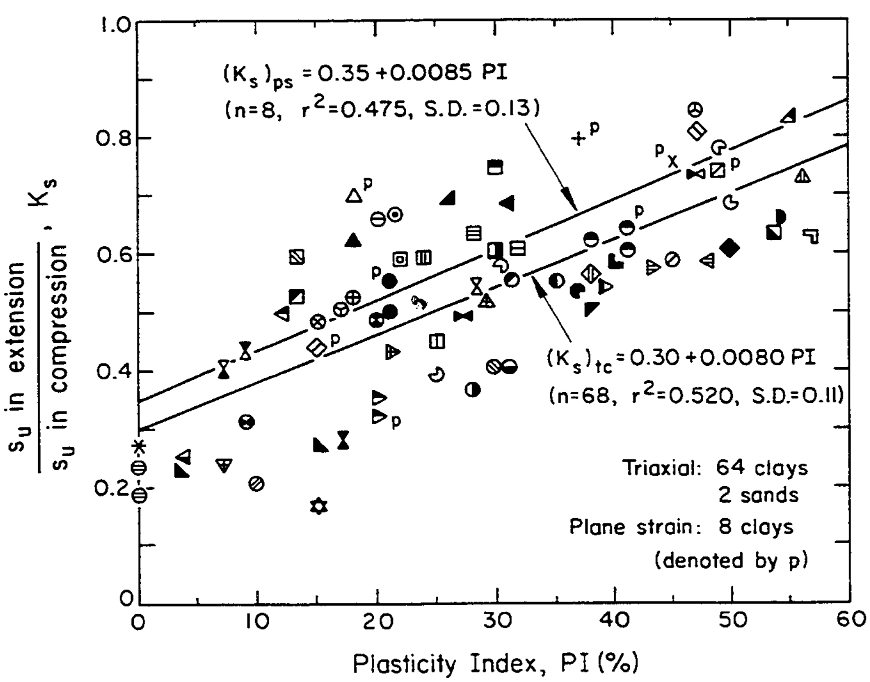

Figure 4-45. Undrained Strength Ratios in Extension and Compression versus Plasticity Index

Source: Data from Mayne and Holtz (26) and others (25, 35, 41, 47).

Table 4-8

EVALUATION OF MODIFIED CAM CLAY EXPONENT Λ

Reference Basis	Test Type	n	Λ mean	Λ COV (%)
Test Evaluation	CIUC	50	0.709	15.5
	PSC	2	0.730	2.0
	CK_oUC	34	0.738	12.7
	DSS	30	0.776	11.7
	PSE	3	0.843	6.8
	CK_oUE	19	0.818	13.8
Design Recommendation	Compression	86	0.72	14.1
	Simple shear	30	0.78	11.7
	Extension	22	0.82	12.8
Overall Mean	All Types	138	0.75	13.4

Source: Data from Mayne and others (26, 35, 41, 44).

Influence of Strain Rate During Testing

Soils exhibit a change in strength as a function of strain rate during loading. In general, for triaxial compression tests, each log cycle increase in strain rate is accompanied by a 10 percent increase in s_u (46). This observation is confirmed by the data shown in Figure 4-46 for 26 clays tested in triaxial compression. Graham, et al. (48) have shown that these trends also are observed for DSS and CK_oUE tests. A testing rate of 1 percent/hour is considered as the standard reference rate. For other than the standard rate, the following should be used:

$$s_u/(s_u \text{ for } \dot{\epsilon} = 1\%/\text{hr}) = 1.0 + 0.1 \log \dot{\epsilon} \qquad (4\text{-}54)$$

For most conventional loading cases, the standard rate would be appropriate for design.

Summary of Factors Influencing the Undrained Strength Ratio

As described previously, many factors influence the measured value of s_u. Using the CIUC test as a standard reference, the value of $s_u/\bar{\sigma}_{vo}$ can be determined as follows:

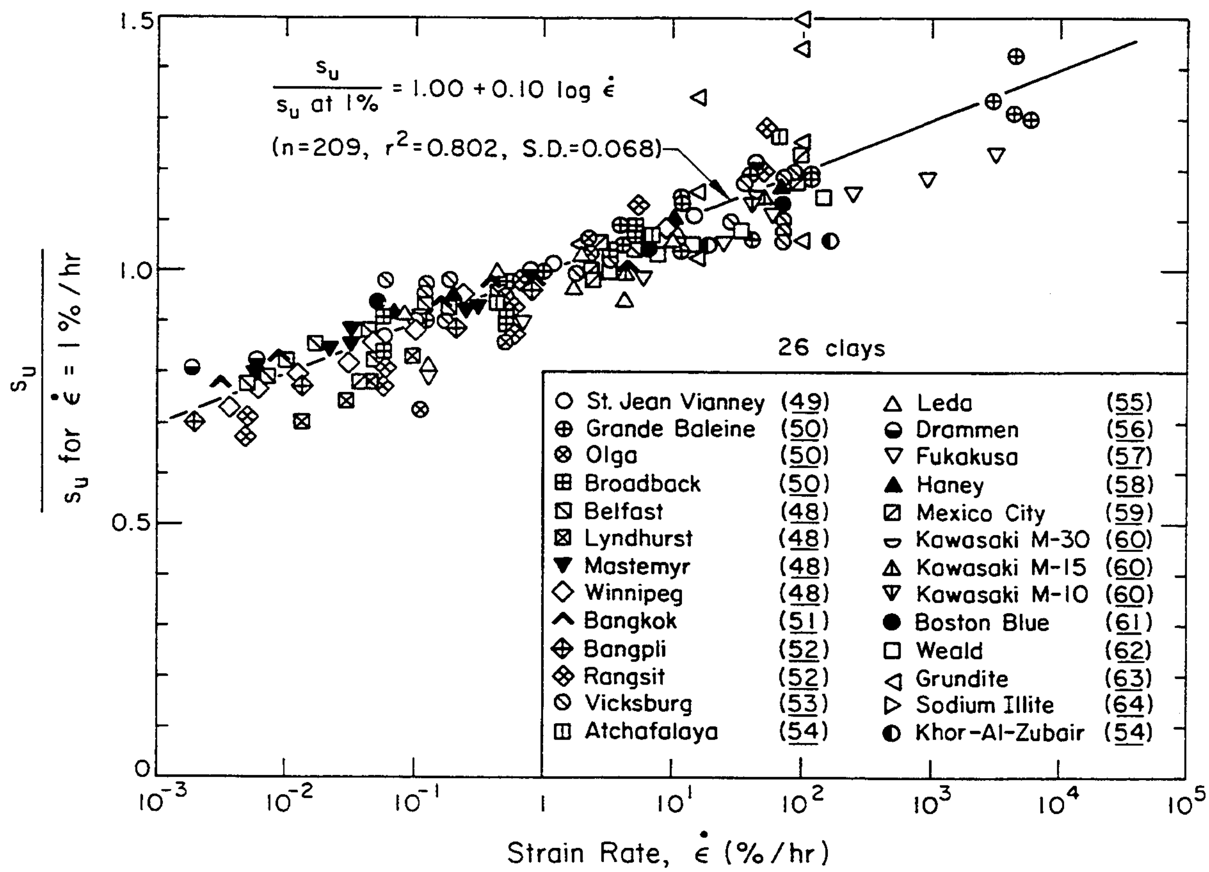

Figure 4-46. Strain Rate Influence on s_u

$$s_u/\bar{\sigma}_{vo} = a_{TEST}\ a_{RATE}\ a_{OCR}\ (s_u/\bar{\sigma}_{vo})_{CIUC} \tag{4-55}$$

in which the a coefficients are given in Table 4-9 and Figure 4-47, and $(s_u/\bar{\sigma}_{vo})_{CIUC}$ is given as:

$$(s_u/\bar{\sigma}_{vo})_{CIUC} = 0.5\ M\ (0.5)^{\Lambda} \tag{4-28}$$

Table 4-9 also gives a simple linear approximation for a_{TEST} which may be useful for first-order estimations.

UNDRAINED SHEAR STRENGTH OF COHESIVE SOILS CORRELATED WITH IN-SITU TESTS

In-situ tests can provide either a measurement or estimation of s_u in clay deposits. At the present time, direct determinations of s_u are obtained from the field vane shear test (VST). The values of s_u from the standard penetration test (SPT), cone penetration test (CPT), piezocone penetration test (CPTU), pressuremeter test (PMT), and dilatometer test (DMT) currently are obtained from analytical models,

Table 4-9

CORRECTION FACTORS FOR s_u COMPARED WITH s_u FROM CIUC TEST RESULTS

Influence	Term	Test Type	Value	Linear Approximation Within $20° < \bar{\phi}_{tc} < 40°$
Test Mode	a_{TEST}	CIUC	1.0	1.0
		PSC	Ratio of Eq. 4-42/Eq. 4-28[a]	$1.22 - 0.0112\ \bar{\phi}_{tc}$
		CK_oUC	Ratio of Eq. 4-29/Eq. 4-28	$1.13 - 0.0094\ \bar{\phi}_{tc}$
		DSS	Ratio of Eq. 4-47/Eq. 4-28	$0.77 - 0.0064\ \bar{\phi}_{tc}$
		PSE	Ratio of Eq. 4-52/Eq. 4-28	$0.71 - 0.0052\ \bar{\phi}_{tc}$
		CK_oUE	Ratio of Eq. 4-53/Eq. 4-28	$0.56 - 0.0046\ \bar{\phi}_{tc}$
Strain Rate	a_{RATE}	All	$1 + 0.1 \log \dot{\epsilon}$[b]	
Overconsolidation	a_{OCR}	All	OCR^{Λ} $\Lambda = 0.72$ for compression[c] $\Lambda = 0.78$ for simple shear[c] $\Lambda = 0.82$ for extension[c]	

a - See plots given in Figure 4-47.
b - Normal reference rate is 1 percent per hour.
c - See Table 4-8 for additional details.

empirical correlations, or calibration with a known reference strength. As noted previously, each in-situ test provides a different s_u particular to the boundary conditions imposed, rate of loading, direction of loading, etc.

Correlations with VST Results

The vane shear test (VST) is one of the oldest in-situ tests for the evaluation of s_u in clays. The value of s_u is determined from the torque required to rotate a four-bladed vane in the clay. Both the peak and remolded s_u can be determined, and therefore the sensitivity (S_t) of the clay can be computed. Details of the VST are given in Appendix E.

The value of s_u determined from the VST should not be used directly in analysis, because it needs to be corrected for the strain rate during testing and the soil anisotropy. Bjerrum (65) reviewed a number of failure case histories from embankments, excavations, and foundations which had been evaluated using s_u from the VST and developed a correction factor (μ) that is to be applied to s_u(VST). This

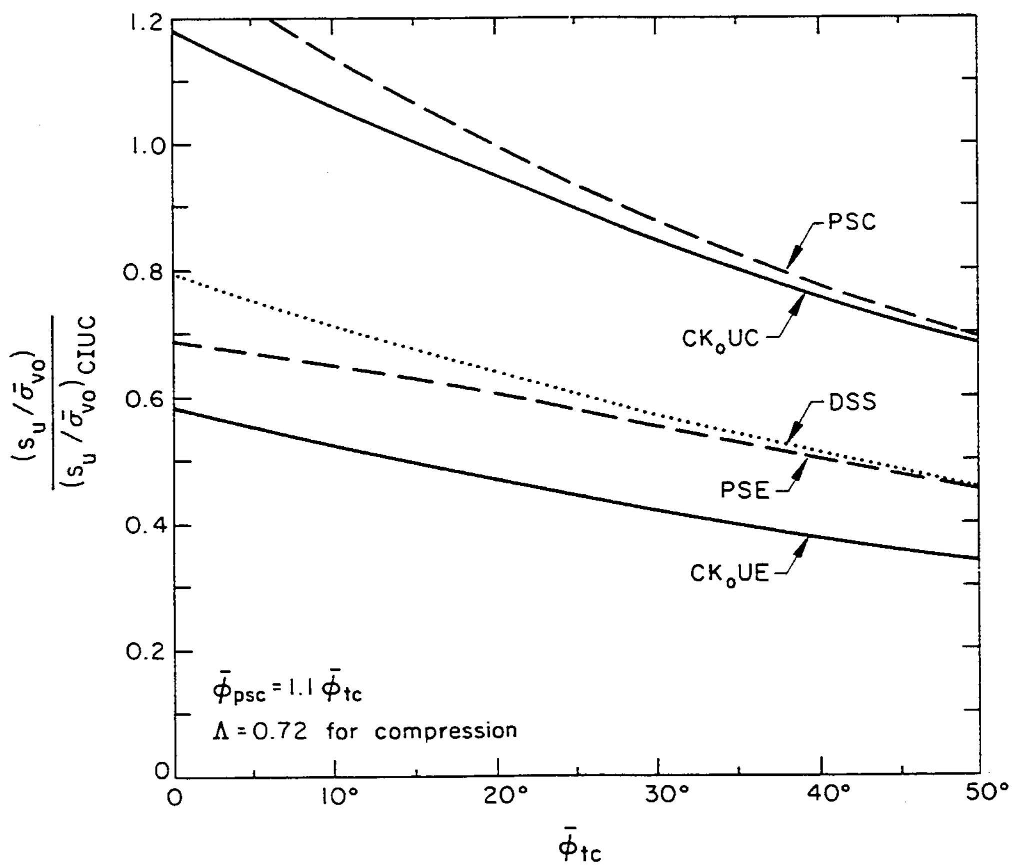

Figure 4-47. Normalized Undrained Strength Ratios for Major Laboratory Shear Test Types

factor apparently is correlated with the plasticity index. A recent update of this correlation is given in Figure 4-48.

In addition to the μ correction for strain rate and anisotropy, Bjerrum noted that there were differences in the apparent preconsolidation stress caused by aging which influenced the computed $s_u/\bar{\sigma}_{vo}$ ratio. To account for this aging, he recommended that the data be presented in terms of the preconsolidation stress, as shown below:

$$s_u(VST)/\bar{\sigma}_p = [s_u(VST)/\bar{\sigma}_{vo}]\ OCR \qquad (4\text{-}56)$$

Figure 4-49 shows a typical plot of this type, which includes the recommended correlations of Bjerrum (66) and Skempton (30), given earlier as Equation 4-18. As can be seen, the Bjerrum correlation fits the data for inorganic clays somewhat better. It should be remembered that Chandler (32) cautions against use of these

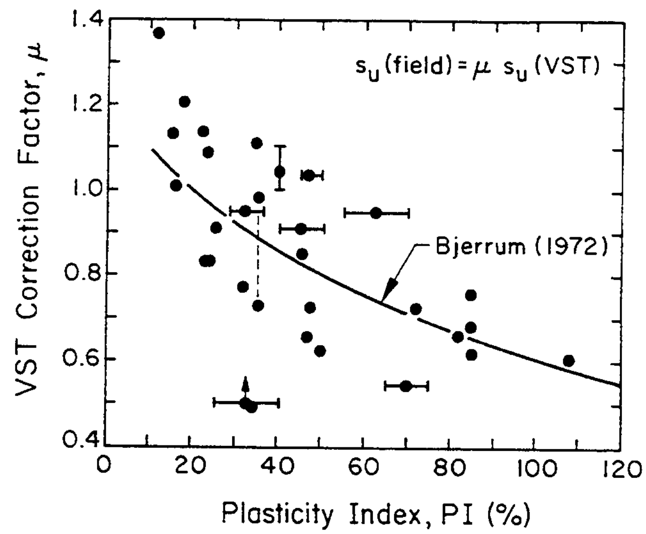

Figure 4-48. Field VST Correction Factor

Source: Ladd, et al. (11), p. 469.

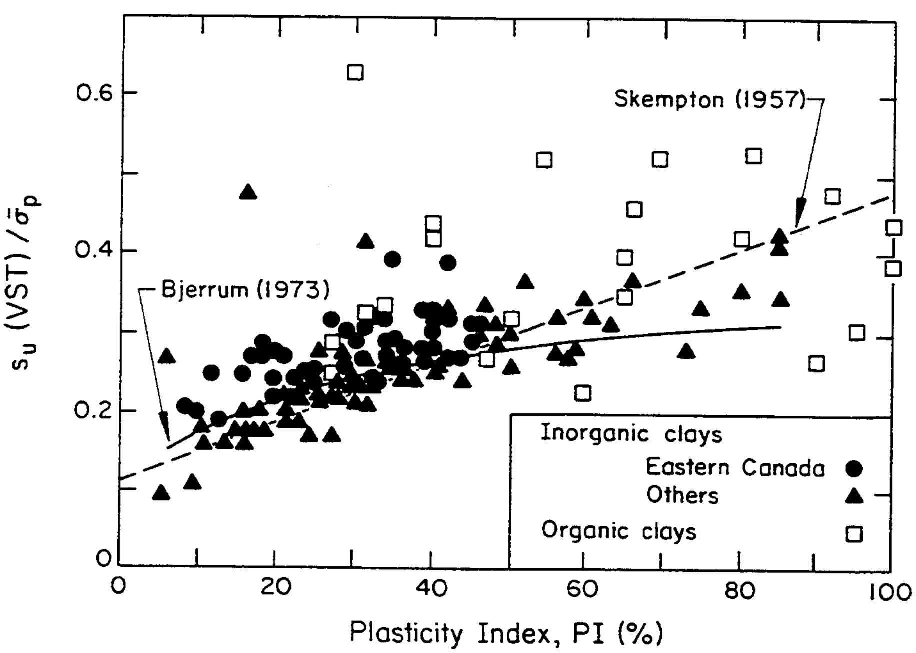

Figure 4-49. Vane Undrained Strength Ratio versus Plasticity Index for NC, Young and Aged Clays

Source: Tavenas and Leroueil (23), p. 21.

types of relationships in fissured, organic, sensitive, or other unusual clays.

Equation 4-56 includes another important difference in evaluating the undrained strength of OC clays using the VST. Earlier it was shown that, for laboratory tests, the strength increased with increasing OCR^{Λ}. Typical Λ values ranged from about 0.7 to 0.8. However, with the VST in the field, Λ basically is equal to unity. This point has been demonstrated effectively by several authors (e.g., 23, 32, 67).

Subsequent examination by Mesri (68) of Bjerrum's correction factor (Figure 4-48) and $s_u(VST)/\bar{\sigma}_p$ relationship (Figure 4-49) suggested the following:

$$s_u(\text{field})/\bar{\sigma}_p \approx \mu \; s_u(VST)/\bar{\sigma}_p \approx 0.22 \tag{4-57}$$

in which s_u(field) represents the average mobilized undrained strength in the field for stability problems such as embankments on soft clay and foundation bearing capacity. This relationship has been corroborated in independent studies by Trak, et al. (69) and Larsson (70). Recent studies by Mesri (36) have reconfirmed this relationship and have noted further that:

$$s_u(\text{field})/\bar{\sigma}_p \approx [s_u(CK_oUC)/\bar{\sigma}_p + s_u(DSS)/\bar{\sigma}_p + s_u(CK_oUE)/\bar{\sigma}_p]/3 \tag{4-58}$$

These last two equations link the direct field and laboratory shear tests and provide a general basis for evaluating the actual field value of s_u for design. As noted previously, caution is warranted in unusual clays.

Correlations with SPT N Value

Correlations have been attempted for estimating s_u from SPT N values, even though it is known that these correlations are weak. The most common of these is shown in Table 4-10, which was developed primarily using unconfined compression tests. From the results of this table, s_u can be approximated as follows:

$$s_u/p_a \approx 0.06 \; N \tag{4-59}$$

Many other relationships have been proposed as well, and several of these are shown in Figure 4-50. It is clear that these relationships represent a wide variety of interpretations of soil types and testing conditions and that a universal relationship between s_u and N is unlikely. Several other serious problems exist with Figure 4-50. First, the SPT N values have not all been standardized to the same energy level. Second, there is no indication of the reference strength used to determine s_u. The mixing of different undrained strength data is inconsistent, and it increases the scatter in the reported trends. Third, the sensitivity of the

Table 4-10

APPROXIMATE s_u VERSUS N RELATIONSHIP

N Value (blows/ft or 305 mm)	Consistency	Approximate s_u/p_a
0 to 2	very soft	< 1/8
2 to 4	soft	1/8 to 1/4
4 to 8	medium	1/4 to 1/2
8 to 15	stiff	1/2 to 1
15 to 30	very stiff	1 to 2
> 30	hard	> 2

Source: Terzaghi and Peck (4), p. 347.

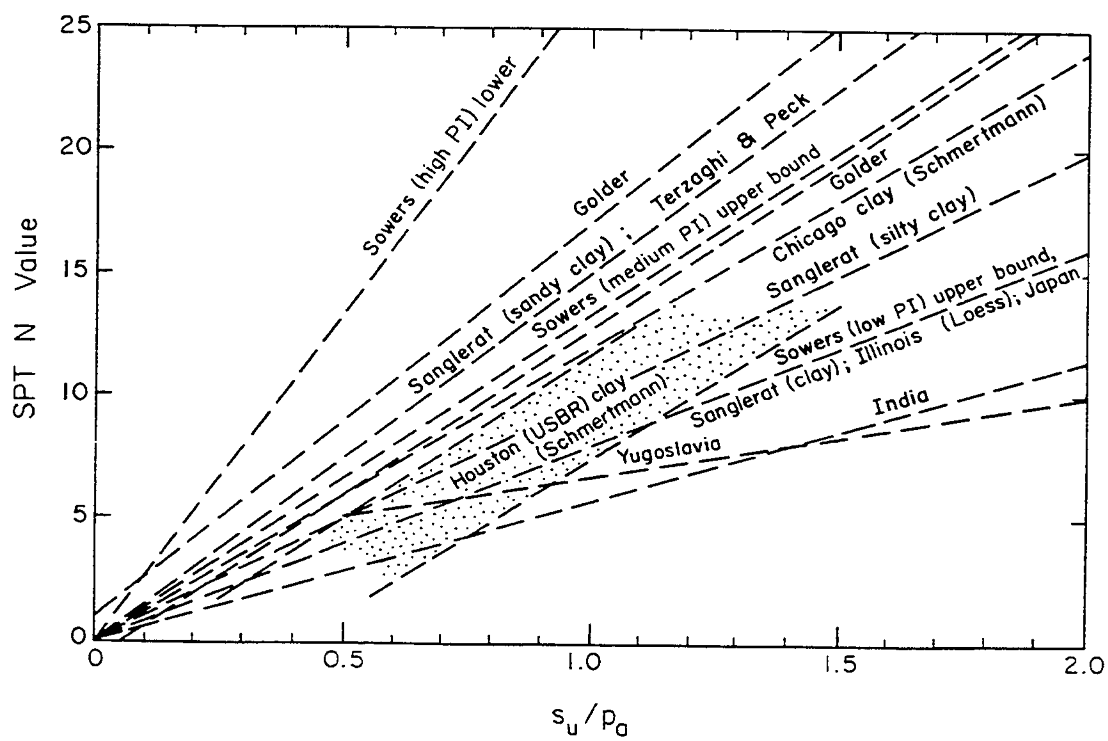

Figure 4-50. Selected Relationships Between N and s_u

Source: Djoenaidi (71), p. 5-93.

clay can affect the N value greatly, as shown in Figure 4-51. Apparently, the penetration process causes temporary excess pore water stresses which reduce the effective stresses in the vicinity of the sampler, thereby resulting in an apparently lower N value.

However, for clays within a given geology, a reasonable correlation might be expected between s_u and N. Figure 4-52 indicates this behavior over a wide range of N values where the same drilling equipment, SPT procedure, and consistent reference strength (UU triaxial) were employed. For these data, the reported regression is given by:

$$s_u/p_a = 0.29\ N^{0.72} \qquad (4\text{-}60)$$

This equation tends to predict s_u/p_a on the high side of the relationships shown in Figure 4-50.

Correlations with CPT q_c Value

The theoretical relationship for the cone tip resistance in clay is given by:

$$q_c = N_k\ s_u + \sigma_{vo} \qquad (4\text{-}61)$$

in which q_c = cone tip resistance, σ_{vo} = total overburden stress, and N_k = cone bearing factor. The application of classical plasticity theory to this bearing capacity problem suggests N_k on the order of 9 for a general shear model. Cavity

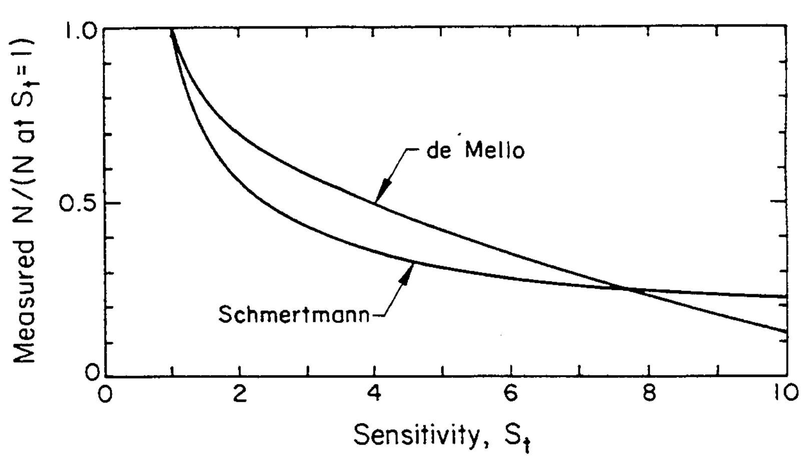

Figure 4-51. Apparent Decrease of N with Increasing Sensitivity

Source: Schmertmann (14), p. 66.

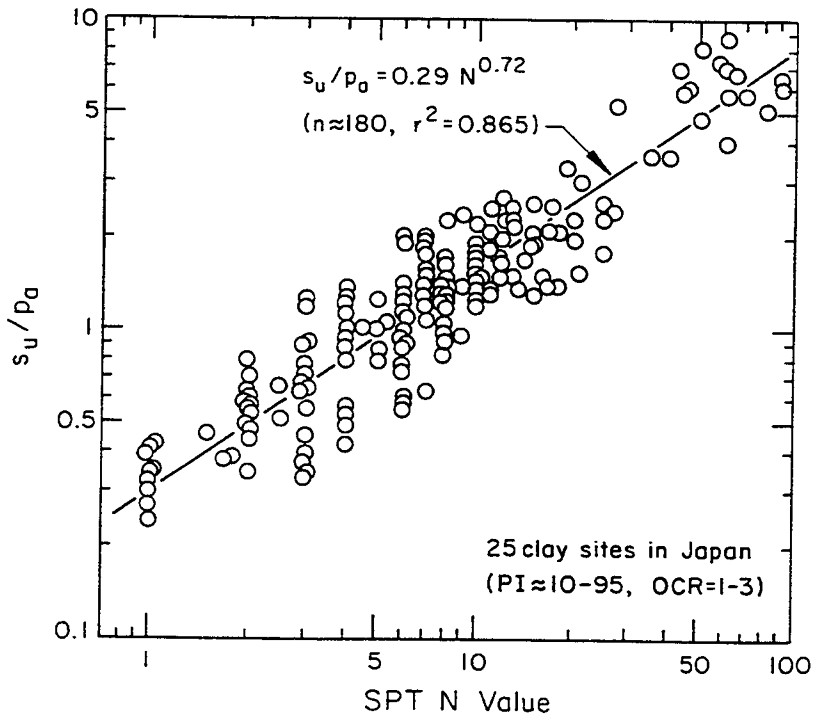

Figure 4-52. Relationship Between s_u and SPT N Value

Source: Hara, et al. (72), p. 9.

expansion theories give N_k increasing in the range of 7 to 13 for increasing values of rigidity index ($I_r = G/s_u$, with G = shear modulus). Steady penetration theory provides a narrow range for N_k between 14 and 18 for a wide range of I_r.

With the various uncertainties in choosing appropriate theoretical models, it is not surprising that N_k usually is determined empirically by calibrating CPT data with a known measured value of s_u. The range of values of N_k back-calculated from CPT data is presented in Figure 4-53. This wide range of N_k values must be scrutinized for several reasons: (1) inconsistent reference strengths, (2) mixing of different type cones (electric and mechanical), and (3) need for correction of q_c for pore water stress effects (Appendix B). These factors can change N_k dramatically.

The importance of correcting q_c for pore water stress effects has been discussed previously and is illustrated by Figure 4-54 for two piezocones with different area ratios. The corrected cone tip resistance (q_T) can be obtained only by use of piezocones with porous elements located behind the tip. Consequently, the large scatter observed in empirical determinations of N_k may result, in part, from use of

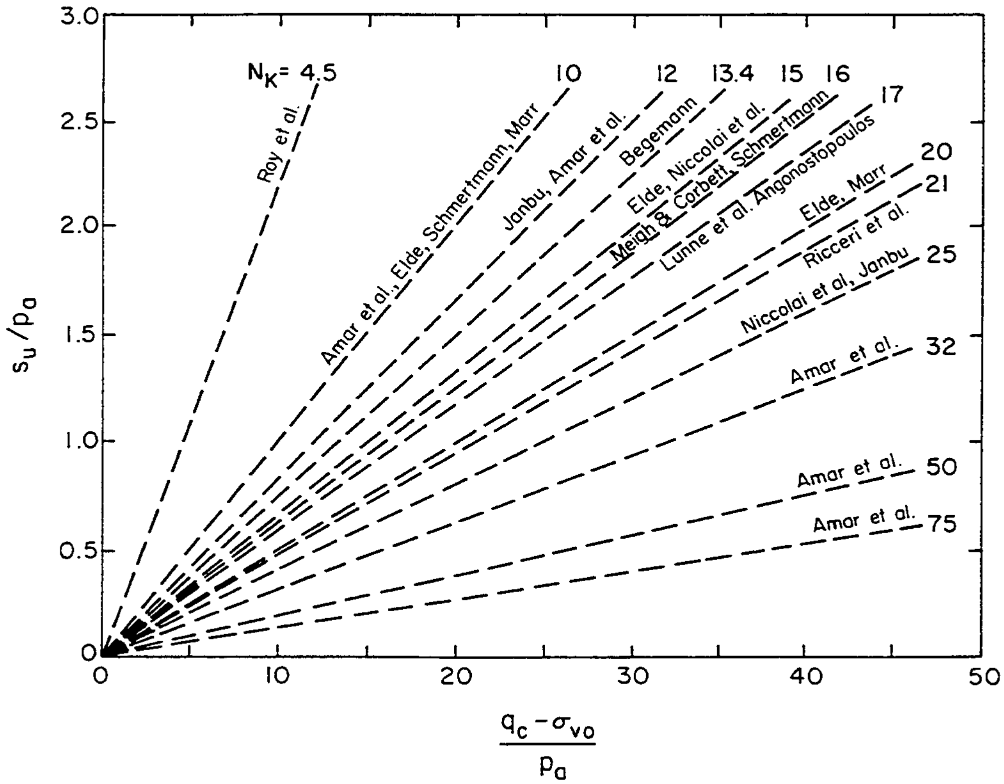

Figure 4-53. Reported Range of N_k Factors from CPT Data

Source: Djoenaidi (71), p. 5-83.

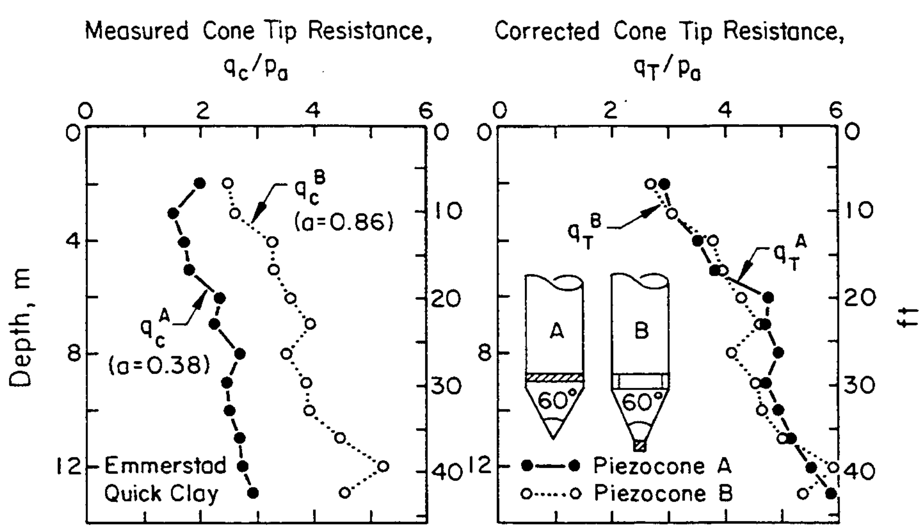

Figure 4-54. Effect of Pore Water Stress on Cone Tip Resistance

Source: Aas, et al. (67), p. 19.

an uncorrected q_c.

The value of N_k ideally should be determined experimentally by comparison with a consistent reference strength. Often, the field VST is used as the reference. In this regard, it is important to recall that the VST requires a correction for s_u in itself. Early correlations (e.g., Battaglio, et al., 73) for N_k using uncorrected VST data suggested a trend for N_k in terms of the plasticity index (PI). However, upon later re-analysis of the same data using the corrected VST strength [μ s_u(VST)], N_k apparently was independent of PI.

Subsequent studies by Keaveny and Mitchell (74) and Konrad and Law (75) have demonstrated that Vesić's cavity expansion theory (76) provides a reasonable estimate for N_k, as given below:

$$N_k = 2.57 + 1.33 (\ln I_r + 1) \tag{4-62}$$

Keaveny and Mitchell suggest using CK_oUC triaxial compression tests to evaluate I_r, while Konrad and Law recommend using the self-boring pressuremeter test.

Recent theoretical developments (Houlsby and Teh, 77) suggest that more refined procedures for determining s_u from the CPT may be appropriate. However, these models currently require a number of parameters that are difficult to determine. Further testing in the future may allow convenient determination of these parameters and a better estimation of s_u.

Correlations with CPTU Results

The piezocone penetration test (CPTU) permits determination of s_u from the corrected cone tip resistance (q_T), as described previously, and also allows for a separate estimate of s_u from the pore water stress measurement. Research on this subject (e.g., Robertson, et al., 78) has suggested the following:

$$s_u = \Delta u / N_{\Delta u} \tag{4-63}$$

in which Δu = measured excess pore water stress (u_m - u_o) and $N_{\Delta u}$ = pore water stress ratio, which may be estimated from A_f and either the PI or rigidity index, as shown in Figure 4-55. Alternative recommendations by Konrad and Law (75) suggest a more complex relationship, including a number of parameters which are somewhat difficult to evaluate.

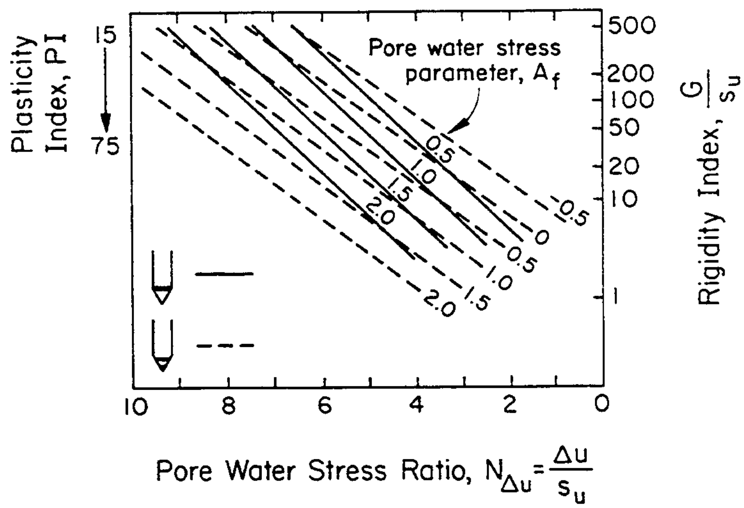

Figure 4-55. s_u as a Function of Δu in the CPTU

Source: Robertson, et al. (78), p. 1273.

Correlations with PMT Results

The pressuremeter test (PMT) ideally provides a measurement of s_u at the PMT limit stress. Based on cavity expansion theory (Baguelin, et al., 79), s_u can be evaluated from:

$$s_u = (p_L - p_o)/N_p \qquad (4\text{-}64)$$

in which p_L = PMT limit stress, p_o = PMT total horizontal stress, $N_p = 1 + \ln(E_{PMT}/3s_u)$, and E_{PMT} = PMT modulus. Values of N_p may range from 2 to 20 (Mair and Wood, 19), but typical values usually range from 5 to 12, with an average of 8.5. Difficulties in choosing the correct value of N_p are compounded by possible measurement errors in both p_L and p_o.

An alternative and more direct method to obtain s_u is shown in Figure 4-56. By re-plotting the basic data as shown in Figure 4-56b, a straight line develops. The slope of this line is s_u. Wroth (3) notes that s_u from the PMT should be close to the value obtained from plane strain compression (PSC) tests.

Correlations with DMT Results

The dilatometer test (DMT) horizontal stress index, $K_D = (p_o - u_o)/\bar{\sigma}_{vo}$, has been correlated with s_u, as shown in Figure 4-57. Based on these data for Italian clays, the following correlation was suggested:

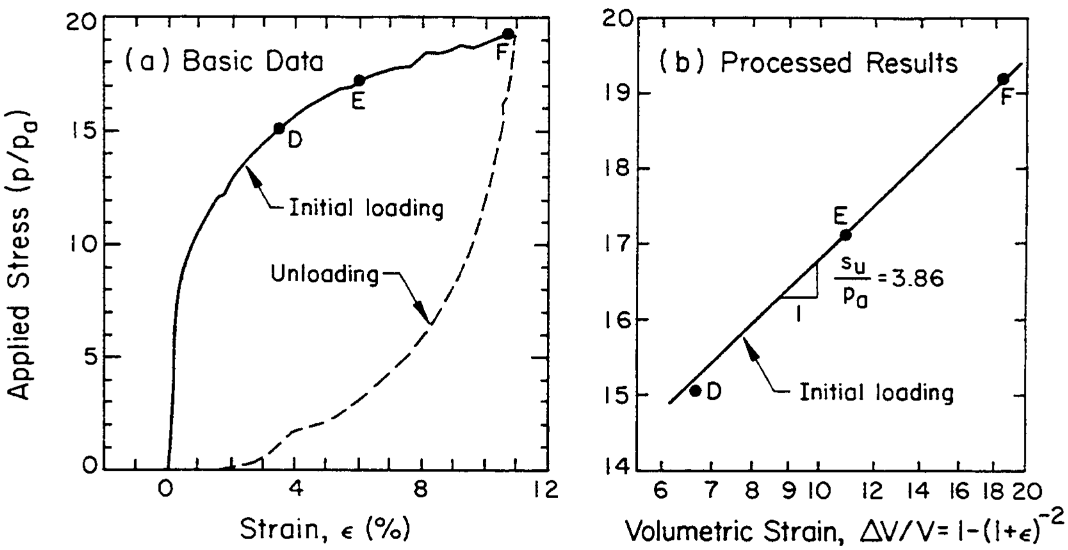

Figure 4-56. PMT Results in Bartoon Clay

Source: Wroth (3), p. 462.

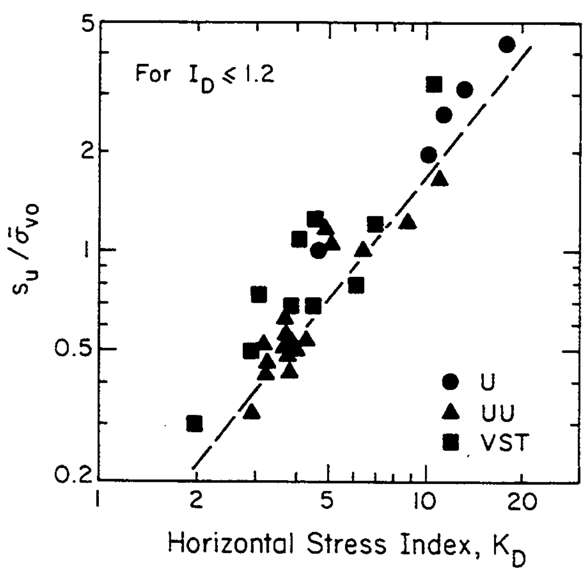

Figure 4-57. s_u as a Function of K_D from the DMT

Source: Marchetti (80), p. 317.

$$(s_u/\bar{\sigma}_{vo})_{PMT} = 0.22\ (0.5\ K_D)^{1.25} \qquad (4\text{-}65)$$

This equation originally was based on clays with a material index, I_D, less than or equal to 1.2. Current recommendations (Schmertmann, 81) are to limit this relationship to clays with $I_D \leq 0.6$. The strength data initially were obtained from unconfined compression tests (U), unconsolidated-undrained triaxial compression tests (UU), and field vane shear tests (VST). Subsequent work by Lacasse and Lunne (82) suggests that the 0.22 coefficient should vary with test type as follows: 0.14 for direct simple shear, 0.20 for triaxial compression, and 0.17 to 0.21 for field VST. Other data by Powell and Uglow (83) indicate different factors for fissured clays and glacial tills if the reference s_u is determined from plate load tests or the self-boring pressuremeter test.

REFERENCES

1. Bishop, A. W., "The Strength of Soils as Engineering Materials", Geotechnique, Vol. 16, No. 2, June 1966, pp. 89-130.

2. Kulhawy, F. H., Trautmann, C. H., Beech, J. F., O'Rourke, T. D., McGuire, W., Wood, W. A., and Capano, C., "Transmission Line Structure Foundations for Uplift-Compression Loading", Report EL-2870, Electric Power Research Institute, Palo Alto, 1983, 412 p.

3. Wroth, C. P., "Interpretation of In-Situ Soil Tests", Geotechnique, Vol. 34, No. 4, Dec. 1984, pp. 449-489.

4. Terzaghi, K. and Peck, R. B., Soil Mechanics in Engineering Practice, 2nd Ed., John Wiley and Sons, New York, 1967, 729 p.

5. Schmertmann, J. H., "Guidelines for Cone Penetration Test Performance and Design", Report FHWA-TS-78-209, U.S. Department of Transportation, Washington, 1978, 145 p.

6. NAVFAC, Soil Mechanics (DM 7.1), Naval Facilities Engineering Command, Alexandria, 1982, 355 p.

7. Baligh, M. M., "Cavity Expansion in Sands with Curved Envelopes", Journal of the Geotechnical Engineering Division, ASCE, Vol. 102, No. GT11, Nov. 1976, pp. 1131-1146.

8. Bolton, M. D., "The Strength and Dilatancy of Sands", Geotechnique, Vol. 36, No. 1, Mar. 1986, pp. 65-78.

9. Rowe, P. W., "The Relation Between the Shear Strength of Sands in Triaxial Compression, Plane Strain and Direct Shear", Geotechnique, Vol. 19, No. 1, Mar. 1969, pp. 75-86.

10. Koerner, R. M., "Effect of Particle Characteristics on Soil Strength", Journal of the Soil Mechanics and Foundations Division, ASCE, Vol. 96, No. SM4, July 1970, pp. 1221-1234.

11. Ladd, C. C., Foote, R., Ishihara, K., Schlosser, F., and Poulos, H. G., "Stress-Deformation and Strength Characteristics", Proceedings, 9th International Conference on Soil Mechanics and Foundation Engineering, Vol. 2, Tokyo, 1977, pp. 421-494.

12. Peck, R. B., Hanson, W. E., and Thornburn, T. H., Foundation Engineering, 2nd Ed., John Wiley and Sons, New York, 1974, 514 p.

13. Meyerhof, G. G., "Penetration Tests and Bearing Capacity of Cohesionless Soils", Journal of the Soil Mechanics and Foundations Division, ASCE, Vol. 82, No. SM1, Jan. 1956, pp. 1-19.

14. Schmertmann, J. H., "Measurement of In-Situ Shear Strength", Proceedings, ASCE Specialty Conference on In-Situ Measurement of Soil Properties, Vol. 2, Raleigh, 1975, pp. 57-138. (closure: pp. 175-179).

15. Robertson, P. K. and Campanella, R. G., "Interpretation of Cone Penetration Tests. Part I: Sand", Canadian Geotechnical Journal, Vol. 20, No. 4, Nov. 1983, pp. 718-733.

16. Villet, W. C. B. and Mitchell, J. K., "Cone Resistance, Relative Density, and Friction Angle", Cone Penetration Testing and Experience, Eds. G. M. Norris and R. D. Holtz, ASCE, New York, 1981, pp. 178-208.

17. Marchetti, S., "On the Field Determination of K_o in Sand", Proceedings, 11th International Conference on Soil Mechanics and Foundation Engineering, Vol. 5, San Francisco, 1985, pp. 2667-2672.

18. Hughes, J. M. O., Wroth, C. P., and Windle, D., "Pressuremeter Tests in Sands", Geotechnique, Vol. 27, No. 4, Dec. 1977, pp. 455-477.

19. Mair, R. J. and Wood, D. M., Pressuremeter Testing, Butterworths, London, 1987, 160 p.

20. Durgunoglu, H. T. and Mitchell, J. K., "Static Penetration Resistance of Soils", Proceedings, ASCE Specialty Conference on In-Situ Measurement of Soil Properties, Vol. 1, Raleigh, 1975, pp. 151-189.

21. Schmertmann, J. H., "A Method for Determining the Friction Angle in Sands from the Marchetti DMT", Proceedings, 2nd European Symposium on Penetration Testing, Vol. 2, Amsterdam, 1982, pp. 853-861.

22. Mitchell, J. K., Fundamentals of Soil Behavior, John Wiley and Sons, New York, 1976, 422 p.

23. Tavenas, F. and Leroueil, S., "State-of-the-Art on Laboratory and In-Situ Stress-Strain-Time Behavior of Soft Clays", Proceedings, International Symposium on Geotechnical Engineering of Soft Soils, Mexico City, 1987, pp. 1-46.

24. Mayne, P. W., "Stress Anisotropy Effects on Clay Strength", Journal of Geotechnical Engineering, ASCE, Vol. 111, No. 3, Mar. 1985, pp. 356-366.

25. Nakase, A. and Kamei, T., "Undrained Shear Strength of Remolded Marine Clays", Soils and Foundations, Vol. 28, No. 1, Mar. 1988, pp. 29-40.

26. Mayne, P. W. and Holtz, R. D., "Effect of Principal Stress Rotation on Clay Strength", Proceedings, 11th International Conference on Soil Mechanics and Foundation Engineering, Vol. 2, San Francisco, 1985, pp. 579-582.

27. Lupini, J. F., Skinner, A. E., and Vaughan, P. R., "The Drained Residual Strength of Cohesive Soils", Geotechnique, Vol. 31, No. 2, June 1981, pp. 181-213.

28. Skempton, A. W., "Residual Strength of Clays in Landslides, Folded Strata, and the Laboratory", Geotechnique, Vol. 35, No. 1, Mar. 1985, pp. 3-18.

29. Lambe, T. W., "Amuay Landslides", Proceedings, 11th International Conference on Soil Mechanics and Foundation Engineering, Jubilee Volume, San Francisco, 1985, pp. 137-159.

30. Skempton, A. W., Discussion of "Planning and Design of New Hong Kong Airport", Proceedings, Institution of Civil Engineers, Vol. 7, June 1957, pp. 305-307.

31. Karlsson, R. and Viberg, L., "Ratio c/p in Relation to Liquid Limit and Plasticity Index, with Special Reference to Swedish Clays", Proceedings, Conference on Shear Strength Properties of Natural Soils and Rocks, Vol. 1, Oslo, 1967, pp. 43-47.

32. Chandler, R. J., "The In-Situ Measurement of the Undrained Shear Strength of Clays Using the Field Vane", Vane Shear Strength Testing in Soils: Field and Laboratory Studies (STP 1014), ASTM, Philadelphia, 1988, pp. 13-44.

33. Bjerrum, L. and Simons, N. E., "Comparison of Shear Strength Characteristics of Normally Consolidated Clays", ASCE Research Conference on Shear Strength of Cohesive Soils, Boulder, 1960, pp. 711-726.

34. Wroth, C. P. and Houlsby, G. T., "Soil Mechanics - Property Characterization and Analysis Procedures", Proceedings, 11th International Conference on Soil Mechanics and Foundation Engineering, Vol. 1, San Francisco, 1985, pp. 1-55.

35. Jamiolkowski, M., Ladd, C. C., Germaine, J. T., and Lancellotta, R., "New Developments in Field and Laboratory Testing of Soils", Proceedings, 11th International Conference on Soil Mechanics and Foundation Engineering, Vol. 1, San Francisco, 1985, pp. 57-153.

36. Mesri, G., "A Re-evaluation of $s_{u(mob)} \approx 0.22\ \sigma_p'$ Using Laboratory Shear Tests", Canadian Geotechnical Journal, Vol. 26, No. 1, Feb. 1989, pp. 162-164.

37. Wood, D. M., "Index Properties and Critical State Soil Mechanics", Proceedings, Symposium on Recent Developments in Laboratory and Field Tests and Analysis of Geotechnical Problems, Bangkok, Dec. 1983, pp. 301-309.

38. Wroth, C. P. and Wood, D. M., "The Correlation of Index Properties with Some Basic Engineering Properties of Soils", Canadian Geotechnical Journal, Vol. 15, No. 2, May 1978, pp. 137-145.

39. Skempton, A. W., "The Pore Pressure Coefficients A and B", Geotechnique, Vol. 4, No. 4, Dec. 1954, pp. 143-147.

40. Mayne, P. W. and Stewart, H. E., "Pore Pressure Behavior of K_o-Consolidated Clays", Journal of Geotechnical Engineering, ASCE, Vol. 114, No. 11, Nov. 1988, pp. 1340-1346.

41. Mayne, P. W., "Determining OCR in Clays from Laboratory Strength", Journal of Geotechnical Engineering, ASCE, Vol. 114, No. 1, Jan. 1988, pp. 76-92.

42. Koutsoftas, D. C. and Ladd, C. C., "Design Strengths for an Offshore Clay", Journal of Geotechnical Engineering, ASCE, Vol. 111, No. 3, Mar. 1985, pp. 337-355.

43. Hansen, L. A. and Clough, G. W., "Characterization of the Undrained Anisotropy of Clays", Application of Plasticity and Generalized Stress-Strain in Geotechnical Engineering, Ed. by R. N. Yong and E. T. Selig, ASCE, New York, 1980, pp. 253-276.

44. Mayne, P. W., "A Review of Undrained Strength in Direct Simple Shear", Soils and Foundations, Vol. 25, No. 3, Sept. 1985, pp. 64-72.

45. Prevost, J. H., "Undrained Shear Tests on Clays", Journal of the Geotechnical Engineering Division, ASCE, Vol. 105, No. GT1, Jan. 1979, pp. 49-64.

46. Ladd, C. C. and Foott, R., "New Design Procedure for Stability of Soft Clays", Journal of the Geotechnical Engineering Division, ASCE, Vol. 100, No. GT7, July 1974, pp. 763-786.

47. Hight, D. W., Shibuya, S., and Symes, M. J., Discussion of "The Engineering Application of Direct and Simple Shear Testing", Geotechnique, Vol. 38, No. 1, Mar. 1988, pp. 139-140.

48. Graham, J., Crooks, J. H. A., and Bell, A. L., "Time Effects on the Stress-Strain Behavior of Natural Soft Clays", Geotechnique, Vol. 33, No. 3, Sept. 1983, pp. 327-340.

49. Vaid, Y. P., Robertson, P. K., and Campanella, R. G., "Strain Rate Behavior of Saint Jean Vianney Clay", Canadian Geotechnical Journal, Vol. 16, No. 1, Feb. 1979, pp. 34-42.

50. Lefebvre, G. and LeBoeuf, D., "Rate Effects and Cyclic Loading of Sensitive Clays", Journal of Geotechnical Engineering, ASCE, Vol. 113, No. 5, May 1987, pp. 476-489.

51. Eide, O. and Holmberg, S., "Test Fills to Failure on Soft Bangkok Clay", Proceedings, ASCE Specialty Conference on Performance of Earth and Earth-Supported Structures, Vol. 1, West Lafayette, 1972, pp. 159-180.

52. Brand, E. W., Discussion of "Time Effects on the Stress-Strain Behavior of Natural Soft Clays", Geotechnique, Vol. 34, No. 3, Sept. 1984, pp. 435-438.

53. Richardson, A. M. and Whitman, R. V., "Effect of Strain Rate Upon Undrained Shear Resistance of a Saturated Remolded Fat Clay", Geotechnique, Vol. 13, No. 4, Dec. 1963, pp. 310-324.

54. Lacasse, S., "Effect of Load Duration on Undrained Behavior of Clay and Sand", Report 40007-1, Norwegian Geotechnical Institute, Oslo, Apr. 1979, 118 p.

55. Crawford, C. B., "The Influence of Rate of Strain on Effective Stresses in Sensitive Clay", Papers on Soils (STP 254), ASTM, Philadelphia, 1959, pp. 36-48.

56. Berre, T. and Bjerrum, L., "Shear Strength of Normally Consolidated Clays", Proceedings, 8th International Conference on Soil Mechanics and Foundation Engineering, Vol. 1.1, Moscow, 1973, pp. 39-49.

57. Akai, K., Adachi, T., and Ando, N., "Existence of a Unique Stress-Strain-Time Relation of Clays", Soils and Foundations, Vol. 15, No. 1, Mar. 1975, pp. 1-16.

58. Vaid, Y. P. and Campanella, R. G., "Time-Dependent Behavior of Undisturbed Clay", Journal of the Geotechnical Engineering Division, ASCE, Vol. 103, No. GT7, July 1977, pp. 693-709.

59. Alberro, J. and Santoyo, E., "Long-Term Behavior of Mexico City Clay", Proceedings, 8th International Conference on Soil Mechanics and Foundation Engineering, Vol. 1.1, Moscow, 1973, pp. 1-9.

60. Nakase, A. and Kamei, T., "Influence of Strain Rate on Undrained Shear Characteristics of K_0-Consolidated Cohesive Soils", Soils and Foundations, Vol. 26, No. 1, Mar. 1986, pp. 85-95.

61. Taylor, D. W., Fundamentals of Soil Mechanics, John Wiley and Sons, New York, 1948, 700 p.

62. Bishop, A. W. and Henkel, D. J., The Measurement of Soil Properties in the Triaxial Test, Edward Arnold, London, 1962, pp. 174-179.

63. Perloff, W. H. and Osterberg, J. O., "The Effect of Strain Rate on the Undrained Shear Strength of Cohesive Soils", Proceedings, 2nd Pan-American Conference on Soil Mechanics and Foundation Engineering, Vol. 1, Rio de Janeiro, 1963, pp. 103-128.

64. Olson, R. E., "Shear Strength Properties of a Sodium Illite", Journal of the Soil Mechanics and Foundations Division, ASCE, Vol. 89, No. 1, Jan. 1963, pp. 183-208.

65. Bjerrum, L., "Embankments on Soft Ground", Proceedings, ASCE Specialty Conference on Performance of Earth and Earth-Supported Structures, Vol. 2, Lafayette, 1972, pp. 1-54.

66. Bjerrum, L., "Problems of Soft Mechanics and Construction on Soft Clays", Proceedings, 8th International Conference on Soil Mechanics and Foundation Engineering, Vol. 3, Moscow, 1973, pp. 111-159.

67. Aas, G., Lacasse, S., Lunne, T., and Høeg, K., "Use of In-Situ Tests for Foundation Design on Clay", Use of In-Situ Tests in Geotechnical Engineering (GSP 6), Ed. S. P. Clemence, ASCE, New York, 1986, pp. 1-30.

68. Mesri, G., Discussion of "New Design Procedure for Stability of Soft Clays", Journal of Geotechnical Engineering, ASCE, Vol. 101, No. GT4, Apr. 1975, pp. 409-412.

69. Trak, B., LaRochelle, P., Tavenas, F., Leroueil, S., and Roy, M., "A New Approach to the Stability Analysis of Embankments on Sensitive Clays", Canadian Geotechnical Journal, Vol. 17, No. 4, Nov. 1980, pp. 526-544.

70. Larsson, R., "Undrained Shear Strength in Stability Calculation of Embankments and Foundations on Soft Clays", Canadian Geotechnical Journal, Vol. 17, No. 4, Nov. 1980, pp. 591-602.

71. Djoenaidi, W. J., "A Compendium of Soil Properties and Correlations", M. Eng. Sc. Thesis, University of Sydney, Sydney, 1985, 836 p.

72. Hara, A., Ohta, T., Niwa, M., Tanaka, S., and Banno, T., "Shear Modulus and Shear Strength of Cohesive Soils", Soils and Foundations, Vol. 14, No. 3, Sept. 1974, pp. 1-12.

73. Battaglio, M., Bruzzi, D., Jamiolkowski, M., and Lancellotta, R., "Interpretation of CPT and CPTU", Proceedings, Field Instrumentation and In-Situ Measurements, Singapore, Nov. 1986, pp. 129-143.

74. Keaveny, J. M. and Mitchell, J. K., "Strength of Fine-Grained Soils Using the Piezocone", Use of In-Situ Tests in Geotechnical Engineering (GSP-6), Ed. S. P. Clemence, ASCE, New York, 1986, pp. 668-685.

75. Konrad, J. M. and Law, K. T., "Undrained Shear Strength from Piezocone Tests", Canadian Geotechnical Journal, Vol. 24, No. 3, Aug. 1987, pp. 392-405.

76. Vesić, A. S., "Design of Pile Foundations", Synthesis of Highway Practice 42, Transportation Research Board, Washington, 1977, 68 p.

77. Houlsby, G. T. and Teh, C. I., "Analysis of the Piezocone in Clay", Proceedings, 1st International Symposium on Penetration Testing (ISOPT-1), Vol. 2, Orlando, 1988, pp. 777-783.

78. Robertson, P. K., Campanella, R. G., Gillespie, D., and Greig, J., "Use of Piezometer Cone Data", Use of In-Situ Tests in Geotechnical Engineering (GSP 6), Ed. S. P. Clemence, ASCE, New York, 1986, pp. 1263-1280.

79. Baguelin, F., Jézéquel, J. F., and Shields, D. H., The Pressuremeter and Foundation Engineering, Trans Tech Publications, Clausthal, 1978, 617 p.

80. Marchetti, S., "In-Situ Tests by Flat Dilatometer", Journal of the Geotechnical Engineering Division, ASCE, Vol. 106, No. GT3, Mar. 1980, pp. 299-321.

81. Schmertmann, J. H., "Personal Communication", 12 Dec. 88 letter to F. H. Kulhawy.

82. Lacasse, S. and Lunne, T., "Calibration of Dilatometer Correlations", Proceedings, 1st International Symposium on Penetration Testing (ISOPT-1), Vol. 1, Orlando, 1988, pp. 539-548.

83. Powell, J. J. M. and Uglow, R. S. T., "Dilatometer Testing in Stiff Overconsolidated Clays", Proceedings, 39th Canadian Geotechnical Conference, Ottawa, 1986, pp. 317-326.

Section 5

ELASTIC DEFORMABILITY

A knowledge of the so-called elastic behavior of soils is necessary for evaluating the initial, time-independent, movement of foundations under static loads. These deformation properties vary with many parameters and therefore are not defined uniquely. In this section, basic definitions are presented first to establish the general background and notation. Methods for estimating Poisson's ratio are presented next, followed by methods for estimating the soil modulus. Both cohesive and cohesionless soils are included. Where available, typical values, influencing factors, and in-situ test correlations are given. For the soil moduli, correlations with dynamic measurements also are given, even though the focus is on static soil properties. The section is concluded with a brief discussion of the concept of subgrade reaction and evaluation of pertinent parameters for this concept.

BASIC DEFINITIONS

The deformation properties of elastic materials are described most often by Young's modulus (E) and Poisson's ratio (ν). Although these parameters strictly are defined only for elastic materials under uniaxial loading, they are used commonly in a "generic" sense with inelastic materials such as soils. These properties are obtained most often from the results of triaxial compression tests. The modulus is the ratio of stress to strain and is obtained from the slope of deviator stress-axial strain curves, as shown in Figure 5-1 and given below:

$$E = \partial(\sigma_1 - \sigma_3)/\partial\epsilon_a \tag{5-1}$$

in which $(\sigma_1 - \sigma_3)$ = deviator stress or principal stress difference and ϵ_a = axial strain. For any particular stress-strain curve, the modulus can be defined as the initial tangent modulus (E_i), the tangent modulus (E_t) at a specified stress level, or the secant modulus (E_s) at a specified stress level. These moduli also will vary with the confining stress (σ_a, σ_b, or σ_c in Figure 5-1) for each stress-strain curve. Therefore, soil moduli are described as being both nonlinear and stress-dependent. In sophisticated numerical models, the actual stress path can be followed, and the modulus can be evaluated for each stress state along the stress

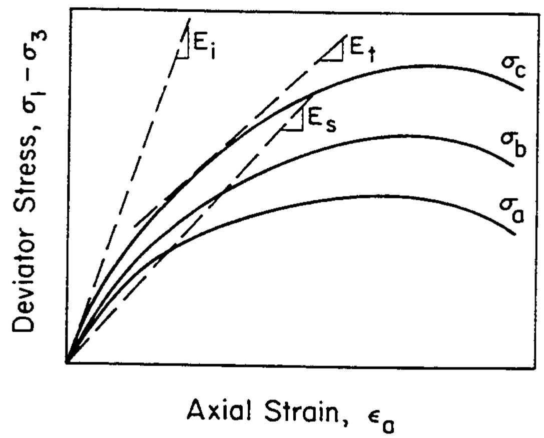

Figure 5-1. Modulus Definitions

path. In simpler, closed-form solutions, an effort must be made to estimate the overall average modulus from the initial to the final stress states.

Poisson's ratio (ν) is defined in an analogous form for triaxial tests in which both axial and volumetric strains are measured. From these data, the axial and radial strains can be obtained. Poisson's ratio is the ratio of the radial strain (ϵ_r) to the axial strain (ϵ_a), as given below:

$$\nu = - \partial\epsilon_r/\partial\epsilon_a \tag{5-2}$$

As with the modulus, Poisson's ratio is both nonlinear and stress-dependent. However, the range of ν is relatively small compared with the range of E, and therefore less effort usually is made in evaluating ν precisely.

For elastic materials, Young's modulus and Poisson's ratio are interrelated uniquely with the shear modulus (G) as follows:

$$G = E/2(1 + \nu) \tag{5-3}$$

The shear modulus also is defined as the slope of the shear stress (τ)-shear strain (γ) curve, which resembles that in Figure 5-1, and is given below:

$$G = \partial\tau/\partial\gamma \tag{5-4}$$

As with E and ν, G is nonlinear and stress-dependent.

Another useful elastic parameter is the constrained modulus (M). This modulus is defined for one-dimensional compression, where the lateral strains are zero, as follows:

$$M = \partial\sigma_v/\partial\epsilon_v = 1/m_v \tag{5-5}$$

in which σ_v = vertical stress, ϵ_v = vertical strain, and m_v = coefficient of volumetric compressibility. From elastic theory, M is related to E and ν as follows:

$$M = \frac{E(1 - \nu)}{(1 + \nu)(1 - 2\nu)} \tag{5-6}$$

The constrained modulus also is nonlinear and stress-dependent.

POISSON'S RATIO

Relatively little information is available in the literature for correlation studies with Poisson's ratio (ν). However, this parameter does not vary greatly. For isotropic elastic materials, the entire range of ν is from 0 to 0.5. For dilatant soils that are inelastic, ν may exceed 0.5. However, it should be remembered that the behavior is no longer elastic in this case.

For undrained ($\phi = 0$) loading of saturated cohesive soil, no volume change occurs. Therefore, the undrained Poisson's ratio (ν_u) is equal to 0.5 by definition.

For drained loading, volume changes occur, and the drained Poisson's ratio (ν_d) varies with soil type and consistency. Typical values are given in Table 5-1, which are representative of secant values at common design stress levels.

For convenience in computer code implementation, Trautmann and Kulhawy (1) approximated ν_d as follows:

$$\nu_d \approx 0.1 + 0.3\,\phi_{rel} \tag{5-7}$$

with

$$\phi_{rel} = (\bar{\phi}_{tc} - 25°)/(45° - 25°) \qquad (0 \le \phi_{rel} \le 1) \tag{5-8}$$

in which ϕ_{rel} = relative friction angle that is convenient to use for approximating the soil density state.

Table 5-1

TYPICAL RANGES OF DRAINED POISSON'S RATIO

Soil	Drained Poisson's Ratio, ν_d
Clay	0.2 to 0.4
Dense sand	0.3 to 0.4
Loose sand	0.1 to 0.3

An alternative approach is to use a hyperbolic model for the initial tangent drained Poisson's ratio, as described by Kulhawy, et al. (2). This value is expressed as:

$$\nu_{di} = G_\nu - F_\nu \log(\bar{\sigma}_{3c}/p_a) \tag{5-9}$$

in which $\bar{\sigma}_{3c}$ = minor principal effective confining stress, and G_ν and F_ν are hyperbolic parameters given in Figure 5-2.

For cohesive soils, the drained Poisson's ratio also has been related to plasticity index for several lightly overconsolidated (LOC) soils, as shown in Figure 5-3. However, ν_d also is nonlinear and stress-dependent, as shown in Figure 5-4 for one clay as a function of stress level (amount of the failure stress mobilized) and OCR. As can be seen in these two figures, the variation of ν_d is not great.

UNDRAINED MODULUS OF COHESIVE SOILS

Cohesive soils exhibit time-dependent response to loading. For initial quick loading conditions, the response is undrained. With time, the excess pore water stresses developed during undrained loading will dissipate, leading to consolidation and other long-term phenomena. These time-dependent phenomena and associated soil properties are described in Section 6.

For undrained loading, the modulus of cohesive soils can be described by either the undrained Young's modulus (E_u) or the shear modulus (G). The shear modulus actually describes the soil "skeleton" response, so it is independent of drainage conditions, all other factors being equal. For undrained loading, E_u is equal to 3G

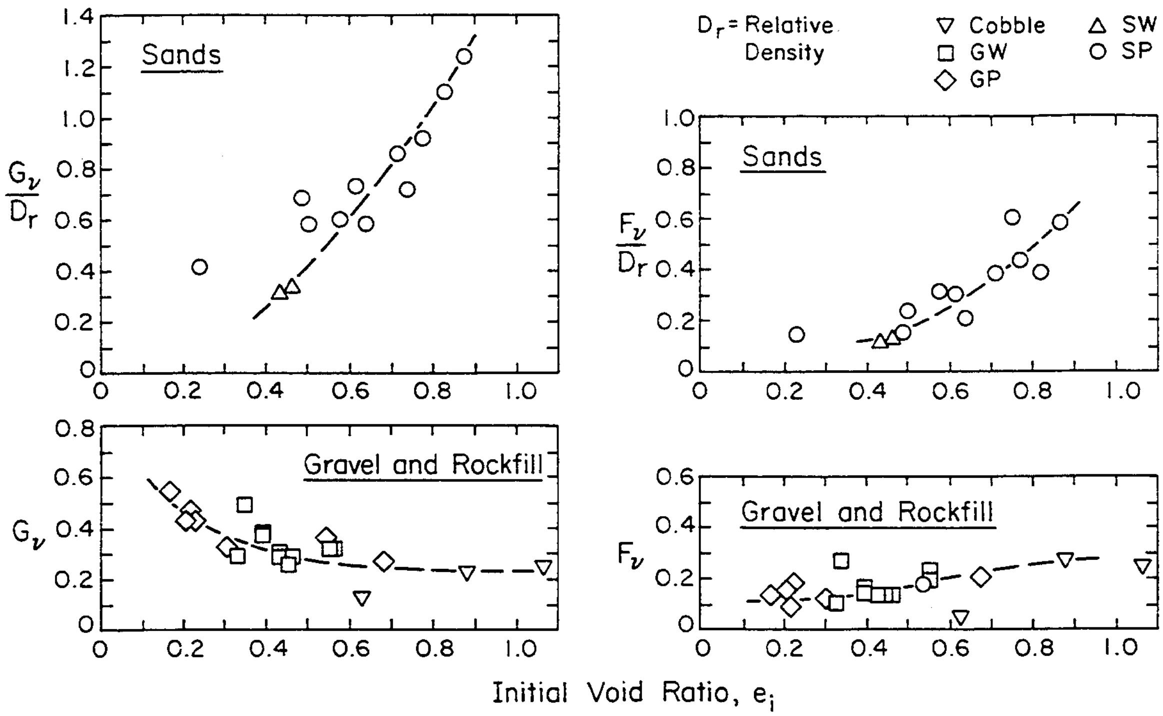

Figure 5-2. Drained Poisson's Ratio Parameters for Granular Soils

Source: Kulhawy (3), p. 76.

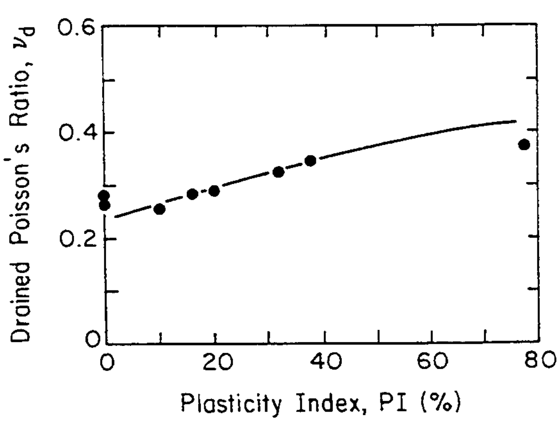

Figure 5-3. Drained Poisson's Ratio versus PI for Several LOC Soils

Source: Wroth (4), p. 187.

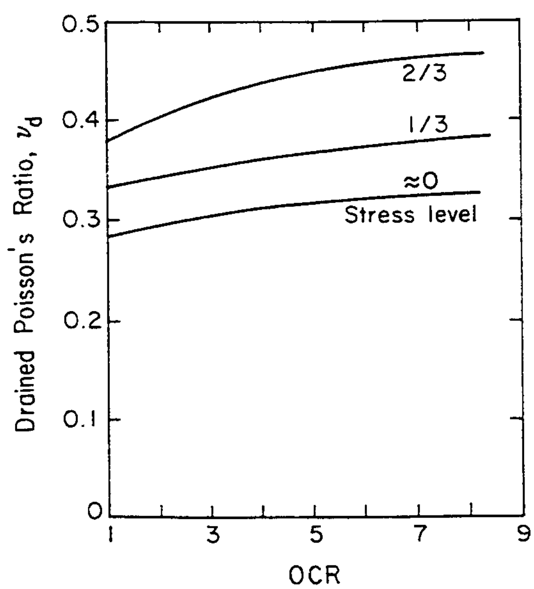

Figure 5-4. Drained Poisson's Ratio versus OCR and Stress Level for Sydney Kaolin

Source: Poulos (5), p. 104.

from Equation 5-3 since $\nu_u = 0.5$.

It should be noted that the factors affecting s_u (discussed in Section 4) also will affect E_u. Therefore, the value of E_u will be dependent on test type and test specifics.

Typical Values

A number of authors have given typical ranges for the undrained modulus, and these ranges are summarized in Table 5-2. These values generally would be representative of secant moduli at common design stress levels.

As an alternative, Kulhawy, et al. (2) suggested use of a hyperbolic model to estimate the undrained tangent modulus (E_{ut}), as given below:

$$E_{ut} = E_{ui}[1 - SL]^2 = \kappa p_a (\sigma_c/p_a)^n [1 - R_f (\sigma_1 - \sigma_3)/(2 s_u)]^2 \quad (5\text{-}10)$$

in which E_{ui} = undrained initial tangent modulus, SL = stress level (fraction of strength mobilized), σ_c = isotropic confining stress, σ_1 = total major principal stress, σ_3 = total minor principal stress, and κ, n, and R_f = modulus parameters given in Table 5-3. For CIUC or CAUC test conditions, σ_c would equal the minor principal effective confining stress ($\bar{\sigma}_{3c}$). For UU test conditions, σ_c would equal σ_3.

Correlations with s_u

More commonly, the undrained modulus (E_u) is normalized directly by the undrained

Table 5-2

TYPICAL RANGES OF UNDRAINED MODULUS FOR CLAY

Consistency	Normalized Undrained Modulus, E_u/p_a
soft	15 to 40
medium	40 to 80
stiff	80 to 200

Table 5-3

TYPICAL UNDRAINED HYPERBOLIC MODULUS PARAMETERS

Unified Soil Classification	κ	n	R_f
CL	100 to 200	1	0.9
CH	100 to 300	1	0.9

Source: Kulhawy, et al. (6), p. 10-19.

shear strength (s_u) from the same test to give E_u/s_u. This ratio is assumed to be independent of test type. Also common is the rigidity index (I_r), which is defined as the ratio of the shear modulus (G) to the strength. For undrained ($\phi = 0$) loading, I_r is given as:

$$I_r = G/s_u \tag{5-11}$$

For undrained loading, E_u is equal to 3G and therefore:

$$E_u/s_u = 3I_r = 3G/s_u \tag{5-12}$$

Figure 5-5 illustrates typical test results obtained for a number of cohesive soils. (The numbered soils were defined in Figure 4-33.) These data were obtained from direct simple shear tests and illustrate the range of the secant undrained modulus ratio (E_{us}/s_u) as a function of stress level (given as shear stress ratio) and OCR. Based on data such as these, Duncan and Buchignani (8) suggested the broad generalization shown in Figure 5-6.

Alternatively, the modified Cam clay model can be used to provide an estimate of the undrained modulus ratio. Wroth, et al. (9) suggested the following:

$$\frac{(E_u/s_u)_{OC}}{(E_u/s_u)_{NC}} = \frac{(G/s_u)_{OC}}{(G/s_u)_{NC}} = [1 + C \ln OCR]\ OCR^{-\Lambda} \tag{5-13}$$

in which C is an experimentally determined constant that is likely to be between 0 and 2. A value of C = 1 appears to be representative of the trends observed in

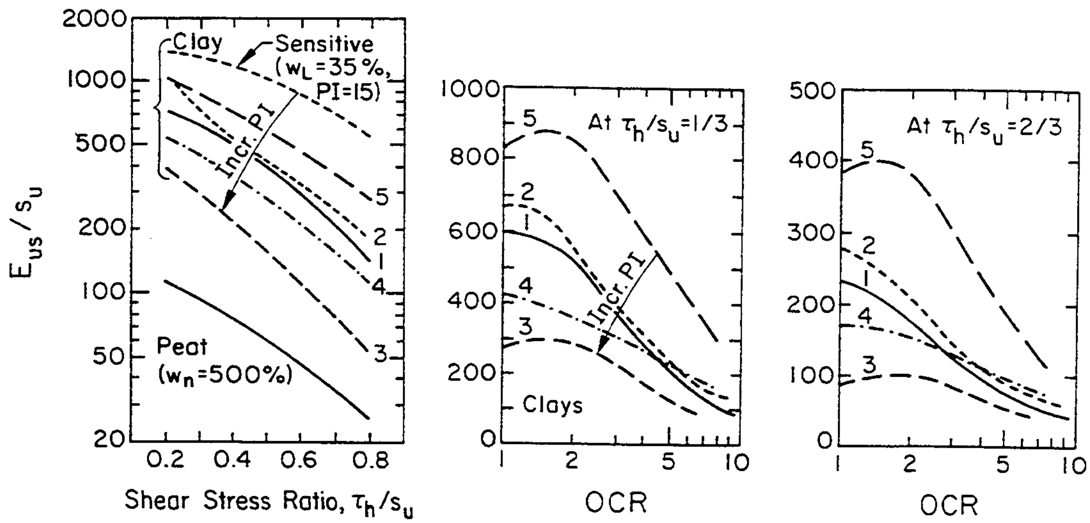

Figure 5-5. Normalized Undrained Modulus versus Stress Level and OCR

Source: Ladd, et al. (7), pp. 436, 441.

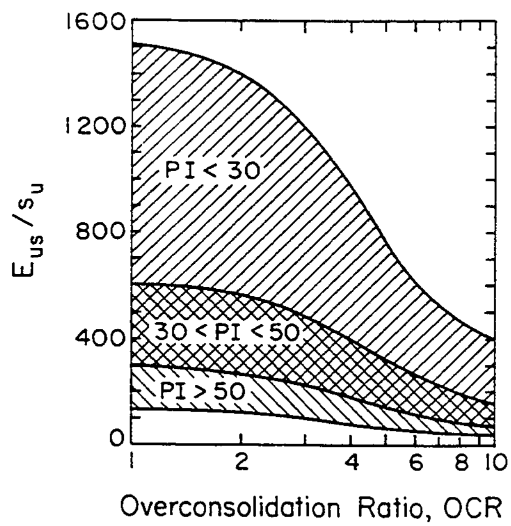

Figure 5-6. Generalized Undrained Modulus Ratio versus OCR and PI

Source: Duncan and Buchignani (8), p. 26.

laboratory test data.

The original Cam clay model can be used to provide an estimate of the undrained initial tangent modulus ratio for normally consolidated clay $(E_{ui}/s_u)_{NC}$. Using relationships given by Mayne and Swanson (10), the initial tangent modulus can be evaluated by differentiation as the strain approaches zero. This modulus then can be normalized by s_u as given by the Cam clay model, resulting in the following:

$$(E_{ui}/s_u)_{NC} = \frac{2M(1 + e_o)\ \ln 10}{C_c\ \Lambda(1 - \Lambda)\ \exp(-\Lambda)} \tag{5-14}$$

in which C_c = virgin compression index (See Section 6.), e_o = initial void ratio, and M and Λ are defined in Appendix G. This equation corresponds to CIUC triaxial compression conditions. Using a typical value of Λ = 0.8, Equation 5-14 simplifies as follows:

$$(E_{ui}/s_u)_{NC} = 64M\ (1 + e_o)/C_c \tag{5-15}$$

Combining Equations 5-15 and 5-13 (with Λ = 0.8 and C = 1) gives:

$$(E_{ui}/s_u) = \frac{64M(1 + e_o)[1 + \ln OCR]}{C_c\ OCR^{0.8}} \tag{5-16}$$

For e_o = 1, Figure 5-7 shows the relationship for E_{ui}/s_u in terms of OCR, C_c, and $\bar{\phi}_{tc}$. This figure is similar in form to Figure 5-6, but it is based on more fundamental soil properties. The tangent modulus at a particular stress level then can be computed from Equation 5-16, using the stress level (SL) reduction as given in

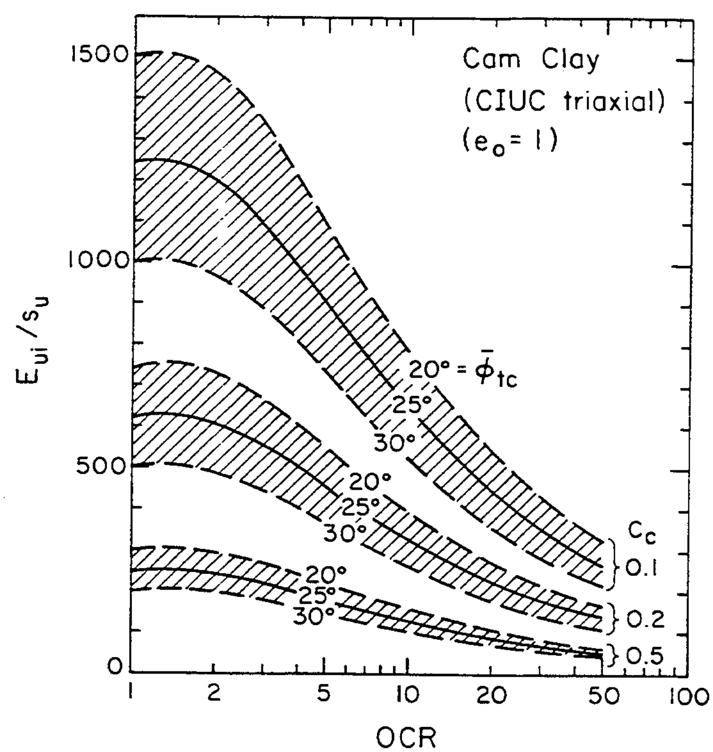

Figure 5-7. Cam Clay Prediction of Undrained Initial Tangent Modulus Ratio

Equation 5-10. Furthermore, the limit value of the secant modulus ratio approaching zero stress level would be E_{ui}/s_u. This value then can be used to estimate E_{us}/s_u at a particular stress level using the experimental relationships shown in Figure 5-5.

Correlations with SPT, CPT, and PMT Results

Apparently, few studies have attempted to relate the undrained modulus (E_u) to the SPT N value or the CPT cone tip resistance in cohesive soils. Ironically, many efforts have instead attempted to correlate the constrained modulus ($M = 1/m_v$) under drained conditions to the N value and q_c, although these penetration resistances occur most likely under undrained conditions. These relationships will be discussed in Section 6.

The pressuremeter test (PMT) provides a measurement of the horizontal modulus in soils. In clays, it is assumed commonly that $E_{PMT} = E_u$. For practical use, attempts have been made to correlate E_{PMT} with the SPT N value, as shown in Figure 5-8. Based on these data, it is clear that more than an order of magnitude variation is possible when using N values as the sole predictor.

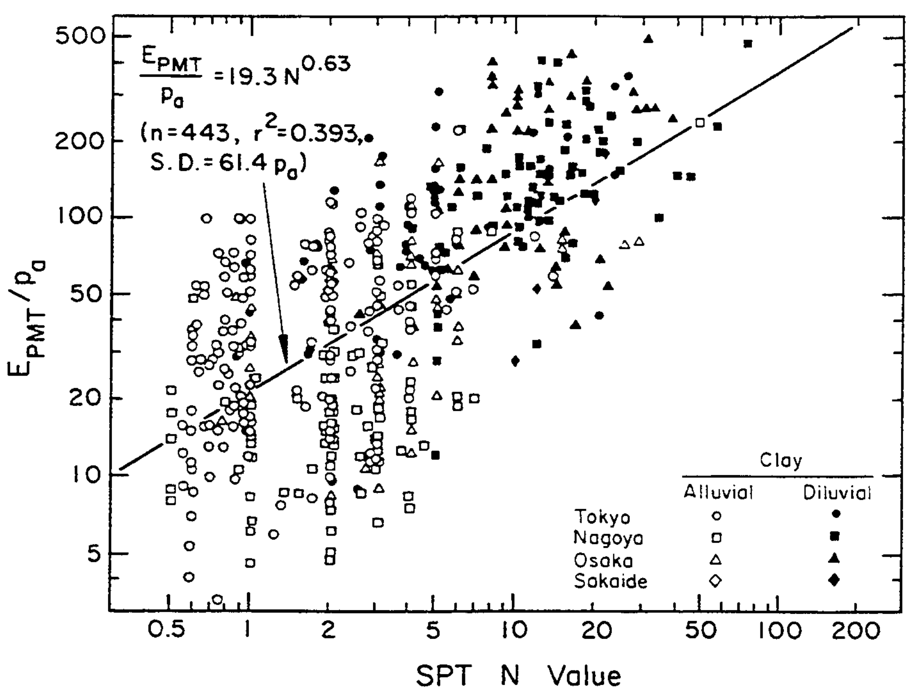

Figure 5-8. PMT Modulus of Clay versus N Value

Source: Ohya, et al. (11), p. 129.

Back-Figured from Full-Scale Load Tests

Perhaps more useful than the in-situ test results are moduli back-figured from analysis of full-scale field load tests. Figure 5-9 shows an interpretation based on limited data for driven piles and drilled shafts.

Figure 5-10a includes more data for drilled shafts as a function of depth (D) to

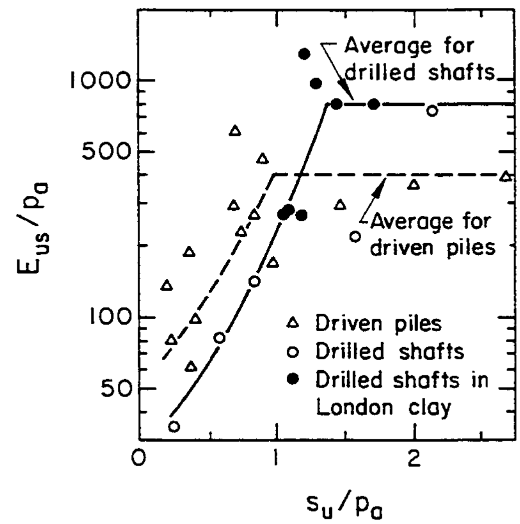

Figure 5-9. Undrained Modulus for Deep Foundations in Compression

Source: Poulos and Davis (12), p. 103.

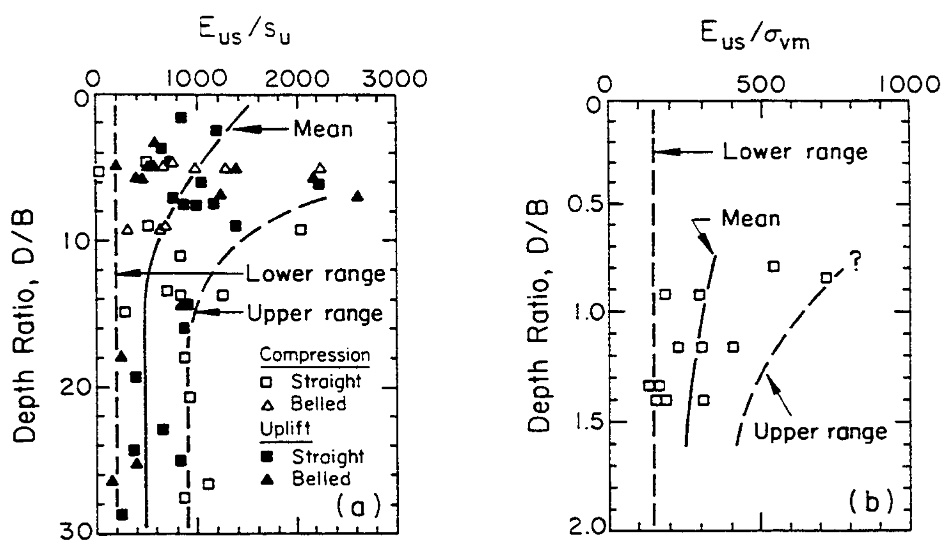

Figure 5-10. Undrained Modulus for (a) Drilled Shafts in Compression and Uplift and (b) Spread Foundations in Uplift

Source: Callanan and Kulhawy (13), pp. 3-28, 3-33.

diameter (B) ratio. Of particular interest to note is that E_{us}/s_u is normally greater than 200. Figure 5-10b shows limited data for spread foundations with cohesive soil backfill. In this figure, σ_{vm} = mean vertical total stress over the foundation depth. Although the data are limited, the range appears to be reasonable.

Lastly, from analyses of the axial deformation of piles at working load levels, Randolph (14) suggested the following range for rigidity index ($I_r = G/s_u$):

$$150 \leq I_r \leq 200 \qquad (5\text{-}17)$$

For lateral loads, the range was suggested to be:

$$75 \leq I_r \leq 100 \qquad (5\text{-}18)$$

These generalized ranges are intended to be representative of common, simple design situations.

Estimation from Dynamic Measurements

Another method for estimating the modulus is based on shear wave velocity measurements from the resonant column test. Hardin and Drnevich (15) developed the following equation to evaluate G_{max} at low-amplitude (dynamic) shear strains:

$$G_{max}/p_a = 321 \frac{(2.97 - e)^2}{1 + e} \, OCR^M \, (\bar{\sigma}_o/p_a)^{0.5} \qquad (5\text{-}19)$$

in which e = void ratio (not to exceed 2), M = exponent given in Table 5-4, and $\bar{\sigma}_o$ = mean principal effective stress.

However, it must be remembered that G_{max} at small dynamic strains is much larger than G at large static strains, as shown in Figure 5-11. From this figure, it is clear that G for static loading is on the order of 5 to 10 percent of G_{max} for dynamic loading. This general pattern holds for all soil types.

Wroth, et al. (9) reviewed a number of relationships for G_{max} at dynamic strains versus N, as shown in Figure 5-12. From this figure, it is clear that considerable scatter is present in the data. From these data, they suggested the following:

$$G_{max}/p_a = 120 \, N^{0.77} \qquad (5\text{-}20)$$

Table 5-4

EXPONENT M FOR SHEAR MODULUS

Plasticity Index, PI	Exponent, M
0	0
20	0.18
40	0.30
60	0.41
80	0.48
≥ 100	0.50

Source: Hardin and Drnevich (15), p. 672.

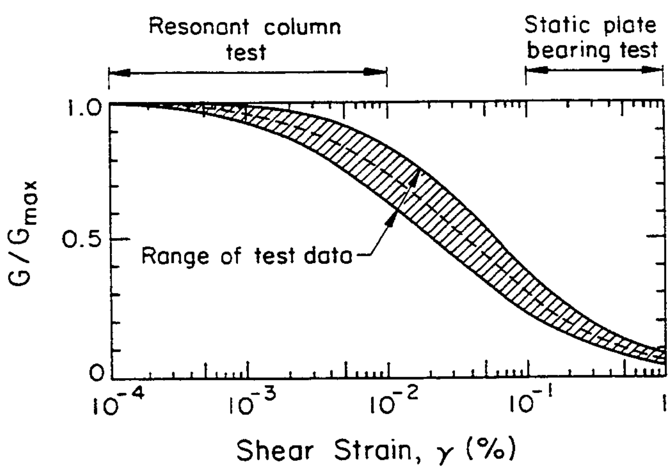

Figure 5-11. Shear Modulus versus Shear Strain for Sands

Source: Seed and Idriss (16).

with limits of the data being $60\ N^{0.71} < G_{max}/p_a < 300\ N^{0.8}$. The static shear modulus then would be some 5 to 10 percent of the computed G_{max} value.

MODULUS FOR COHESIONLESS SOILS

Cohesionless soils such as sands do not exhibit significant time-dependency to loading caused by excess pore water stress dissipation, and therefore the modulus under undrained loading conditions exists only briefly. Almost always, the modulus

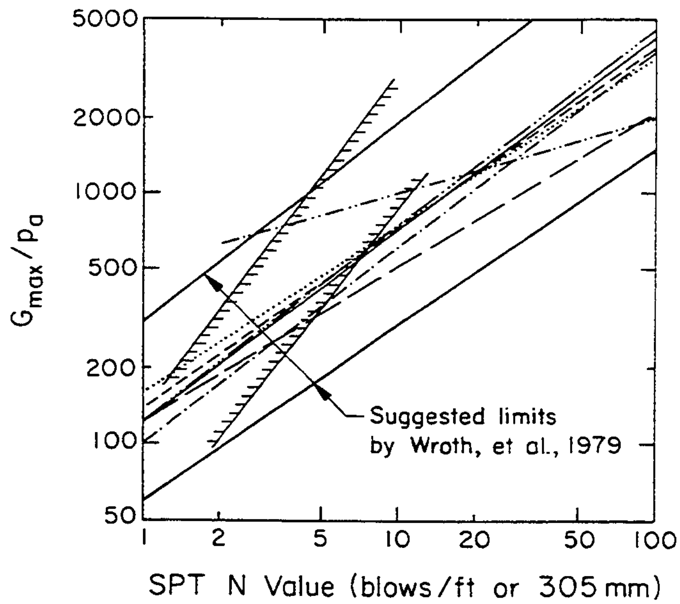

Figure 5-12. Dynamic Shear Modulus versus N for Cohesive Soils

Source: Wroth, et al. (9), p. 96.

is considered for drained conditions. However, for finer-grained silts, some significant time-dependency may develop which will have to be considered on a case-by-case basis.

For drained loading, the modulus can be described by the drained elastic modulus (E_d), the shear modulus (G), or the drained constrained modulus (M_d). E and G commonly are evaluated in triaxial compression, while M is evaluated in one-dimensional compression. All of these are interrelated through Poisson's ratio, as noted previously in Equations 5-3 and 5-6. Unless otherwise stated, the moduli will be secant values given by E_{ds} and M_{ds}.

Typical Values

A number of authors have given typical ranges for the modulus of cohesionless soils. Table 5-5 is representative of these ranges for sands in general and for driven piles in particular. These values generally would be representative of secant moduli within common design stress levels.

Alternatively, Duncan and Chang (18) suggested a hyperbolic model to estimate the drained tangent modulus, starting from an initial isotropic stress, as follows:

Table 5-5

TYPICAL RANGES OF DRAINED MODULUS FOR SAND

Consistency	Normalized Elastic Modulus, E_d/p_a Typical	Driven Piles[a]
loose	100 to 200	275 to 550
medium	200 to 500	550 to 700
dense	500 to 1000	700 to 1100

a - Source: Poulos (17), p. 207.

$$E_t = \kappa p_a (\bar{\sigma}_3/p_a)^n [1 - R_f (1 - \sin \bar{\phi}_{tc})(\bar{\sigma}_1 - \bar{\sigma}_3)/(2 \bar{\sigma}_3 \sin \bar{\phi}_{tc})]^2 \quad (5\text{-}21)$$

in which $\bar{\sigma}_1$ and $\bar{\sigma}_3$ = effective major and minor principal stresses, respectively, $\bar{\phi}_{tc}$ = effective stress friction angle in triaxial compression, and κ, n, and R_f = modulus parameters given in Table 5-6. For convenience in computer code implementation, Trautmann and Kulhawy (1) approximated κ as follows:

$$\kappa \approx 300 + 900 \phi_{rel} \quad (5\text{-}22)$$

with ϕ_{rel} defined in Equation 5-8.

Correlations with Strength

The shear modulus commonly is correlated to the effective soil strength through the rigidity index (I_r), as defined below for drained loading:

$$I_r = G/(\bar{\sigma} \tan \bar{\phi}_{tc}) \quad (5\text{-}23)$$

Selected values for I_r are given in Table 5-7. Of particular interest to note is that I_r increases with increasing relative density and decreases with increasing normal stress. It also is lower with more compressible soil minerals.

When using the rigidity index (I_r) for drained loading, volume changes normally have to be considered. Therefore, I_r must be corrected for the volumetric strains (ϵ_v) to yield a reduced rigidity index (I_{rr}), as given below by Vesić (20):

Table 5-6

TYPICAL DRAINED HYPERBOLIC MODULUS PARAMETERS

Unified Soil Classification	κ	n	R_f
GW	300 to 1200	1/3	0.7
GP	500 to 1800	1/3	0.8
SW	300 to 1200	1/2	0.7
SP	300 to 1200	1/2	0.8
ML	300 to 1200	2/3	0.8

Source: Kulhawy, et al. (6), p. 10-19.

Table 5-7

VALUES OF RIGIDITY INDEX FOR SELECTED COHESIONLESS SOILS

Soil	Relative Density D_r (%)	Normalized Mean Normal Stress, $\bar{\sigma}_o/p_a$	Rigidity Index, I_r
Chattahoochee sand	80	0.1	200
	80	1	118
	80	10	52
	80	100	12
	20	0.1	140
	20	1	85
Ottawa sand	82	0.05	265
	21	0.05	89
Piedmont silt	-	0.70	10 to 30

Source: Vesić (20), p. 68.

$$I_{rr} = I_r/(1 + I_r\ \epsilon_v) \qquad (5\text{-}24)$$

Vesić (20) noted that ϵ_v would be zero for dense soils and range from 0 to 0.05 for loose soils in the stress range from 1 to 10 atmospheres. For convenience in computer code implementation, Trautmann and Kulhawy (1) approximated ϵ_v as follows:

$$\epsilon_v \approx 0.005(\bar{\sigma}_v/p_a)(1 - \phi_{rel}) \qquad (5\text{-}25)$$

in which $\bar{\sigma}_v$ = vertical effective stress (up to 10 atmospheres), and ϕ_{rel} is defined in Equation 5-8.

Correlations with SPT N Value

Young's Modulus. Early correlations in the literature related E_{ds} of sands directly to the standard penetration test (SPT) N value. Several of these correlations are shown in Figure 5-13. Others within the same ranges are given by Mitchell and Gardner (23). Later correlations attempted to relate the constrained modulus (M) and N as a function of overburden stress (e.g., 24).

However, all attempts to date which correlate a modulus with N show considerable scatter. This lack of correlation is to be expected because the SPT N value varies with many factors, as described in Section 2, and these factors have yet to be incorporated in these correlations. Therefore, as a first order estimator, the following may be used:

$$E/p_a \approx 5\ N_{60} \qquad \text{(sands with fines)} \qquad (5\text{-}26a)$$

$$\approx 10\ N_{60} \qquad \text{(clean NC sands)} \qquad (5\text{-}26b)$$

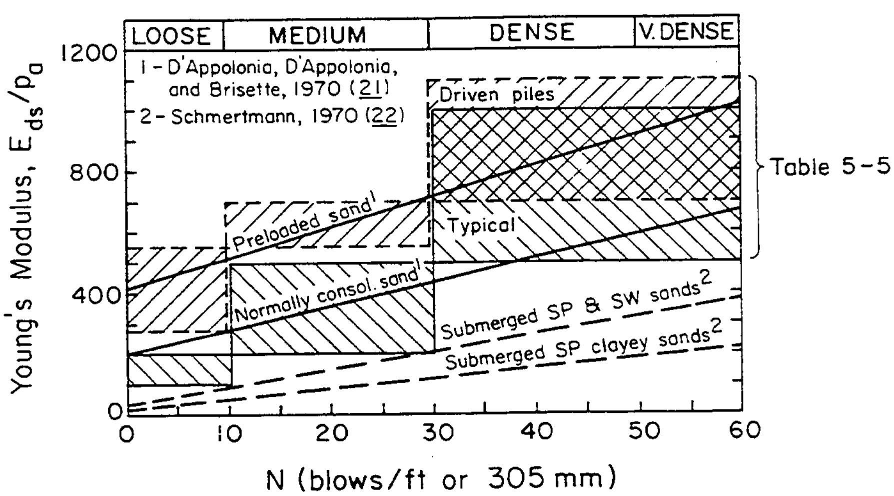

Figure 5-13. Comparative Plot of Drained Modulus Correlations for Sand

Source: Callanan and Kulhawy (13), p. 3-16.

$\approx 15\ N_{60}$ (clean OC sands) (5-26c)

in which N_{60} is the N value corrected for field procedures to an average energy ratio of 60 percent. Equation 2-11 gives the appropriate correction factors.

Pressuremeter Modulus. The pressuremeter test (PMT) provides a direct measurement of the horizontal modulus of cohesionless soils. This modulus (E_{PMT}) often is presumed to be roughly equivalent to Young's modulus (E). Correlations between the N value and E_{PMT} have been developed, as shown in Figure 5-14. The scatter shown is typical of other N correlations because of the reasons noted above.

Dilatometer Modulus. The dilatometer test (DMT) also provides a direct modulus measurement for cohesionless soils. The dilatometer modulus (E_D) is related to Young's modulus as follows:

$$E_D = E/(1 - \nu^2) \quad (5\text{-}27)$$

No general correlations of E_D with N have been presented at this time. However, the DMT and other in-situ tests can be used effectively to develop convenient

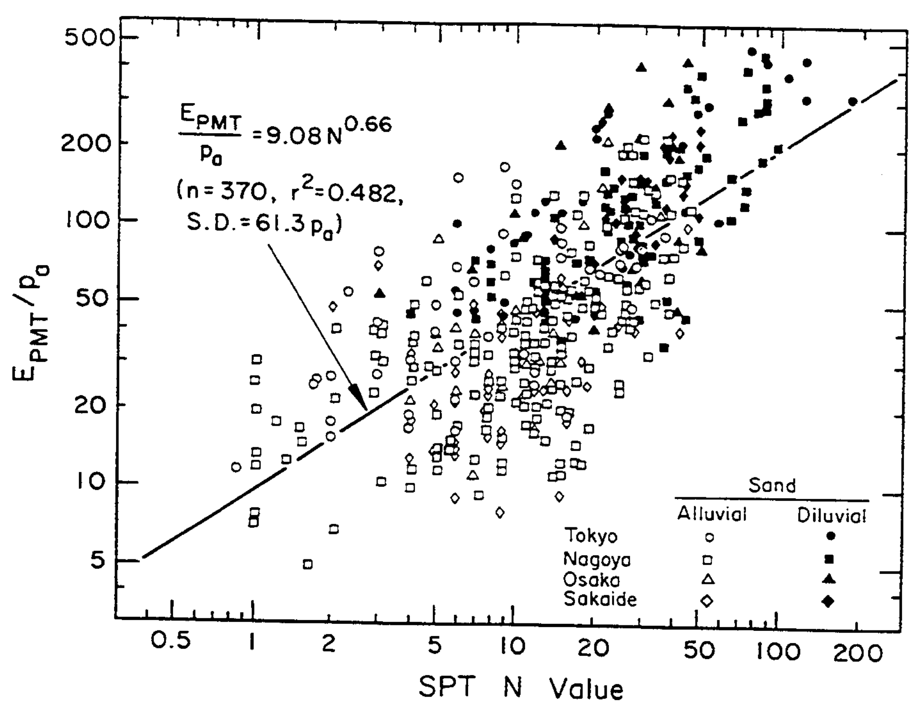

Figure 5-14. PMT Modulus of Sand versus N Value

Source: Ohya, et al. (11), p. 129.

correlations within a specific geologic setting. For example, Mayne and Frost (25) developed the relationship shown in Figure 5-15, which correlates the SPT N value with both the E_D and the secant modulus (E_{ds}) back-calculated from eight case histories of field performance data on building foundations. All of these data were obtained in sandy silts of the Piedmont geologic province, in and around the Washington, D.C. area. Local correlations of this type normally are much more accurate than generalized global correlations.

Correlations with CPT q_c Value

Modulus values for cohesionless soils have been correlated with the cone penetration test (CPT) q_c value. Initial correlation studies attempted to link E_{ds} with q_c directly, using the general form below:

$$\alpha = E_{ds}/q_c \tag{5-28}$$

in which α = empirical parameter and E_{ds} and q_c are in the same units. Webb, et al. (26) have shown that existing relationships suggest α values ranging from 1.5 to 2.5 and intercepts for E_{ds}/p_a ranging from 0 to 80. However, as noted previously, the q_c relationships actually are nonlinear and stress-dependent.

The majority of studies actually have focused on the tangent constrained modulus (M_{dt}) instead of Young's modulus (E), primarily because M_{dt} corresponds to

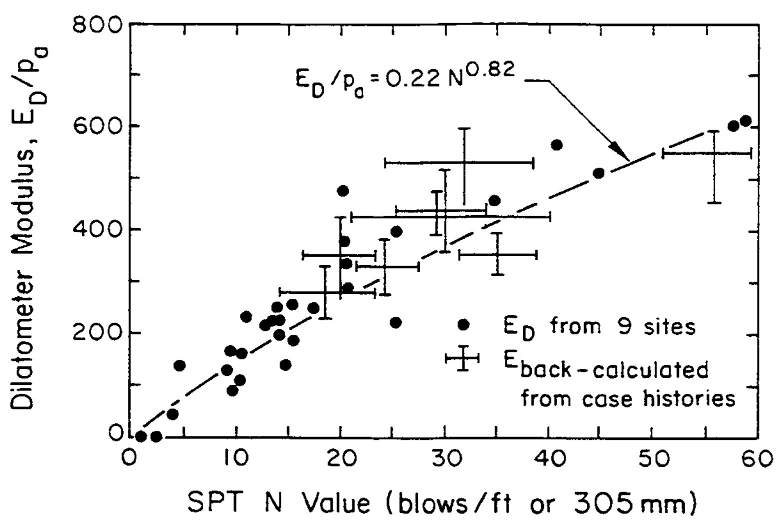

Figure 5-15. Trend Between Dilatometer Modulus and N in Piedmont Sandy Silts

Source: Mayne and Frost (25), p. 22.

one-dimensional compression and is easier to determine. The correlations typically take the form:

$$\alpha = M_{dt}/q_c \qquad (5\text{-}29)$$

in which α = empirical parameter and M_{dt} and q_c are in the same units. Values of α quoted in the literature typically range from 3 to 8 for normally consolidated (NC) sands. However, Figure 5-16a shows further ranges in α and a definite trend with relative density. These data were obtained from the calibration chamber studies reported in Appendix H.

For overconsolidated (OC) sands, α is much higher. Values quoted in the literature typically range from 7 to 25 or more. However, Figure 5-16b shows further ranges in α and a definite trend with relative density. These data also were from the calibration chamber studies.

For one sand tested extensively in a calibration chamber, the effects of relative density, overconsolidation, and stress level adopt consistent patterns, as shown in Figure 5-17. These patterns can be used as guidelines for other sands.

Figures 5-16 and 5-17 show that the modulus is a function of relative density. In Section 2, it was shown that the relative density is a function of the cone tip resistance normalized by $(\bar{\sigma}_{vo})^{0.5}$. Therefore, the modulus should have the same proportionality with the effective vertical stress, as shown by Janbu (28). This issue will be discussed further in Section 6.

Back-Figured from Full-Scale Load Tests

Perhaps more useful than the in-situ test results are moduli back-figured from analysis of full-scale field load tests. Figure 5-18a shows secant modulus values from analyses of drilled shafts in uplift, where the modulus was normalized by the mean unit side resistance (f). Comparable data are shown in Figure 5-18b for spread foundations in uplift, except that the modulus was normalized by the mean vertical effective stress over the foundation depth. A lower bound on both E_{ds}/f and $E_{ds}/\bar{\sigma}_{vm}$ is 200.

Estimation from Dynamic Measurements

Another method of estimating the modulus is based on shear wave velocity measurements from the resonant column test. These measurements have been used to evaluate

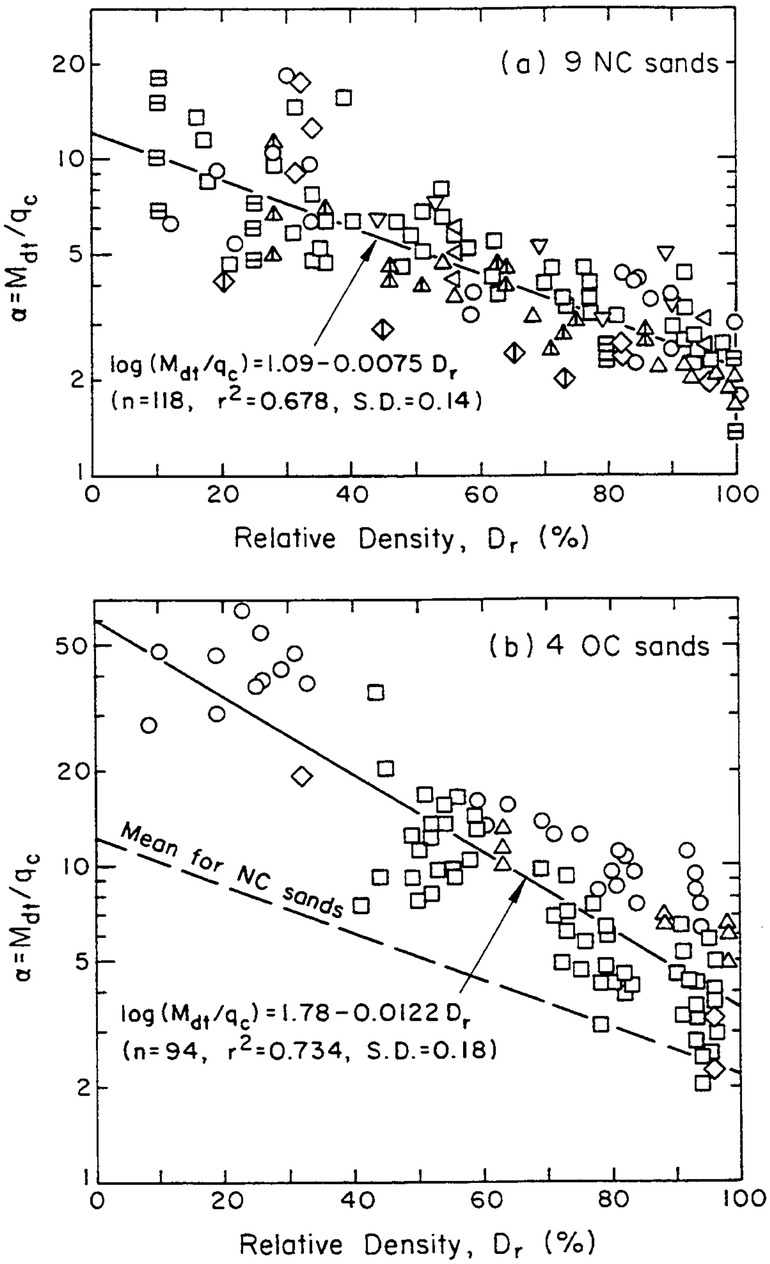

Figure 5-16. Variation of α with D_r for Sands in Calibration Chambers

G_{max} at low-amplitude (dynamic) shear strains. As shown with Figure 5-11, this dynamic modulus represents an upper bound, and therefore it is denoted G_{max}. For static loading with relatively large strains, G is on the order of 5 to 10 percent of G_{max}.

Early laboratory studies on rounded and angular sands gave the relationships shown in Figure 5-19. More recent studies by Hardin (30) suggested the following:

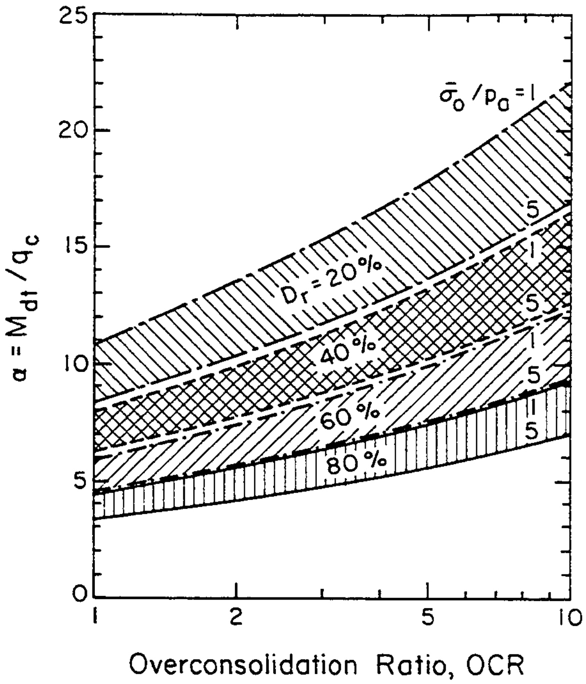

Figure 5-17. CPT α Correlation for Ticino Sand

Source: Jamiolkowski, et al. (27), p. 277.

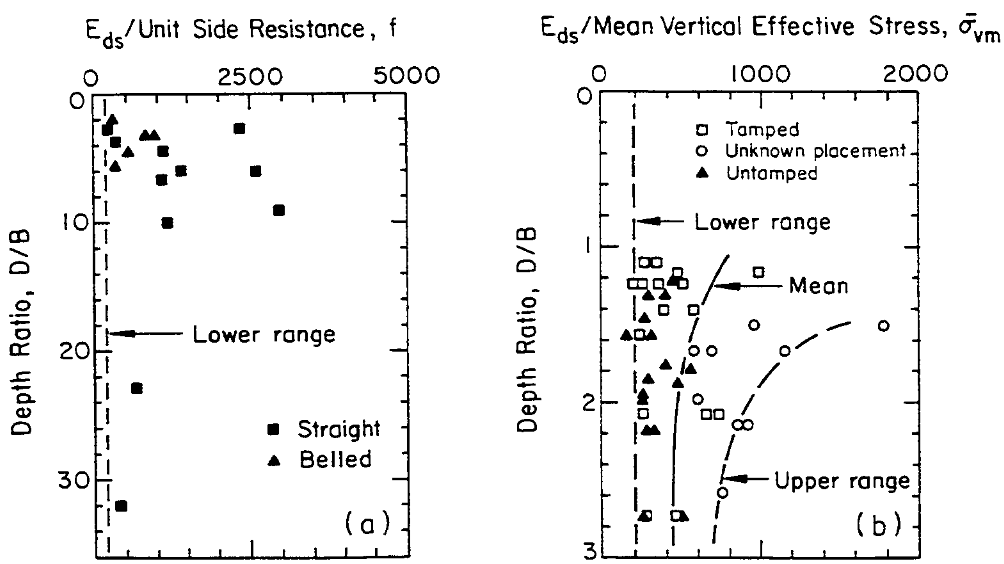

Figure 5-18. Normalized Drained Modulus for (a) Drilled Shafts in Uplift and (b) Spread Foundations in Uplift

Source: Callanan and Kulhawy (13), pp. 3-30, 3-36.

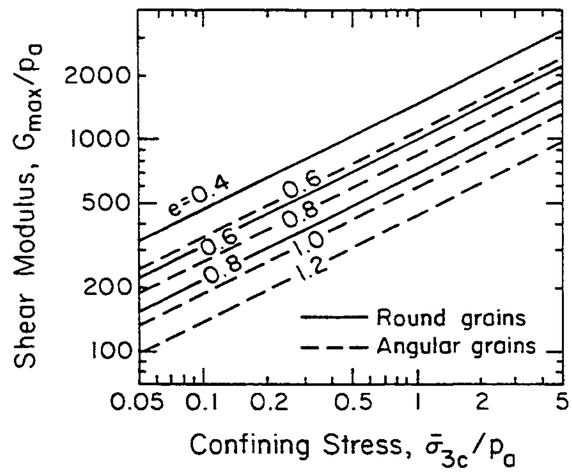

Figure 5-19. Variation of Shear Modulus of Dry Sands with Void Ratio and Confining Stress

Source: Richart, Hall, and Woods (29), p. 385.

$$G_{max}/p_a = \frac{S\ OCR^M\ (\bar{\sigma}_o/p_a)^{0.5}}{2(1 + \nu)(0.3 + 0.7e^2)} \tag{5-30}$$

in which S = stiffness coefficient, M = exponent, $\bar{\sigma}_o$ = mean principal effective stress, and e = void ratio. Hardin (30) notes that OCR^M often is taken as 1 for convenience and that S for clean sands is in the range of 1200 to 1500.

SUBGRADE REACTION

In contrast with elastic theories that use Young's modulus (E), an alternative method for analyzing load-displacement response is the concept of subgrade reaction. This concept is used often for evaluating the behavior of footings, mat/raft foundations, and laterally loaded deep foundations. In subgrade reaction models, there is a basic parameter which is analogous to a spring constant. This parameter is defined as the modulus of subgrade reaction (k_s), given by:

$$k_s = p/\delta \tag{5-31}$$

in which p = applied stress and δ = displacement under p. By this definition, k_s is in units of force per length cubed. As with Young's modulus, k_s varies with stress level. However, unlike Young's modulus, k_s also varies with foundation width (e.g., Horvath, 31).

To account for this width dependence, another subgrade reaction modulus (K_s) was introduced as below:

$$K_s = k_s B \qquad (5\text{-}32)$$

in which K_s has units of force per length squared and B = foundation width. For deep foundations where k_s varies with depth, z (and k_s sometimes is known as k_h), an alternative coefficient of subgrade reaction (n_h) sometimes is used, as given by:

$$k_s = k_h = n_h(z/B) \qquad (5\text{-}33)$$

Perhaps the most logical procedure to evaluate k_s is to present it in terms of Young's modulus (E) and Poisson's ratio (ν) of the soil. Vesić (32) reinterpreted k_s in this manner and determined the following:

$$k_s = \left(\frac{0.65}{B}\right) \left(\frac{E\ B^4}{E_f\ I_f}\right)^{1/12} \left(\frac{E}{1 - \nu^2}\right) \qquad (5\text{-}34)$$

in which E_f = foundation Young's modulus, I_f = foundation moment of inertia, and $E_f\ I_f$ = foundation stiffness. E_f and I_f normally are constants depending on the foundation material and geometry. Procedures for evaluating E and ν were presented earlier in this section.

REFERENCES

1. Trautmann, C. H. and Kulhawy, F. H., "CUFAD - A Computer Program for Compression and Uplift Foundation Analysis and Design", Report EL-4540-CCM, Vol. 16, Electric Power Research Institute, Palo Alto, Oct. 1987, 148 p.

2. Kulhawy, F. H., Duncan, J. M., and Seed, H. B., "Finite Element Analysis of Stresses and Movements in Embankments During Construction", Contract Report S-69-8, U.S. Army Engineer Waterways Experiment Station, Vicksburg, Nov. 1969, 169 p.

3. Kulhawy, F. H., "Finite Element Analysis of the Behavior of Embankments", Ph.D. Dissertation, University of California, Berkeley, 1969, pp. 40-80.

4. Wroth, C. P., "In-Situ Measurement of Initial Stresses and Deformation Characteristics", Proceedings, ASCE Specialty Conference on In-Situ Measurement of Soil Properties, Vol. 2, Raleigh, 1975, pp. 180-230.

5. Poulos, H. G., "Normalized Deformation Parameters for Kaolin", Research Report R336, School of Civil Engineering, University of Sydney, 1978, 18 p.

6. Kulhawy, F. H., Trautmann, C. H., Beech, J. F., O'Rourke, T. D., McGuire, W., Wood, W. A., and Capano, C., "Transmission Line Structure Foundations for Uplift-Compression Loading", Report EL-2870, Electric Power Research Institute, Palo Alto, Feb. 1983, 412 p.

7. Ladd, C. C., Foott, R., Ishihara, K., Schlosser, F., and Poulos, H. G., "Stress-Deformation and Strength Characteristics", Proceedings, 9th International Conference on Soil Mechanics and Foundation Engineering, Vol. 2, Tokyo, 1977, pp. 421-494.

8. Duncan, J. M. and Buchignani, A. L., An Engineering Manual for Settlement Studies, Department of Civil Engineering, University of California, Berkeley, June 1976, 94 p.

9. Wroth, C. P., Randolph, M. F., Houlsby, G. T., and Fahey, M., "A Review of the Engineering Properties of Soils with Particular Reference to the Shear Modulus", CUED/D - SOILS TR 75, University of Cambridge, 1979, 79 p.

10. Mayne, P. W. and Swanson, P. G., "The Critical State Pore Pressure Parameter from Consolidated-Undrained Shear Tests", Laboratory Shear Strength of Soil (STP 740), Ed. R. N. Yong and F. C. Townsend, ASTM, Philadelphia, 1981, pp. 410-430.

11. Ohya, S., Imai, T., and Matsubara, M., "Relationships Between N Value by SPT and LLT Pressuremeter Results", Proceedings, 2nd European Symposium on Penetration Testing, Vol. 1, Amsterdam, 1982, pp. 125-130.

12. Poulos, H. G. and Davis, E. H., Pile Foundation Analysis and Design, John Wiley and Sons, New York, 1980, 397 p.

13. Callanan, J. F. and Kulhawy, F. H., "Evaluation of Procedures for Predicting Foundation Uplift Movements", Report EL-4107, Electric Power Research Institute, Palo Alto, Aug. 1985, 124 p.

14. Randolph, M. F., "PIGLET - A Computer Program for the Analysis and Design of Pile Groups Under General Loading Conditions", Engineering Department Report, University of Cambridge, July 1983, 69 p.

15. Hardin, B. O. and Drnevich, V. P., "Shear Modulus and Damping in Soils: Design Equations and Curves", Journal of the Soil Mechanics and Foundations Division, ASCE, Vol. 98, No. SM7, July 1972, pp. 667-692.

16. Seed, H. B. and Idriss, I. M., "Soil Moduli and Damping Factors for Dynamic Response Analysis", Report EERC 70-10, University of California, Earthquake Engineering Research Center, Berkeley, Dec. 1970.

17. Poulos, H. G., "Settlement of Isolated Foundations", in Soil Mechanics - Recent Developments, Eds. S. Valliappan, S. Hain, and I. K. Lee, William H. Sellen Pty., Zetland, 1975, pp. 181-212.

18. Duncan, J. M. and Chang, C.-Y., "Nonlinear Analysis of Stress and Strain in Soils", Journal of the Soil Mechanics and Foundations Division, ASCE, Vol. 96, No. SM5, Sept. 1970, pp. 1629-1653.

19. Vesić, A. S., "Design of Pile Foundations", Synthesis of Highway Practice 42, Transportation Research Board, Washington, 1977, 68 p.

20. Vesić, A. S., "Bearing Capacity of Shallow Foundations", Chapter 3 in Foundation Engineering Handbook, Eds. H. Winterkorn and H. Y. Fang, Van Nostrand Reinhold Company, New York, 1975, pp. 121-147.

21. D'Appolonia, D. J., D'Appolonia, E., and Brisette, R. F., Discussion of "Settlement of Spread Footings in Sands", Journal of the Soil Mechanics and Foundations Division, ASCE, Vol. 96, No. SM2, Mar. 1970, pp. 754-761.

22. Schmertmann, J. H., "Static Cone to Compute Static Settlement Over Sand", Journal of the Soil Mechanics and Foundations Division, ASCE, Vol. 96, No. SM3, May 1970, pp. 1011-1043.

23. Mitchell, J. K. and Gardner, W. S., "In-Situ Measurement of Volume Change Characteristics", Proceedings, ASCE Specialty Conference on In-Situ Measurement of Soil Properties, Vol. 2, Raleigh, 1975, pp. 279-345.

24. Schultz, E. and Melzer, K. J., "The Determination of the Density and the Modulus of Compressibility of Non-Cohesive Soils by Soundings", Proceedings, 6th International Conference on Soil Mechanics and Foundation Engineering, Vol. 1, Montreal, 1965, pp. 354-358.

25. Mayne, P. W. and Frost, D. D., "Dilatometer Experience in Washington, D.C. and Vicinity", Research Record 1169, Transportation Research Board, Washington, 1989, pp. 16-23.

26. Webb, D. L., Mival, K. N., and Allinson, A. J., "A Comparison of the Methods of Determining Settlements in Estuarine Sands from Dutch Cone Penetration Tests", Proceedings, 2nd European Symposium on Penetration Testing, Vol. 2, Amsterdam, 1982, pp. 945-950.

27. Jamiolkowski, M., Ghionna, V., Lancellotta, R., and Pasqualini, E., "New Correlations of Penetration Tests for Design Practice", Proceedings, 1st International Symposium on Penetration Testing (ISOPT-1), Vol. 1, Orlando, 1988, pp. 263-296.

28. Janbu, N., "Soil Models in Offshore Engineering", Geotechnique, Vol. 35, No. 3, Sept. 1985, pp. 241-281.

29. Richart, F. E., Jr., Hall, J. R., Jr., and Woods, R. D., Vibrations of Soils and Foundations, Prentice-Hall, Englewood Cliffs, 1970, 414 p.

30. Hardin, B. O., "Nature of Stress-Strain Behavior for Soils", Proceedings, ASCE Specialty Conference on Earthquake Engineering and Soil Dynamics, Vol. 1, Pasadena, 1978, pp. 3-90.

31. Horvath, J. S., "Modulus of Subgrade Reaction: New Perspective", Journal of Geotechnical Engineering, ASCE, Vol. 109, No. 12, Dec. 1983, pp. 1591-1596.

32. Vesić, A. S., "Beams on Elastic Subgrade and the Winkler Hypothesis", Proceedings, 5th International Conference on Soil Mechanics and Foundation Engineering, Vol. 1, Paris, 1961, pp. 845-850.

Section 6

TIME-DEPENDENT DEFORMABILITY

The parameters that define the time-dependent deformability of soils are important for evaluating the settlement of foundations. In this section, basic definitions are covered first to describe the pertinent terms. Correlations then are presented to evaluate the consolidation settlement of both cohesive and cohesionless soils. Where available, in-situ test correlations are included. The parameters defining the time-dependency of consolidation settlement are covered next, again including in-situ test correlations where available. The final topic addresses the parameters that control the long-term settlement caused by secondary compression.

BASIC DEFINITIONS

The time-dependent deformability covered in this section refers to the processes of hydrodynamic consolidation and secondary compression. Without addressing theoretical issues in detail, the basic terms are described below.

The effective preconsolidation stress ($\bar{\sigma}_p$ or $\bar{\sigma}_{vmax}$) is the maximum vertical (overburden) stress experienced by the soil during its geologic history, as shown in Figure 6-1. Most natural soils are preconsolidated to some degree, either by erosion, desiccation, past glacial activity, aging, or other factors. The ratio of preconsolidation stress to current effective overburden stress is defined as the overconsolidation ratio (OCR = $\bar{\sigma}_p/\bar{\sigma}_{vo}$) and is a convenient term for describing the stress state. Methods for estimating $\bar{\sigma}_p$ and OCR have been presented in Section 3.

The compression index (C_c) is defined as the slope of the void ratio (e) versus log vertical effective stress ($\bar{\sigma}_v$) curve for virgin loading. This slope corresponds to the normally consolidated (NC) state with OCR = 1. An alternative form is to plot the vertical strain (ϵ_v) versus log $\bar{\sigma}_v$. The virgin compression slope in this case is defined as the compression ratio [CR = $C_c/(1 + e_o)$].

If the soil is unloaded vertically, it will rebound or swell along an unloading line, as shown in Figure 6-1. Subsequent reloading follows a similar path, also shown in Figure 6-1. The differences between unloading and reloading normally are

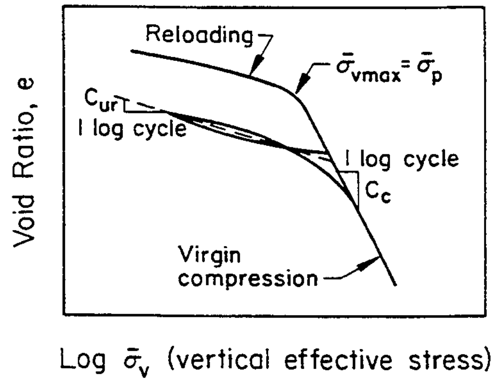

Figure 6-1. Consolidation Behavior

small and are neglected in practice. Therefore, an average value (C_{ur}) often is used. Soils existing on the C_{ur} line represent overconsolidated (OC) states.

The coefficient of consolidation (c_v) expresses the rate of primary settlement with time and is found by interpreting laboratory curves of settlement with time. From these data, the value of c_v is computed as:

$$c_v = T\,H^2/t \tag{6-1}$$

in which T = time factor, H = height of drainage path, and t = time. The coefficient of consolidation includes the permeability (k) and constrained modulus ($M = 1/m_v$) as follows:

$$c_v = k\,M/\gamma_w = k/\gamma_w m_v \tag{6-2}$$

in which γ_w = unit weight of water.

The time factor (T) depends upon the drainage boundaries, geometry, and percent dissipation of excess pore water stresses. For one-dimensional loading, the time factor for 50 percent consolidation (T_{50}) is 0.197. For 90 percent consolidation, the time factor (T_{90}) is 0.848.

Secondary compression follows primary consolidation and is defined by the coefficient of secondary compression (C_α). If expressed in terms of vertical strain, $C_{\alpha\epsilon}$ is defined over one log cycle of time, as shown in Figure 6-2. If the coefficient of secondary compression is expressed by change of void ratio with logarithm of time, then:

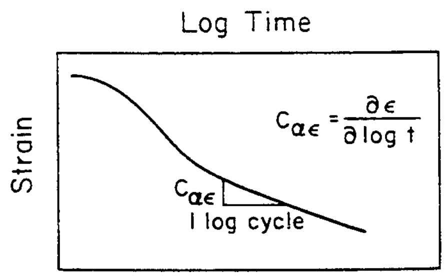

Figure 6-2. Time-Settlement Behavior

$$C_{\alpha e} = C_{\alpha\epsilon}(1 + e_o) \qquad (6\text{-}3)$$

in which e_o = initial void ratio.

An alternate procedure for representing consolidation data is to use vertical strain versus vertical stress curves on arithmetic scales. In this way, the stress-strain curve provides a constrained modulus (M) which can be related to the more familiar compression index (C_c) as follows:

$$M = \frac{\partial \bar{\sigma}}{\partial \epsilon} = \frac{(1 + e) \ln 10\ \bar{\sigma}_v}{C_c} = \frac{2.3\ (1 + e)\ \bar{\sigma}_v}{C_c} \qquad (6\text{-}4)$$

For overconsolidated soils, C_c should be replaced by C_{ur} in Equation 6-4.

COMPRESSION AND UNLOAD-RELOAD INDICES FOR COHESIVE SOILS

The compression and unload-reload indices have been examined in detail by many authors, and a variety of correlations have been proposed. Representative correlations are presented below.

Typical Values

The degree of compressibility of clay, expressed in terms of the compression index (C_c), commonly is described as in Table 6-1. Over 70 different correlations have been published for correlating C_c to the index properties of clays, and Figure 6-3 illustrates the ranges involved. Apparently, the correlations between C_c and w_n are more consistent than those cited between C_c and w_L or e_o.

Although there is considerable scatter, the Terzaghi and Peck (2) relationship for NC natural clay is still popular. This relationship is given by:

Table 6-1

DEGREE OF COMPRESSIBILITY

Compressibility	C_c
slight or low	< 0.2
moderate or intermediate	0.2 to 0.4
high	> 0.4

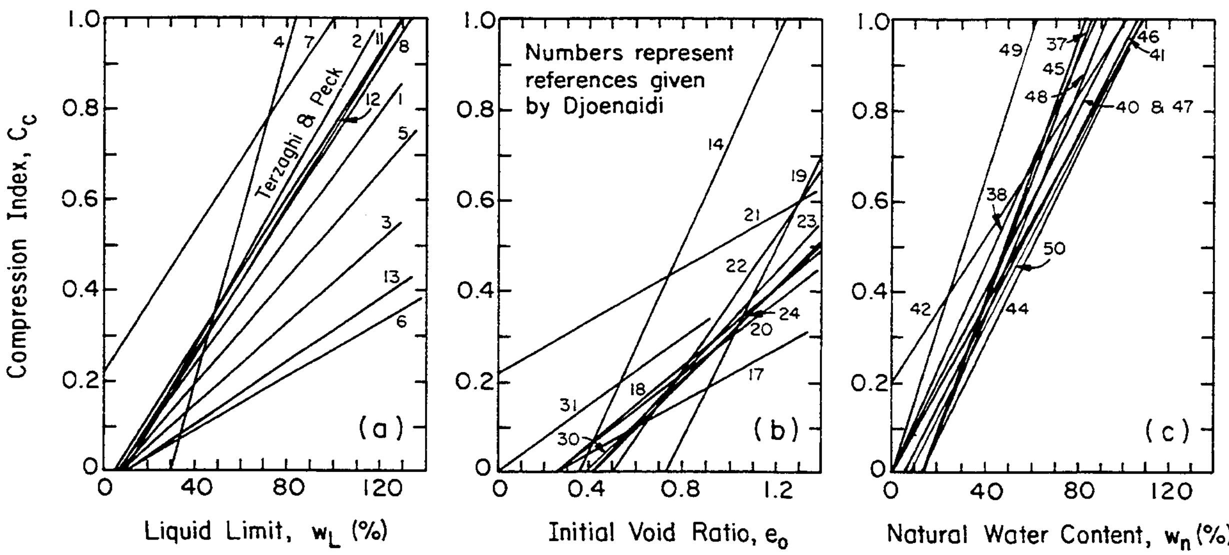

Figure 6-3. Representative C_c Relationships for Cohesive Soils

Source: Djoenaidi (1), p. 6-67.

$$C_c \approx 0.009\ (w_L - 10) \qquad (6\text{-}5)$$

Based on the modifed Cam clay model, Wroth and Wood (3) showed that C_c also can be estimated as follows:

$$C_c \approx 0.5\ G_s\ (PI/100) \qquad (6\text{-}6)$$

in which G_s = specific gravity of solids. Using a typical G_s = 2.7 for clays gives:

$$C_c \approx PI/74 \qquad (6\text{-}7)$$

Furthermore, the modified Cam clay model utilizes the Λ parameter, which is relatively constant for natural clays at approximately 0.8. Re-writing Equation G-2 (in Appendix G) for Λ, the unload-reload index can be calculated as:

$$C_{ur} = C_c\ (1 - \Lambda) \qquad (6\text{-}8)$$

Using the typical value of $\Lambda = 0.8$ with $G_s = 2.7$ gives:

$$C_{ur} \approx PI/370 \qquad (6\text{-}9)$$

Figure 6-4 indicates general agreement between the measured values of C_c and C_{ur} and those predicted using the modified Cam clay model. Furthermore, the regression lines are within several percent of the model values. These data confirm that the average C_{ur} is approximately 20 percent of the average C_c.

The sensitivity of the clay (S_t) also affects C_c, particularly for marine deposits. Figure 6-5 shows the dramatic influence of sensitivity on C_c.

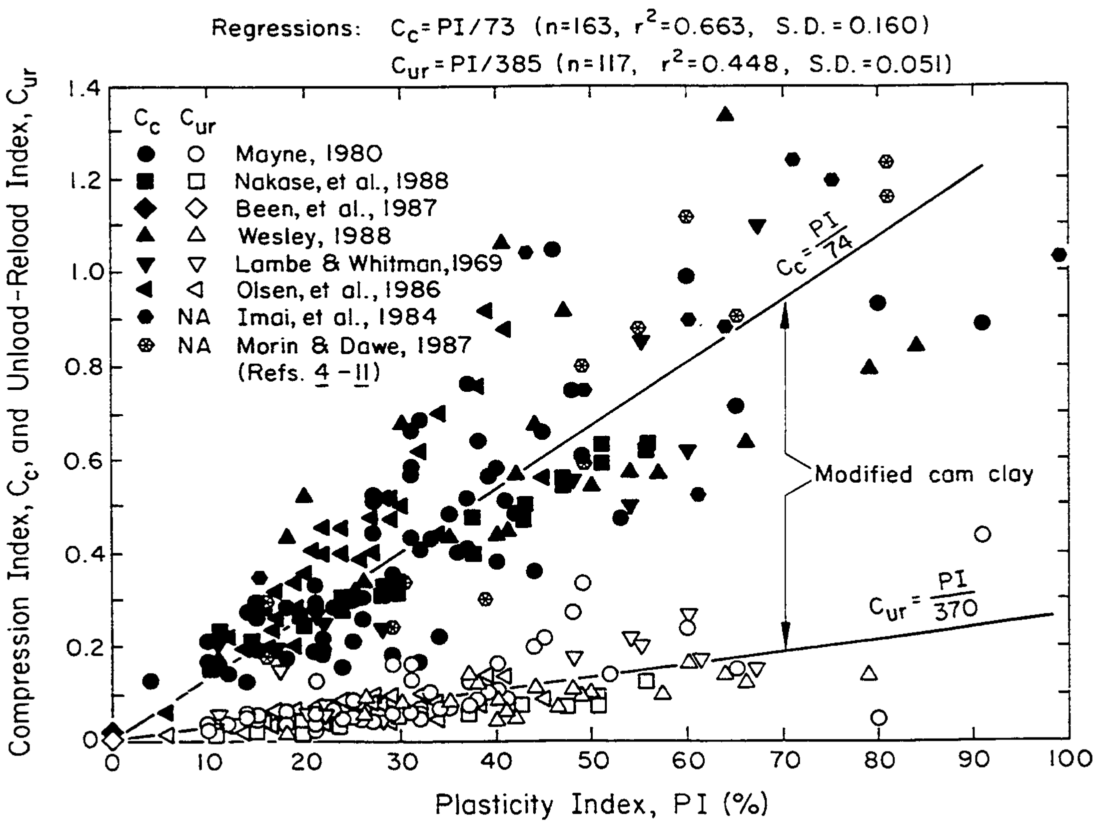

Figure 6-4. Compression and Unload-Reload Indices versus PI

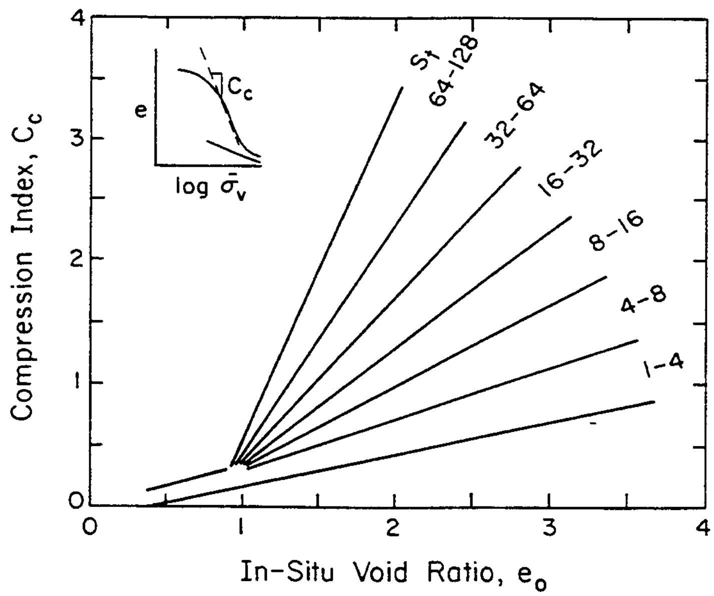

Figure 6-5. Sensitivity-Compression Index Relationships

Source: Leroueil, et al. (12), p. 696.

An alternative to the compression index (C_c) is the compression ratio (CR), defined as $C_c/(1 + e_o)$, in which e_o = initial void ratio. Normalizing C_c in this manner tends to reduce the data scatter, (e.g., 8). Figure 6-6 shows the typical ranges in CR reported by Lambe and Whitman (8).

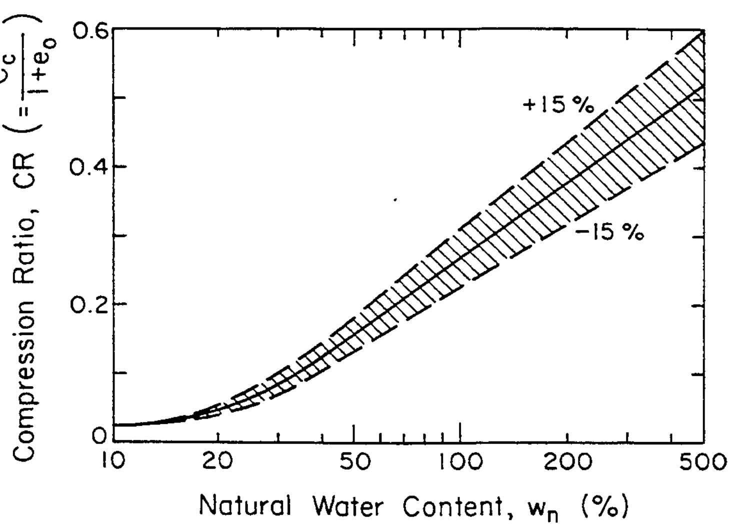

Figure 6-6. Compression Ratio versus Water Content

Source: Lambe and Whitman (8), p. 321.

Correlations with CPT q_c Value

Attempts also have been made to corrrelate C_c with the cone tip resistance, as described by Sanglerat (13). However, these correlations have not proved to be useful to date. For example, they show that for $q_c/p_a > 20$, C_c is likely to be between 0.05 and 0.2. For $q_c/p_a < 10$, C_c could be nearly any value above 0.1.

CONSTRAINED MODULUS FOR COHESIVE SOILS

Typical Values

As described previously, the constrained modulus (M) is an alternative to C_c. Early work on this subject by Janbu (14) demonstrated that the drained secant constrained modulus (M_{ds}) is a function of the vertical effective stress ($\bar{\sigma}_v$) and a modulus number (m). For NC clays, M_{ds} is given by:

$$M_{ds} = m\ \bar{\sigma}_v \qquad (6\text{-}10)$$

For NC silts and sands, M is given by:

$$M_{ds}/p_a = m\ (\bar{\sigma}_v/p_a)^{0.5} \qquad (6\text{-}11)$$

Figure 6-7 shows the general trend in m as a function of porosity for a variety of NC soils and rocks.

Since the constrained modulus is defined as $\partial\bar{\sigma}/\partial\epsilon$ for one-dimensional compression, it can be shown simply that:

$$M_{ds} = \bar{\sigma}_v\ \left(\frac{1 + e_o}{C_c}\right)\ \ln 10 = m\ \bar{\sigma}_v \qquad (6\text{-}12)$$

Therefore, the modulus number for clays is simply 2.3/CR, where CR = compression ratio. Figure 6-8 shows that the trend for m with water content for NC clays is consistent with the previous correlation for CR and water content (Figure 6-6). For OC clays, the modulus number is 5 to 10 times that for the NC range.

Correlations with SPT N Value

The constrained modulus from oedometer tests on clay also has been correlated by Stroud (16) with N values obtained from the standard penetration test (SPT). This relationship is given by:

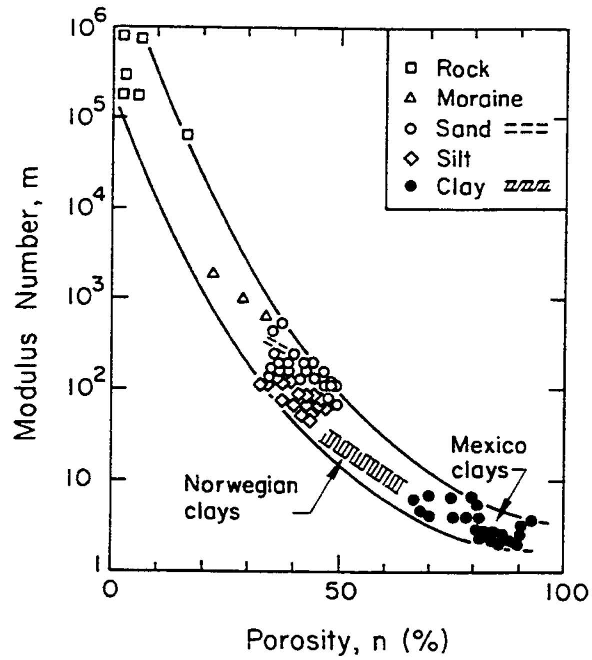

Figure 6-7. General Relationship Between Modulus Number and Porosity for NC Soils

Source: Janbu (14), p. 20.

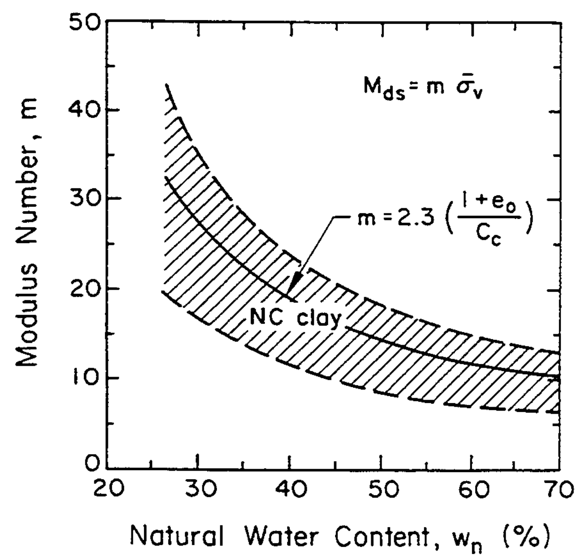

Figure 6-8. Modulus Number for NC Clay

Source: Janbu (15), p. 261.

$$M_{ds}/p_a = f\ N \tag{6-13}$$

in which the empirical coefficient, f, has been related to PI, as shown in Figure

6-9. This correlation is not very strong and should be used with caution.

Correlations with CPT Results

Numerous correlations have been suggested to relate the cone penetration test (CPT) q_c value to the constrained modulus of cohesive soils. All generally take the form below:

$$M_{ds}/q_c = \alpha \qquad (6\text{-}14)$$

in which α = empirical coefficient. Compilations of α (e.g., 17) have shown suggested values ranging from 0.4 to 8, with the majority of values between 1 and 3. However, most of these values have been obtained using a variety of mechanical and electric cones of different geometries and test procedures.

Figure 6-10 shows the variation of M_{ds} with high quality cone tip resistance data from 12 sites tested by piezocone. This figure provides a more useful estimator for M in clays.

Correlations with DMT Results

The dilatometer test (DMT) provides an estimate of M_{ds} through an empirical relationship between the dilatometer parameters E_D and K_D, as shown in Figure 6-11. The effect of the dilatometer parameter I_D on this relationship is given in explicit equations by Marchetti (19).

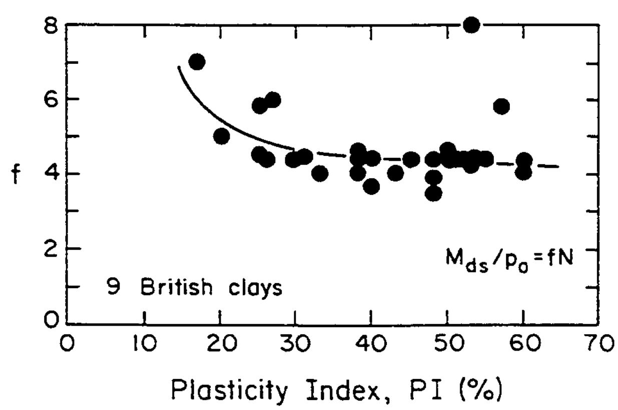

Figure 6-9. SPT Constrained Modulus Coefficient f versus PI

Source: Stroud (16), p. 373.

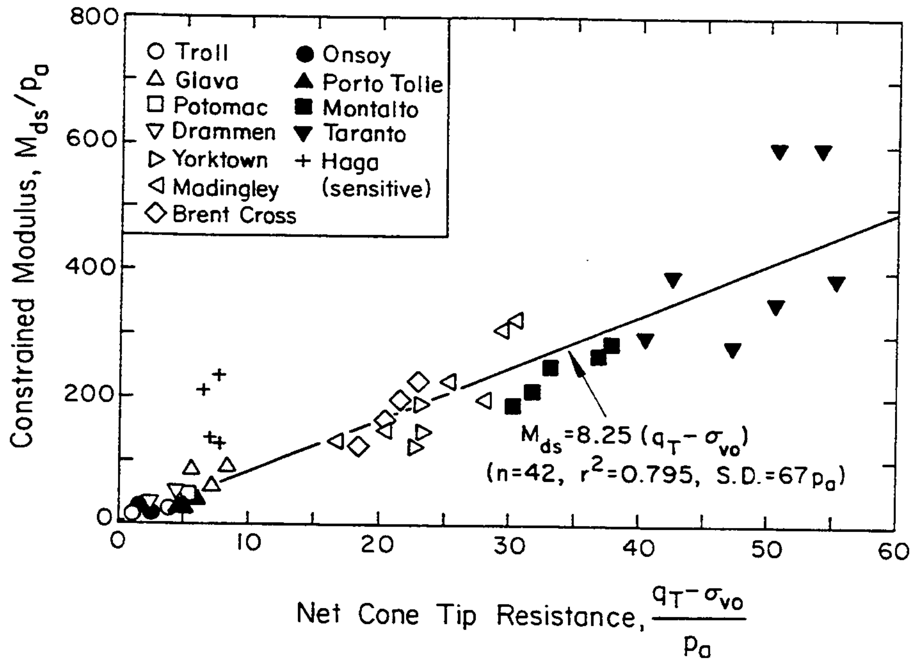

Figure 6-10. Constrained Modulus versus q_T from CPTU for Clays

Source: Database from Mayne, et al. (18).

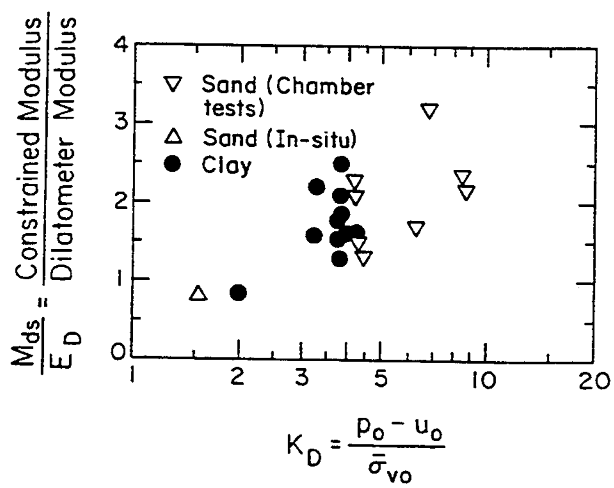

Figure 6-11. Constrained Modulus from DMT Parameters

Source: Marchetti (19), p. 317.

COMPRESSION INDEX FOR COHESIONLESS SOILS

For the predominant quartz-type cohesionless soils found throughout the world, the compressibility characteristics are much less than for cohesive soils. Exceptions to this observation could include micaceous sands and the calcareous sands associated with coralline deposits, which show significant compressibility compared with the more prevalent silica sands. The compression index of cohesionless soils is somewhat stress-dependent, indicating that e-log $\bar{\sigma}_v$ plots are perhaps not the most appropriate means of presenting one-dimensional compression data. Typical values for the compression index and unload-reload index of six different sands are given in Table 6-2.

The effect of grain size distribution on sand compressibility is illustrated in Figure 6-12 at a reference relative density of 40 percent. The effect of relative density on sand compressibility is given in Figure 6-13. In both of these figures, the notation used is defined in Table 2-7.

CONSTRAINED MODULUS FOR COHESIONLESS SOILS

Typical Values

The stress-dependency effect on sand compressibility may be taken into account more directly by using the constrained modulus (M_{ds}):

Table 6-2

COMPRESSIBILITY DATA FOR SIX SANDS IN CALIBRATION CHAMBER TESTS

Sand	e_o	C_c: $\bar{\sigma}_v/p_a$ = 1 to 3	C_c: $\bar{\sigma}_v/p_a$ = 20 to 30	C_{ur}
Monterey 0	0.854	0.021	0.085	0.006
	0.782	0.018	0.090	0.007
Ticino	0.917	0.025	0.130	0.007
	0.827	0.026	0.085	0.006
Hokksund	0.870	0.024	0.095	0.005
	0.790	0.018	0.056	0.005
Ottawa	0.760	0.025	0.030	0.007
	0.560	0.005	0.100	0.003
Reid-Bedford	0.900	0.013	0.090	0.005
	0.650	0.005	0.019	0.003
Hilton Mines	0.950	0.038	0.210	0.009
	0.732	0.022	0.100	0.006

Note: Details on these sands are given in Appendix H.
Source: Been, et al. (6), p. 295.

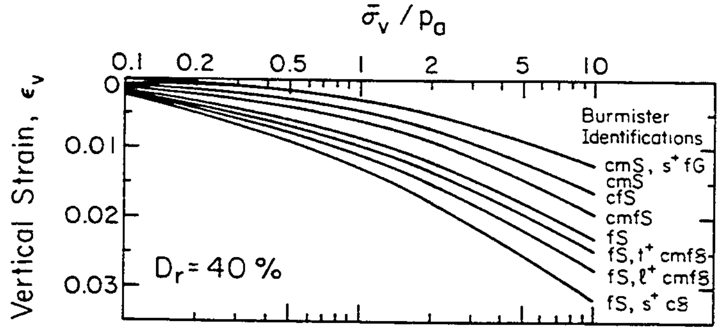

Figure 6-12. Effect of Grain Size on Sand Compressibility

Source: Burmister (20), p. 82.

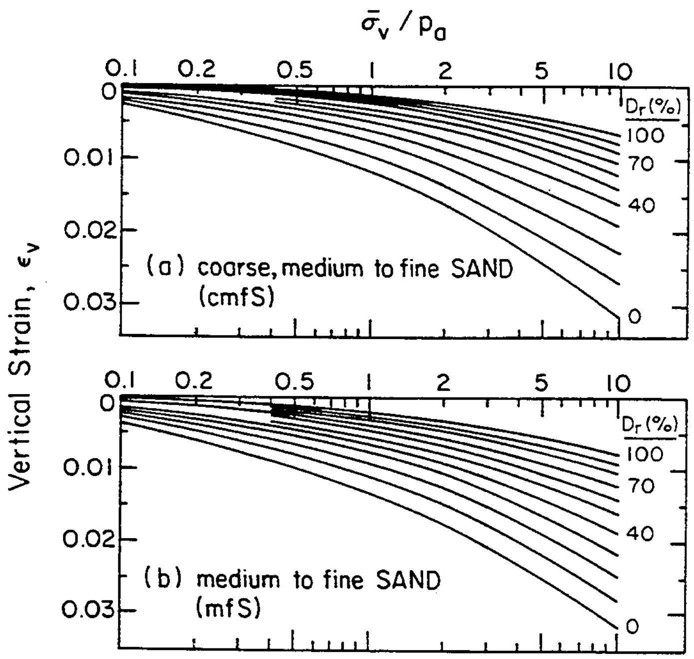

Figure 6-13. Effect of D_r on Sand Compressibility

Source: Burmister (20), p. 83.

$$M_{ds}/p_a = m\,(\bar{\sigma}_v/p_a)^{0.5} \tag{6-15}$$

in which the modulus number (m) has been correlated with porosity, as shown previously in Figure 6-7. More specific general relationships are shown in Figure 6-14 for silts and sands.

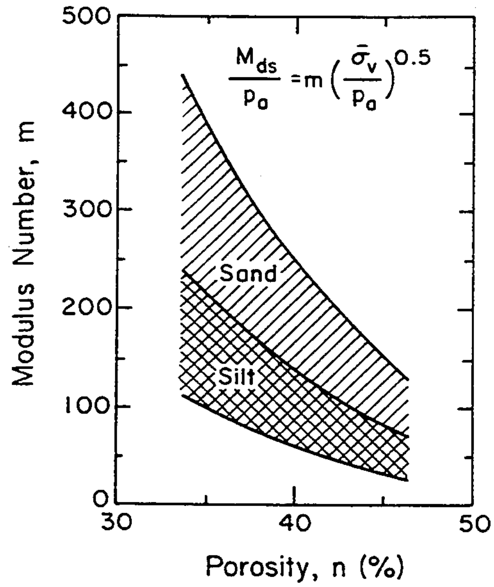

Figure 6-14. Modulus Number for NC Silts and Sands

Source: Janbu (15), p. 261.

Correlations with SPT, CPT, and DMT Results

In Section 5, correlations are presented which relate the constrained modulus of cohesionless soils to the SPT N value and CPT q_c value. DMT correlations were given in Figure 6-11.

COEFFICIENT OF CONSOLIDATION

Typical Values

The field value of the coefficient of consolidation (c_v) is a difficult parameter to estimate because common field situations include sand seams and lenses, varves, etc., which make laboratory-predicted values of c_v different from in-situ values. However, Figure 6-15 provides a first-order estimate for c_v of clays using the liquid limit.

Correlations with CPT and DMT Results

Several of the recent in-situ tests, particularly the piezocone and dilatometer, have been utilized to give field estimates of horizontal permeability (k_h) and horzontal coefficient of consolidation (c_{vh}) in clays. The basic equation for the horizontal coefficient of consolidation is:

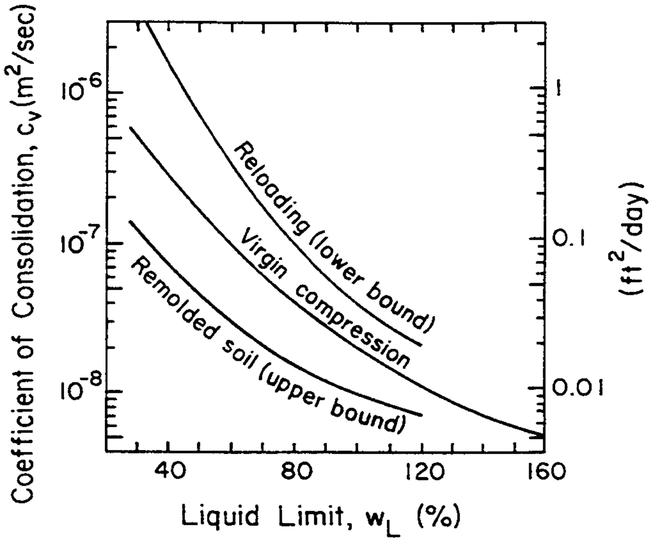

Figure 6-15. c_v versus w_L

Source: NAVFAC (21), p. 7.1-144.

$$c_{vh} = T\,R^2/t \tag{6-16}$$

in which T = time factor, R = equivalent cavity (piezocone) radius, and t = time to achieve desired degree of excess pore water stress dissipation. The approach is based on cavity expansion theory, and therefore it depends on the rigidity index of the soil ($I_r = G/s_u$, in which G = shear modulus and s_u = undrained shear strength).

Figure 6-16 gives the piezocone time factors. Most commonly, the dissipation test is conducted for a period of time (t) which will allow 50 percent dissipation of the original insertion excess pore water stress (Δu). The time factor corresponding to this dissipation time then is introduced into Equation 6-16 to compute the coefficient of consolidation. Cylindrical theory would be used for a pore water sensor behind the tip, while spherical theory would be used for a sensor at the tip.

Similar developments by Robertson, et al. (23) have led to an empirical method for determining c_{vh} from the dilatometer C readings, using the following:

$$c_{vh} = T\,R_e{}^2/t \tag{6-17}$$

in which R_e = equivalent radius for the 14 mm by 95 mm dilatometer blade (i.e., $R_e \approx 20.6$ mm) and the time factor (T) is given in Figure 6-17. In this figure, p_2 is the dilatometer C reading at a particular time. The test procedure for the DMT

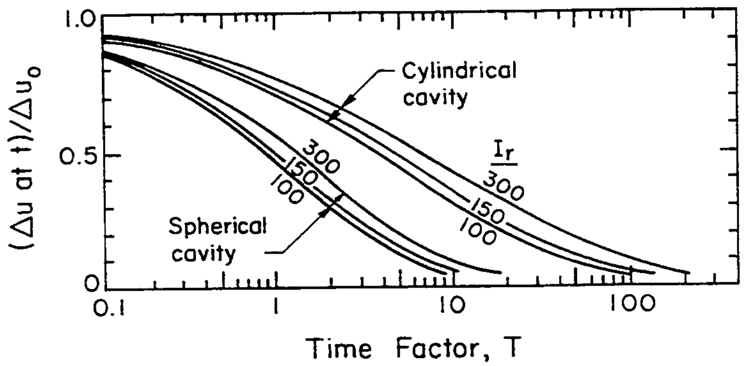

Figure 6-16. Pore Water Stress Decay versus Piezocone Time Factor

Source: Jamiolkowski, et al. (22), p. 128.

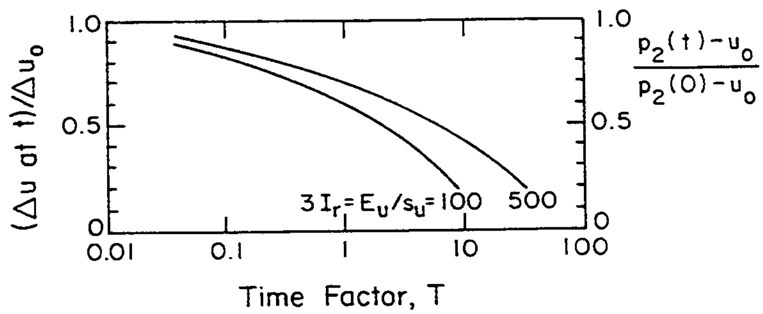

Figure 6-17. Pore Water Stress Decay versus Dilatometer Time Factor

Source: Robertson, et al. (23), p. 574.

dissipation readings is similar to that for the piezocone.

COEFFICIENT OF SECONDARY COMPRESSION

The coefficient of secondary compression (C_α) defines the rate of settlement with time after primary consolidation is complete. This coefficient may be expressed either in units of strain ($C_{\alpha\epsilon}$) or void ratio ($C_{\alpha e}$) per log cycle of time, as shown in the following:

$$C_{\alpha\epsilon} = \partial\epsilon/\partial \log t \quad (6\text{-}18)$$

$$C_{\alpha e} = \partial e/\partial \log t \quad (6\text{-}19)$$

For a wide variety of clays, $C_{\alpha\epsilon}$ has been correlated to the natural water content, as shown in Figure 6-18. Based on this figure, the following was suggested for NC clay:

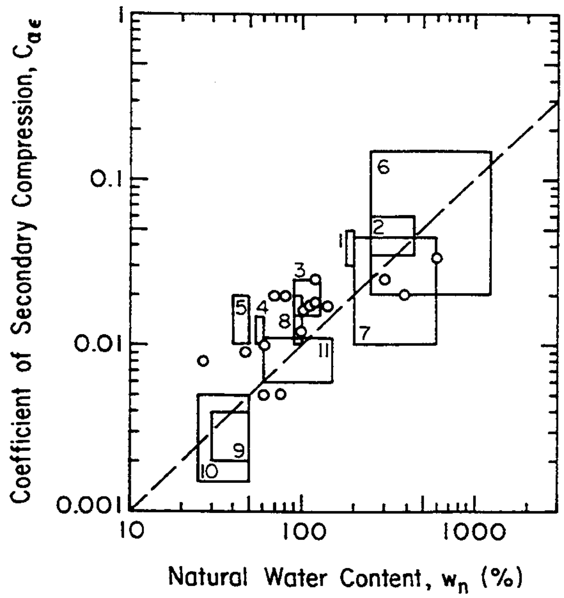

Figure 6-18. Coefficient of Secondary Compression versus Water Content for NC Clays

Source: Mesri (24), p. 125.

$$C_{\alpha\epsilon} \approx 0.0001\ w_n \qquad (6\text{-}20)$$

Examination of available data indicates that $0.0005 < C_{\alpha\epsilon} < 0.001$ for most OC clays.

For NC clays, the ratio of the coefficient of secondary compression to the compression index ($C_{\alpha e}/C_c = C_{\alpha\epsilon}/CR$) is relatively constant for a given soil. Table 6-3 lists $C_{\alpha e}/C_c$ for a variety of clays. On the average, the value of $C_{\alpha e}/C_c$ is 0.04 ± 0.01 for the inorganic clays and silts. For the organic clays and silts, the value averages 0.05 ± 0.01. For the peats, the value averages 0.075 ± 0.01. This constant also is applicable for inorganic OC clays which have $C_{\alpha e}/C_{ur}$ equal to 0.04 ± 0.01.

Table 6-3

COMPILATION OF $C_{\alpha e}/C_c$ FOR NATURAL SOILS

Grouping	Soil Type	$C_{\alpha e}/C_c$
Inorganic Clays and Silts	Whangamarino clay	0.03 to 0.04
	Leda clay	0.025 to 0.06
	Soft blue clay	0.026
	Portland sensitive clay	0.025 to 0.055
	San Francisco bay mud	0.04 to 0.06
	New Liskeard varved clay	0.03 to 0.06
	Silty clay C	0.032
	Nearshore clays and silts	0.055 to 0.075
	Mexico City clay	0.03 to 0.035
	Hudson River silt	0.03 to 0.06
Organic Clays and Silts	Norfolk organic silt	0.05
	Calcareous organic silt	0.035 to 0.06
	Post-glacial organic clay	0.05 to 0.07
	Organic clays and silts	0.04 to 0.06
	New Haven organic clay silt	0.04 to 0.075
Peats	Amorphous and fibrous peat	0.035 to 0.083
	Canadian muskeg	0.09 to 0.10
	Peat	0.075 to 0.085
	Peat	0.05 to 0.08
	Fibrous peat	0.06 to 0.085

Source: Mesri and Godlewski (25), p. 421.

REFERENCES

1. Djoenaidi, W. J., "A Compendium of Soil Properties and Correlations", M. Eng. Sc. Thesis, University of Sydney, 1985, 836 p.

2. Terzaghi, K. and Peck, R. B., Soil Mechanics in Engineering Practice, 2nd Ed., John Wiley and Sons, New York, 1967, 729 p.

3. Wroth, C. P. and Wood, D. M., "The Correlation of Index Properties with Some Basic Engineering Properties of Soils", Canadian Geotechnical Journal, Vol. 15, No. 2, May 1978, pp. 137-145.

4. Mayne, P. W., "Cam-Clay Predictions of Undrained Strength", Journal of the Geotechnical Engineering Division, ASCE, Vol. 106, No. GT11, Nov. 1980, pp. 1219-1242.

5. Nakase, A., Kamei, T., and Kusakabe, O., "Constitutive Parameters Estimated by Plasticity Index", Journal of Geotechnical Engineering, ASCE, Vol. 114, No. 7, July 1988, pp. 844-858.

6. Been, K., Jeffries, M. G., Crooks, J. H. A., and Rothenburg, L., "The Cone Penetration Test in Sands: Part II, General Inference of State", Geotechnique, Vol. 37, No. 3, Sept. 1987, pp. 285-299.

7. Wesley, L. D., "Compression Index: A Misleading Parameter?", Journal of Geotechnical Engineering, ASCE, Vol. 114, No. 6, June 1988, pp. 718-723.

8. Lambe, T. W. and Whitman, R. V., Soil Mechanics, John Wiley and Sons, New York, 1969, 553 p.

9. Olsen, H. W., Rice, T. L., Mayne, P. W., and Singh, R. D., "Piston Core Properties and Disturbance Effects", Journal of Geotechnical Engineering, ASCE, Vol. 112, No. 2, June 1986, pp. 608-625.

10. Imai, G., Yano, K., and Aok, S., "Applicability of Hydraulic Consolidation Test for Very Soft Clayey Soils", Soils and Foundations, Vol. 24, No. 2, June 1984, pp. 29-42.

11. Morin, P. and Dawe, C. R., "Geotechnical Properties of Two Deep-Sea Marine Soils from The Labrador Sea", Canadian Geotechnical Journal, Vol. 24, No. 4, Nov. 1987, pp. 536-548.

12. Leroueil, S., Tavenas, F., and LeBihan, J. P., "Propriétés Caractéristiques des Argiles de l'est du Canada", Canadian Geotechnical Journal, Vol. 20, No. 4, Nov. 1983, pp. 681-705.

13. Sanglerat, G., The Penetrometer and Soil Exploration, Elsevier, Amsterdam, 1972, 464 p.

14. Janbu, N., "Soil Compressibility as Determined by Oedometer and Triaxial Tests", Proceedings, 3rd European Conference on Soil Mechanics and Foundation Engineering, Vol. 1, Wiesbaden, 1963, pp. 19-25.

15. Janbu, N., "Soil Models in Offshore Engineering", Geotechnique, Vol. 35, No. 3, Sept. 1985, pp. 241-281.

16. Stroud, M. A., "The SPT in Insensitive Clays and Soft Rocks", Proceedings, European Symposium on Penetration Testing, Vol. 2.2, Stockholm, 1974, pp. 367-375.

17. Mitchell, J. K. and Gardner, W. S., "In-Situ Measurement of Volume Change Characteristics", Proceedings, ASCE Specialty Conference on In-Situ Measurement of Soil Properties, Vol. 2, Raleigh, 1975, pp. 279-345.

18. Mayne, P. W., Kulhawy, F. H., and Kay, J. N., "Observations on the Development of Pore Water Stresses During Cone Penetration in Clays", Canadian Geotechnical Journal, Vol. 27, No. 3, Aug. 1990.

19. Marchetti, S., "In-Situ Tests by Flat Dilatometer", Journal of the Geotechnical Engineering Division, ASCE, Vol. 106, No. GT3, Mar. 1980, pp. 299-321.

20. Burmister, D. M., "Physical, Stress-Strain, and Strength Responses of Granular Soils", Symposium on Field Testing of Soils (STP 322), ASTM, Philadelphia, 1962, pp. 67-97.

21. NAVFAC, Soil Mechanics (DM 7.1), Naval Facilities Engineering Command, Alexandria, 1982, 355 p.

22. Jamiolkowski, M., Ladd, C. C., Germaine, J. T., and Lancellotta, R., "New Developments in Field and Laboratory Testing of Soils", Proceedings, 11th International Conference on Soil Mechanics and Foundation Engineering, Vol. 1, San Francisco, 1985, pp. 57-154.

23. Robertson, P. K., Campanella, R. G., Gillespie, D., and By, T., "Excess Pore Pressures and the Flat Dilatometer Test", Proceedings, 1st International Symposium on Penetration Testing (ISOPT-1), Vol. 1, Orlando, 1988, pp. 567-576.

24. Mesri, G., "Coefficient of Secondary Compression", Journal of the Soil Mechanics and Foundations Division, ASCE, Vol. 99, No. SM1, Jan. 1973, pp. 123-137.

25. Mesri, G. and Godlewski, P. M., "Time and Stress - Compressibility Interrelationship", Journal of the Geotechnical Engineering Division, ASCE, Vol. 103, No. GT5, May 1977, pp. 417-430.

Section 7

PERMEABILITY

The coefficient of permeability (k) of soil, also known as the hydraulic conductivity, describes the rate of water flow through soil. This soil property often is difficult to evaluate with certainty, because it varies over many orders of magnitude and in-situ soil conditions are highly variable. In addition to controlling the amount and rate of ground water inflow into foundation excavations, the coefficient of permeability also governs the rate of primary consolidation and equalization of pore water stresses.

TYPICAL VALUES

The value of the coefficient of permeability can vary over a wide range, as shown in Table 7-1. From this table, it is clear that k is highly dependent upon soil particle size. To obtain a first-order estimate of k in sands, Figure 7-1 suggests

Table 7-1

COEFFICIENT OF PERMEABILITY

Soil	Coefficient of Permeability, k (m/sec)	Relative Permeability
gravel	$> 10^{-3}$	high
sandy gravel, clean sand, fine sand	10^{-3} to 10^{-5}	medium
sand, dirty sand, silty sand	10^{-5} to 10^{-7}	low
silt, silty clay	10^{-7} to 10^{-9}	very low
clay	$< 10^{-9}$	practically impermeable

Source: Based on Terzaghi and Peck (1).

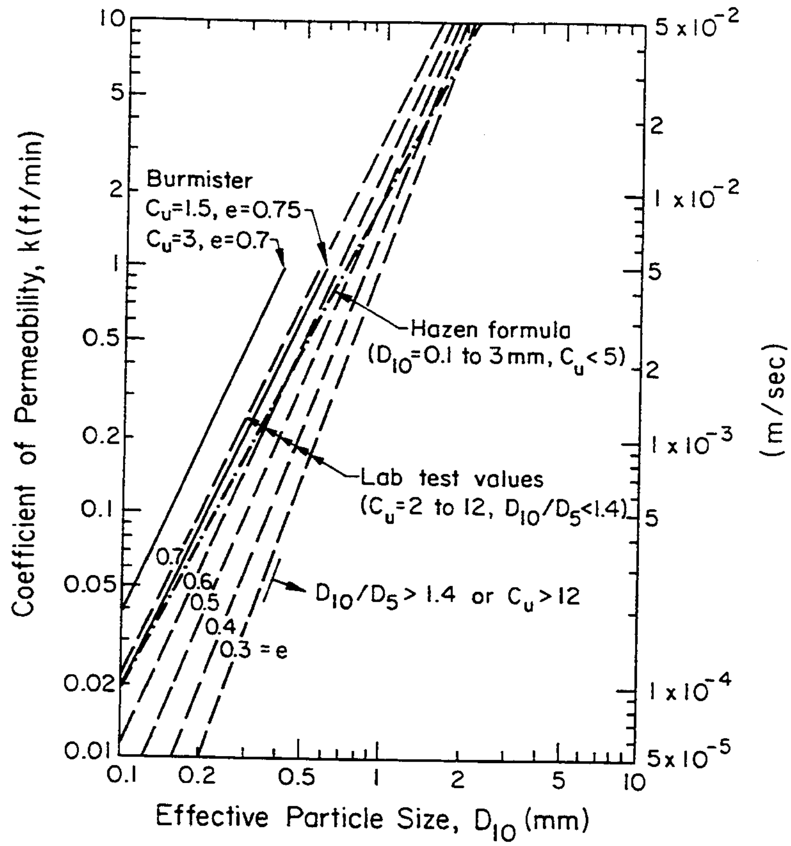

Figure 7-1. Coefficient of Permeability versus Particle Size

Source: NAVFAC (2), p. 7.1-139.

an approach in terms of void ratio (e) and effective particle size (expressed as D_{10}). The effect of particle size distribution and relative density on k is shown for several sands in Figure 7-2. The notation used is given in Table 2-7.

The in-situ vertical permeability (k_v) of clay may be estimated from the void ratio, plasticity index (PI), and clay fraction (CF), as shown in Figure 7-3. In geotechnical problems, drainage can occur horizontally as well as vertically. The ratio of horizontal to vertical permeability (k_h/k_v) generally is less than 1.5 for marine clays and other massive deposits. However, in varved clays and stratified fluvial deposits, k_h/k_v easily can exceed 10, as shown in Figure 7-4. Values of k_h/k_v over 100 are possible.

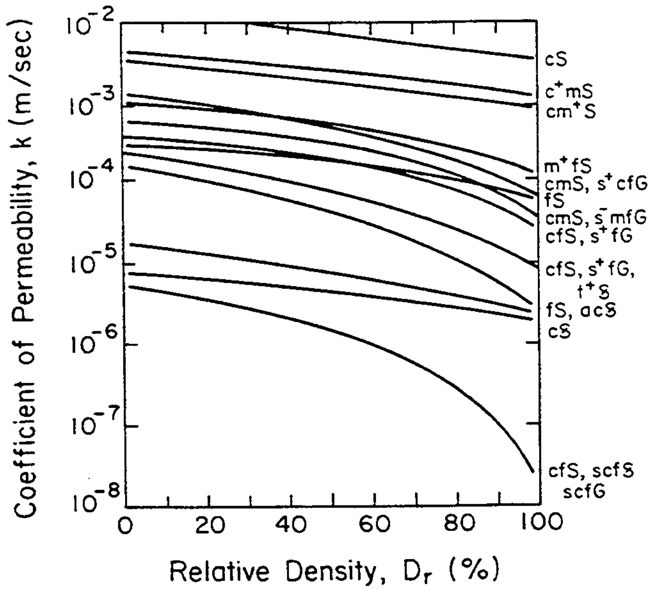

Figure 7-2. Coefficient of Permeability versus Particle Size and Relative Density

Source: Burmister (3), p. 78.

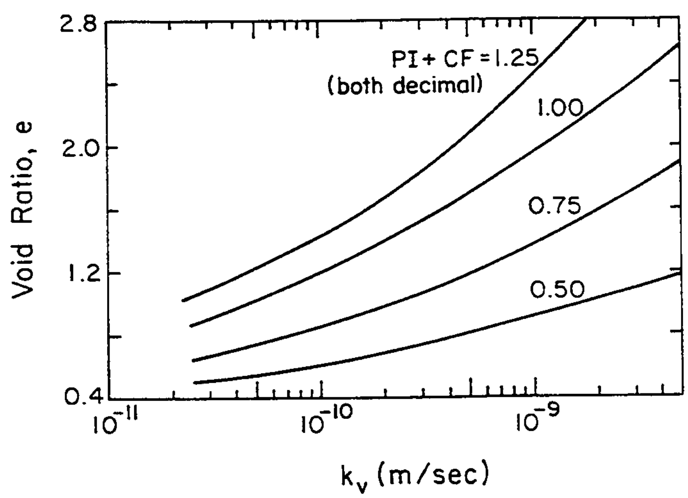

Figure 7-3. Vertical Coefficient of Permeability for Clay

Source: Tavenas, et al. (4), p. 658.

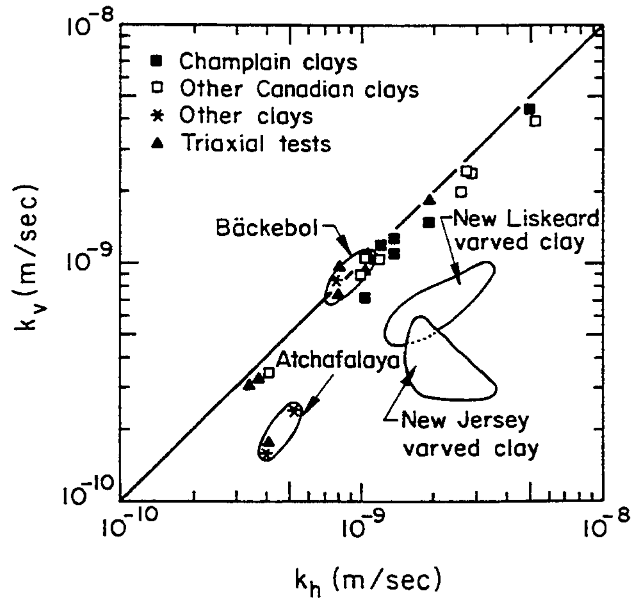

Figure 7-4. Permeability Anisotropy for Various Natural Clays

Source: Tavenas and Leroueil (5), p. 34.

REFERENCES

1. Terzaghi, K. and Peck, R. B., Soil Mechanics in Engineering Practice, 2nd Ed., John Wiley and Sons, New York, 1967, 729 p.

2. NAVFAC, Soil Mechanics (DM 7.1), Naval Facilities Engineering Command, Alexandria, 1982, 355 p.

3. Burmister, D. M., "Physical, Stress-Strain, and Strength Responses of Granular Soils", Symposium on Field Testing of Soils (STP 322), ASTM, Philadelphia, 1962, pp. 67-97.

4. Tavenas, F., Jean, P., LeBlond, P., and Leroueil, S., "The Permeability of Natural Soft Clays. Part II, Permeability Characteristics", Canadian Geotechnical Journal, Vol. 20, No. 4, Nov. 1983, pp. 645-660.

5. Tavenas, F. and Leroueil, S., "State-of-the-Art on Laboratory and In-Situ Stress-Strain-Time Behavior of Soft Clays", Proceedings, International Symposium on Geotechnical Engineering of Soft Soils, Mexico City, 1987, pp. 1-46.

Section 8

LIQUEFACTION RESISTANCE

For foundations in seismic regions, it is important to assess the potential for liquefaction occurring in cohesionless soils. If the cyclic stresses become too large and last for a long enough period of time, looser sands below the water table can liquefy and lose essentially all of their supporting capacity. Although liquefaction analysis is complex, simplified guidelines have been developed for three common in-situ tests, as described in this section.

CYCLIC STRESS RATIO

In all of the in-situ test evaluations, the loading is described by the average cyclic stress ratio at depth, given by $\tau_{av}/\bar{\sigma}_{vo}$, in which τ_{av} = average cyclic stress and $\bar{\sigma}_{vo}$ = effective overburden stress. This ratio can be evaluated experimentally using cyclic triaxial compression or direct simple shear tests or by using shaking table tests. Seed (1) discusses these tests and their interrelationships.

Alternatively, the average cyclic stress ratio can be estimated from the following (Tokimatsu and Yoshimi, 2):

$$\tau_{av}/\bar{\sigma}_{vo} = 0.1\ (M-1)\ a_{max}\ (\sigma_{vo}/\bar{\sigma}_{vo})\ (1 - 0.015z) \qquad (8\text{-}1)$$

in which M = earthquake magnitude (7.5 is used commonly), a_{max} = maximum horizontal acceleration at ground surface (as a fraction of g, the acceleration from gravity), σ_{vo} = total overburden stress, $\bar{\sigma}_{vo}$ = effective overburden stress, and z = depth in meters (for z < 25 m).

CORRELATIONS WITH SPT, CPT, AND DMT RESULTS

Extensive work has been done on evaluating the liquefaction potential of loose sands using the standard penetration test (SPT) N value and the cone penetration test (CPT) q_c value. A recent summary of this work by Seed and de Alba (3) is given in Figure 8-1. In this figure, the N value has been corrected for the overburden stress and a constant energy ratio of 60 percent, as described in Section 2. Data for this figure were developed from Pan-American, Japanese, and Chinese

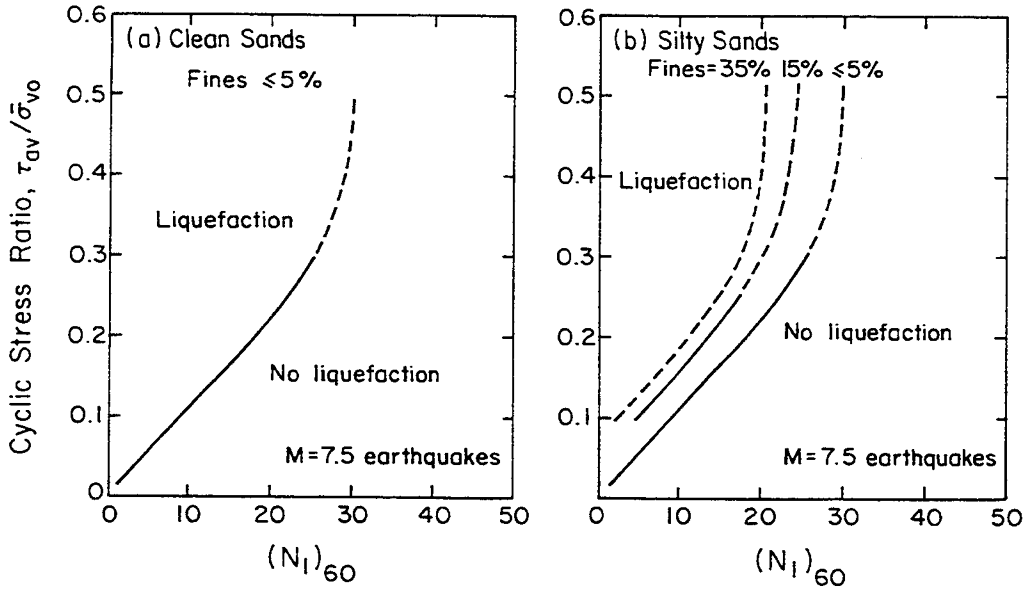

Figure 8-1. Liquefaction Resistance Correlated with Modified SPT N Value

Source: Seed and de Alba (3), pp. 290, 291.

sources. As can be seen, silty sands exhibit a greater resistance to liquefaction at a given N value.

By cross-correlating SPT and CPT data, Seed and de Alba (3) developed a comparable relationship for liquefaction resistance in terms of the CPT q_c value. This relationship is shown in Figure 8-2 and uses q_n, the cone tip resistance corrected for the overburden stress which, from Equations 2-18 and 2-19, is given by:

$$q_n = q_c \ (p_a/\bar{\sigma}_{vo})^{0.5} \qquad (8\text{-}2)$$

Recently, a more direct relationship has been proposed by Shibata and Teparaksa (4). This relationship was developed directly from CPT data obtained at earthquake sites in Japan, China, and the U.S. As shown in Figure 8-3, this new approach provides further refinement over prior recommendations.

A correlation also has been developed by Robertson and Campanella (6) to evaluate liquefaction resistance in terms of the dilatometer test (DMT) horizontal stress index (K_D), as shown in Figure 8-4. This correlation is new and based on limited data for normally consolidated, unaged, uncemented sands. Further refinements and generalizations are likely in the future.

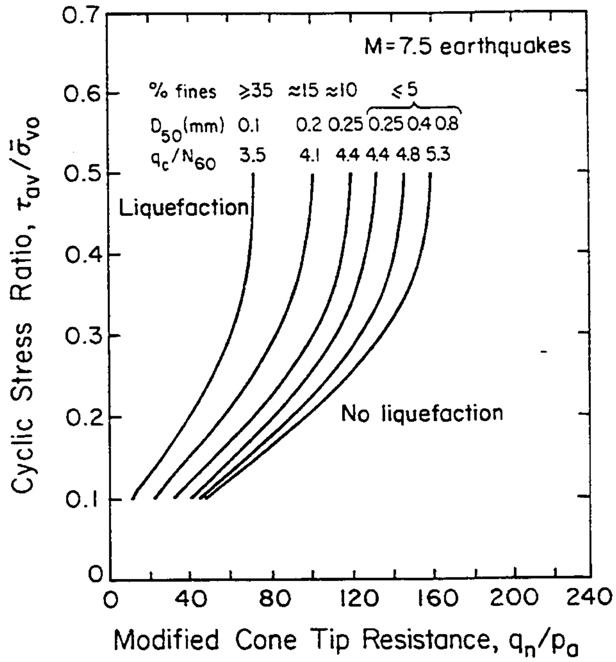

Figure 8-2. Liquefaction Resistance Correlated Indirectly with CPT Results

Source: Seed and de Alba (3), p. 295.

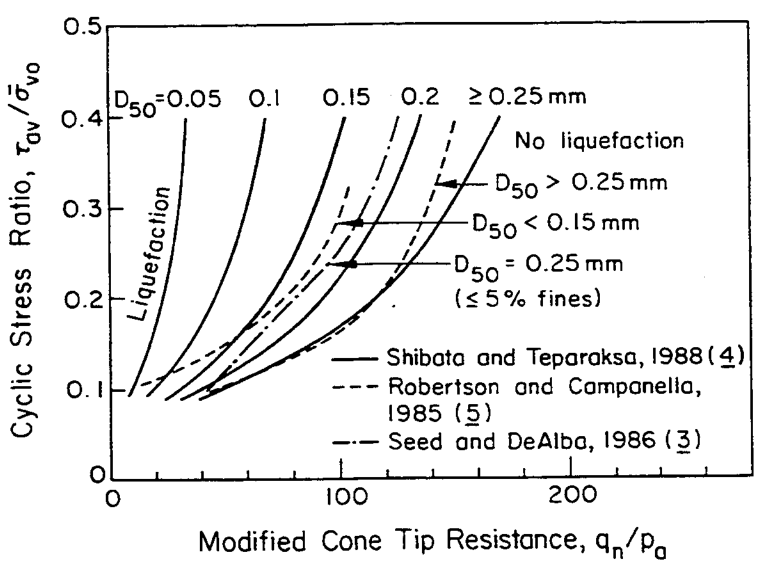

Figure 8-3. Liquefaction Resistance Correlated Directly with CPT Results

Source: Shibata and Teparaksa (4), p. 57.

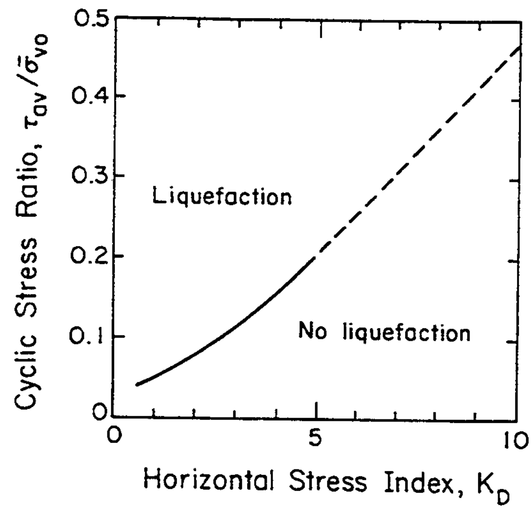

Figure 8-4. Liquefaction Resistance Correlated with DMT K_D

Source: Robertson and Campanella (6), p. 39.

REFERENCES

1. Seed, H. B., "Soil Liquefaction and Cyclic Mobility Evaluation for Level Ground During Earthquakes", Journal of the Geotechnical Engineering Division, ASCE, Vol. 105, No. GT2, Feb. 1979, pp. 201-256.

2. Tokimatsu, K. and Yoshimi, Y., "Empirical Correlation of Soil Liquefaction Based on SPT N Value and Fines Content", Soils and Foundations, Vol. 23, No. 4, Dec. 1983, pp. 56-74.

3. Seed, H. B. and de Alba, P., "Use of SPT and CPT Tests for Evaluating the Liquefaction Resistance of Sands", Use of In-Situ Tests in Geotechnical Engineering (GSP 6), Ed. S. P. Clemence, ASCE, New York, 1986, pp. 281-302.

4. Shibata, T. and Teparaksa, W., "Evaluation of Liquefaction Potential of Soils Using Cone Penetration Tests", Soils and Foundations, Vol. 28, No. 2, June 1988, pp. 49-60.

5. Robertson, P. K. and Campanella, R. G., "Liquefaction Potential of Sands Using the CPT", Journal of Geotechnical Engineering, ASCE, Vol. 111, No. 3, Mar. 1985, pp. 384-403.

6. Robertson, P. K. and Campanella, R. G., "Estimating Liquefaction Potential of Sands Using the Flat Plate Dilatometer", Geotechnical Testing Journal, ASTM, Vol. 9, No. 1, Mar. 1986, pp. 38-40.

Appendix A

STANDARD PENETRATION TEST

The standard penetration test (SPT) is performed during a test boring to obtain an approximate measure of the soil resistance to dynamic penetration and a disturbed sample of the soil. Although the test can be performed in a wide variety of soils, the most consistent results are found in sandy soils where large gravel particles are absent. Almost all U.S. soil drilling rigs are equipped to perform the SPT. In fact, the SPT is the most common in-situ geotechnical test in the world (1).

PROCEDURE

The detailed procedure for the SPT is described in ASTM D1586 (2), and a complete theoretical analysis of the statics and dynamics of the SPT is given by Schmertmann (3, 4).

To perform the test, the drilling crew, after advancing the test boring to the desired depth, first removes the string of drill rods slowly and cleans out the hole to the desired depth of testing. During this procedure, the head of water in the hole is maintained at or above the ground water level to avoid an inflow of water into the hole that can disturb the soil and cause erroneously low (conservative) test results. After the drilling tools are removed, a standard 51 mm (2 in) O.D. split spoon sampler, as shown in Figure A-1, is attached to the drill rods and lowered carefully to the bottom of the hole. With the sampler resting at the bottom of the hole, a 63.6 kg (140 lb) weight is allowed to fall freely 762 mm (30 in)

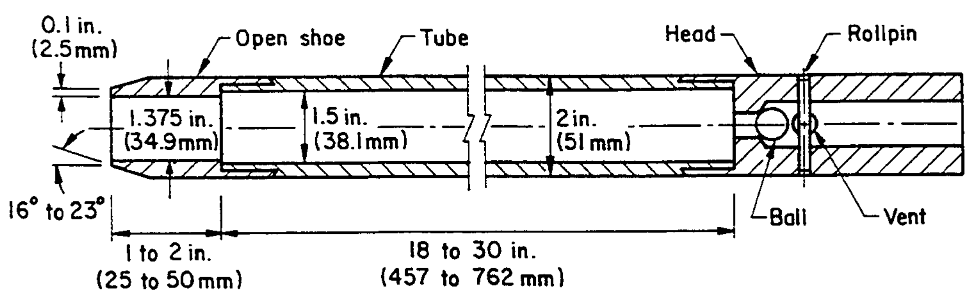

Figure A-1. Standard Split-Spoon Sampler

Source: American Society for Testing and Materials (2), p. 223.

onto a collar that is attached to the top of the drill string until 460 mm (18 in) of penetration has been achieved (or 100 blows have been applied).

The two most common hammers in North American practice are the safety and donut hammers. The safety hammer illustrated in Figure A-2 is a long weight which slides over the drill rods and impacts against an internal anvil. The donut hammer illustrated in Figure A-3 is a short, wide weight centered on a guide pipe which strikes an external anvil above the drill rods. Alternatively, but now uncommon in U.S. practice, a 63.6 kg (140 lb) pin-guided weight is allowed to drop freely on the top of the drill string. The overall equipment and setup for the SPT are shown in Figure A-4.

The number of blows (or drops of the weight) is recorded for each of three 152 mm (6 in) intervals; the first generally is considered a seating drive, and the number of blows for the final 305 mm (12 in) is reported as the standard penetration resistance or N value. After the sampler has been brought back to the surface, the

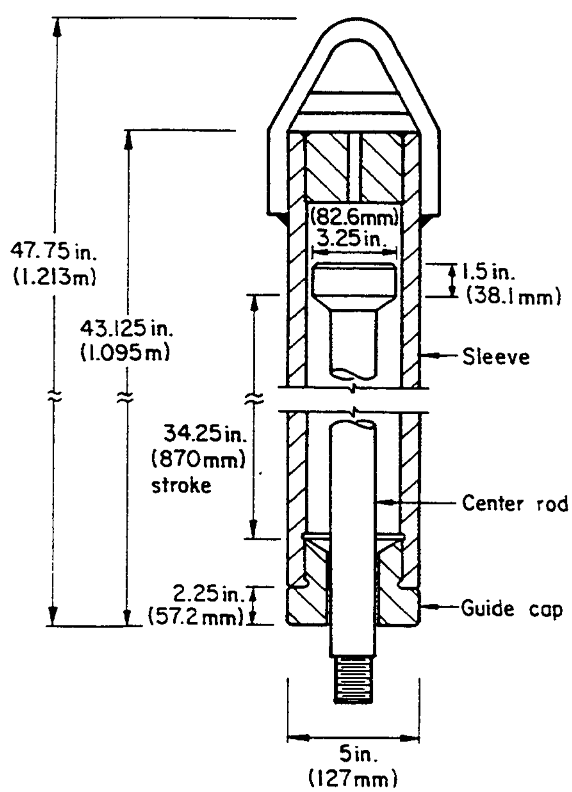

Figure A-2. SPT Safety Hammer

Source: Kovacs, et al. (5), p. 11.

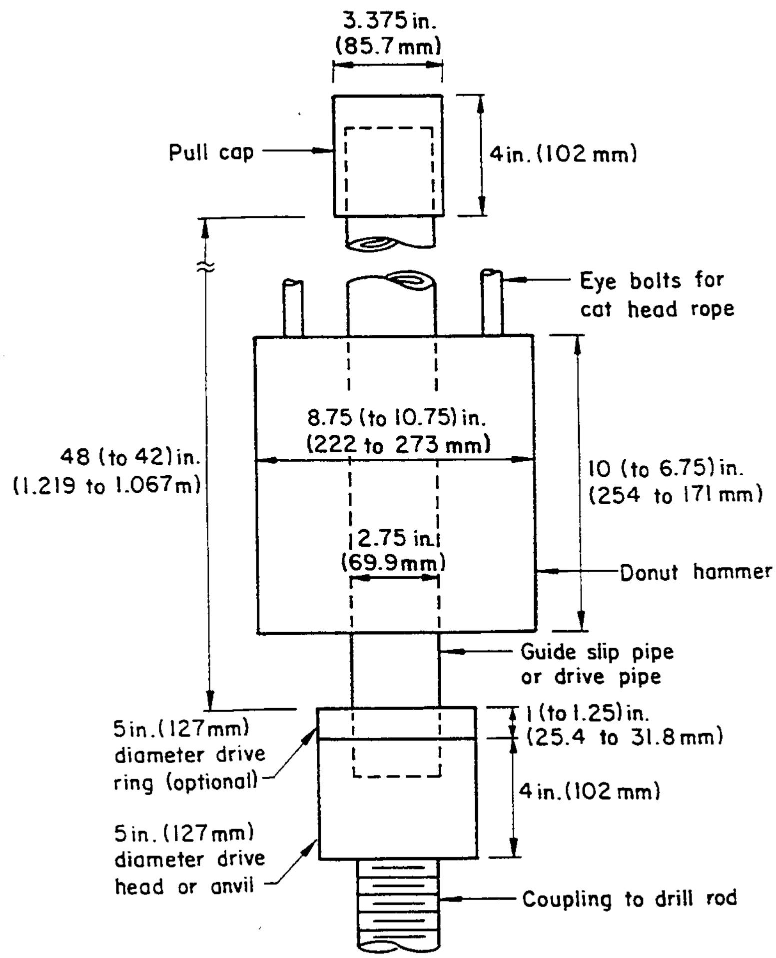

Figure A-3. SPT Donut Hammer

Source: Kovacs, et al. (5), p. 10.

samples are removed and classified, before being placed into jars, labeled, and sealed with wax for transport.

ADVANTAGES AND DISADVANTAGES

The advantages of the SPT are that it is relatively quick and simple to perform, and it is widely available. It is relatively inexpensive and provides, with one procedure, both a sample and a soil test result. The test also provides a useful index of the relative strength and compressibility of the soil in the immediate vicinity of the test. In addition, the test is able to penetrate relatively difficult materials such as dense layers, gravels, and fills.

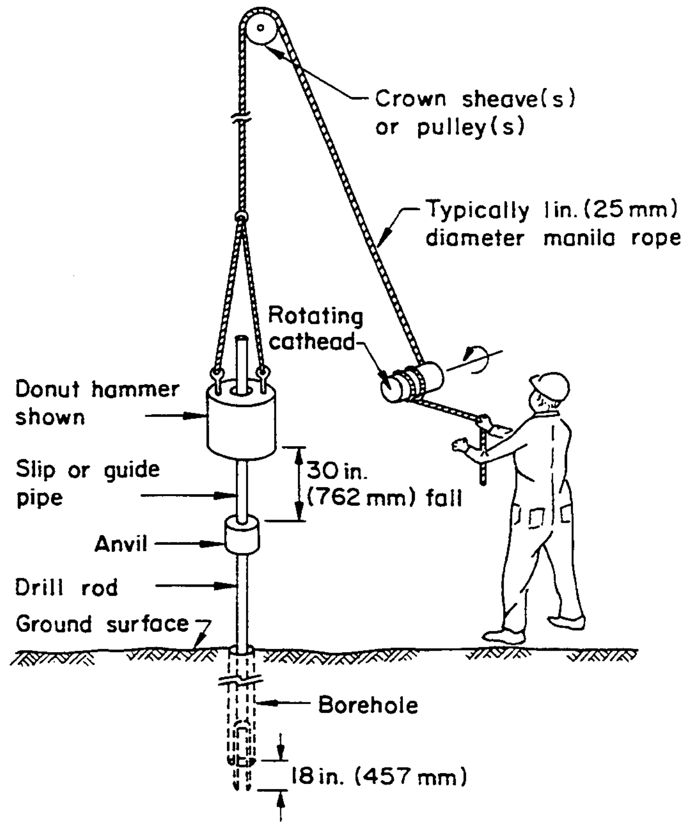

Figure A-4. Equipment Used to Perform the SPT

Source: Kovacs, et al. (6), p. 3.

The disadvantage of the SPT is that it has many sources of error, both random and systematic (7 - 10). The accuracy of the test is in large part dependent on the details of the procedure followed and the equipment used by the drilling crew, so that the care and knowledge of the drillers forms a critical factor in the test accuracy.

The SPT should not be relied on in soils containing coarse gravel, cobbles, or boulders, because the sampler can become obstructed, giving erroneously high and unconservative N values. The test also should not be relied on for cohesionless silts, because dynamic effects at the sampler tip can lead to erroneous strength and compressibility determinations. In addition, the test has little meaning in soft and sensitive clays. In such soils, the SPT yields results inconsistent with actual in-situ conditions.

If the head of water in the hole is not maintained at or above the ground water level, piping can occur at the bottom of the hole which can loosen the soil and invalidate the test results. This problem can be minimized by returning water to the hole as the drilling tools are removed prior to conducting the SPT.

Studies by Kovacs (11) showed that the SPT is highly dependent on the method of winding the hammer rope around the cathead on the drill rig. While seemingly a minor detail, these studies showed that when two turns of rope are used, as is common practice in the U.S., N values are about 40 percent higher than when a free-fall trip monkey or one turn was used. This example illustrates the level of uncertainty involved.

In addition, many older correlations of N values with engineering properties were based on pin-guided weights, which are no longer used for the SPT. The rod-guided hammers in present use can lead to slightly higher (unconservative) N values.

SOURCES OF ERROR, RELIABILITY, AND COST

The SPT has numerous sources of error that limit its use in foundation design. A list of many of the important sources of error and their probable effects on the SPT results is given in Table A-1. Factors that tend to increase the N values err on the unconservative side by overestimating soil strength and/or stiffness. However, most correlations of the SPT with engineering properties tend to be somewhat conservative. Other important issues influencing the N value are discussed in detail by Schmertmann (10).

In addition to these sources of error, a number of soil mechanics factors affect the test results and the correlations of N value with engineering properties. These factors include particle size, shape, and mineralogy; soil sensitivity, permeability, and degree of saturation; time lapse between drilling and testing; spacing of samples; depth of sampler penetration; relative depth of the boring; and size of the vent area of the sampler.

The reliability of the SPT is best where it is used as an index test to determine the approximate strength and compressibility of sandy soil strata for preliminary design purposes. For example, a soil with an N value of 50 is unlikely to exhibit any major problems with respect to strength or compressibility for spread footings; on the other hand, a soil with an N value of 2 or 3 can be expected to pose significant difficulties.

Although it is difficult to quantify the costs of SPT in remote areas, one approach

Table A-1

MAJOR SOURCES OF ERROR IN THE STANDARD PENETRATION TEST

Cause	Effect	Influence on N Value
Inadequate cleaning of hole	SPT is not made in original in-situ soil, and therefore soil may become trapped in sampler and be compressed as sampler is driven, reducing recovery	Increases
Failure to maintain adequate head of water in the borehole	Bottom of borehole may become quick	Decreases
Careless measurement of hammer drop	Hammer energy varies (generally, variations cluster on the low side)	Increases
Hammer weight inaccurate	Hammer energy varies (driller supplies weight; variations of 5 to 7 percent are common)	Increases or decreases
Hammer strikes drill rod collar eccentrically	Hammer energy reduced	Increases
Lack of hammer free fall because of ungreased sheaves, new stiff rope on weight, more than two turns on cathead, incomplete release of rope during each drop	Hammer energy reduced	Increases
Sampler driven above bottom of casing	Sampler driven in disturbed, artificially densified soil	Increases greatly
Careless blow count	Inaccurate results	Increases or decreases
Use of non-standard sampler	Correlations with standard sampler invalid	Increases or decreases
Coarse gravel or cobbles in soil	Sampler becomes clogged or impeded	Increases
Use of bent drill rods	Inhibited transfer of energy of sampler	Increases

Source: Kulhawy, et al. (12), p. 5-24.

is to determine the daily drill rig charge and divide by the number of tests obtainable in one day. All-terrain vehicles in 1990 cost about $1000 to $1500 per day and, during a typical day, 10 to 20 tests might be obtained. Therefore, the unit charge could be approximated as $50 to $150 per test, including drilling 1.0 to 1.5 m (3 to 5 ft) between tests. These figures are intended only as a relative measure of the cost of performing the SPT for comparison with other field exploration techniques.

REFERENCES

1. DeCourt, L., Muromachi, T., Nixon, I. K., Schmertmann, J. H., Thorburn, S., and Zolkov, E., "Standard Penetration Test: International Reference Test Procedures", Proceedings, 1st International Symposium on Penetration Testing (ISOPT-1), Vol. 1, Orlando, 1988, pp. 3-26.

2. American Society for Testing and Materials, "Standard Method for Penetration Test and Split-Barrel Sampling of Soils (D1586-84)", Annual Book of Standards, Vol. 4.08, ASTM, Philadelphia, 1989, pp. 221-225.

3. Schmertmann, J. H., "Statics of SPT", Journal of the Geotechnical Engineering Division, ASCE, Vol. 105, No. GT5, May 1979, pp. 665-670.

4. Schmertmann, J. H. and Palacios, A., "Energy Dynamics of SPT", Journal of the Geotechnical Engineering Division, ASCE, Vol. 105, No. GT8, Aug. 1979, pp. 909-926.

5. Kovacs, W. D., Salomone, L. A., and Yokel, F. Y., "Comparison of Energy Measurements in the Standard Penetration Test Using the Cathead and Rope Method", Report NUREG/CR-3545, Nuclear Regulatory Commission, Washington, 1983, 69 p.

6. Kovacs, W. D., Salomone, L. A., and Yokel, F. Y., "Energy Measurements in the Standard Penetration Test", Building Science Series 135, National Bureau of Standards, Washington, 1981, 73 p.

7. Fletcher, G. F. A., "Standard Penetration Test: Its Uses and Abuses", Journal of the Soil Mechanics and Foundations Division, ASCE, Vol. 91, No. SM4, July 1965, pp. 67-75.

8. Ireland, H. O., Moretto, O., and Vargas, M., "The Dynamic Penetration Test: A Standard That Is Not Standardized", Geotechnique, Vol. 20, No. 2, June 1970, pp. 185-192.

9. Orchant, C. J., Kulhawy, F. H., and Trautmann, C. H., "Reliability-Based Foundation Design for Transmission Line Structures: Critical Evaluation of In-Situ Test Methods", Report EL-5507, Vol. 2, Electric Power Research Institute, Palo Alto, 1988, 214 p.

10. Schmertmann, J. H., "Use the SPT to Measure Soil Properties? - Yes, But..!", Dynamic Geotechnical Testing (STP 654), ASTM, Philadelphia, 1978, pp. 341-355.

11. Kovacs, W. D., "What Constitutes a Turn?", Geotechnical Testing Journal, ASTM, Vol. 3, No. 3, Sept. 1980, pp. 127-130.

12. Kulhawy, F. H., Trautmann, C. H., Beech, J. F., O'Rourke, T. D., McGuire, W., Wood, W. A., and Capano, C., "Transmission Line Structure Foundations for Uplift-Compression Loading", Report EL-2870, Electric Power Research Institute, Palo Alto, 1983, 412 p.

Appendix B

CONE PENETRATION TEST

The cone penetration test (CPT), once known as the Dutch cone test, is a versatile sounding procedure that can be used to classify the materials in a soil profile and to estimate their engineering properties. The CPT is becoming perhaps the most popular and versatile in-situ test in the world (1). In the CPT, a conical penetrometer tip is pushed slowly into the ground and monitored. The earlier versions of the CPT still are used widely and are known as mechanical friction cone (Begemann) penetrometers (Figure B-1). Some of these penetrometers lack a friction sleeve and measure only tip resistance, such as the Delft mantle cone (Figure B-1). These devices provide less information about the soil conditions. Modern devices, such as those shown in Figure B-2, contain electrical transducers to measure both tip and side resistances as the instrument is advanced; such devices are known as electric friction cone penetrometers. In the U.S., the electric cone in

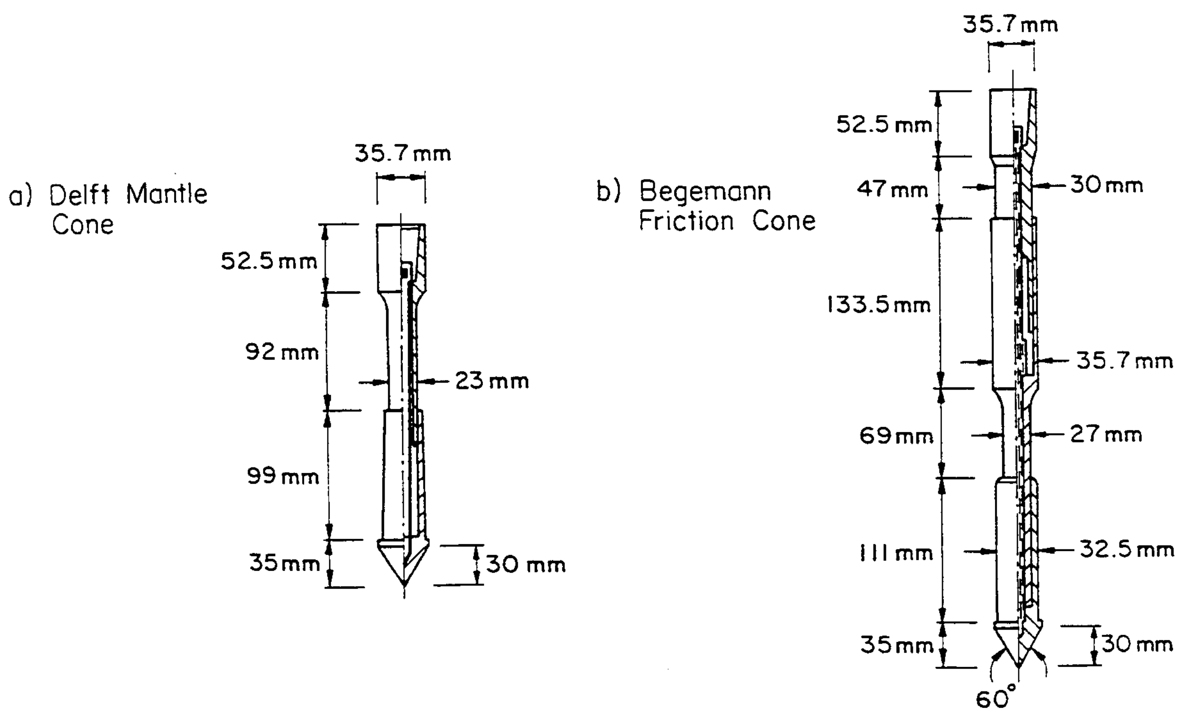

Figure B-1. Mechanical Cone Penetrometers

Source: American Society for Testing and Materials (2), pp. 415, 416.

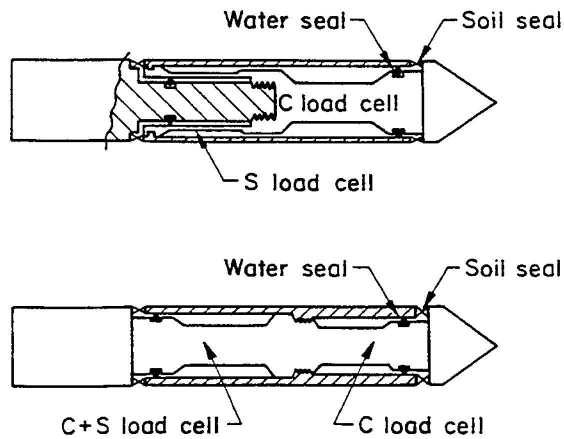

Figure B-2. Typical Designs of Electric Cone Penetrometers

Source: Schaap and Zuidberg (3), p. 842.

most common use is the Fugro cylindrical cone. Unless otherwise noted, this cone is assumed. More recently, piezocone penetrometers (CPTU) have been developed which measure the pore water stresses during penetration, as well as the cone tip resistance and sleeve side resistance. Furthermore, several new cone devices have been introduced to measure additional parameters, including the seismic cone (for P and S waves), acoustic cone, pressuremeter cone (with full-displacement PMT), vibrating cone (for liquefaction assessment), lateral stress cone (for pile analysis and K_o evaluation), logging cone (for nuclear density readings), and cone penetrometers for environmental work, including water sampling capabilities.

PROCEDURE

The detailed procedure for the CPT is described in ASTM D3441 (2). To perform the test, an electric cone penetrometer tip is attached to a string of steel rods and is pushed vertically into the ground at a constant rate of approximately 20 mm (0.8 in)/sec. Wires from the transducers are threaded through the center of the rods, and the tip and side resistances are recorded continuously on a strip chart recorder (Figure B-3) until the desired depth is reached. A similar procedure is used for electric piezocone soundings, except that special measures are required for ensuring saturation of the porous stone element.

The procedure is modified slightly when a mechanical penetrometer tip is used. In this case, the penetrometer tip is connected to an inner set of rods and is first advanced about 40 mm (1.6 in), giving the tip resistance. With further thrusting, the tip engages the side friction sleeve and, as the inner rods advance, the rod

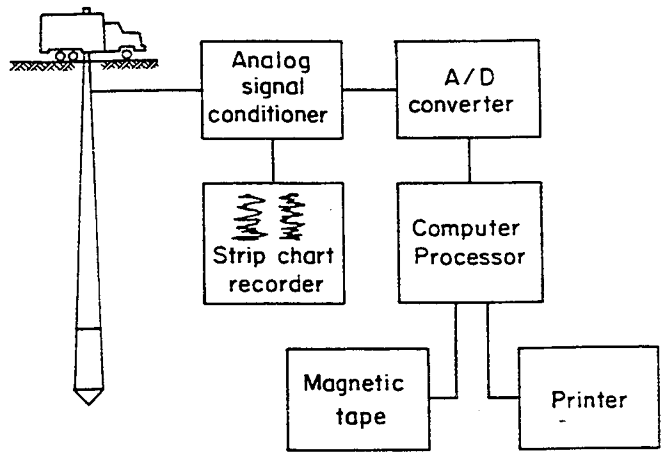

Figure B-3. Electric CPT Data Acquisition System

Source: DeRuiter (4), p. 393.

force equals the sum of the tip and side resistances. The tip resistance is subtracted to give the side resistance. Finally, the outer rods are pushed to collapse the entire device, and the process is repeated at approximate 200 mm (8 in) intervals. This mechanical process has several important sources of error not characteristic of the electrical process and, where available, the electric penetrometer is recommended.

With standard mechanical and electric cones, the two most useful parameters measured by the test are the tip resistance, q_c, and the side resistance, f_s. Piezocones also provide readings of the maximum pore water stress, u_m.

The CPT can be used where a sample is not needed and soil conditions do not prevent its penetration. In general, the CPT is less suitable in soils containing gravelly soils, cobbles or boulders, or cemented seams.

Cone penetrometers have been in general use since the 1930s in Europe, but only within the past two decades have they gained wide usage in the U.S. Cone penetrometers can be employed in a variety of soils and, although they do not provide a sample, they have a number of advantages over the standard penetration test. The CPT, especially when performed with an electrical tip, provides a continuous log of soil conditions, while the SPT usually shows conditions only at discrete locations in the soil profile, typically at 1 to 1.5 m (3 to 5 ft) intervals. Because the CPT measures at least two parameters, it ideally gives more information about in-situ soil consistency than the SPT. Furthermore, when comparisons of cone soundings using both electric and mechanical cone tips are made, the profiles give similar trends, as shown in Figure B-4. However, the electric cone provides more tip detail and shows less scatter in the side resistance profile, indicating that soil boundaries can be located more accurately with an electric penetrometer tip.

The mechanical and electric cones do not give the same results, largely because of the different geometry of the cones. The Delft and Begemann cones shown in Figure B-1, as well as the Gouda cone (similar to the Delft), all have a reduction in diameter beyond the cone tip. In contrast, the Fugro electric cone has the same sleeve and tip diameter. Approximate correlations between these mechanical and electric cones have been suggested (e.g., 6 - 10). These studies generally have shown that q_c for electric cones is greater than q_c for mechanical cones in sands, while the reverse is true in clays and silts. To quantify these studies further, data were summarized from 14 sands and 10 clays and silts tested by both Fugro electric cones and several mechanical cones. The results are shown in Figure B-5 and indicate a good correlation.

For side resistance (f_s), the mechanical cones apparently give higher readings than the electric cones in all soils. In sands, the ratio is about 2 (e.g., 5, 7). In marine clays, the ratio varies from 2.5 to 3.5 (e.g., 18).

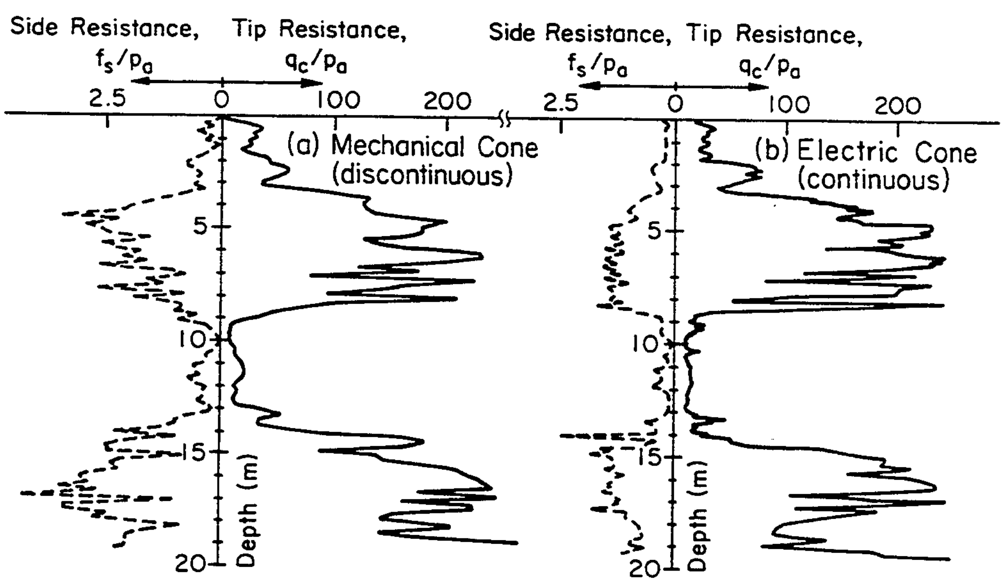

Figure B-4. Comparison of Begemann Mechanical and Fugro Electric Cones

Source: DeRiuter (5), p. 466.

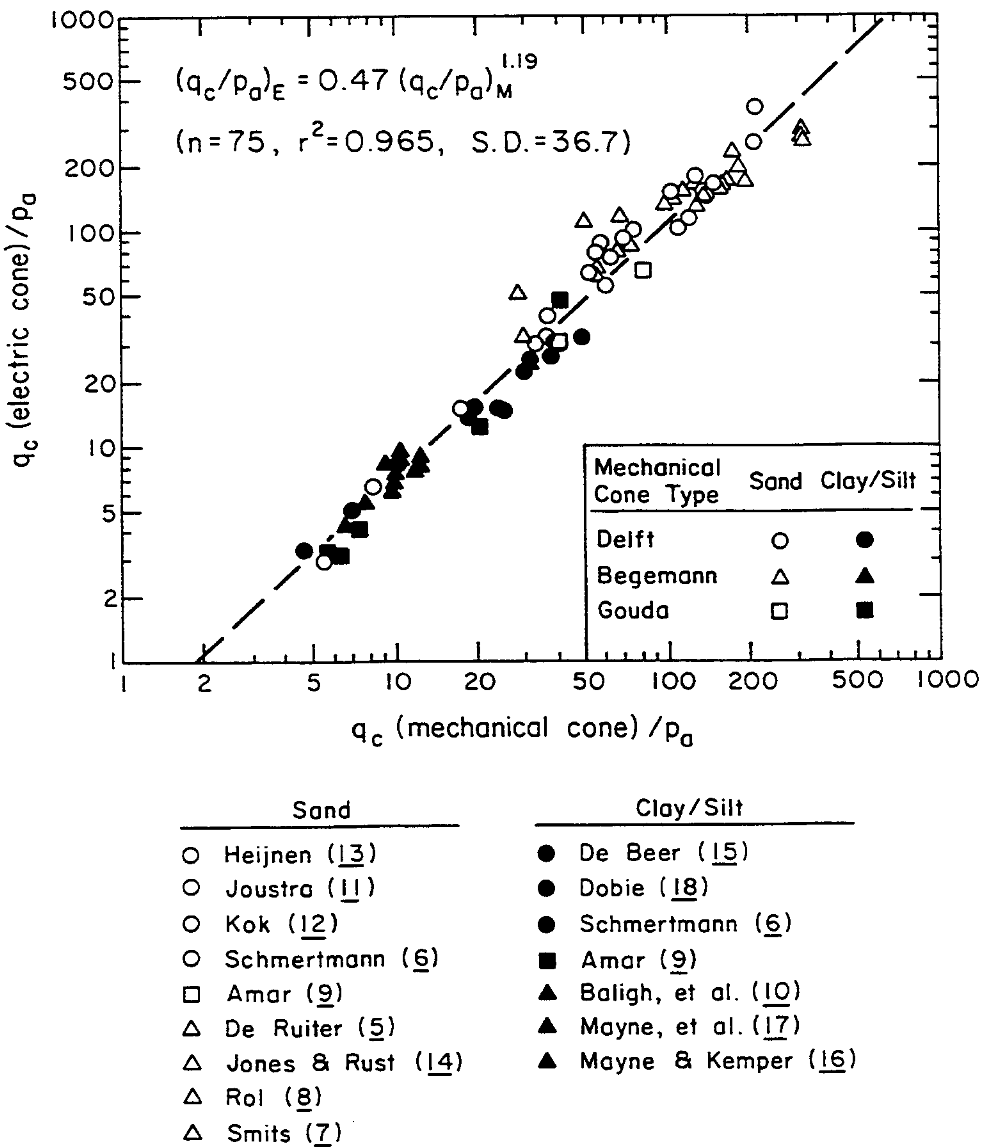

Figure B-5. Correlation of q_c Between Electric and Mechanical Cones

CPT results also may vary as a function of electric cone type. A recent study by Lunne, et al. (19) compared the results of 14 different types of commercially-available electric cones in the same sand. The variations in q_c were relatively small, but values of f_s varied dramatically, in some cases by a factor of 3. These results undoubtedly would influence all interpretations made from the test results, so it is prudent to conduct verification and local calibration tests with specific CPT equipment.

The introduction of the piezocone (CPTU) and the resulting comparative studies of the CPT and CPTU have shown that all cones require a correction for pore water stresses acting on any unequal areas of the cone. Correction of the tip resistance is most important in soft clays where the values of q_c and u_m are of comparable magnitude. Studies by Lunne, et al. (19) using 14 different cones at the Onsoy site in Norway showed a wide range in the uncorrected cone tip resistance (q_c), but a relatively narrow range in the corrected cone tip resistance (q_T). The value of f_s also must be corrected, but this correction requires additional pore water stress measurements behind the cone sleeve. These additional measurements are not yet practical for commercial CPTU testing.

One further complication with the piezocone is that its design has not yet been standardized (e.g., 20). Most commercially-available piezocones place the porous element either on the cone tip face or just behind the cone tip, as shown in Figure B-6. Technically, the measurement of pore water stresses behind the tip (u_{bt}) is required to correct the cone tip resistance (q_c) for pore water stresses acting on unequal areas of the cone. On the other hand, pore water stress measurements on the cone tip or face provide the maximum reading, which may be best for delineation of stratigraphy.

Many electric cone penetrometers in commercial use do not have the ability to measure pore water stresses during penetration. Therefore, it is of interest to examine means of empirically correcting the measured cone tip resistance (q_c) to obtain the corrected cone tip resistance (q_T), as follows:

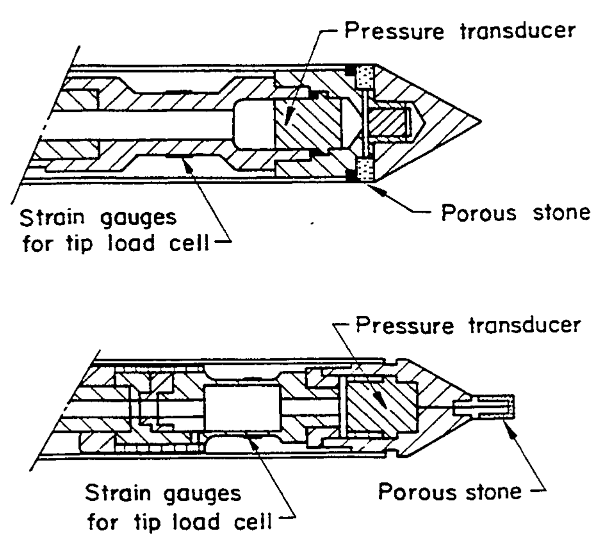

Figure B-6. Common Piezocone Geometries

Source: Campanella and Robertson (21), p. 7.

$$q_T = q_c + (1 - a)u_{bt} \quad \text{(B-1)}$$

in which a = net area ratio defined in Figure 2-11. Lunne, et al. (19) give typical values of "a" for commercial cones. The actual value of "a" should be determined by site calibration.

Piezocone data from numerous soil sites are summarized in Figure B-7 to illustrate the variation in u_{bt} as a function of soil type and structure. From regression analyses, $u_{bt} = 0.53\ q_T$ for intact clays and $u_{bt} = 0.58\ q_T$ for the highly sensitive Leda clays. Silts and micro-fissured clays show values of u_{bt} that are only a small fraction of q_T. For fissured clays, u_{bt} is about zero. These trends will be useful for estimating the corrected cone tip resistance on a preliminary basis.

ADVANTAGES AND DISADVANTAGES

The CPT has a number of advantages over other routine forms of in-situ testing. Current trends indicate that usage will continue to increase, as more engineers become familiar with the types of information that it provides, and as more drilling firms acquire the equipment to perform the test.

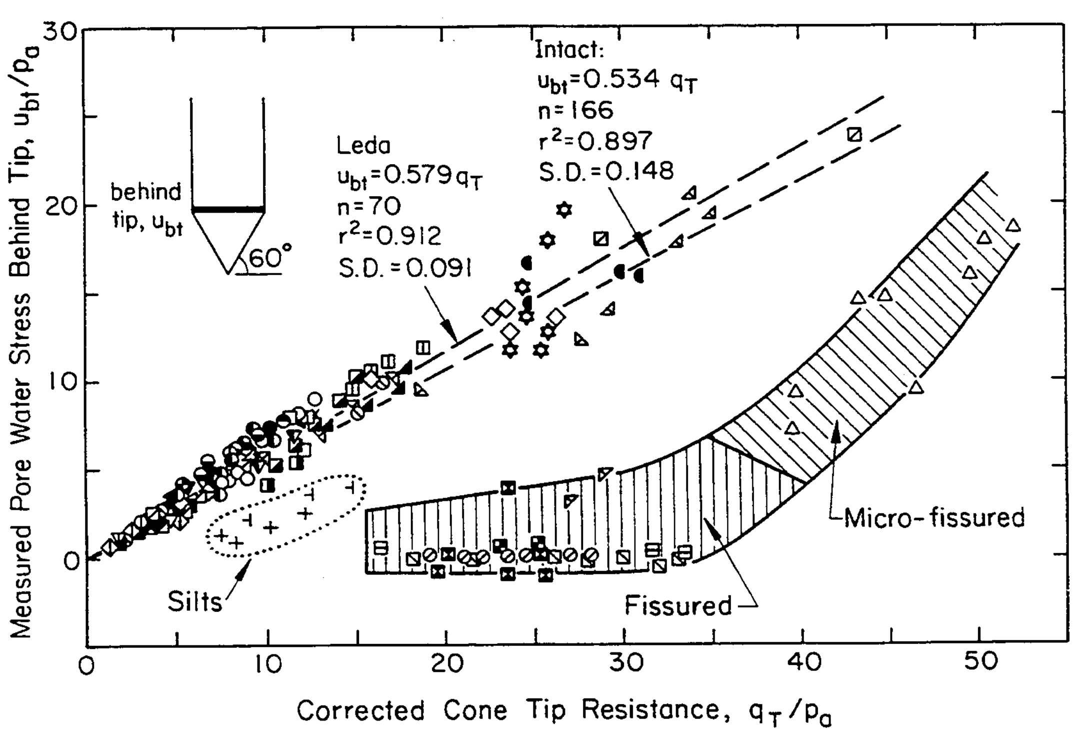

Figure B-7. Measured Pore Water Stresses in CPTU Tests

Source: Mayne, et al. (22).

The CPT is one of the faster and less expensive forms of in-situ testing in relatively soft or loose soils. It provides a rapid method of identifying potential problem soils, such as peat or soft clay strata, so that more sophisticated sampling and testing procedures can be used as efficiently as possible. Typical penetration rates during testing average about 1.2 m (4 ft) per minute and, except for problems caused by cemented layers or gravel, penetration is interrupted only to add additional rods as the test advances. Data are recorded concurrently with the test and, when the instrument is calibrated, the test personnel have a relatively minor influence on the results, compared to the SPT. The test can be performed in a wide range of soils, although very hard soils or gravel can not be penetrated at the present time. Except for special, high-capacity cone trucks, most standard cone equipment can penetrate soils with SPT N values up to 50 or thereabouts.

A significant advantage of the electric cone penetration test is that it provides a continuous record of soil conditions. Stratigraphy and soil identification are inferred from empirical classification charts developed for the mechanical and electric cones. The new piezocone equipment offers the most accurate means of profiling soil strata today (20). Subsurface conditions therefore may be inferred without retrieval of soil samples. In general, however, samples should be obtained whenever feasible to confirm the interpretation of soil types made with the CPT. As with the SPT, the empirical correlations vary with soil type.

The CPT also has several disadvantages. First, no sample is obtained and the penetrometer can not penetrate very dense soils or soils containing cobbles or boulders. Excessive force in these materials can damage the penetrometer tip. These problems, however, also are faced by most other forms of in-situ testing. Second, many drilling contractors do not have the test equipment at the present time. Third, the penetrometer may drift from vertical at depths below about 50 ft (15 m). Many new electric penetrometer tips include an inclinometer to monitor verticality, so that if the instrument does wander, the operator can determine immediately if the test should be repeated.

SOURCES OF ERROR, RELIABILITY, AND COST

Errors in the CPT have been described by several authors (6, 23, 24), and Table B-1 lists many of the sources of error in the standard mechanical and electric CPT. For the more sophisticated cone penetrometers such as the piezocone, specialized personnel, electronics, and computer hardware are required, and therefore numerous other factors may affect the measurements.

Table B-1

MAJOR SOURCES OF ERROR IN THE CONE PENETRATION TEST

Cause	Effect	Influence on Results
Gravel or cobbles in soil	Impedes penetration of penetrometer tip (can break tip or rods)	Increases q_c greatly
	Causes penetrometer to wander off vertical	Increases or decreases q_c and f_s
Worn penetrometer tip	Tip may become dull and/or surface roughness may become greater or lesser than standard	Increases or decreases q_c and f_s slightly
Soil clogging end of friction sleeve (mechanical tips only)	Adds an erroneous end bearing component to f_s	Increases f_s up to about 80 percent
Rusted or clogged inner rods (mechanical tips only)	Impedes free travel of inner rods because of friction against outer rods	Increases q_c and f_s
Hard soils (mechanical tips only)	Causes elastic compression of inner rods, giving false indication that penetration has occurred	Measurement of q_c and f_s may not be possible
Leaky water seal (electrical tips only)	Electrical transducers may become corroded	Increases or decreases q_c and f_s
Improper calibration (electrical tips only)	Inaccurate measurements	Increases or decreases q_c and f_s

Source: Kulhawy, et al. (23), p. 5-30.

The reliability is stated effectively in ASTM D3441 (2), "Because of the many variables involved and the lack of a superior standard, engineers have no direct data to determine the accuracy of this method. Judging from its observed reproducibility in approximately uniform soil deposits, plus the q_c and f_s measurement effects of special equipment and operator care, persons familiar with this method estimate its precision as follows: (1) mechanical tips - standard deviation of 10 percent in q_c and 20 percent in f_s, (2) electric tips - standard deviation of 5 percent in q_c and 10 percent in f_s".

The CPT may be conducted using either standard drilling rigs or special cone trucks which maximize the effort by pushing through the system center of gravity. The former generally weigh about 10 tons (89 kN) and can achieve q_c/p_a up to 250, while the special 20 ton (178 kN) cone trucks can reach q_c/p_a values of 600 or more. Mobilization costs for the latter are higher. However, unit costs for both run about $4 to $6/ft ($13 to $20/m) for CPT profiling. The more specialized CPTU version costs about $5 to $9/ft ($16 to $30/m).

REFERENCES

1. De Beer, E. E., Goelen, E., Heynen, W. J., and Joustra, K., "Cone Penetration Test: International Reference Test Procedures", Proceedings, 1st International Symposium on Penetration Testing (ISOPT-1), Vol. 1, Orlando, 1988, pp. 27-52.

2. American Society for Testing and Materials, "Standard Test Method for Deep, Quasi-Static, Cone and Friction-Cone Penetration Tests of Soil (D3441-86)", Annual Book of Standards, Vol. 4.08, ASTM, Philadelphia, 1989, pp. 414-419.

3. Schaap, L. H. J. and Zuidberg, H. M., "Mechanical and Electrical Aspects of the Electric Cone Penetrometer Tip", Proceedings, 2nd European Symposium on Penetration Testing, Vol. 2, Amsterdam, 1982, pp. 841-851.

4. De Ruiter, J., "The Static Cone Penetration Test: State-of-the-Art Report", Proceedings, 2nd European Symposium on Penetration Testing, Vol. 2, Amsterdam, 1982, pp. 389-405.

5. De Ruiter, J., "Electric Penetrometer for Site Investigations", Journal of the Soil Mechanics and Foundations Division, ASCE, Vol. 97, No. SM2, Feb. 1971, pp. 457-472.

6. Schmertmann, J. H., "Guidelines for Cone Penetration Test Performance and Design", Report FHWA-TS-78-209, Federal Highway Administration, Washington, 1978, 145 p.

7. Smits, F. P., "Cone Penetration Tests in Dry Sand", Proceedings, 2nd European Symposium on Penetration Testing, Vol. 2, Amsterdam, 1982, pp. 887-881.

8. Rol, A. H., "Comparative Study on Cone Resistances Measured with Three Types of CPT Tips", Proceedings, 2nd European Symposium on Penetration Testing, Vol. 2, Amsterdam, 1982, pp. 813-819.

9. Amar, S., "The Use of the Static Penetrometer in the Laboratoires des Ponts et Chaussées", Proceedings, European Symposium on Penetration Testing, Vol. 2.2, Stockholm, 1974, pp. 7-12.

10. Baligh, M. M., Vivatrat, V., and Ladd, C. C., "Exploration and Evaluation of Engineering Properties for Foundation Design of Offshore Structures", Report R78-40, Dept. of Civil Engineering, M.I.T., Cambridge, Dec. 1978, 268 p.

11. Joustra, K., "Comparative Measurements on the Influence of the Cone Shape on Results of Soundings", Proceedings, European Symposium on Penetration Testing, Vol. 2.2, Stockholm, 1974, pp. 199-200.

12. Kok, L., "The Effect of the Penetration Speed and Cone Shape on CPT Results", Proceedings, European Symposium on Penetration Testing, Vol. 2.2, Stockholm, 1974, pp. 215-216.

13. Heijnen, W. J., "The Dutch Cone Test: Study of the Shape of the Electrical Cone", Proceedings, 8th International Conference on Soil Mechanics and Foundation Engineering, Vol. 1.1, Moscow, 1973, pp. 79-83.

14. Jones, G. and Rust, E., "Piezometer Penetration Testing", Proceedings, 2nd European Symposium on Penetration Testing, Vol. 2, Amsterdam, 1982, pp. 607-613.

15. De Beer, E. E., "Scale Effects in Results of Penetration Tests Performed in Stiff Clays", Proceedings, European Symposium on Penetration Testing, Vol. 2.2, Stockholm, 1974, pp. 105-115.

16. Mayne, P. W. and Kemper, J. B., "Profiling OCR in Stiff Clays by CPT and SPT", Geotechnical Testing Journal, ASTM, Vol. 11, No. 2, June 1988, pp. 139-147.

17. Mayne, P. W., Frost, D. D., and Swanson, P. G., "Geotechnical Report, CEBAF Project, Newport News, VA", Law Engineering NK5-1182 to Daniel, Mann, Johnson, and Mendenhall, Washington, Dec. 1986, 580 p.

18. Dobie, M. J. D., "A Study of Cone Penetration Tests in the Singapore Marine Clay", Proceedings, 1st International Symposium on Penetration Testing (ISOPT-1), Vol. 2, Orlando, 1988, pp. 737-744.

19. Lunne, T., Eidsmoen, D., Gillespie, D., and Howland, J., "Laboratory and Field Evaluation of Cone Penetrometers", Use of In-Situ Tests in Geotechnical Engineering (GSP 6), Ed. S. P. Clemence, ASCE, New York, 1986, pp. 714-729.

20. Campanella, R. G. and Robertson, P. K., "Current Status of the Piezocone Test", Proceedings, 1st International Symposium on Penetration Testing (ISOPT-1), Vol. 1, Orlando, 1988, pp. 93-116.

21. Campanella, R. G. and Robertson, P. K., "State-of-the-Art in In-Situ Testing of Soils; Developments Since 1978", Proceedings, Engineering Foundation Conference on Updating Subsurface Sampling of Soils and Rocks and Their In-Situ Testing, Santa Barbara, 1982, 23 p.

22. Mayne, P. W., Kulhawy, F. H., and Kay, J. N., "Observations on the Development of Pore Water Stresses During Cone Penetration in Clays", Canadian Geotechnical Journal, Vol. 27, No. 3, Aug. 1990.

23. Kulhawy, F. H., Trautmann, C. H., Beech, J. F., O'Rourke, T. D., McGuire, W., Wood, W. A., and Capano, C., "Transmission Line Structure Foundations for Uplift-Compression Loading", Report EL-2870, Electric Power Research Institute, Palo Alto, 1983, 412 p.

24. Orchant, C. J., Kulhawy, F. H., and Trautmann, C. H., "Reliability-Based Foundation Design for Transmission Line Structures: Critical Evaluation of In-Situ Test Methods", Report EL-5507, Vol. 2, Electric Power Research Institute, Palo Alto, 1988, 214 p.

Appendix C

PRESSUREMETER TEST

The pressuremeter test (PMT) can be used in soil to determine the in-situ stress, deformability, and strength. A cylindrical probe is advanced to the test depth by one of several means and is then expanded incrementally with either liquid or gas pressure. During expansion, the diameter or volume of the expanding probe is measured accurately to yield a volume versus pressure curve, from which the in-situ stress, stress-strain behavior, and strength properties can be estimated. The original Menard-type PMT is performed in a prebored hole. A more sophisticated device is the self-boring pressuremeter (SBPMT), which minimizes stress relaxation and soil disturbance during insertion. More recently, the push-in pressuremeter and full-displacement pressuremeter have been introduced, primarily for offshore work, and these may be operated more quickly without need for a prebored hole.

PROCEDURE

A standard procedure for the prebored PMT has been developed recently in the U.S. as ASTM D4719 (1). Specific details on the traditional test equipment and interpretation are given by Baguelin, et al. (2). After calibration, the pressuremeter probe is installed at the test location by lowering it down a borehole, jacking it into the ground, or by self-boring. The latter technique is useful in soft and medium clays, but specialized equipment is required, and shells and gravel particles can obstruct proper functioning of the probe. Figure C-1 illustrates a PMT installation.

The test is carried out by applying pressure in about ten equal steps. The pressure is maintained constant for each step for the same period of time, such as 60 seconds. The volumetric expansion of the probe is measured at 15, 30, and 60 seconds after each pressure step to determine a creep curve. The test ends when the probe has been expanded to twice its deflated volume or when the pressure limit of the device has been reached. Once the test has been completed, the probe is deflated, and the device is either advanced to a new depth or returned to the surface.

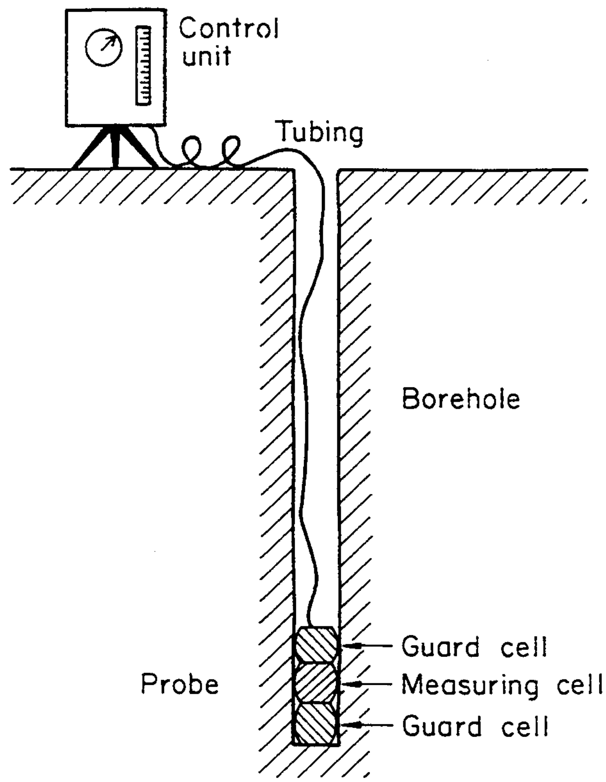

Figure C-1. Menard Pressuremeter Equipment

Source: Baguelin, et al. (2), p. 47.

PMT results are presented generally as a plot of pressure versus volume, as shown in Figure C-2. Three characteristic pressures are determined from this curve:

- p_o, representing the pressure at which recompression of disturbed soil is complete and expansion into undisturbed material is initiated (It often is assumed that $p_o = \sigma_{ho}$, the in-situ total horizontal stress.)

- p_f, an inflation point, known as the creep or yield pressure, where the soil behavior changes from pseudo-elastic to plastic and shearing is initiated

- p_L, the limit pressure, representing the pressure to which the curve becomes asymptotic

The limit pressure is never measured directly. Instead, it is determined by extrapolation as the pressure at which the probe has expanded to twice its original volume. A review of the available methods for interpreting p_o, p_f, and p_L is given by Ladd, et al. (3). These three characteristic pressures are used to estimate a number of engineering soil properties and for direct semi-empirical correlations to

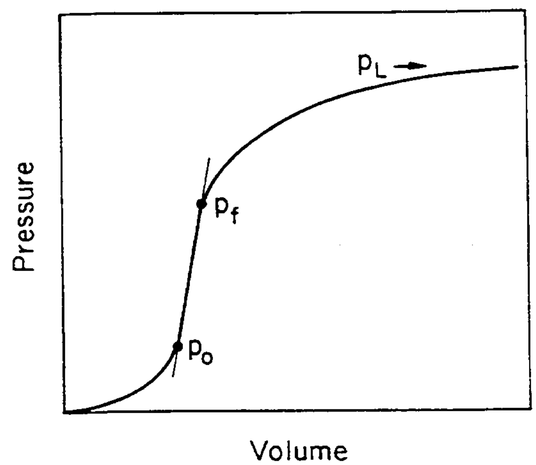

Figure C-2. Typical Pressuremeter Test Curve

foundation capacity and settlement. The PMT is considered a specific soil property test and not a logging tool. Therefore, the soil must be characterized in advance of the test for the PMT results to be used efficiently and economically.

The self-boring pressuremeter test (SBPMT) is a relatively recent development, and as such it is just reaching maturity in terms of the equipment and procedures employed. Two basic types of self-boring probes are currently in use: a French version, known as the PAFSOR, and an English device called the Camkometer. Both are shown in Figure C-3.

Among the most attractive features of the SBPMT is its ability to provide reasonable estimates of the in-situ horizontal stress. A graphical procedure is used to estimate σ_{ho} from Camkometer data. An enlarged plot of the initial portion of the expansion curve for each displacement transducer is analyzed. Then σ_{ho} equals the "lift off" pressure or the pressure at which volumetric expansion of the membrane is first recognized. An example of this procedure is shown in Figure C-4. As noted in this figure, the three feeler arms may display substantially different "lift off" pressures. This phenomenon has been attributed to one or more of the following factors (e.g., 4): soil stiffness, relative stiffnesses of each feeler arm, noncircular shape of SBPMT hole, mechanical compliance of the instrument, deviation of the probe from the vertical, non-uniform shear stress at the probe soil interface, and anisotropy of the in-situ horizontal stress.

In terms of deformation parameters, the pressure-strain curve obtained from the

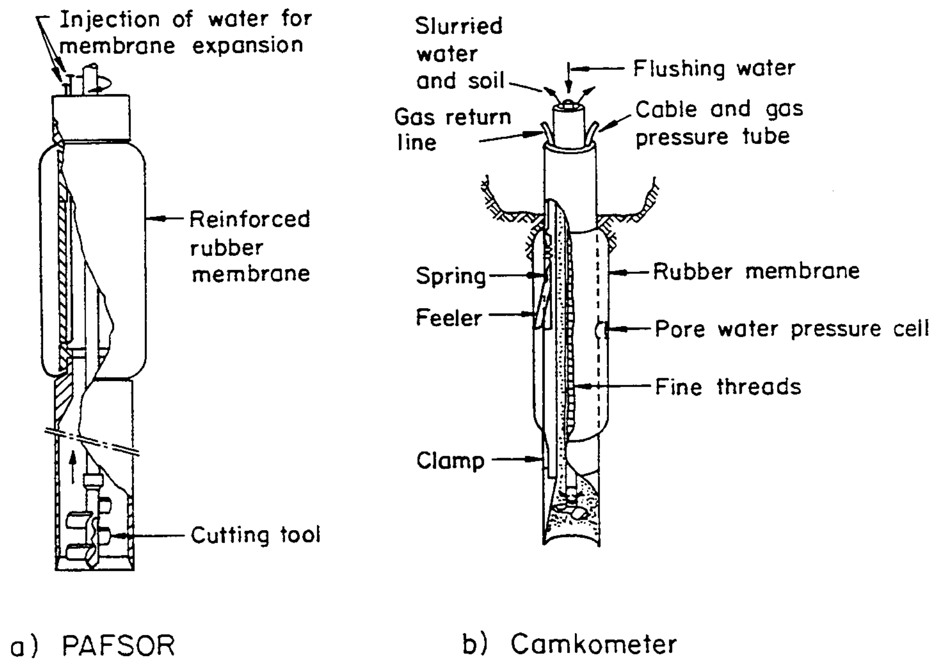

Figure C-3. Self-Boring Pressuremeters

Source: Jamiolkowski, et al. (4), pp. 98, 99.

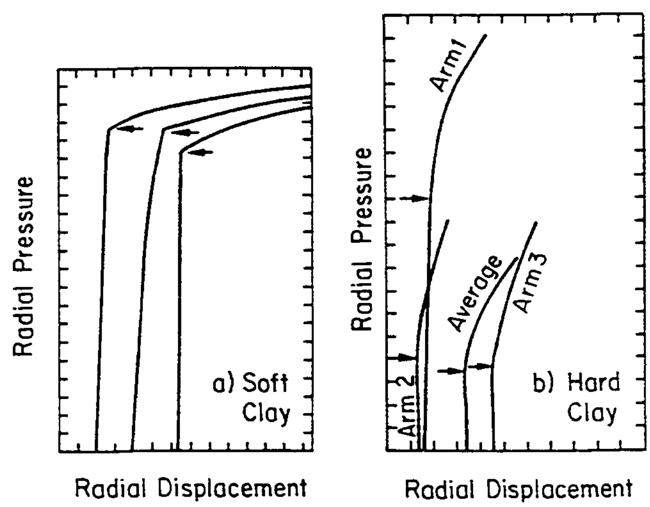

Figure C-4. Examples of "Lift Off" Pressure

Source: Jamiolkowski, et al. (4), p. 100.

SBPMT can provide estimates of the initial tangent shear modulus (G_i), secant shear modulus (G_s), unload-reload shear modulus (G_{ur}), and reload-unload shear modulus (G_{ru}).

ADVANTAGES AND DISADVANTAGES

The main advantage of the pressuremeter test is that it is one of the few in-situ measurement techniques that can assess directly the state of horizontal stress in soil. This capability is a significant advantage for the design of deep foundations because the capacity of these foundations is directly related to the in-situ stress. In addition, the PMT is capable of yielding data on soil modulus and shearing resistance when performed carefully in appropriate materials.

The PMT also has a number of disadvantages. It generally is performed in soil deposits that have been identified previously using other forms of in-situ testing or sampling. Therefore, like the vane shear test, prior exploration is required for proper interpretation of the test results.

From a soil mechanics point of view, the test has several limitations. The drainage conditions in soils of intermediate permeability are generally unknown during the test, which can seriously impair test interpretation. Pressuremeters of the self-boring variety can, in some cases, provide the most accurate data because they cause minimal soil disturbance, but they are most reliable in relatively soft, fine-grained soils that do not contain shells, gravel particles, or cohesionless sands. Recent improvements in self-boring techniques have extended the range of soils that can be penetrated, but gravel particles remain an important limitation for self-boring pressuremeters. Test accuracy is still subject to drilling procedures, insertion techniques, and the human element in both performance and interpretation, which includes instrument calibration, the theory used for interpretation, and prior knowledge of soil stratification. Strain-rate effects are important, and semi-empirical correlations with documented case histories still are required to use the test results in design. Also, long test times may be required for testing some relatively impermeable cohesive soils.

SOURCES OF ERROR, RELIABILITY, AND COST

The PMT has a number of potential sources of error, largely because of the complex nature of the test equipment and procedure (2, 4 - 6). Equipment calibration, leakage, borehole preparation, probe insertion, prior knowledge of soil stratification, and test interpretation are all important considerations, and trained personnel must perform the test. In addition, the strength and modulus values obtained from the PMT are not strictly comparable to those derived from other forms of in-situ testing, so the values can not be used indiscriminately in classical design methods without leading to erroneous results in some cases. A list of the major variables affecting the PMT and SBPMT is given in Table C-1.

The reliability of the PMT is greatest in homogeneous, finer-grained soil. With skilled operators and good equipment and procedural controls, the test is highly reproducible in these soil types.

Pressuremeter tests are higher in cost compared with the SPT and VST. All three require the same type of test boring, but the PMT requires a skilled operator in addition to the drilling crew. Taking into account drilling costs, the operator, and a productivity of 5 to 8 tests per shift, the cost per test in 1990 is in the

Table C-1

MAJOR PMT AND SBPMT VARIABLES

Variable	Relative Effect on Test Results
Gage error	Minor
Expansion of tubing	Minor to moderate
Frictional losses in tubing	Minor
Probe dimensions	Minor to moderate
Probe design (PMT)	Minor
Membrane aging	Minor
Size of cutting shoe (SBPMT)	Moderate to significant
Cutter position (SBPMT)	Minor
Shape of probe (SBPMT)	Minor to moderate
Drilling equipment (SBPMT)	Minor to moderate
Compliance of electrical sensors (SBPMT)	Minor
Method of drilling and borehole preparation (PMT)	Significant
Rate of probe inflation	Minor to moderate
Relaxation time (SBPMT)	Moderate to significant
Rate of probe advance (SBPMT)	Moderate to significant

Source: Orchant, et al. (6), pp. 4-49, 4-51.

range of $150 to $250 for the standard PMT and $300 to $600 for the SBPMT.

REFERENCES

1. American Society for Testing and Materials, "Test Method for Pressuremeter Testing in Soils (D4719-87)", Annual Book of Standards, Vol. 4.08, ASTM, Philadelphia, 1989, pp. 881-888.

2. Baguelin, F, Jézéquel, J. F., and Shields, D. H., The Pressuremeter and Foundation Engineering, Trans Tech Publications, Clausthal, 1978, 617 p.

3. Ladd, C. C., Germaine, J. T., Baligh, M. M., and Lacasse, S. M., "Evaluation of Self-Boring Pressuremeter Tests in Boston Blue Clay", Report FHWA/RD-80/052, Federal Highway Administration, Washington, 1980, 224 p.

4. Jamiolkowski, M., Ladd, C. C., Germaine, J. T., and Lancellotta, R., "New Developments in Field and Laboratory Testing of Soils", Proceedings, 11th International Conference on Soil Mechanics and Foundation Engineering, Vol. 1, San Francisco, 1985, pp. 57-153.

5. Kulhawy, F. H., Trautmann, C. H., Beech, J. F., O'Rourke, T. D., McGuire, W., Wood, W. A., and Capano, C., "Transmission Line Structure Foundations for Uplift-Compression Loading", Report EL-2870, Electric Power Research Institute, Palo Alto, 1983, 412 p.

6. Orchant, C. J., Kulhawy, F. H., and Trautmann, C. H., "Reliability-Based Foundation Design for Transmission Line Structures: Critical Evaluation of In-Situ Test Methods", Report EL-5507, Vol. 2, Electric Power Research Institute, Palo Alto, 1988, 214 p.

Appendix D

DILATOMETER TEST

The flat-plate dilatometer test (DMT) became commercially available in the U.S. in 1979. Although the use of this test in routine site investigation practice has been relatively recent, a number of factors associated with the DMT, including its relative ease of operation and durability, suggest that its use will increase.

PROCEDURE

The equipment required to perform DMT tests is shown in Figure D-1. The dilatometer itself is a flat blade or plate, 14 mm (0.55 in) thick, 95 mm (3.74 in) wide, and 220 mm (8.66 in) long. A flexible stainless steel membrane, 60 mm (2.36 in) in diameter, is located on the center and flush with one side of the blade. A combination gas and electrical line extends from a surface control box through the push rods and into the blade. A special hydraulic system has been developed for offshore use.

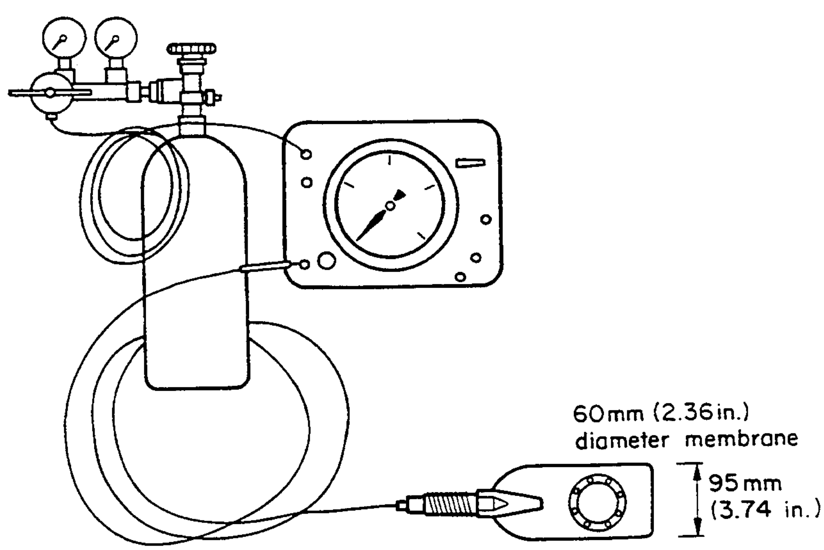

Figure D-1. Dilatometer Test Equipment

Source: Schmertmann (1), p. 95.

Although the test is not yet standardized, a recommended ASTM procedure has been developed by Schmertmann (1). The test is performed by pushing the blade to the desired test depth at a typical rate of penetration of 20 mm (0.8 in)/sec. Test depths may be taken as frequently as 200 mm (8 in), although more typically in the U.S., the intervals are 300 mm (1 ft). The blade can be pushed with a CPT hydraulic jacking rig, the hydraulics of a rotary drilling rig, or a hammer and rod system as used in the SPT. Upon achieving the desired test depth, the operator uses a control valve at the surface to inflate the membrane with high pressure nitrogen gas. Typically two readings are recorded, prompted by audio and visual signals at the control box. The first, called the A reading, represents the pressure at which the membrane "lifts off" its sensing disc, which ideally represents initial contact with the soil. The second, called the B reading, is made after 1 mm (0.04 in) deflection has occurred. The operator vents the pressure after obtaining the B reading. Recently, a third reading, designated as the closing pressure or C reading, has been proposed as a measure of the total pore water stress. The C reading is similar to the A reading, except that it is obtained during deflation. After these measurements, the blade is pushed to the next test depth, at which the test cycle is repeated. Each cycle typically takes 1 to 2 minutes to complete. After each complete profile, the membrane response of the dilatometer should be calibrated.

Recent devices include load cells capable of measuring static thrust (1) and piezometric elements to monitor the pore water stresses generated during penetration (2). The inclusion of these electronic sensors enhances the information obtained from the DMT, but they also increase the complexity of the test substantially.

The A and B readings obtained during the test must be corrected by calibration of the measuring gage and the membrane response. During calibration of the device, two readings, ΔA and ΔB, are made. ΔA is the vacuum pressure required to keep the membrane in contact with its seating, because after a number of expansions the membrane develops an outward curvature. ΔB is the air pressure required to deflect the membrane 1.1 mm (0.043 in) in air. The corrected in-situ data for the contact stress (p_o) and the expansion stress (p_1) are expressed as:

$$p_o = 1.05(A + \Delta A - z_m) - 0.05\ p_1 \qquad \text{(D-1)}$$

$$p_1 = B - \Delta B - z_m \qquad \text{(D-2)}$$

with z_m = gage pressure deviation from zero when vented to atmospheric pressure.

Using these values, three index parameters are defined as follows (1):

$$I_D = (p_1 - p_o)/(p_o - u_o) \quad \text{(D-3)}$$

$$K_D = (p_o - u_o)/\bar{\sigma}_{vo} \quad \text{(D-4)}$$

$$E_D = 34.7(p_1 - p_o) \quad \text{(D-5)}$$

in which I_D = material index, u_o = assumed hydrostatic pore water stress, K_D = horizontal stress index, $\bar{\sigma}_{vo}$ = in-situ effective vertical stress, and E_D = dilatometer modulus. In the original work for this test (3), Equations D-1 and D-2 were somewhat different, and the coefficient in Equation D-5 was equal to 38.2. When this test was introduced, correlations of these index parameters to a variety of soil properties were proposed. Most were based on limited field data and are empirical, although some of the more recent relationships have a more theoretical basis.

ADVANTAGES AND DISADVANTAGES

The DMT offers a number of advantages. First, the test is simple and rapid to perform. The equipment is rugged, and the test can be used in a wide variety of soils. Also, the blade-like shape reduces the shear and volumetric strain associated with other penetration tests. As indicated above, the DMT tentatively has been correlated to a number of soil properties. Specifically, the test may provide reasonable estimates of the horizontal stress and the overconsolidation ratio, which are traditionally difficult properties to measure. The proposed empirical correlations, although requiring a substantial database for verification, relate the test results to basic geotechnical engineering parameters. The test data can be reduced quickly in the field, which allows evaluation of anomalous results. In addition, these test results and inferred soil properties can be plotted in a nearly continuous profile to illustrate the variations with depth. Also, the test equipment is relatively inexpensive and, because the test is rapid, numerous data points can be obtained quickly.

The DMT also possesses several notable disadvantages. First and most important, it is a recent test which has had limited field exposure. Therefore, the general validity of the soil property correlations is uncertain. Second, most contractors do not possess the equipment required to perform the DMT. Third, as with any penetration test, the DMT has limited use in very dense or cemented soils and in soils containing appreciable gravel or coarser fragments. In the case of gravelly deposits, the blade may deviate from vertical penetration, causing difficulty in interpreting the horizontal stress parameters and, in some cases, the blade may be bent or the inflatable membrane may be torn. Fourth, the test requires the additional measurement of thrust to evaluate the strength and stress history of cohesionless soils. These thrust measurements, as well as other electronic sensors such as pore water stress elements which facilitate interpretation of the DMT, detract from the simplicity, ruggedness, and low cost of the test. Finally, this test suffers from the common limitation that it does not obtain soil samples.

SOURCES OF ERROR, RELIABILITY, AND COST

The DMT has a number of potential sources of error, as noted in Table D-1. Perhaps most important is that the test is quite new, and experience with the test is limited. Its real potential as a field production tool has yet to be assessed, and correlations with the DMT parameters have been limited to date.

The reliability of the test is difficult to determine precisely at the present time

Table D-1

MAJOR DMT VARIABLES

Variable	Relative Effect on DMT Results
Leaking seals	Minor to significant
Deformed membrane	Moderate to significant
Bent or deformed push rods	Minor to moderate
Damaged blade	Minor to significant
Poor electrical ground	Significant
Inclination of push rods	Minor to moderate
Rate of testing	Minor to moderate
Method of driving	Minor to significant
Rod friction	Minor (except for thrust measurement)
Calibration error	Minor to moderate
Waiting time after insertion	Significant in silts

Source: Modified after Orchant, et al. (4), p. 4-42.

because of a shortage of detailed test data. However, the limited data to date are encouraging and suggest good reproducibility and relatively high reliability.

The costs associated with dilatometer testing are comparable, to slightly more expensive, than those described for the CPT. Typical DMT costs have been reported to be about $12 to $15/ft ($40 to $50/m) with a CPT truck and about $15 to $20/ft ($50 to $65/m) with a standard drill rig. Because of its simple and expedient operation, the DMT is becoming popular and available for production testing. Many specialty in-situ testing firms with large cone trucks also offer DMT services.

REFERENCES

1. Schmertmann, J. H., "Suggested Method for Performing the Flat Dilatometer Test", Geotechnical Testing Journal, ASTM, Vol. 9, No. 2, June 1986, pp. 93-101.

2. Lutenegger, A. J., "Current Status of the Marchetti Dilatometer Test", Proceedings, 1st International Symposium on Penetration Testing (ISOPT-1), Vol. 1, Orlando, 1988, pp. 137-156.

3. Marchetti, S., "In-Situ Tests by Flat Dilatometer", Journal of the Geotechnical Engineering Division, ASCE, Vol. 106, No. GT3, Mar. 1980, pp. 299-321.

4. Orchant, C. J., Kulhawy, F. H., and Trautmann, C. H., "Reliability-Based Foundation Design for Transmission Line Structures: Critical Evaluation of In-Situ Test Methods", Report EL-5507, Vol. 2, Electric Power Research Institute, Palo Alto, 1988, 214 p.

Appendix E

VANE SHEAR TEST

The vane shear test (VST) is a moderately rapid and economical in-situ method for determining the peak and remolded undrained shear strength of soft to medium stiff clays. The test involves pushing a four-bladed vane into a clay stratum and slowly rotating it while measuring the resisting torque.

PROCEDURE

The procedure for the VST is described in ASTM D2573 (1). Important related issues are given elsewhere (2, 3, 4). The test generally is used to determine the shear strength of a cohesive soil once its location has been established. In the test, a shear vane similar to those shown in Figure E-1 is pushed into undisturbed soil and is rotated from the surface at a standard rate of 0.1 degrees per second. The peak

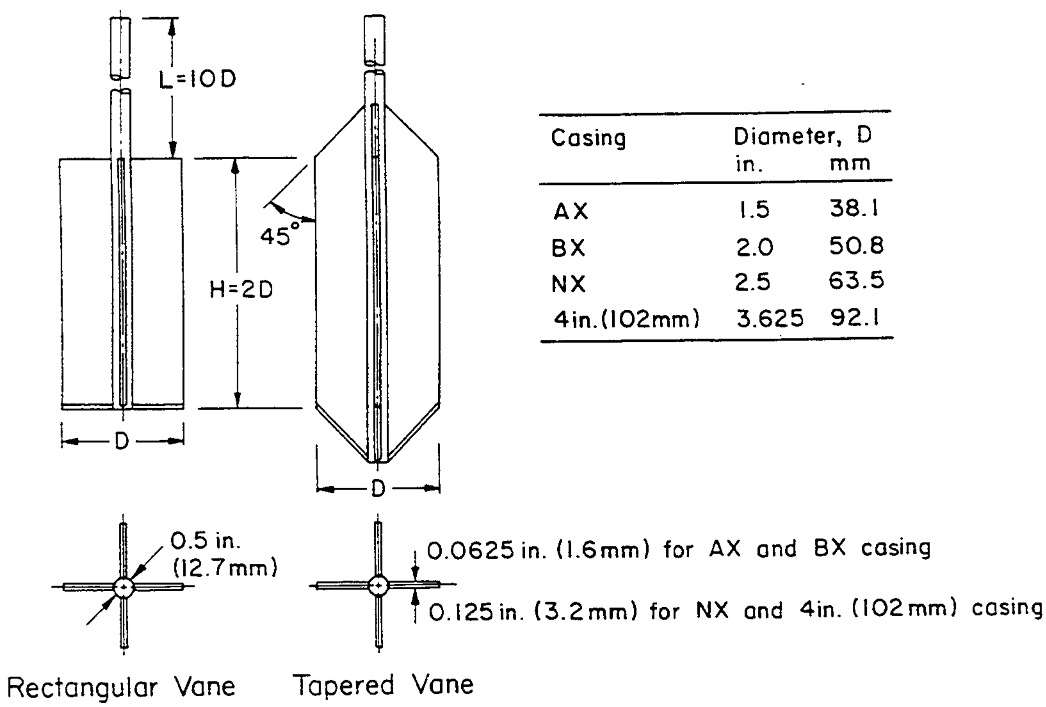

Casing	Diameter, D in.	mm
AX	1.5	38.1
BX	2.0	50.8
NX	2.5	63.5
4in.(102mm)	3.625	92.1

Figure E-1. Vane Geometries and Sizes

Source: American Society for Testing and Materials (1), p. 304.

torque which develops is related to the peak shear strength on a cylindrical failure surface by a constant, which is a function of the shape and dimensions of the vane. Details are given in ASTM D2573 (1). The VST may be conducted either at the bottom of a prebored hole or, in soft clays, by merely pushing the vane rods to the desired test depth. The latter method requires a correction for rod friction.

After the peak torque has been determined, the vane is rotated quickly about ten times to remold the soil. The torque then is measured again to determine the remolded shear strength. The sensitivity (S_t) may be calculated as the ratio of the peak to remolded strength. Numerous tests can be performed sequentially in the same deposit, but individual tests should be separated vertically by at least 0.75 m (30 in).

Another method of testing uses vane borers, as shown in Figure E-2. With the SGI device, the rods are surrounded by a sleeve to minimize friction losses, and the vane is covered by a protective shoe during penetration. At the desired test

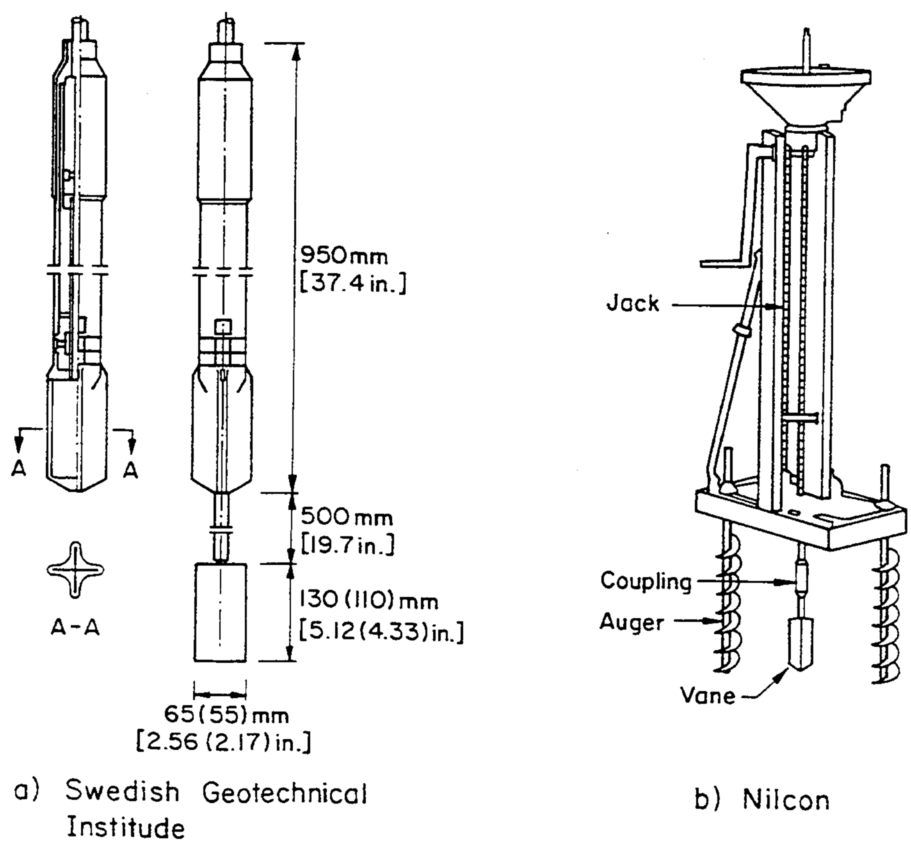

Figure E-2. Common Vane Borers

Source: Walker (2), p. 68.

depth, the vane is advanced into the soil beneath the protective shoe. The other device is the Nilcon vane borer, which does not have either a protective sleeve or shoe. However, the vane is followed by a slip coupling during penetration, which provides for rod friction calibration before each test.

The maximum measured torque (T) in the VST is used to calculate the undrained shear strength (s_u) as follows (1):

$$s_u = T/K \tag{E-1}$$

in which T = torque in N-m or lb-ft and K = constant depending on the dimensions and shape of the vane (m^3 or ft^3), where:

$$K = \pi(D^2H/2)\ [1 + (D/3H)] \qquad \text{for D and H in meters} \tag{E-2}$$

$$K = (\pi/1728)\ (D^2H/2)\ [1 + (D/3H)] \qquad \text{for D and H in inches} \tag{E-3}$$

A number of assumptions are made in calculating the undrained shear strength from these torque measurements (3), including:

- The soil is completely undrained, i.e., no consolidation takes place during insertion of the vane or during the test.
- No disturbance is caused by the boring operation or installation of the vane.
- The remolded zone around the vane is very small.
- There is no progressive failure so that the maximum applied torque overcomes the fully-mobilized shear strength along the cylindrical surface.
- Isotropic strength conditions exist in the soil mass.

ADVANTAGES AND DISADVANTAGES

The VST has many advantages when used in soil deposits for which it is intended. The test is moderately rapid and economical, and it is reproducible in homogeneous deposits. The scatter in test results is on the same order as that for the confined and unconfined compression tests with which it is compared. The test has had extensive usage during the past few decades, and a large body of literature is available for use in correlations with other test and design methods. The effect of the vane size is minor in most types of soil and, by using two vanes with different length to diameter ratios in the same stratum, the soil strength anisotropy can be inferred. Additionally, the test is an inexpensive way to determine the properties of sensitive clays, which are characteristically difficult to obtain in the laboratory without extreme care.

The VST has a number of important limitations that influence its usefulness. The test is most easily interpreted for soft and medium stiff clays which have been previously identified by some other test or sampling procedure. Also, it is useful mainly for analyses requiring the undrained shear strength.

SOURCES OF ERROR, RELIABILITY, AND COST

The VST may be in error because of excessive rod friction, poor torque calibrations, non-standard rotation rates, and other factors (4, 5, 6). A list of the major sources of error with the VST is given in Table E-1.

In addition to these test uncertainties, the theoretical nature of the failure

Table E-1

MAJOR SOURCES OF ERROR IN THE VANE SHEAR TEST

Cause	Effect	Influence on Strength Measurement
Friction between torque rods and soil or casing	Measured torque includes spurious component of resistance	Increases
Poorly calibrated torque measurement	Inaccurate torque	Increases or decreases
Vane rotated too quickly	Soil sheared too rapidly	Increases
Test performed in disturbed soil	Soil structure broken down	Decreases
Damaged vane	Disturbed soil excessively	Decreases peak strength
Unknown sand/silt/shell lenses	Drainage during test	Increases
Isolated gravel/cemented nodules	Measured torque includes spurious component of resistance	Increases

Source: Adapted from Kulhawy, et al. (5), p. 5-34.

mechanism is not fully understood. Therefore, the correlation between field and laboratory measurements of the same soil contains a significant element of uncertainty. On the basis of published studies, the random variations between tests made in the same soil are much smaller than the uncertainties associated with the test procedure.

Vane shear tests are comparable in cost to the SPT, taking into account that both require a test boring. During an average shift, approximately 10 to 15 tests can be performed. Based on 1990 drilling costs, this indicates that the average cost of a VST is about $70 to $150. However, it should be noted that the VST can be alternated with the SPT in a single test boring to optimize the return of information from a single borehole.

REFERENCES

1. American Society for Testing and Materials, "Standard Test Method for Field Vane Shear Test in Cohesive Soil [D2573-72(1978)]", Annual Book of Standards, Vol. 4.08, ASTM, Philadelphia, 1989, pp. 308-310.

2. Walker, B. F., "Vane Shear Strength Testing", In-Situ Testing for Geotechnical Investigations, Ed. M. C. Ervin, A. A. Balkema, Rotterdam, 1983, pp. 65-72.

3. Flaate, K., "Factors Influencing the Results of Vane Tests", Canadian Geotechnical Journal, Vol. 3, No. 1, Feb. 1966, pp. 18-31.

4. Richards, A. F., "Overview", Vane Shear Strength Testing in Soils: Field and Laboratory Studies (STP 1014), ASTM, Philadelphia, 1988, pp. 1-9.

5. Kulhawy, F. H., Trautmann, C. H., Beech, J. F., O'Rourke, T. D., McGuire, W., Wood, W. A., and Capano, C., "Transmission Line Structure Foundations for Uplift-Compression Loading", Report EL-2870, Electric Power Research Institute, Palo Alto, 1983, 412 p.

6. Orchant, C. J., Kulhawy, F. H., and Trautmann, C. H., "Reliability-Based Foundation Design for Transmission Line Structures: Critical Evaluation of In-Situ Test Methods", Report EL-5507, Vol. 2, Electric Power Research Institute, Palo Alto, 1988, 214 p.

Appendix F

COMPARISON OF IN-SITU TEST METHODS

Mitchell (1) has reviewed the various types of in-situ test procedures and classified each according to a variety of parameters. A modified version of his summary is shown in Table F-1 and can be used qualitatively in designing a field exploration program, once a preliminary study has been completed to determine the general types of geologic materials likely to be encountered along the route.

In addition to the common in-situ tests described in Appendices A through E, a number of other tests exist which serve special purposes or have not gained wide usage to date. These other tests include the Iowa borehole shear device, the Glötzl

Table F-1

ASSESSMENT OF IN-SITU TESTS

Comparison Basis	Standard Penetration Test	Cone Penetration Test	Vane Shear Test	Pressure-meter Test	Flat Dilatometer Test
Simplicity of apparatus	Simple, rugged	Complex, rugged	Simple, rugged	Complex, delicate	Simple, rugged
Ease of testing	Easy	Easy	Easy	Complex	Easy
Continuous profile or point values	Point	Continuous	Point	Point	Semi-continuous
Basis for interpretation	Empirical	Empirical, theory	Theory	Empirical, theory	Semi-empirical, theory
Suitable soils	Most types	Most types	Softer clays	Most types	Most types
Suitability in practice	Routine	Routine	Routine	Limited	Routine

Source: Modified from Mitchell (1), pp. 121, 123.

total pressure cell, seismic cone, K_o-stepped blade, acoustic cone, large diameter penetration test (LPT), Becker probes, and screw-plate tests, among others. Some of these tests may become common in the future.

When comparing test methods, it is very important to consider the cost-effectiveness of the information obtained. Handy (2) considered this point and developed qualitative relationships for both field and laboratory tests. Table F-1 summarizes the general applicability of the five major types of in-situ tests covered in this manual. The usefulness of the various in-situ test methods in different soils is summarized in Table F-2.

The degree of historical use and the general familiarity of an in-situ technique commonly are important considerations in assessing their applicability to a given project, because there is an added element of risk involved in using techniques

Table F-2

USEFULNESS OF IN-SITU TESTS IN COMMON SOIL CONDITIONS

Test	Soil Type					
	gravel	sand		silt	clay	
		loose	dense		soft	stiff
SPT	2 to 3	1	1	2	3	3
MCPT	2 to 3	1	2	1	1	2
ECPT	3	1	2	1	1	2
CPTU	3	1	2	1	1	2
VST	4	4	4	3	1	2
DMT	3	1	2	1	1	2
PMT	2	2	1	1	1	1
SBPMT	3	2	2	1	1	1

Notes:
1 - Highly applicable
2 - Moderately applicable
3 - Limited applicability
4 - Not applicable

MCPT - Mechanical CPT
ECPT - Electric CPT
CPTU - Piezometric CPT
SBPMT - Self-boring PMT

Source: Orchant, et al. (3), p. 2-61.

which have not been field-proven.

Also, access to testing locations for some projects may be difficult. Therefore, logistical concerns of equipment mobilization and access requirements must be considered in the overall applicability of in-situ techniques for transmission line site characterization. These considerations must be evaluated on a project by project basis because requirements will vary.

Test costs are related to the above logistical concerns. Since limited allocations are available for most geotechnical projects, test economics may govern their application for a given project. Table F-3 summarizes the historical use, mobilization and access requirements, and relative costs of the tests reviewed.

Selection of the most suitable test for a specific project is governed by the type of information required for the applied design method. In some cases, specific soil property estimates are required; in others, empirical design models based on in-situ test results are employed. These factors must be addressed as well.

Table F-3

HISTORICAL USE, MOBILIZATION AND ACCESS REQUIREMENTS, AND COSTS OF IN-SITU TESTS

Test	Historical Use	Availability	Access	Unit Cost
SPT	Substantial	Excellent	Truck, trailer	Medium
MCPT	Substantial	Good	Limited portability - truck, trailer	Low
ECPT	Moderate	Good	Limited portability - truck, trailer	Low
CPTU	Limited	Poor	Limited portability - truck, trailer	Medium
VST	Substantial	Excellent	Limited portability - truck, trailer	Medium
DMT	Limited	Fair	Limited portability - truck, trailer	Low
PMT	Moderate	Good	Limited portability - truck, trailer	Medium
SBPMT	Limited	Poor	Limited portability - truck, trailer	High

Source: Orchant, et al. (3), p. 2-62.

In addition to the test conditions summarized in the above tables, the sources of error and the magnitude of uncertainty associated with particular tests will influence their applicability. These factors are considered in a qualitative sense in assessing the ability of the test to obtain specific soil property data. However, to allow direct comparisons between tests and assess their potential to provide reliable design input, quantitative information regarding the variability of the test results is required.

The variability of the various in-situ testing methods has been evaluated by Orchant, et al. (3), and the expected coefficient of variation (COV = ratio of standard deviation to mean value) for each test is summarized in Table F-4. The analysis is based on a statistical review of data from numerous sites tested by each apparatus. In terms of reliability, the electric cone and dilatometer appear to be less variable than the vane shear test and pressuremeter. The mechanical cone and standard penetration test are the most variable test methods.

Finally, the relative accuracy of the device must be weighed against its relative cost. A qualitative relationship between relative cost and accuracy for the various field test methods is given in Figure F-1.

Table F-4

ESTIMATES OF IN-SITU TEST VARIABILITY

Test	COV[a] (%) Equipment	COV (%) Procedure	COV (%) Random	COV[b] (%) Total	COV[c] (%) Range
Standard Penetration Test (SPT)	5[d] to 75[e]	5[d] to 75[e]	12 to 15	14[d] to 100[e]	15 to 45
Mechanical Cone Penetration Test (MCPT)	5	10[f] to 15[g]	10[f] to 15[g]	15[f] to 22[g]	15 to 25
Electrical Cone Penetration Test (ECPT)	3	5	5[f] to 10[g]	7[f] to 12[g]	5 to 15
Vane Shear Test (VST)	5	8	10	14	10 to 20
Dilatometer Test (DMT)	5	5	8	11	5 to 15
Pressuremeter Test (PMT)	5	12	10	16	10 to 20[h]
Self-Boring Pressuremeter Test (SBPMT)	8	15	8	19	15 to 25[h]

Notes:

a - COV = standard deviation/mean

b - COV(Total) = $[COV(Equipment)^2 + COV(Procedure)^2 + COV(Random)^2]^{1/2}$

c - Because of limited data and the judgment involved in estimating COV values, ranges represent probable magnitudes of field test measurement error

d - Best case scenario for SPT test conditions

e - Worst case scenario for SPT test conditions

f - Tip resistance CPT measurements

g - Side resistance CPT measurements

h - It is likely that results may differ for p_o, p_f, and p_L, but the data are insufficient to clarify this issue

Source: Orchant, et al. (3), p. 4-63.

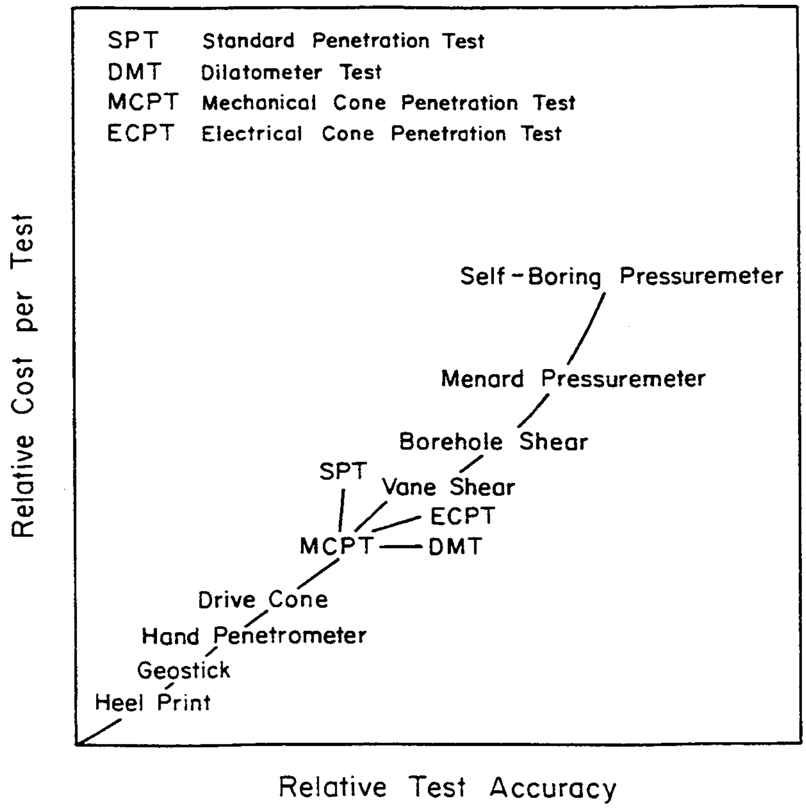

Figure F-1. Qualitative Relationship Between Relative Test Cost and Accuracy

Source: Handy (2), p. 242.

REFERENCES

1. Mitchell, J. K., "In-Situ Techniques for Site Characterization", Proceedings, NSF Specialty Workshop on Site Characterization and Exploration, Ed. C. H. Dowding, Northwestern University, Evanston, June 1978, pp. 107-129.

2. Handy, R. L., "Realism in Site Exploration: Past, Present, Future, and Then Some - All Inclusive", Proceedings, Symposium on Site Exploration in Soft Ground Using In-Situ Techniques, Report FHWA-TS-80-202, Federal Highway Administration, Washington, 1980, pp. 239-248.

3. Orchant, C. J., Kulhawy, F. H., and Trautmann, C. H., "Reliability-Based Foundation Design for Transmission Line Structures: Critical Evaluation of In-Situ Test Methods", Report EL-5507, Vol. 2, Electric Power Research Institute, Palo Alto, 1988, 214 p.

Appendix G

CRITICAL STATE SOIL MECHANICS (CSSM) CONCEPT

The concept of critical state soil mechanics (CSSM) evolved at the University of Cambridge (e.g., 1) and has been instrumental in improving our understanding of soil behavior (e.g., 2, 3). Basically (and very simplistically), the concept states that there is uniqueness of soil behavior at the critical state in void ratio (e) - shear stress (q) - effective mean normal stress ($\bar{p}$) space. The details are well beyond the scope of this manual; however, the general soil behavior is illustrated in Figure G-1.

For the stiff soil, a peak strength is achieved which is followed by strain softening to a state of constant volume (i.e., constant void ratio) deformation. For the soft soil, a peak strength is achieved at the state of constant volume deformation. This state is known as the critical state and represents the limit strength of soil. Different critical states exist for different confining stresses (or, more precisely, effective mean normal stresses) to define a unique e-$\bar{p}$-q envelope in void ratio-stress space.

With this concept, a number of theoretical/experimental soil models were developed, known as Cam clay, Granta gravel, and modified Cam clay (e.g., 1). From these models, a general predictive tool for soil behavior emerged. Strictly speaking, this tool is applicable only to remolded, insensitive soils without aging,

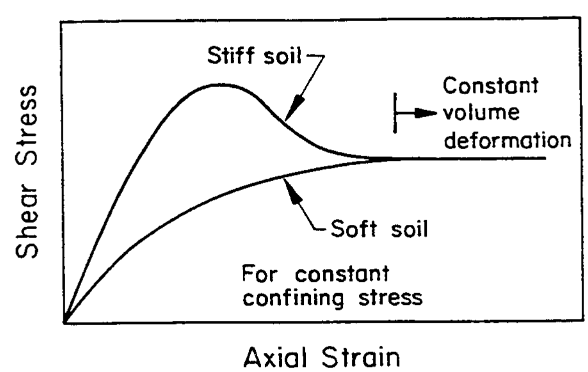

Figure G-1. Typical Soil Stress-Strain Behavior cementing, and other environmental influences. However, research has shown that the modified Cam clay model predicts well the behavior of normally consolidated, insensitive soils, also without aging, cementing, and other environmental influences. In other soils, the model effectively provides a lower bound.

The following is some of the notation used with the modified Cam clay model:

$$M = \frac{6 \sin \bar{\phi}_{tc}}{3 - \sin \bar{\phi}_{tc}} \quad \text{(G-1)}$$

$$\Lambda = \frac{\lambda - \kappa}{\lambda} = 1 - \frac{C_s}{C_c} \quad \text{(typically} \approx 0.8) \quad \text{(G-2)}$$

$$OCR_i = \bar{p}_{max}/\bar{p}_o \quad \text{(G-3)}$$

r = spacing ratio, defined in Figure G-2 (typically r = 2 for modified Cam clay)

in which $\bar{\phi}_{tc}$ = effective stress friction angle in triaxial compression, λ = isotropic compression index, κ = isotropic swelling index, C_c = compression index, C_s = swelling (or unload-reload) index, $\bar{p}$ = effective mean normal stress = $(\bar{\sigma}_1 + \bar{\sigma}_2 + \bar{\sigma}_3)/3$, $\bar{\sigma}_1$, $\bar{\sigma}_2$, and $\bar{\sigma}_3$ = effective maximum, intermediate, and minor principal stresses, $\bar{p}_{max}$ = maximum $\bar{p}$ to which soil has been subjected, $\bar{p}_o$ = current $\bar{p}$, and OCR_i = isotropic overconsolidation ratio.

In its most basic form, CSSM assumes that all stress paths terminate on a line (termed the critical state line or CSL) which is parallel to the virgin compression

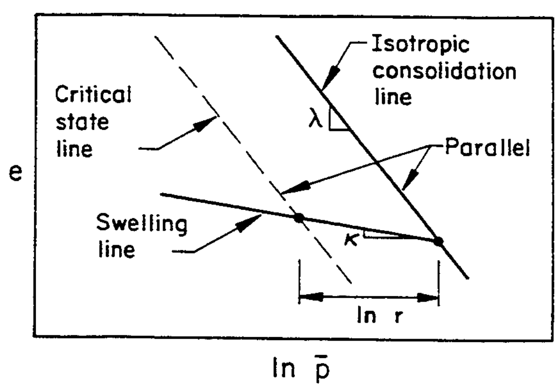

Figure G-2. CSSM Notation

line. It is able to account for undrained and drained behavior and normally consolidated as well as overconsolidated states of stress (See Figure G-2.) The advantage of the Cam clay models is their simplicity and ability to relate effective stress analysis with total stress analysis. In its most basic form, only three soil parameters ($\bar{\phi}_{tc}$, C_c, C_s) are required to represent a variety of common stress paths and boundary conditions.

REFERENCES

1. Schofield, A. N. and Wroth, C. P., Critical State Soil Mechanics, McGraw-Hill Book Company, London, 1968, 310 p.

2. Wroth, C. P., "Interpretation of In-Situ Soil Tests", Geotechnique, Vol. 34, No. 4, Dec. 1984, pp. 449-489.

3. Wroth, C. P. and Houlsby, G. T., "Soil Mechanics - Property Characterization and Analysis Procedures", Proceedings, 11th International Conference on Soil Mechanics and Foundation Engineering, Vol. 1, San Francisco, 1985, pp. 1-55.

Appendix H

CPT CALIBRATION CHAMBER DATA FOR SANDS

It is very difficult to obtain undisturbed samples of clean sands for laboratory testing. New methods of sampling by freezing techniques are available now, but they are difficult to use and expensive. Therefore, most CPT correlations for sands have been developed from data obtained in laboratory calibration chambers which allow control of the sand uniformity, density, initial stress state, and stress history. Triaxial compression tests on identically prepared samples allow determination of the friction angle and modulus for comparison. In this appendix, the calibration chamber data used within this manual are described for reference.

DATA SUMMARY

In this manual, CPT correlations with relative density (D_r), effective stress friction angle ($\bar{\phi}$), constrained modulus (M), and in-situ or at-rest horizontal soil stress coefficient (K_o) have been developed from 24 different sets of calibration chamber data on sands. A listing of these sands and their properties is given in Table H-1. The symbol column refers to that used on the correlation plots.

All of the calibration chamber tests were conducted on reconstituted sands which were unaged. The majority were clean quartz sands. The percent fines (percent less than No. 200 sieve) ranged from 0 to 6 percent, although most of the sands had less than 1 percent fines. The particle size at 50 percent finer (D_{50}) ranged from 0.16 to 1.0 mm, with an average of 0.38 mm. The particle size at 10 percent finer (D_{10}) ranged from 0.10 to 0.70 mm, with an average of 0.25 mm. All of the sands were uniformly graded, with a range of uniformity coefficient (C_u) from 1.10 to 2.60 and an average of 1.79. The specific gravity ranged from 2.65 to 3.02, with an average of 2.68. The maximum void ratio ranged from 0.73 to 1.05, while the minimum void ratio ranged from 0.40 to 0.65.

For testing, the sands were prepared over a range of relative density (D_r) and overconsolidation ratio (OCR). D_r varied from 8 to 100 percent, while the OCR ranged from 1 (normally consolidated) to about 14 (heavily overconsolidated). In general, the sands were consolidated under K_o conditions prior to testing.

Table

CALIBRATION CHAMBER

No.	Symbol	Sand (Reference)	D_{50}	D_{10}	C_u	G_s	e_{max}	e_{min}
1	⟐	Earlston (1)	0.33	0.16	2.60	2.65	0.727	0.404
2	◁◀	Edgar (1, 2)	0.45	0.29	1.79	NA	0.919	0.543
3	⊕	Erksak (3)	0.35	0.18	2.20	2.65	0.963	0.525
4	△▲	Frankston (4)	0.31	0.18	2.05	NA	0.792	0.462
5	⊞	Hilton Mines (5)	0.20	0.15	2.00	3.02	1.050	0.620
6	○●	Hokksund (6, 7)	0.44	0.27	2.20	2.70	0.906	0.539
7	◇◆	Hokksund (8)	0.39	0.21	2.20	2.70	0.878	0.535
8	◈	Hostun Fine (9)	0.35	0.18	2.22	NA	1.000	0.650
9	⊟	Lanchester 25/52 (10)	0.40	0.30	1.40	NA	0.818	0.563
10	◁	Leighton Buzzard (11)	0.37	0.26	1.50	NA	0.815	0.489
11	⦶	Leighton Buzzard (12)	0.85	0.70	1.30	NA	0.790	0.490
12	⧄	Lone Star 2 (13)	1.00	0.60	2.00	2.66	0.766	0.482
13	⧅	Lone Star 30 (13)	0.39	0.22	1.86	2.66	0.824	0.537
14	▷▶	Lone Star 60 (13)	0.30	0.18	1.48	2.66	0.908	0.566
15	⊠	Monterey 0 (14)	0.37	0.25	1.60	2.65	0.820	0.540
16	◫	Monterey 0/30 (15)	0.45	0.35	1.37	2.65	0.803	0.563
17	⟠	Oostershelde (16)	0.17	0.10	1.80	NA	0.887	0.562
18	▽	Ottawa (17)	0.28	0.26	1.10	NA	0.868	0.545
19	⊖	Ottawa 90 (5)	0.22	0.13	1.85	2.65	0.789	0.486
20	⊗	Reid-Bedford (5)	0.24	0.15	1.70	2.66	0.871	0.549
21	△	S. Oakleigh Fine (1)	0.17	0.12	1.60	2.65	0.932	0.570
22	▽▼	S. Oakleigh Medium (1)	0.32	0.17	2.20	NA	0.754	0.412
23	□■	Ticino (8)	0.50	0.41	1.58	2.67	0.915	0.568
24	⟡	Toyoura (18)	0.16	0.13	1.46	2.64	0.977	0.605

Symbols: D_{50} - particle size at 50% finer
D_{10} - particle size at 10% finer
C_u - uniformity coefficient
G_s - specific gravity of solids

H-1

DATABASE FOR SANDS

Angularity	Mineralogy	Chamber Diameter (mm)	Cone Diameter (mm)	D_r in Tests (%)	OCR in Tests
subrounded	quartz	760	50.0	20,45,65,73	1
subangular	quartz	1220	35.7	56,95	1 to 10
subrounded	quartz, 6% fines, trace chert	1400	35.7	69 to 99	1
subangular to rounded	quartz	1200	35.7	54 to 100	1 to 7.7
angular (S = 0.72, R = 0.23)	feldspar, quartz, mica, muscovite, iron, 3% fines	1220	35.7	30 to 84	1
angular	45% feldspar, 35% quartz, 10% mica	762,1220	25.2,35.7	8 to 100	1,8
subangular to angular	35% quartz, 10% mica	1200	20,25.4, 35.7	31,82,96	1,7.3, 14.5
subangular	quartz	180	11.3	15 to 95	1
subangular	95% quartz	254	9.5	0 to 100	1
subrounded	quartz	1200	35.7	40 to 97	1
subrounded	quartz	900	35.7	20 to 90	1
subrounded to subangular	quartz with feldspar	760	35.7	22 to 66	1
subrounded to subangular	quartz with feldspar	760	35.7	20 to 84	1
subrounded to subangular	quartz with feldspar	760	35.7	17 to 79	1,1.5, 3.6,5.9
subrounded (S = 0.80, R = 0.35)	quartz, trace feldspar	760	35.7	27 to 72	1
subrounded to subangular	quartz with feldspar	1500	23.2,35.7	24,64	1
rounded	quartz	1900	35.7	30 to 87	1
well-rounded	quartz	71.1	12.7	57	1,2,4
rounded	quartz, 0.2% fines	1220	35.7	20 to 83	1
subangular (S = 0.76, R = 0.29)	quartz, some feldspar, trace calcite	1220	35.7	24 to 81	1
subangular	quartz	760	35.7,50.0	28 to 86	1
subangular	quartz	760	35.7,50.0	44 to 89	1,2,4,8
subangular to angular (S = 0.79, R = 0.38)	30% quartz, 5% mica	1200	20,25.4, 35.7	16 to 98	1 to 14.7
subangular	high feldspar content	790	35.7	33 to 86	1

e_{max} - maximum void ratio
e_{min} - minimum void ratio
S - particle sphericity = (6 x particle volume/π)$^{1/3}$/particle length
R - particle roundness (See Figure 2-2.)

Most of the sands were placed in a dry state by air-pluviation (raining). Exceptions include Erksak sand (3), which was tamped moist, and Lanchester sand (10), which was prepared by raining, tamping, and vibrating methods. In addition, most of the CPT tests were performed on dry sand. The exceptions include Erksak sand (3), which was saturated using back pressure, and Monterey 0 sand (14) and Ticino sand (8), which were both dry and saturated. Furthermore, Jamiolkowski, et al. (19) state that the Edgar, Ottawa, Reid-Bedford, and Hilton Mines sands were tested both "drained" and "submerged".

All tests used electric cones with a 60° cone angle. The cone diameters ranged from 9.5 to 50.0 mm, although 85 percent of the data were obtained with the standard 35.7 mm diameter cone. All of the cones were of the standard Fugro cylindrical shape, except for that of Villet and Mitchell (13), which had a reduced diameter behind the cone.

CHAMBER BOUNDARY INFLUENCE

Most of the available data were obtained using flexible-wall calibration chambers, which allow yielding during cone penetration. This yielding gives measured cone tip resistance (q_c) values which are less than they would be in an infinite medium, and therefore the q_c values need to be corrected for these boundary effects. No generally accepted approach has been developed yet for making these corrections. However, research has shown (e.g., 20) that q_c increases with increasing ratio of chamber to cone diameter (B_c/B). In addition, the increase is more pronounced as the relative density increases (e.g., 7). The correction factor used herein was derived from six available data sets from Table H-1 where the B_c/B ratio was varied to allow evaluation of the boundary effects. These data are summarized in Figure H-1. Based upon examination of these data and the trends noted above, the following correction factor was developed:

$$q_c \text{ (corrected)} = q_c \text{ (measured) } [(B_c/B - 1)/70]^{-0.005 \, D_r} \qquad \text{(H-1)}$$

in which D_r = relative density in percent. This equation assumes that there are no boundary effects when B_c/B equals or exceeds 70. A plot of this equation is given in Figure H-2, which shows increasing corrections needed for smaller B_c/B ratios and higher relative densities.

Four different types of boundary conditions may be applied in flexible-wall calibration chambers (e.g., 21), as shown in Table H-2. Most of the tests summarized

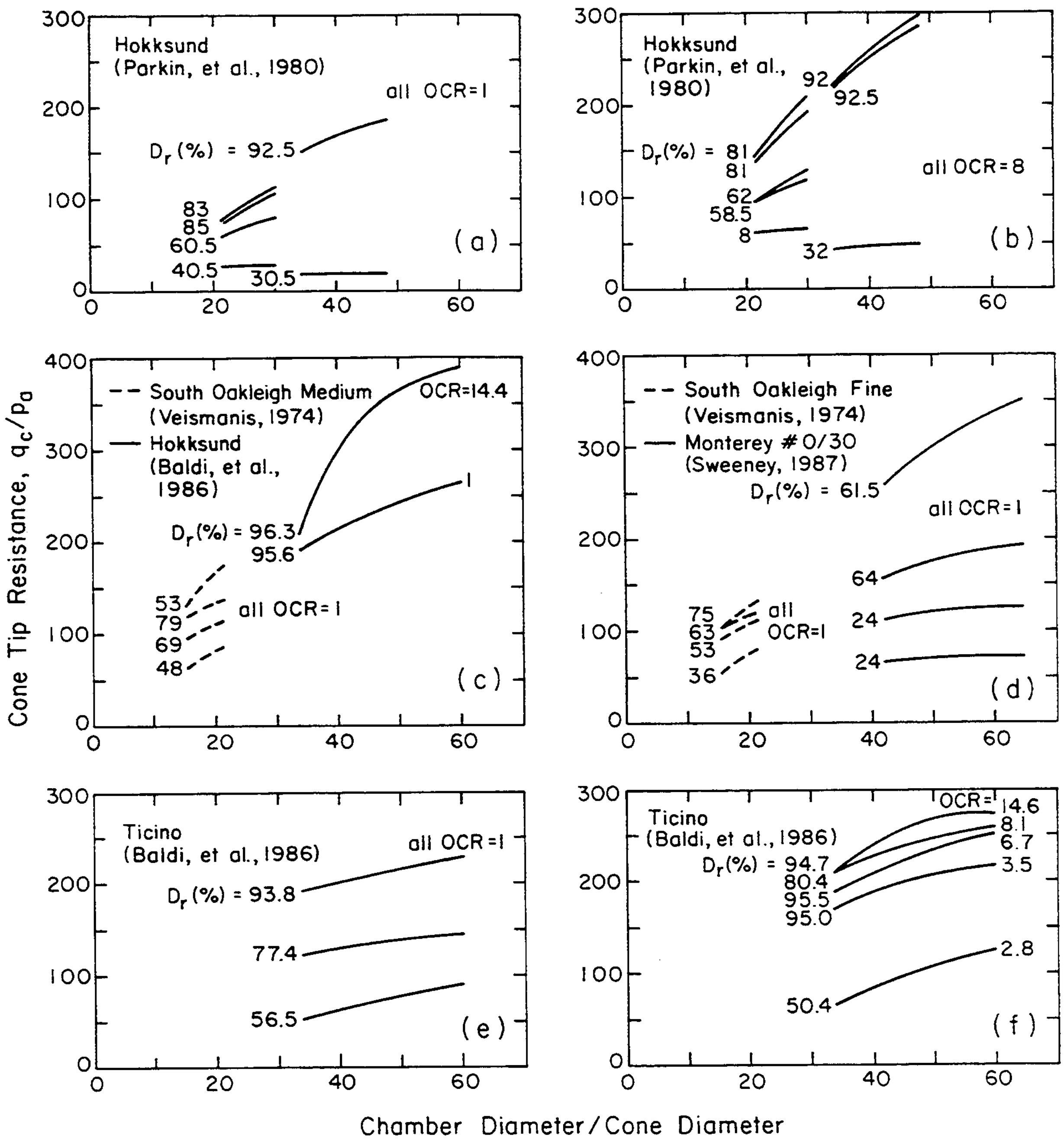

Figure H-1. Calibration Chamber Data for Various Sands

in Table H-1 used Type A or C conditions, which more closely simulate field conditions. The proposed correction factor applies to these cases.

Only two of the sands tested used either Type B or D boundary conditions. The

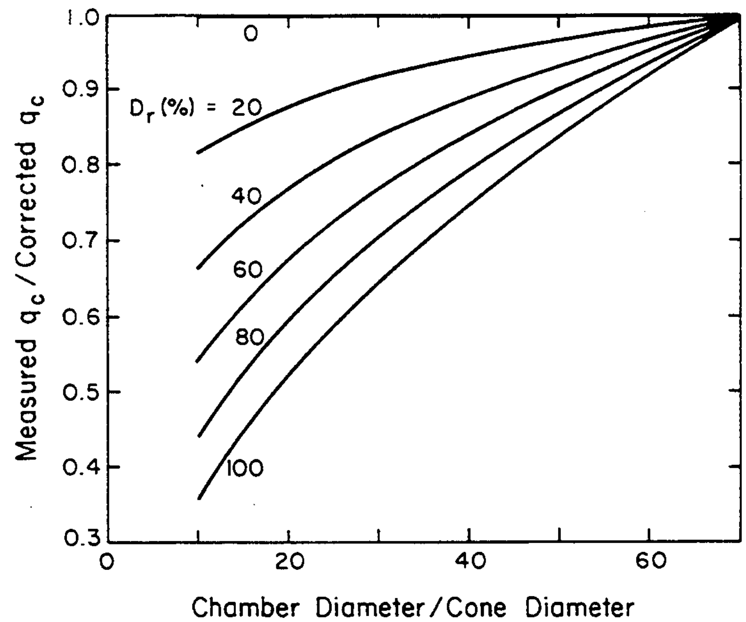

Figure H-2. CPT Calibration Chamber Correction Factor

Table H-2

BOUNDARY CONDITIONS IN FLEXIBLE-WALL CALIBRATION CHAMBERS

Type	Vertical	Horizontal
A	Stress constant	Stress constant
B	Change in strain is zero	Change in strain is zero
C	Stress constant	Change in strain is zero
D	Change in strain is zero	Stress constant

first was Toyoura sand (18), where Type B conditions were imposed. The second was the three Lone Star sands (13), where the chamber used was of a different design than most and Type D conditions were imposed. For these sands, no correction factor was introduced because the data are insufficient to develop this factor.

REFERENCES

1. Veismanis, A., "Laboratory Investigation of Electrical Friction Cone Penetrometers in Sand", Proceedings, European Symposium on Penetration Testing, Vol. 2.2, Stockholm, 1974, pp. 407-419.

2. Holden, J. C., "The Determination of Deformation and Shear Strength Parameters for Sands Using the Electrical Friction Cone Penetrometer", Report 110, Norwegian Geotechnical Institute, Oslo, 1976, pp. 55-60.

3. Been, K., Lingnau, B. E., Crooks, J. H. A., and Leach, B., "Cone Penetration Test Calibration for Erksak Sand", Canadian Geotechnical Journal, Vol. 24, No. 4, Nov. 1987, pp. 601-610.

4. Chapman, G. A. and Donald, I. B., "Interpretation of Static Penetration Tests in Sand", Proceedings, 10th International Conference on Soil Mechanics and Foundation Engineering, Vol. 2, Stockholm, 1981, pp. 455-458.

5. Schmertmann, J. H., "Study of Feasibility of Using Wissa-Type Piezometer Probe to Identify Liquefaction Potential of Saturated Fine Sands", Report S-78-2, U. S. Army Engineer Waterways Experiment Station, Vicksburg, 1978, 60 p.

6. Parkin, A. K., Holden, J., Aamot, K., Last, N., and Lunne, T., "Laboratory Investigation of CPT's in Sand", Report 52108-9, Norwegian Geotechnical Institute, Oslo, 1980, 45 p.

7. Lunne, T. and Christoffersen, H. P., "Interpretation of Cone Penetrometer Data for Offshore Sands", Report 156, Norwegian Geotechnical Institute, Oslo, 1985, pp. 1-11.

8. Baldi, G., Bellotti, R., Ghionna, V., Jamiolkowski, M., and Pasqualini, E., "Interpretation of CPT's and CPTU's: Drained Penetration of Sands", Proceedings, 4th International Geotechnical Seminar: Field Instrumentation and In-Situ Measurements, Nanyang Technological Institute, Singapore, 1986, pp. 143-156.

9. Canou, J., El Hachem, M., Kattan, A., and Juran, I., "Mini Piezocone Investigation Related to Sand Liquefaction Analysis", Proceedings, 1st International Symposium on Penetration Testing (ISOPT-1), Vol. 2, Orlando, 1988, pp. 699-706.

10. Thomas, D., "Deep Sounding Test Results and the Settlement of Spread Footings on Normally Consolidated Sands", Geotechnique, Vol. 20, No. 4, Dec. 1968, pp. 472-488.

11. Chong, M. K., "Density Changes of Sand on Cone Penetration Resistances", Proceedings, 1st International Symposium on Penetration Testing (ISOPT-1), Vol. 2, Orlando, 1988, pp. 707-714.

12. Houlsby, G. T. and Hitchman, R., "Calibration Chamber Tests of a Cone Penetrometer in Sand", Geotechnique, Vol. 38, No. 1, Mar. 1988, pp. 39-44.

13. Villet, W. C. B. and Mitchell, J. K., "Cone Resistance, Relative Density, and Friction Angle", Cone Penetration Testing and Experience, Ed. G. M. Norris and R. D. Holtz, ASCE, New York, 1981, pp. 178-207.

14. Huntsman, S. R., Mitchell, J. K., Klejbuk, L. W., and Shinde, S. B., "Lateral Stress Measurement During Cone Penetration", Use of In-Situ Tests in Geotechnical Engineering (GSP 6), Ed. S. C. Clemence, ASCE, New York, 1986, pp. 617-634.

15. Sweeney, B. P., "Liquefaction Evaluation Using a Miniature Cone Penetrometer and Large Scale Calibration Chamber", Ph.D. Thesis, Stanford University, Mar. 1987, 281 p.

16. Greeuw, G., Smits, F. P., and van Driel, P., "Cone Penetration Tests in Dry Oosterschelde Sand and the Relation with a Cavity Expansion Model", Proceedings, 1st International Symposium on Penetration Testing (ISOPT-1), Vol. 2, Orlando, 1988, pp. 771-776.

17. Lambrechts, J. R. and Leonards, G. A., "Effects of Stress History on Deformation of Sand", Journal of the Geotechnical Engineering Division, ASCE, Vol. 104, No. GT11, Nov. 1978, pp. 1371-1388.

18. Iwasaki, K., Tanizawa, F., Zhou, S., and Taksuoka, F., "Cone Resistance and Liquefaction Strength of Sand", Proceedings, 1st International Symposium on Penetration Testing (ISOPT-1), Vol. 2, Orlando, 1988, pp. 785-791.

19. Jamiolkowski, M., Baldi, G., Bellotti, R., Ghionna, V., and Pasqualini, E., "Penetration Resistance and Liquefaction of Sands", Proceedings, 11th International Conference on Soil Mechanics and Foundation Engineering, Vol. 4, San Francisco, 1985, pp. 1891-1896.

20. Parkin, A. K. and Lunne, T., "Boundary Effects in the Laboratory Calibration of a Cone Penetrometer for Sand", Proceedings, 2nd European Symposium on Penetration Testing, Vol. 2, Amsterdam, 1982, pp. 761-768.

21. Bellotti, R., Bizzi, G., Ghionna, V., Jamiolkowski, M., Marchetti, S., and Pasqualini, E., "Preliminary Calibration Tests of Electrical Cone and Flat Dilatometer in Sand", Proceedings, 8th European Conference on Soil Mechanics and Foundation Engineering, Vol. 2, Brighton, 1979, pp. 195-200.

Appendix I

UNIT CONVERSIONS

Parameter	Measure	Conversions
length	foot (ft)	0.3048 meters (m)
	inch (in)	25.4 millimeters (mm)
mass	pound (lb)	0.4526 kilograms (kg)
force	ton (t)	2000 pounds (lb)
		2 kips (k)
		8.896 kiloNewtons (kN)
stress	atmosphere (atm)	1.058 tons/square foot (tsf)
		2.116 kips/square foot (ksf)
		1.033 kilograms/square centimeter (ksc)
		101.3 kiloNewtons/square meter (kN/m^2)
		101.3 kiloPascals (kPa)
		0.1013 MegaNewtons/square meter (MN/m^2)
		14.70 pounds/square inch (psi)
		1.013 bars
unit weight	pound/cubic foot (pcf) (actually pound-force)	0.157 kiloNewtons/cubic meter (kN/m^3)
density	pound/cubic foot (pcf) (actually pound-mass)	16.02 kilograms/cubic meter (kg/m^3)

Note: 1 atm (p_a) $\approx$ 1 tsf $\approx$ 2 ksf $\approx$ 1 ksc $\approx$ 100 kN/m^2 $\approx$ 100 kPa $\approx$ 0.1 MN/m^2 $\approx$ 14.7 psi $\approx$ 1 bar

unit weight of fresh water (γ_w) = 62.4 pcf = 9.80 kN/m^3

Appendix J

SUMMARY CORRELATION TABLES

Within this manual, numerous correlations have been presented that allow the user to estimate a desired soil property from the results of laboratory index tests or in-situ field tests, or from other simple procedures. To assist the user in locating specific recommended correlations, Tables J-1 and J-2 have been prepared for cohesive and cohesionless soils, respectively. In each table, the broad property category is noted in the first column, followed by the specific soil property to be estimated in Column 2. Column 3 gives the laboratory or other test methods used to develop the laboratory or theoretical correlations noted in Column 4. The remaining columns identify the correlations available for the common in-situ field tests.

These tables are not intended to be a substitute for the text, which puts the correlations in proper perspective. Instead, they are intended to be a quick reference guide for the experienced user.

Table

CORRELATIONS FOR

Property Category	Soil Property	Lab/Field Test Method	Lab/Theory Correlation
Basic Characterization (Sec. 1, 2)	Simple description	Atterberg limits, gradation, simple field tests	pp. 2-1 to 2-7
	Soil classification	Atterberg limits, gradation, visual - manual	pp. 2-9,10
	Unit weight, γ	gradation	Table 2-8
	Consistency	-	-
In-Situ Stress (Sec. 3)	Preconsolidation stress, $\bar{\sigma}_p$	Atterberg limits	Eq. 3-13 Fig. 3-6
	Overconsolidation ratio, OCR	Atterberg limits, triaxial shear	Eq. 3-17 to 22
	Coef. of horizontal soil stress, K_o	Atterberg limits, oedometer, triaxial	Eq. 3-10 Fig. 3-22,25,26
Strength (Sec. 4)	Effective stress friction angle, $\bar{\phi}$	Atterberg limits	Fig. 4-20,24,25 Table 4-5
	Undrained shear strength, s_u	Atterberg limits, triaxial, etc.	Fig. 4-21,22,24,55 Fig. 4-26 to 29 Table 4-9
Elastic Deformability (Sec. 5)	Poisson's ratio, ν	-	$\nu_u = 0.5$
	Young's modulus, E	Atterberg limits, field load tests, resonant column	Eq. 5-16,19,20 Fig. 5-6,7,9,10
	Subgrade modulus, k_s	-	Eq. 5-34
Time-Dependent Deformability (Sec. 6)	Compression indices, $C_c + C_{ur}$	Atterberg limits	Eq. 6-7,9 Fig. 6-4,5,6
	Constrained modulus, M	oedometer	Eq. 6-12 Fig. 6-7,8
	Coef. of consolidation, c_v	Atterberg limits	Fig. 6-15
	Coef. of secondary compression, C_α	water content	Fig. 6-18 Table 6-3
Permeability (Sec. 7)	Coef. of permeability, k	constant head	Fig. 7-3,4 Table 7-1

a - SPT - standard penetration test
CPT - cone penetration test
CPTU - piezocone test
PMT - pressuremeter test
DMT - dilatometer test
VST - vane shear test

J-1

COHESIVE SOILS

Field Test Correlation[a]					
SPT[b] (App. A, F)	CPT[b] (App. B, F)	CPTU (App. B, F)	PMT (App. C, F)	DMT (App. D, F)	VST (App. E, F)
-	-	-	-	-	-
-	Fig. 2-8	Fig. 2-9,10	-	Fig. 2-12	-
-	-	-	-	-	-
Table 2-13,14	Table 2-14	-	-	-	-
Fig. 3-9	Fig. 3-10	Fig. 3-11, 12,13	Fig. 3-14,15	Fig. 3-16	Eq. 3-15 Fig. 3-7
Fig. 3-18	-	Fig. 3-19	-	Eq. 3-25 Fig. 3-21	Fig. 3-17
Fig. 3-30	Fig. 3-31	Fig. 3-32	Fig. 3-27 (direct measurement)	Eq. 3-30 Fig. 3-28,29	-
-	-	-	-	-	-
Fig. 4-50 Table 4-10	Eq. 4-61,62 Fig. 4-53	Eq. 4-63 Fig. 4-55	Eq. 4-64	Eq. 4-65	Eq. 4-57,58 Fig. 4-49
-	-	-	-	-	-
-	-	-	Fig. 5-8	-	-
-	-	-	-	-	-
-	-	-	-	-	-
Fig. 6-9	Fig. 6-10	-	-	Fig. 6-11	-
-	-	Fig. 6-16	-	Fig. 6-17	-
-	-	-	-	-	-
-	-	-	-	-	-

b - See interrelationship of CPT q_c and SPT N values in Figures 2-29 to 2-32.

Table

CORRELATIONS FOR

Property Category	Soil Property	Lab/Field Test Method	Lab/Theory Correlation
Basic Characterization (Sec. 1, 2)	Simple description	gradation, simple field tests	pp. 2-1 to 2-7
	Soil classification	gradation, visual - manual	p. 2-9,10
	Unit weight, γ	gradation	Table 2-8
	Relative density, D_r	relative density	-
In-Situ Stress (Sec. 3)	Coef. of horizontal soil stress, K_o	triaxial	-
Strength (Sec. 4)	Effective stress friction angle, $\bar{\phi}$	triaxial, etc.	Eq. 4-5,6,8 Table 4-2
Deformability (Sec. 5, 6)	Poisson's ratio, ν	triaxial, etc.	Eq. 5-7,9
	Young's modulus, E	triaxial, etc., field load tests, resonant column	Eq. 5-21,23,30 Fig. 5-18,19
	Constrained modulus, M	oedometer	Fig. 6-14
	Compression index, C_c	gradation, oedometer	Fig. 6-12,13
	Subgrade modulus, k_s	-	Eq. 5-34
Permeability (Sec. 7)	Coef. of permeability, k	falling head	Fig. 7-1,2 Table 7-1
Liquefaction Resistance (Sec. 8)	Cyclic stress ratio, $\tau_{av}/\bar{\sigma}_{vo}$	cyclic triaxial, etc.	-

a - SPT - standard penetration test
CPT - cone penetration test
CPTU - piezocone test
PMT - pressuremeter test
DMT - dilatometer test
VST - vane shear test

COHESIONLESS SOILS

Field Test Correlation[a]				
SPT[b] (App. A, F)	CPT[b] (App. B, F)	CPTU (App. B, F)	PMT (App. C, F)	DMT (App. D, F)
-	-	-	-	-
-	Fig. 2-8	Fig. 2-9,10	-	Fig. 2-12
-	-	-	-	-
Eq. 2-17	Eq. 2-21	Eq. 2-21	-	Fig. 2-28
-	Fig. 3-35,37,39	-	direct measurement	Fig. 3-34
Fig. 4-13	Fig. 4-15,16,17	-	Fig. 4-19	Eq. 4-17
-	-	-	-	-
Eq. 5-26 Fig. 5-13	-	-	Fig. 5-14	Eq. 5-27
-	Fig. 5-16	-	-	-
-	-	-	-	-
-	-	-	-	-
-	-	-	-	-
Fig. 8-1	Fig. 8-2,3	-	-	Fig. 8-4

b - See interrelationship of CPT q_c and SPT N values in Figures 2-29 to 2-32.

About EPRI

EPRI creates science and technology solutions for the global energy and energy services industry. U.S. electric utilities established the Electric Power Research Institute in 1973 as a nonprofit research consortium for the benefit of utility members, their customers, and society. Now known simply as EPRI, the company provides a wide range of innovative products and services to more than 1000 energy-related organizations in 40 countries. EPRI's multidisciplinary team of scientists and engineers draws on a worldwide network of technical and business expertise to help solve today's toughest energy and environmental problems.

EPRI. Electrify the World

Printed on recycled paper in the United States of America

EPRI • 3412 Hillview Avenue, Palo Alto, California 94304 • PO Box 10412, Palo Alto, California 94303 • USA
800.313.3774 • 650.855.2121 • askepri@epri.com • www.epri.com